Department of Mechanics, Faculty of Mechanical Engineering,
Czech Technical University in Prague, Czech Republic

Mechanist's Jotter 2006

Tomáš Mareš, editor

September 2006, Prague

ISBN 80-01-03454-2

Aims and Scopes:

The aim and scope of the *Mechanist's Jotter* is to convey scientific progress in applied mechanics to those concerned with application of this knowledge for the engineering practice. It addresses itself primarily to students, teachers, as well as to mechanical, civil and biomedical engineers involved in the study and practical application of mechanics. The *Mechanist's Jotter* publishes original contributions in the field of experimental and numerical mechanics, mechanics of materials, biomechanics and review articles by experts on new developments in theoretical mechanics and advances in experimental techniques.

The creation of this editorial project was substantially supported by the Czech Ministry of Education under Project MSM6840770012/FIS3405121.
Printing of 100
(EN) Mechanist's Jotter 2006
Date of issue: 2006–09–25
Editor: Tomáš Mareš
Editorial office address: Department of Mechanics, Faculty of Mechanical Engineering, Czech Technical University in Prague, Czech Republic, Technická 4, 166 07 Prague, Czech Republic
e-mail: Tomas.Mares@fs.cvut.cz
http://drone.fsid.cvut.cz/jotter/
ISBN 80-01-03454-2

Contents

Propagation of Acoustic Waves in Composite Materials and Cortical Bone

Author: Tomáš Goldmann

Department of Mechanics, Faculty of Mechanical Engineering, Czech Technical University in Prague, Czech Republic, Karlovo nám. 13, 121 35 Praha 2, Czech Republic
<Marek.Stefan@fs.cvut.cz>

Annotation

This work contributes to the methodology of an evaluation of elastic properties of cortical bones by ultrasonic wave inversion, whilst the bone is considered to be a linear elastic anisotropic continuum. Velocities of acoustic waves are used as an input data into inverse problem and they are experimentally detected by means of the ultrasonic based pulse-echo immersion technique. This method was developed on composite structures such as plates and cylindrical shells. The geometry of bone specimens is also implicated into algorithm by the model of wave propagation through curvilinear anisotropic sample based on the simplified ray method. The stability of resulting data is evaluated by the statistical method based on the Monte-Carlo simulation. Two additional ultrasonic based experimental techniques, the pulse through transmission contact method and the resonant ultrasound spectroscopy (RUS), are tested here in order to validate and improve a wave inversion access.

The immersion method based on the wave inversion has shown to be a reliable tool for determination of some elastic constants only, the remaining coefficients need to be measured or improved by another experimental method. The ultrasonic contact pulse through transmission technique was rated as an acceptable experimental approach for this purposes. The RUS was found to be an unsuitable method for the measurement of the elastic coefficients of the cortical bone tissue.

List of the most often used symbols

General notation

a	... scalar quantity
$\mathbf{a}$	... vector quantity
a^{cont}	... experimentally detected value of a via contact ultrasonic technique
a^{imm}	... experimentally detected value of a via immersion ultrasonic technique
$\mathbf{a}_{\mathsf{INC}}$	... incident vector quantity
$\mathbf{a}_{\mathsf{r}}$	... reflected vector quantity
$\mathbf{a}_{\mathsf{t}}$	... transmitted vector quantity
a_i, a_x	... vector quantity component
a_{ij}, a_{ijkl}	... component of a matrix or tensor
a^{exp}	... experimentaly obtained value of a
$\overline{a}$	... mean value of a
$a^{(undistorted)}$	... result of some algorithm undistorted by errors
$\mathrm{grad}_{\mathbf{a}}$	... gradient in coordinates $\mathbf{a}$
$\min_a$	... minimum with respect to a
$\dot{a}$	... time derivation od a

Mathematical symbols

$\mathbf{I}$	... unit matrix
$\mathbf{R}^n$	... space of n-dimensional real vectors
e	... Eulerian constant
i	... imaginary unit
L	... Lagrangian
δ_{ij}	... Kronecker symbol
π	... circular constant

Physical quantities

c_{ij}	... matrix of elastic coefficients [Pa]
C_{ijkl}	... tensor of elastic coefficients [Pa]
d	... thickness of specimen [m]
E	... Young modulus [Pa]
E_1, E_2, E_3	... Young modulus in three main directions of stress [Pa]
k	... wave number
$\mathbf{k}$	... wave vector [m^{-1}]
L,L1	... proportions of experimental set-up [m]
$\mathbf{n}$	... unit vectors in directions of a wave vector
P, Q, R	... Biot parameters
q_1, q_2	... distances in x coordinate from inner (1) and outer (2) boundaries of specimen [m]
Q	... quadratic sum
$\mathbf{s}$	... slowness vector [$\mathrm{s} \cdot \mathrm{m}^{-1}$]
SD_{ij}	... standard deviation
t	... time coordinate [s]
T	... temperature of water bath [C]
$\mathbf{u}(\mathbf{x}, t)$	... elastic wave (displacement field) [m]
$\mathbf{U}$	... amplitude of elastic wave [m]
V	... volume of solid [m^3]
v_ϕ^L, v_ϕ^T	... experimentaly obtained longitudinal and transverse phase velocities [$\mathrm{mm} \cdot \mathrm{s}^{-1}$]
v_φ	... phase velocity of bulk waves [$\mathrm{m} \cdot \mathrm{s}^{-1}$]
$v_\varphi^{\mathsf{fluid}}$	... phase velocity of incident wave propagating in fluid [$\mathrm{m} \cdot \mathrm{s}^{-1}$]
$\mathbf{v}_G$	... group velocity of bulk waves [$\mathrm{m} \cdot \mathrm{s}^{-1}$]
x_i, x, y, z	... cartesian coordinate system [m]
$X_i^1, Y_i^1, X_i^2, Y_i^2$	... coordinates defining sets of points of inner (1) and outer (2) boundaries of specimen [m]
Γ_{ij}	... Christoffel tensor
α	... angular deviation of specimen or reflector rotation []
β_{qL}, β_{qT}	... angular coordinate of refracted qL/qT wave's slowness vector [rad]
ϑ	... angular coordinate []
ε_{ij}	... strain tensor
ν	... normal direction
ρ	... density [$\mathrm{kg} \cdot \mathrm{m}^{-3}$]
σ_{ij}	... stress tensor [Pa]
τ	... tangential direction
υ	... Poisson ratio
ϕ	... angular coordinate [rad]
ψ	... angular coordinate between vectors of group and phase velocity [rad]
ψ_{qL}, ψ_{qT}	... angular coordinate of refracted qL/qT wave's energy fluxes [rad]
ψ	... angle of reflector or specimen rotation []
ω	... angular frequency [s^{-1}]
Ω	... Christoffel secular equation in wave vector components

Abbreviations

A	... anterior anatomical direction
ASCR	... Academy of Sciences of the Czech Republic
BMD	... bone mineral density
CAD	... Computer Aided Design
CFRP	... Carbon Fiber Reinforced Plastic
CNC	... Computer Numerical Control
CT	... computed tomography
DXA	... dual-energy X-ray absorptiometry
DSO	... digital oscilloscope
FEA	... finite element analysis
FEM	... finite element method
I	... inferior
L	... longitudinal wave or lateral anatomical direction
M	... medial anatomical direction
MIL	... mean intercept length
MRI	... magnetic resonance imaging
P	... posterior anatomical direction
PC	... personal computer
PMMA	... Polymethylmethacrylate
fiber fibre PS/PR	... Point-Source/Point Receiver
PT	... pure transverse
qL	... quasi-longitudinal
qT	... quasi-transverse
QUS	... quantitative ultrasound
RUS	... resonant ultrasound spectroscopy
S	... superior
SAW	... surface acoustic waves
SOS	... speed of sound
SW	... software
T, T1, T2	... transverse
TOF	... time of flight
μCT	... micro-computed tomography

Introduction

The general purpose of this study is a development of methodology for determination of the elastic coefficient of a cortical bone by means of dynamic testing. The elastic properties of single parts of a human skeleton are necessary to know for modeling the bone tissue-implants interactions as well as for disease diagnostics purposes. The knowledge of elastic constants of the bone tissue is also fundamental for a modelling of a mechanical response of bone loading and a micro-mechanical modelling that conduces to new findings concerning the microstructure of a bone tissue. This knowledge may, for example, help to answer a bone tissue remodelling problem.

Bone tissue is, from the mechanical point of view, an inhomogeneous, anisotropic and viscoelastic material with a composite structure. Compared to other tissues of the human body, the strain of a bone tissue is comparatively small, hence it is possible to assume a linear dependence between the stress and the strain. The damping of a cortical bone, in the terms of time dependency on material constants, is relatively small. Therefore, it is possible to contemplate a cortical bone as a linear elastic material, which is approximately homogenous and anisotropic with an orthotropic material symmetry [Lasayques and Pithioux, 1998,

Lee *et al.*, 2002, Pithioux *et al.*, 2002, Rho, 1996].

Dynamical mechanical tests are based on the fundamental theory of acoustic waves (also called elastic waves) propagation in anisotropic homogenous solids. In practise, these techniques are ultrasonic, it means that mechanical disturbance occurs at frequencies higher than approximately 20 kHz (the upper limit of the human audible range), and pulse transmission, consisting in measurement time of ultrasonic pulse flight between transmitting and receiving transducers. The pulse transmission method can be modified to a pulse echo technique, where only one transducer is used as a transmitter and receiver at the same time. The reflected waves from a specimen boundary or an acoustic reflector are detected then instead of the refracted ones. The ultrasonic pulse methods can be adjusted to a contact or immersion experimental set-up.

Contact tests are characterized by a direct contact among the specimen and transducers. The resultant elastic coefficients are dependent on specimen's dimensions and density, which are the easily measurable quantities, particulary in the case of cubical specimens. The contact technique is very suitable for determination of elastic properties of isotropic solids, however the measurement in a case of higher crystal symmetries (a bone is regarded to be an orthotropic or transversely isotropic anisotropic material [Lasayques and Pithioux, 1998, Lee *et al.*, 2002, Pithioux *et al.*, 2002, Rho, 1996, Yoon and Katz, 1976]) is embarrassed by requirement of necessary preparation of specimens for every crystallographic direction.

The immersion pulse transmission technique consists of a specimen immersion into a liquid between transmitting and receiving ultrasonic transducers. The specimen is rotated and ultrasonic waves propagating in various direction through a specimen are detected. Elastic coefficients of specimen can be obtained either analytically from the velocity measurements in different directions [Enderby *et al.*, 1998, Geiske and Allred, 1974, Harper and Clarke, 2002] or the problem can be solved by a multi-dimensional optimization approach [Sachse *et al.*, 1998, Seiner, 2004, Seiner and Landa, 2005, Wu and Ho, 2005] (inverse problem).

This PhD study will start with a literature overview, where the fundamental knowledge of a bone tissue structure, hierarchy and biomechanical properties will be introduced. The main scope of this work is the evaluation of elastic properties of a cortical bone, however the research in mechanical properties of a cancellous bone is no less important and the porosity and fluid flow of a cancellous bone make this task a much more complex problem. The mechanical properties of a cortical bone, their experimental and theoretical evaluation as well as advances in modelling of this porous tissue with a special reference to Biot theory will be also surveyed. The contemporary state of art in an evaluation of the elastic coefficients of a cortical bone via the ultrasonic pulse and resonant based techniques will be discussed in the final part of the literature overview.

The successive chapters will be devoted to theoretical background necessary to encompassment of the elastic constants evaluation by the experimental procedure used in this thesis. Widely known principles such as the Hooke's law, the Christoffel's equation, examples of characteristic surfaces of waves and the application of the Snell-Descartes law to a proposed experimental technique. Further theoretical part will deal with an original approach to the wave propagation in a curvilinear anisotropic specimen, which will be explored at the elastic constant evaluation of a generally shaped bone specimen later on. The last theoretical part will describe an applied access to the solution of an inverse problem of the Christoffel equation (determination of elastic coefficients from known velocities of wave propagation) by the optimization procedure which will be practically utilized during the immersion measurements. The method for the statistical evaluation of resulting data from optimization procedure will be presented, too.

The description of experimental procedures, list and characterization of specimens preparation will be accomplished in following chapter. Totally three ultrasonic techniques will be here planned. The pulse based immersion technique is going to be the most fundamental for purposes of this study, because of the automated measurement and results evaluation, an absence of a precise specimen cutting as well as a challenge to solution of the wave propagation through the

specimen of a general geometry are expected at a contemporary observance of a high result accuracy. The other two techniques, the pulse contact technique and the RUS (resonant ultrasound spectroscopy), will be used for a validation of results eventually results improvement. The result discussion and concluding remarks will be stated at the end of this work.

Aim of the work

The thesis specific aims are to develop an ultrasonic-pulse immersion scanning device and methodology based on an ultrasonic wave inversion for the evaluation of elastic constants of a homogenous anisotropic material and its application on an experimental determination of the elastic constants of the cortical bone. The part of this study is to deal with the solution of an inverse problem of Christoffel's equation for phase velocities and its application to measured data, to develop the statistical method for evaluation of the stability of inverse problem resulting data, to propose model of wave propagation through anisotropic solids of a planar, cylindrical and general shape, to validate this model on an immersion measurement of composite technical materials samples and its application to the cortical bone samples, to suggest an usage of the additional ultrasonic techniques such as the contact ultrasonic-pulse technique and the resonant ultrasound spectroscopy for an elastic coefficients measurement and their experimental verification on bone samples, to discuss advantages and disadvantages of particular experimental techniques and to outline the theoretical parameters for a future research.

Review of literature

Fundamental biomechanical properties of bone

A bone tissue represents a porous tissue containing a fluid phase, a solid matrix, and cells. It is a living tissue consisting of 25 % fluid. The remaining 75 % of a bone's structure contains organic and mineral components [Piekarski, 1970]. These solid and liquid phases are optimally resolved as a composite structure, which is hierarchically organized from the skeleton to an organ, tissue, cellular, subcellular and molecular level [Tate, 2003]. The interaction between solid and fluid phases is important for mechanical (elastic properties, viscoelastic behaviour) [Buechner *et al.*, 2001], metabolic and adaptive behaviour.

A bone tissue consists of a cortical and a cancellous (trabecular) bone. The cortical bone forms the major (80 % [Liebschner, 2004]) bone content in the body and it typically occurs in the diaphysis of long bones such as the radius, tibia and femur. The cancellous bone serves as a shock absorber and can be found at bones diaphysis and in the cores of flat bones. The cancellous bone is always protected by a thin layer of the cortical bone.

The skeleton is considered to be a system of bones accomplishing bearing, protecting and damping functions necessary for survival and mobility of a human [Pauwels, 1973, Piekarski, 1973]. A bone is an adaptive tissue and has optimal mechanical properties, specific to each part of the skeleton. The structure of the bone is exposed to dynamic loading, where the functional adaptation of the bone is necessary for surviving. The bone tissue remodeling is realized among osteocytes, osteoblasts and osteoclasts and ensures functional adaptation of the bone. The osteocytes are the most frequent cells in the bone and they participate in a mineralized structure (solid phase) of the bone and their death is associated with a lapse of the the solid matrix of the bone [Junqueira *et al.*, 1995]. Osteocytes are thought to be mechanosensors in bone [Burger and Klein-Nuled, 1999]. The transmission of mechanical signals to the cytoskeleton of osteocyte via the cell surface receptors can arise directly (through the solid matrix of the tissue) [Burger and Klein-Nuled, 1999, Carter, 1987, Huiskes and Hollister, 1993] or

indirectly (fluid pressure and shear stress) [Cowin *et al.*, 1991, Smalt *et al.*, 1997] imparted by the fluid movement.

Physical description of bone

The adaptive response of a bone tissue to mechanical stimuli is described by numerous different parameters such as a magnitude of a stress and a strain, number of loading cycles, strain tensor and strain energy density. The numerous strain/stress based bone adaptation theories were published, from the surface modelling as a function of the strain magnitude [Frost, 1990, Fyhrie and Carter, 1986, Huiskes *et al.*, 1987] to the time dependent modelling and remodelling [Beaupre *et al.*, 1990]. There is a lot of studies which are engaged in an overall relationship between the intensity of a stimulus and the magnitude of the response, but there is a very little evidence that the magnitudes of strains and stresses directly correlate to the bone's morphological response [Brown *et al.*, 1990, Gross *et al.*, 1997].

Composite and hierarchical structure of bone

The bone can be also considered as a highly structured composite material, which is composed of a collagen hydroxyapatite matrix and a hierarchical system of lacunae canals. These tubes permit the intersticial flow of a fluid through micro porosities [Cowin, 1999, Cowin *et al.*, 1995]. This flow induces loading, that leads to a change in the fluid velocity or pressure and ensures a tool by which a physical signal could be translated to the cell [Burger and Klein-Nuled, 1999, Jacobs *et al.*, 1998].

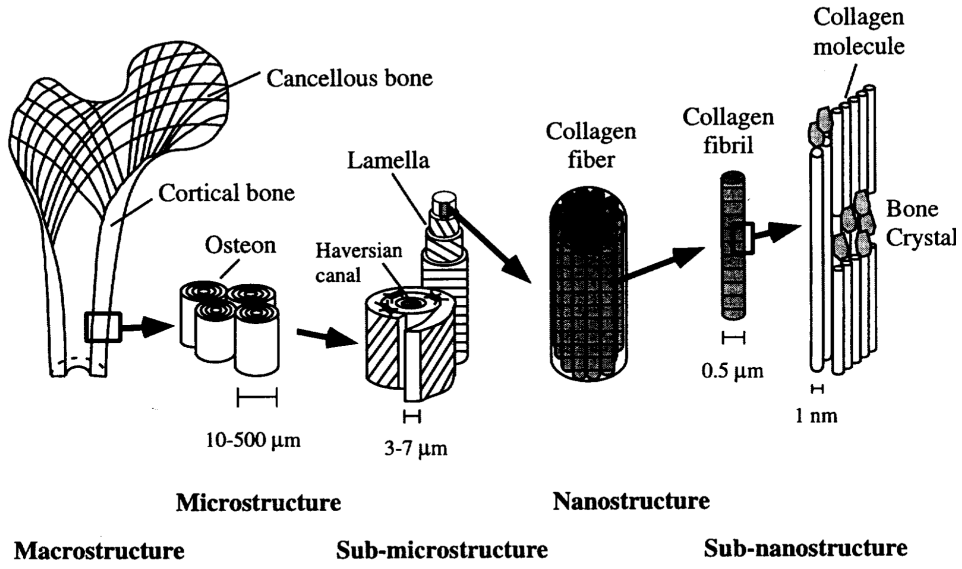

Fig. 1: The hierarchical structural organisation of a bone: (a) cortical and cancellous bone; (b) osteons with Haversian systems; (c) lamellae; (d) collagen fiber assemblies of collagen fibrils; (e) bone mineral crystals, collagen molecules, and non-collagenous proteins (After Rho et al 1998) [Rho *et al.*, 1998]).

The material structure of a bone varies at different scales which perform different mechanical, biological and chemical functions. The knowledge of mechanical characteristics of these scales is important for understanding of the mechanical properties of a structural relationship between them at the various levels of structural organization [Liebschner, 2004, Rho *et al.*, 1998] (Figure 1). These levels are: (1) the macrostructure (the cancellous and the cortical bone); (2)

the microstructure (from 10 to 500 μm: Haversian systems, osteons, single trabeculae); (3) the sub-microstructure (1 - 10μm: lamellae); (4) the nanostructure (from a few hundred nanometers to 1 μm: fibrillar collagen and embedded mineral); (5) the sub-nanostructure (below a few hundred nanometers: the molecular structure of constituent elements). This hierarchically organized structure makes the material of a bone heterogeneous and anisotropic, and mechanical properties vary at these different structural levels [RHO *et al.*, 1998].

Biomechanical characterization of cancellous bone

The cancellous bone is compounded of a system of trabeculae surrounded by a bone marrow. The cancellous bone has relatively high porosity (50-95 %) [MARTIN *et al.*, 1998] and low density (0.5-1.0 g/cm^3) [RHO, 1996]. From a biomechanical point of view, the elastic properties of the cancellous bone depend on a volume fraction, trabecular architecture and the elastic tissue properties of the mineralized matrix. A frequently used quantity, the bone mineral density (BMD) involves both, the volume fraction and the degree of mineralization of a mineralized matrix, but doesn't include an information in the trabecular architecture. However, the increasing resolution of imaging techniques (μCT - micro-computed tomography) and MRI - magnetic resonance imaging) develop the possibility of in vivo analysis of trabecular structure [MAJUMDAR *et al.*, 1998, MUELLER *et al.*, 1994]. These non-invasive techniques contain a range of gray values such a indicator of degree of a mineralization of the bone and a prediction of the apparent elastic moduli of the cancellous bone trabeculas [HOMMINGA *et al.*, 2001]. The further parameters of the trabecular structure such as a volume fraction, a surface density, a trabecular thickness, an inter-trabecular spacing, a trabecular number [HILDEBRAND *et al.*, 1999], a connectivity [ODGAARD and GUENDERSEN, 1993] and a fractal dimension [CROSS *et al.*, 1993] can be determined by the digital image analysis of these gray values maps.

The measurement of an architectural anisotropy of the cancellous bone is possible due to the methods such as the mean intercept length (MIL) [WHITEHOUSE, 1974] or the volume orientation distribution [ODGAARD *et al.*, 1990]. These techniques describe the spatial distribution of the bone architecture with a function that can be approximated by an ellipsoid or spherical Fourier series. Both approaches lead to the definition of the positive definite second order tensor that characterizes the three planes of an orthotropic symmetry and a degree of anisotropy of the cancellous bone.

Experimental determination of mechanical properties of cancellous bone

The measurement of mechanical properties of the cancellous bone in conjunction with the knowledge of the trabecular architecture is currently one of the most desirable topics in the bone research. The mathematical basis for assessment of both, the bone elastic properties and the bone architecture is given by nine orthotropic elastic constants, a volume fraction and a fabric tensor [COWIN, 1985]. The number of constants must be determined to satisfy these theoretical relationships by measurement of fabric and mechanical parameters. Several attempts (especially convectional mechanical tests) were made earlier to measure these constants, but a general and accurate approach has not been found yet.

The recent development of imaging techniques (μCT or MRI) in conjunction with new computer methods such as the finite element analysis FEA and frequent use of ulltrasonic experimental tests conduce to find the relationship between architectural and mechanical parameters.

Mechanical tests The volume fraction and an apparent density were measured in the earliest studies [CARTER and HAYES, 1977, LINDE *et al.*, 1989] in order to quantify the bone architecture, whilst the dependence between the bone density end the elastic modulus was found. The fabric measure was implicated in later studies [GOULET *et al.*, 1994, TURNER *et al.*, 1990] of a

large number of specimens in order to state the anisotropy of the bone architecture, but only a subset of the nine orthotropic elastic constants were determined.

Generally, the convectional mechanical probes are not very useful for the measurement of the anisotropic mechanical properties of bone specimens. For example, to determine the nine independent elastic coefficients of an orthotropic material, the three tensile or compressive, three deflection and three torsion tests in different directions are required. These tests require multiple measuring of the same specimen that is nearly impossible. Just a few efforts to quantify orthotropic elastic coefficients of the cancellous bone are known from the literature [Giesen *et al.*, 2001, Snyder and Hayes, 1990, Yahia *et al.*, 1988].

An interesting attempt of using a combination of mechanical testing and high-resolution nonlinear finite element modelling for a comparison of elastic modulus of the trabecular and the cortical bone was made by Bayraktar [Bayraktar *et al.*, 2004]. Results indicated that the mean elastic modulus was 10% lower for the trabecular tissue than for the cortical tissue. The similar conclusion was predicted in earlier work of Turner [Turner *et al.*, 1999], where acoustic and nanoindentation measurement technique were compared.

Micro-finite element analysis The micro-finite element analysis [Homminga *et al.*, 2003] has been developed to calculate the elastic coefficients computer models of the trabecular micro architecture. The finite element models are generated from micro-computed tomography (μCT) images of a region of interest of bone specimen. These images are digitalized in order to rebuild the original structure of the specimen as a 3D voxel model and a tensor of elastic coefficients is calculated for a given set of boundary conditions [Hollister and Kikuchi, 1992].

The results of conventional compression versus the μFE analysis show good agreement [Kabel *et al.*, 1999] indicating that the FEA approach can provide information similar to mechanical tests. Another study [Taylor *et al.*, 2002] has performed a FE and experimental modal analysis and compared the determined elastic constants with ultrasound results. It has been shown that a modal analysis can be used, together with FE models incorporating CT scan data, to determine the distribution of elastic constants throughout a long bone.

The comparison of the experimental techniques such as abilities of the bone mineral density (BMD) as measured by dual-energy X-ray absorptiometry (DXA), and the quantitative ultrasound (QUS) parameter and the speed of sound (SOS) to predict elastic constants as assessed by μFEA was done in work of van den Bergh [van den Bergh *et al.*, 2000]. For this purpose, BMD measurements were performed on bovine specimens, and, in addition, the SOS was measured in three directions. The specimens were μCT-scanned, and elastic constants were determined in three directions with μFEA analysis.

Ultrasound wave propagation Another technique for measuring elastic properties of the trabecular bone is ultrasound wave propagation. The velocity measurement of longitudinal and transverse wave velocities propagating through the trabecular microstructure along the principal material orientations provides calculation of elastic coefficients of an orthotropic material. However, theoretical limitations arise due to the characteristic length of the inter trabecular spacing with respect to a specimen size that determines together with the selected wavelength the actual ultrasound propagation mode.

The group of researches (Rho, Ashman, Turner et al. [Ashman *et al.*, 1989], [Rho, 1996], [Rho and ad C.Turner, 1993], [Rho *et al.*, 1995] and Strelitski [Strelitski *et al.*, 1997]) dealt with the measurement of orthotropic elastic coefficients by the ultrasound. The three important questions were claimed in their earlier work [Rho and ad C.Turner, 1993]: (1) Is the Young's modulus of an individual trabeculae same as that of microspecimens of the cortical bone? (2) Can the Young's modulus of the trabecular bone material be extrapolated from the

Young's modulus vs. density relationship for a cancellous bone? (3) Can the Young's modulus of a cortical bone be extrapolated from the Young's modulus vs density relationship for a cancellous bone? The ultrasonics through transmission tests and a mechanical micro-tensile test were performed in order to answer these three questions successively: (1)Young's moduli between the trabecular and the cortical bone were found significantly different; (2); Results from the multiple regression analysis showed that the Young's modulus of the trabecular bone material could be extrapolated from that of the cancellous bone using a quadratic relationship; (3) The Young's modulus of the cortical bone could not be extrapolated from relationships between a density and the Young's modulus of the cancellous bone.

The following research has addressed a problem of relations between elastic properties and CT numbers (density) [Rho *et al.*, 1995]. Mechanical properties of the cortical and the cancellous bone were determined using an ultrasonic transmission technique. CT values obtained from scans of the bones in water were corrected to Hounsfield units [Hvid *et al.*, 1989]. The correlations between CT numbers and a mechanical property estimated from the cortical bone were found to be low, while these relationships for the cancellous bone were found to be higher. These results suggest that CT values may be useful in predicting mechanical properties only for the cancellous bone.

The subsequent study [Rho, 1996] mapped the anisotropic elastic properties of the human tibia1 cortical and the cancellous bone using the ultrasonic pulse transmission contact technique. Cortical bone specimens were assumed to be orthotropic with nine independent elastic constants and were satisfactorily determined. The measurement of elastic properties of the cancellous bone was a much more complex problem. The cancellous bone was in this measurement also considered to be a continuous, linearly elastic and anisotropic structure. To assume this material as a continuous structure, the propagating wavelength must be greater than the characteristic dimensions of the structure and larger than the cross-sectional dimensions of the specimen. The elastic properties in three different directions were determined. Their average magnitudes E_1, E_2 and E_3 (standard deviations) are equal to 202(154), 232(180) and 769(534) MPa respectively. The shear moduli and poisson's ratios were not measured. The variation of elastic properties over several orders can be explained by porosity and the inhomogeneity of the structure due to different load conditions.

The convenience of the ultrasonic pulse through transmission or the echo contact techniques for measuring elastic properties of the cortical bone at macrostructural level can be deduced from these works of Rho et al. in fine. The necessity of another experimental technique such as the nanoindentation [Rho *et al.*, 1997, Silva *et al.*, 2004, Turner *et al.*, 1999, Zysset *et al.*, 1999] for the measurement of mechanical properties of the cancellous and the cortical bone at a microstructural level was proposed.

Anisotropy and elastic properties of the trabecular bone were clearly detected in a recent study [Jørgensen and Kundu, 2002] at the micrometer level. This work uses the $V(z)$-curve method, which involves surface acoustic waves (SAW) that are propagating along the surface of a specimen. The $V(z)$-curves are plots of lens output voltage of an acoustic microscope as a function of the lens focal point position with a respect to the specimen surface. The SAW subject of interest are Rayleight waves (R-waves) and longitudinal lateral waves (L-waves), which strongly reflect mechanical properties of a material. Both waves can be recorded and their propagation velocities can be determined, and when assumption of the trabecular bone density (ρ) is made, computation of the Poisson's ratio ($\upsilon = 0.23 \pm 0.07$), the Young's modulus ($E = 19.9 \pm 2.5$ GPa), and the shear modulus ($G = 8.4 \pm 0.5$ GPa) is possible and the qualitative measure of anisotropy at the micrometer level is obtained.

The measured and estimated elastic properties (Young's modulus) of the trabecular bone material published in a literature are introduced in the Table 1. The table was presented by Rho [Rho and ad C.Turner, 1993] and is extended. The table shows the great variance in the Young's modulus (from 0.2 to 20 GPa) and large standard deviations for all different testing techniques of the trabecular bone measured as a macrostructure. It is evident, that determination of elastic properties of the cancellous bone at macro and lower hierarchical levels is still a matter of considerable interest.

Table 1: Estimated and measured elastic modulus (standard deviation) of the trabecular bone material. Table presented by Rho [Rho and ad C.Turner, 1993] and is extended. E, G and ν are the Young's modulus, the shear modullus and the Poisson ratio. E_1, E_2 and E_3 are Young's modulus in a proximo-distal, an anterio-posterior and a mediolateral direction.

Literature source	Type of bone	Test method	Estimated elastic module
Wolf (1892)	Human	Hypothesis	17-20 GPa (wet)
Runkle & Pugh (1975)	Human, distal femur	Buckling	8.69 (3.17) GPa (dry)
Townsend et al. (1975)	Human, proximal tibia	Inelastic buckling	11.38 GPa (wet) 14.13GPa (dry)
Ryan & Williams (1986)	Fresh bovine femur	Tensile testing	0.76 (0.39)GPa
Ku et al. (1987)	Fresh frozen human tibia	Three-point bending	3.17(1.5) GPa
Ashman & Rho (1988)	Bovine femur, human femur	Ultrasonic testing	10.9 (1.6) GPa 12.7 (2.0) GPa
Mente & Lewis (1989)	Dried human femur, fresh human tibia	Cantilever bending with finite element analysis	7.8 (5.4) GPa
Ryan & Williams (1989)	Bovine femur	Tensile testing	1.0 GPa
Choi et al. (1991)	Human tibia	Four-point bending	5.35 (1.36) GPa (wet)
Rho (1993)	Human tibia	Tensile testing Ultrasonic testing	10.4 (3.5) GPa (dry) 14.8 (1.4) GPa (wet)
Rho (1996) [Rho, 1996]	Human tibia	Ultrasonic pulse transmission method	E_1 = 769 (534) MPa (wet) E_2 = 202 (154) MPa E_3 = 232 (180) MPa
Strelitzki (1997) [Strelitski *et al.*, 1997]	Human calcaneus	Ultrasonic pulse transmission method	E_1 = 834 (248) MPa (wet) E_2 = 440 (125) MPa E_3 = 299 (98) MPa
Jørgensen (2002) [Jørgensen and Kundu, 2002] $V(z)$	Dog femoral shaft E = 19.9 (2.5) GPa (dry)	curve method	G = 8.4 (0.5) GPa ν = 8.4 (0.5)

Theoretical models of wave propagation through porous media

Several theoretical approaches were adapted to model an ultrasonic wave propagation through the cancellous bone in order to understand the dependence of the ultrasound velocity and the attenuation upon the material and structural properties of the bone tissue. Different scattering theories and Biot theory belong among mentioned approaches [Haire and Langton, 1999]. Also a new cellular multi-layered models [Hughes *et al.*, 1999, Kaczmarek *et al.*, 2002] resulting from Biot theory were invented.

Biot theory The Biot theory is an optional model to the conventional scattering theories for the prediction of an acoustic wave propagation through the cancellous bone and it can be also applied to the less porous cortical bone [Haire and Langton, 1999]. This theory was first published by the Biot [Biot, 1956a, Biot, 1956b] and it was originally used for geophysical

purposes. The basic principle of Biot theory is a consideration of the separate motion of the solid elastic frame and the intersticed fluid. The loss of energy due to frictional and viscous forces opposing the fluid motion relative to the solid frame is analyzed. This motion is induced by three acoustic waves (two dilatational and one rotational) propagating through an investigate porous media. The fast wave represents the fluid and solid vibrating in phase and the slow corresponds to a vibration in an antiphase. The Biot theory also predicts two modes of wave dispersion separated by critical frequency: only the fast wave propagates (1st mode) and both fast and slow waves propagate (2nd mode). The existence of two compressional waves in the cortical bone was first reported by Lakes [Lakes *et al.*, 1983], but the two compressional waves in the cancellous bone were discovered due to the recent work of Hosokawa [Hosokawa and Otani, 1997], where an agreement between a prediction of the phase velocity and a measurement were obtained for both waves, thereby, the the Biot theory for the cancellous bone was confirmed. The critical frequency for the cancellous bone was estimated by Hughes [Hughes *et al.*, 2003].

The Biot theory is applied today to the cancellous bone with some difficulties. The greatest problem is a necessity of the experimental determination of large number of material and structural parameters. Originally, the Biot theory defined four nondimensional characteristic parameters and a characteristic frequency for the elastic waves propagation in a fluid-saturated porous media in a low-frequency range [Biot, 1956a], and six numerical combinations of the characteristic parameters of the porous system in a higher frequency range [Biot, 1956b]. Lately, the Biot theory was modified by Johnson [Johnson *et al.*, 1987]. According the review article of Haire [Haire and Langton, 1999], following parameters resulting from the Biot theory need to be determined for the characterization of the cortical and the cancellous bone: three Biot parameters P, Q and R, which are dependent on the intrinsic bulk modulus of the solid material, a bulk modulus of the solid frame, a bulk modulus of the solid, a shear modulus of the solid frame and a porosity (the volume fraction of the fluid phase). Additional four parameters describes the effective density of the solid moving through a liquid, an effective density of the fluid moving through the solid, an inertial drag that the solid exerts on the fluid and a dynamic tortuosity defined by Johnson [Johnson *et al.*, 1987]. The frequency of propagating waves also needs to be known. These parameters cannot be easily evaluated in vivo or in vitro. Many attempts to estimate or to measure these parameters by various groups of researches are overviewed by Haire [Haire and Langton, 1999]. The isotropic assumption of an observed material is a further limitation of the Biot theory application to the cancellous bone.

A new anisotropic model was proposed [Hughes *et al.*, 1999] in order to avoid the difficulties linked to the Biot theory, i.e. the isotropic behavior and a large number of parameters. This model consists of a simple layered structure of alternating fluid and solid plates. The geometry of the model is very simple for the investigation of the ultrasonic propagation through this system by applying the theory of the wave propagation in alternating solid and fluid layers developed by the Schoenberg [Schoenberg, 1984]. This model predicts two compressional waves for all propagation angles, except that perpendicular to plates, where there is only one. Two waves are equivalent to the waves of the first and the second kind of the Biot theory. Schoenberg theory requires six parameters (densities, speeds in component media and a porosity) and does not include a viscosity of fluid. The application of the Schoenberg model to the acoustic wave propagation through cancellous bone was validated experimentally.

Biomechanical characterization of cortical bone

The cortical bone is composed of osteons that are formed parallel to the long axis of the bone. This arrangement is due to a bone's ability to organize its structure in order to optimize its strength according to applied loading in different directions. The cortical bone has a relatively high density (1.7-2.2-0 g/cm^3 [Rho, 1996]) and a low porosity (5-10 % [Martin *et al.*, 1998]). The cortical bone is, from the mechanical point of view, an inhomogeneous, anisotropic, and visco-

elastic material having a composite structure. Compared to other tissues of the human body, the strain of a bone tissue is comparatively small, hence it is possible to assume a linear dependence between the stress and the strain. The porosity can be, contrary to the cancellous bone, vanished [Lakes *et al.*, 1986], [Lakes *et al.*, 1983], [Lasayques and Pithioux, 1998], [Lee *et al.*, 2002], [Pithioux *et al.*, 2002], [Rho, 1996] and the trabecular bone can be rated as a homogenous continuum. The visco-elasticity of the cortical bone is, in the terms of time dependency on material constants, relatively small. A bone is considered to be a composite structure that consists of stiff mineral particles embedded in a flexible matrix made of collagen fibres. Mineral particles are anisotropic, so the cortical bone has anisotropic mechanic properties [Fratzl *et al.*, 1992]. Therefore, it is possible to contemplate a cortical bone as a linear elastic material, which is approximately homogenous and anisotropic with an orthotropic material symmetry [Lee *et al.*, 2002], [Lasayques and Pithioux, 1998], [Pithioux *et al.*, 2002], [Yoon and Katz, 1976], [Rho, 1996]. The greatest strength and stiffness can be found in main loading direction, and has a structure designed to resist torsional and bending forces where these occur [Lakes *et al.*, 1986], [Pithioux *et al.*, 2002], [Rho, 1996].

Experimental determination of mechanical properties of cortical bone

The determination of the elastic coefficients of a bone tissue is very important for the description of mechanical properties of bones. Static mechanical tests (e.g. compressive, bending, and torsional tests) are currently used for assessment of the elastic coefficients of bones. Elastic coefficients are possible to detect experimentally by means of dynamics tests (ultrasonic tests), such as the contact pulse transmission technique (contact or specimen immersed in a liquid) or the resonant ultrasound spectroscopy (RUS).

The knowledge of elastic constants of a bone tissue is fundamental for modelling of the mechanical response of bone loading. The specification of elastic coefficients of bones is also very important for micro mechanical modelling that conduces to new findings concerning the microstructure of a bone tissue. This knowledge may, for example, help to answer a bone tissue remodelling problem.

Mechanical tests The classical mechanical tests were historically the first attempts of an experimental observation of cortical bone properties. One of the earliest and very valuable studies was a work of Park and Lakes [Park and Lakes, 1986]. This experiment was carried out on prismatic, square cross sectional bars of a wet and dry cortical bovine bone. The specimens were subjected to a torsion and strain distribution was measured by strain gauges around the surface of the bar. However, even through simplicity of this experiment, the Young modulus was firstly specified and an important conclusion, that the dry and wet bovine bone behaves quite differently was assessed. In the dry bone, the strain distribution was very close to the linear elastic model, while the strain distribution of wet followed micropolar (Cosserat) model [Park and Lakes, 1986]. Another important experiment was performed by Rho [Rho and ad C.Turner, 1993], where the Young modulus of the cortical and the cancellous bone was measured ultrasonically and mechanically (micro-tensile test) and results of the both, the experimental technique and the bone structure were compared. The ultrasonic and mechanical moduli differed by 11 % for the specimens of the cortical bone in comparison to 42 % for the trabecular bone.

The classical mechanical tests are still used in more recent studies [Dong and Guo, 2004, Iyo *et al.*, 2004]. The tensile and torsional testing system [Dong and Guo, 2004] was used for an examination of the dependence of the anisotropic elastic properties of the cortical bone as a transversely isotropic material on its porosity. This study proved, that the longitudinal Young and shear moduli of the human cortical bone are negatively correlated with the porosity of the cortical bone. Conversely, the elastic properties in the transverse direction did not have statistically significant correlations with the porosity of the cortical bone. The experimental

study of Iyo [Iyo *et al.*, 2004] takes advantage of three point bending testing method for the measuring of anisotropic viscoelastic properties of the cortical bone, where the relaxation process was investigated for different directions of the cortical bone and experimental results were fitted to empirically proposed relaxation models of the cortical bone [Iyo *et al.*, 2004].

Ultrasonic tests

Contact pulse transmission technique The pulse transmission contact technique is the simplest experimental technique of elastic constants determination of material properties via the ultrasound. The two transducers (a transmitter and a receiver) are attached to the examined material through the contact medium. The planar pulse waves are emitted from the transmitter, directly through the specimen and detected by the receiver. The thickness of the specimen and the time of the wave flight through the specimen in the investigated crystallographic direction is measured and the velocity of wave propagation is calculated. The elastic constants can be evaluated from velocities analytically [Buskirk *et al.*, 1981], [Degtyar and Rokhlin, 1997], [Every and Sachse, 1990], [Rho, 1996], [Royer and Dieulesaint, 1996] or numerically [Balasubramaniam and Whitney, 1996], [Rokhlin and Wang, 1992], [Seiner and Landa, 2005]. The velocity measurement needs to be performed with a high accuracy, hence the precise shape preparation of the specimen is necessary, which is a main disadvantage of this method. The specimen must have a constant thickness, a sufficient dimension in direction of the wave propagation and a smooth surface.

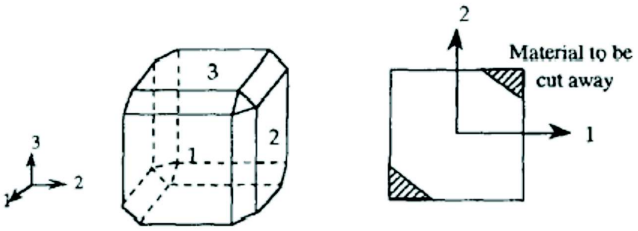

Fig. 2: Cubic specimen developed by Van Buskirk et al. [Buskirk *et al.*, 1981]. (After Rho 1996) [Rho, 1996]).

The contact pulse transmission technique is most widely used and oldest approach of the bone elastic constants measurement. The work of Rho [Rho, 1996] is for example a very comprehensive attempt to improve the contact technique for elastic constant measurement of the cortical bone as an orthotropic linear elastic material. Eight human tibiae were used in this study. Bones were cut into cube shaped specimens developed by Van Buskirk [Buskirk *et al.*, 1981] (Figure 2) so, that the velocities of propagation of longitudinal and transversal waves through the specimen could be measured in each crystallographic direction of orthotropic material symmetry. The average values of evaluated elastic coefficients of the human cortical bone are introduced in the Table 2.

Table 2: Elastic properties of the human tibial cortical bone obtained by the contact technique. The table presented by Rho [Rho, 1996]. Values are expressed in GPa.

c_{11}	c_{12}	c_{13}	c_{22}	c_{23}	c_{33}	c_{44}	c_{55}	c_{66}
19.41	11.32	12.50	20.01	12.55	30.91	5.73	5.18	4.05

Recently, the contact pulse transmission technique was used for elastic properties mapping of the human mandible cortical bone [Schwartz-Dabney and Dechow, 2002],

[Schwartz-Dabney and Dechow, 2003]. This was a problematic issue because of a lack of information about the principal material axes and a thickness of the cortex lower than in long bones. This study appeared from a cubic specimen developed by Van Buskirk [Buskirk *et al.*, 1981] and a new cylindrical specimen [Schwartz-Dabney and Dechow, 2002] was suggested. All nine elastic constants of the orthotropic specimen can be evaluated by the contact measurement of this cylindrical specimen. This technique proposes considerably less wastage of the bone than the standard technique of machining cubic specimens, and allows for the principal axis determination. Totally 31 samples of 10 human mandibles [Schwartz-Dabney and Dechow, 2003] were measured and statistically evaluated and a complete map of the orthotropic elastic constant of the mandibular cortex was drawn.

Immersion pulse transmission technique The immersion technique appears from the contact technique, but the specimen is not in a direct contact with ultrasonic transducers. It is widely used for evaluation of technical composite materials (e.g. [Darras *et al.*, 1995], [Enderby *et al.*, 1998], [Harper and Clarke, 2002], [Hine *et al.*, 1997], [Liaw *et al.*, 1996], [Wu and Ho, 2005]). The specimen is placed between a transmitter and a receiver and the entire measuring configuration is immersed in the liquid, where the transmitter generates well defined planar waves. This method allows the specimen rotation in the wide range of directions and a determination of the phase velocity propagation in these paths. The immersion technique is non-destructive and does not require the use of samples with precise dimensions and perfectly parallel faces. The evaluation of velocities of propagation is described by Gieske [Geiske and Allred, 1974] in a detail. The elastic constants are evaluated from detected velocities and they are described by Christoffel's equations [Auld, 1973], [Geiske and Allred, 1974], [Royer and Dieulesaint, 1996], which connect the velocity and shear pulses in the sample to an elastic stiffness for different angles of a refraction and can be calculated for the orthotropic material either analytically [Enderby *et al.*, 1998], [Harper and Clarke, 2002], [Hine *et al.*, 1997] or numerically (e.g. Newton-Raphson method [Wu and Ho, 2005]) or the problem can be converted to a multidimensional optimization approach. The multidimensional optimization approach can be solved by means of a differential method [Seiner and Landa, 2005] or by neural network [Sachse *et al.*, 1998].

The immersion pulse transmission technique was successfully used for a measurement of elastic coefficients of a wet bovine cortical femoral bone considered as the orthotopic and transversely isotropic material by Lasaygues and Pithioux [Lasayques and Pithioux, 1998], [Pithioux *et al.*, 2002]. Focussed 1MHz frequency transducers were used in this study in order to focus on small surfaces and to perform the measurement in different points on the sample. The Christoffel's equation was in this case solved numerically by using the Newton method. The measurement was performed only in a few points and all nine elastic constants are stated in the Table 3.

Table 3: Elastic properties of the bovine femoral cortical bone obtained by the immersion technique. The table presented by Lasaygues and Pithioux [Lasayques and Pithioux, 1998, Pithioux *et al.*, 2002]. Values are expressed in GPa.

c_{11}	c_{12}	c_{13}	c_{22}	c_{23}	c_{33}	c_{44}	c_{55}	c_{66}
23.50	7.6	8.4	26	8.20	34.60	9.20	6.00	6.28

Previously described attempts didn't look at a geometrical specification of the measured specimen, the general shape of the bone was substituted by a plane in the surroundings of the measurement location. The one case of the wave propagation through the bone-like shape specimen was performed by Detti [Detti *et al.*, 2002]. In this study the bone diaphysis was modeled by a cylindrical hollow tube. The internal cavity of the tube model was assumed to

be filled with a medullar marrow, so acoustic waves propagate as in a liquid environment. The water bath constituted the coupling medium between the acoustic transmitter and the examined specimen. The theory of rays, which is a special case of the geometrical theory of diffraction for a homogenous environment [Fekih and Quentin, 1983, Folacci and Rossi, 1997] was used in order to propose the wave propagation in a model situation of the cylindrical tube (Figure 3).

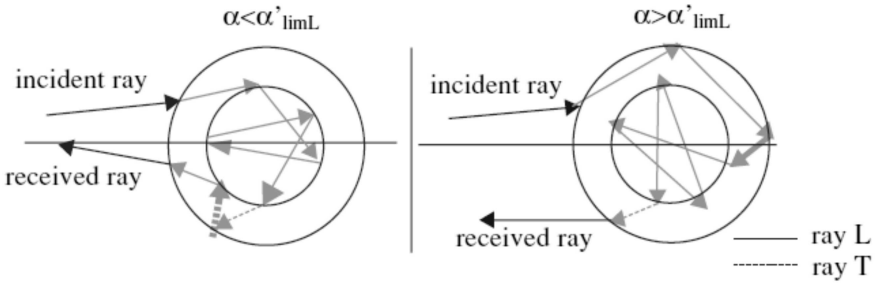

Fig. 3: Two cases of the theory of rays based model of the propagation through the cylindrical tube specimen in dependence on an angle of the specimen . (After Detti et al 2002 [Detti *et al.*, 2002]). α - angle of incidence, $\alpha\prime_{LIML}$ - limit angle of incidence for a longitudinal wave. [Detti *et al.*, 2002]

However, this model hasn't dealt with a specimen anisotropy (only the isotropic material was considered) and a more general geometry. Material properties of the specimen weren't also monitored, only the internal and external dimensions and the speed of sound were evaluated. The proposed method was validated on a bone specimen by the ultrasonic experiment and the conclusion, that the *a priori* chosen cylindrical model is more or less close to the real bone anatomy, was declared.

Resonant ultrasound spectroscopy (RUS) The resonant ultrasound spectroscopy is an experimental technique made for the determination of elastic properties of anisotropic materials developed by Demarest [Demarest, 1971]. It is the study of resonant frequencies spectra obtained by a forced mechanical oscillation of a sample at a known frequency of excitation. The resonant frequency is dependent on its symmetry, density, geometry and boundary condition. The resonant frequencies can be calculated from known elastic constants, density and dimensions of the specimen. Inversely, the elastic constants can be determined through the iterative calculations from the measured resonance frequencies as shown in Figure 4 [Ichitsubo *et al.*, 2002].

The full matrix of elastic coefficients can be determined by RUS to a great precision with one measurement, using the specimen with a simple geometry (cube, parallelepiped, cylinder and sphere). The specimen is supported by its opposite corners between the transmitter and receiver in the case of the cube or parallelepiped. The RUS has the advantage of a simple sample handling (no gluing or clamping) since the specimen is held by a contact force and a possibility of measuring both large and small specimens. Anisotropic samples need not to be oriented with respect to their crystal symmetry axes.

The usage of the RUS is very suitable for elastic constant measurement of single crystals and composite or technical materials with low attenuation properties. Some difficulties may occur while complex materials having the complicated structure and attenuation such as the cortical bone are being measured. The key factor for the reliable determination is to identify the vibration modes (eight independent groups for the orthotropic material symmetry - one dilatational, one torsional, three shear and three bend modes). The exact correspondence between the resonance peaks and the vibration modes should be known. Otherwise the results should be unrealistic.

The RUS experiment on the cortical bone was performed for example by Lee [Lee *et al.*, 2002]. Cubic-shaped specimens obtained from different locations of the bovine wet femur were used in this study. Only the lowest mode of resonant frequencies was observed. This mode corresponds

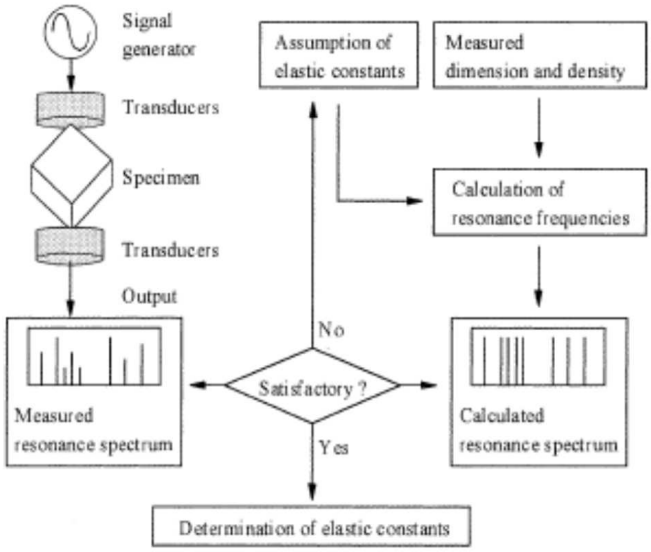

Fig. 4: Determination of elastic constants from the measurement and calculation of resonance frequencies by the RUS method. (After Itchisubo et al 2002 [Ichitsubo *et al.*, 2002]).

to the torsional vibration mode and it is clearly distinguishable, because the torsional frequency is far from the others [Demarest, 1971]. Only the torsional shear elastic constants c_{44}, c_{55} and c_{66} can be evaluated by this technique. Even through the simplicity of this experiment several serious difficulties have occurred, the noise caused by the resonance of air interfered with the RUS spectrum and one torsion mode was separated enough to be revealed by the RUS, but the other two overlapped in the RUS spectrum. The average magnitudes of elastic constants c_{44}, c_{55} and c_{66} resulting from this study correspond to 5.1, 4.9 and 4.2 GPa respectively. The following conclusion was declared by Lee [Lee *et al.*, 2002]: the RUS of cubical specimens was found not to be an effective tool for the study of damping and anisotropy of the bone because of the overlapping resonant peaks due to high damping of the bone at an ultrasonic frequency. The use of rectangular samples rather than cubes in RUS allows determination of three shear moduli and three shear damping values. For a future work, experiments using more rectangular specimens rather than cubes are recommended.

Wang [Wang and Lakes, 2003] suggested usage of shear transducers instead of compressional ones. This has the following advantages: a meaningfully stronger signal at the fundamental frequency, a rapid determination of the shear modulus, an identification of the vibration modes using the polarization of the shear transducers and no resonance of air. Those advantages of shear transducers were verified experimentally in this work on a technical material, but a verification on a bone specimen is still missing.

On the other hand, the RUS scanning was used by Kinney [Kinney *et al.*, 2004] on the human dentin, which is similar in its composition to a bone. The human dentin was assumed to be the transversely isotropic material and RUS measurement was performed in the vacuum using the foil transducers. All five elastic constants of transversely isotropic symmetry was successfully determined without reporting any involvement and the RUS was rated as a suitable technique for measuring elastic constants of the dentin.

Theoretical background

Elastic waves in anisotropic solid

Hooke's law

For a linear, elastic, homogenous, anisotropic material, assuming small deformations the generalized Hooke's law

$$\sigma_{ij} = C_{ijkl}\varepsilon_{kl} \tag{1}$$

is valid, where σ_{ij} and ε_{kl} are the stress and infinitesimal strain tensors and C_{ijkl} is stiffness tensor, of rank four, which expresses linear relation between stress and strain tensors of rank two. The tensor C_{ijkl} has 81 coefficients and due to a symmetry of the stress and strain tensor

$$\sigma_{ij} = \sigma_{ji} \tag{2}$$

$$\varepsilon_{kl} = \varepsilon_{lk} \tag{3}$$

is this count reduced to 36 and furthermore due to a total differentiability of the deformation energy [HEARMON, 1961] to 21 coefficients. Then the tensor C_{ijkl} is often rewritten in the shorten Voight's notation as a matrix of elastic coefficients c_{ij} [CHANDRASEKHARAIAH and DEBNATH, 1994, HEARMON, 1961].

Christoffel equation

The equation of motion

$$\rho\frac{\partial^2 u_i}{\partial t^2} = C_{ijkl}\frac{\partial^2 u_k}{\partial x_j \partial x_l} \,, \tag{4}$$

where ρ is the mass density, and $\mathbf{u}(\mathbf{x},t)$ is a planar elastic wave propagating in direction $\mathbf{n}$ through an observed material, can be obtained by substituting the Hooke's law into an equation of the equilibrium of a small volume of solid with no body forces acting

$$\rho\frac{\partial^2 u_i}{\partial t^2} = \frac{\partial \sigma_{ij}}{\partial x_j} \,, \tag{5}$$

considering the infinitesimal strain tensor

$$\varepsilon_{kl} = \frac{1}{2}\left(\frac{u_k}{x_l} + \frac{u_l}{x_k}\right) \,. \tag{6}$$

A planar elastic wave $\mathbf{u}(\mathbf{x},t)$ propagating in a material can be represented by

$$\mathbf{u} = \mathbf{U}e^{\mathrm{i}(\mathbf{kx}-\omega t)} \,, \tag{7}$$

where $\mathbf{U}$ is the wave amplitude, ω is the angular frequency, $\mathbf{x}$ is the position vector, and $\mathbf{k}$ is the wave vector. On substituting (7) into (4), it is obvious, that ω and U_k must satisfy the following system of the so-called Christoffel equation

$$\left(C_{ijkl}k_j k_l - \rho\omega^2\delta_{ik}\right)U_k = 0 \,, \tag{8}$$

where δ_{ik} is the Kronecker's symbol.

The phase velocity of a planar wave (7) and a wave vector $\mathbf{k}$ are defined as

$$v_\varphi = \frac{\omega}{k} \tag{9}$$

$$\mathbf{k} = k \cdot \mathbf{n} \,, \tag{10}$$

where k is the wave number, and $\mathbf{n}$ is the wave normal. Thus, the Christoffel equation can be rewritten in the terms of the phase velocity

$$\left(C_{ijkl} n_j n_l - \rho v_\varphi^2 \delta_{ik}\right) = 0 \,. \tag{11}$$

Introducing the Christoffel's tensor

$$\Gamma_{ik} = C_{ijkl} n_j n_l \,, \tag{12}$$

the Christoffel's equation becomes

$$\left(\Gamma_{ik}(\mathbf{n}) - \rho v_\varphi^2 \delta_{ik}\right) U_k = 0 \tag{13}$$

and it can be treated as an eigenvalue problem of following relation

$$\left|\Gamma_{ik} - \rho v_\varphi^2 \delta_{ik}\right| = 0 \,. \tag{14}$$

It stands of a reason of the equation (13) that resultant phase velocities v_φ are independent on the angular frequency ω and the magnitude of the wave vector $\mathbf{k}$, they are dependent only on a direction of the vector $\mathbf{k}$. As it follows from the definition of (12), the Christoffel matrix Γ_{ik} is symmetric and positively definitive, therefore its eigenvalues ρv_φ^2 are real positive and its eigenvectors $\mathbf{U}$ create an orthogonal triplet. The equation (14) has in general three solutions corresponding to the different modes of phase velocities propagation in a given direction $\mathbf{n}$.

If the direction of one of vectors $\mathbf{U}$ is consistent with $\mathbf{n}$, then this mode is denoted as a longitudinal mode (L). Other two modes, which are polarized perpendicularly to the $\mathbf{k}$ are marked as transversal (T). Both modes L and T correspond with the solution of the Christoffel equation for an isotropic solid. For an anisotropic solid, the wave with the polarization closest to $\mathbf{n}$ is called quasi-longitudinal (qL), and others are called quasi-transverse (qT).

The Christoffel's tensor (12) for general anisotropic solid can be itemized into the following expressions:

$$\begin{gathered}
\Gamma_{11} = c_{11}n_1^2 + c_{66}n_2^2 + c_{55}n_3^2 + 2c_{16}n_1n_2 + 2c_{15}n_1n_3 + 2c_{56}n_2n_3 \\
\Gamma_{12} = c_{16}n_1^2 + c_{26}n_2^2 + c_{45}n_3^2 + (c_{12}+c_{66})n_1n_2 + (c_{14}+c_{56})n_1n_3 + (c_{46}+c_{25})n_2n_3 \\
\Gamma_{13} = c_{15}n_1^2 + c_{46}n_2^2 + c_{35}n_3^2 + (c_{14}+c_{56})n_1n_2 + (c_{13}+c_{55})n_1n_3 + (c_{36}+c_{45})n_2n_3 \\
\Gamma_{22} = c_{66}n_1^2 + c_{22}n_2^2 + c_{44}n_3^2 + 2c_{26}n_1n_2 + 2c_{46}n_1n_3 + 2c_{24}n_2n_3 \\
\Gamma_{23} = c_{56}n_1^2 + c_{24}n_2^2 + c_{34}n_3^2 + (c_{46}+c_{25})n_1n_2 + (c_{36}+c_{45})n_1n_3 + (c_{23}+c_{44})n_2n_3 \\
\Gamma_{33} = c_{55}n_1^2 + c_{44}n_2^2 + c_{33}n_3^2 + 2c_{45}n_1n_2 + 2c_{35}n_1n_3 + 2c_{34}n_2n_3 \\
\Gamma_{21} = \Gamma_{12} \,, \Gamma_{31} = \Gamma_{13} \,, \Gamma_{32} = \Gamma_{23}.
\end{gathered} \tag{15}$$

Group velocity

The $\rho\left(\frac{\omega}{k}\right)^2$is the eigenvalue of $\Gamma_{ik}(\mathbf{n})$ if the secular equation

$$\left|\Gamma_{ik}(\mathbf{n}) - \rho\frac{\omega^2}{k^2}\delta_{ik}\right| = 0 \tag{16}$$

is valid. This equation can be written in the form

$$\Omega\left(\mathbf{k}, \omega\right) = \left|k_j C_{ijkl} k_l - \rho\omega^2 \delta_{ik}\right| = 0 \tag{17}$$

after multiplying by k^2. This relations represents an implicit dispersion relation $\omega = \omega(\mathbf{k})$ for (qL) and (qT) modes of a wave polarization and it enables the i-th group velocity component to be evaluated as

$$\left(v_G\right)_i = -\frac{\partial\omega}{\partial k_i} = -\frac{\partial\Omega/\partial k_i}{\partial\Omega/\partial\omega} \,. \tag{18}$$

Written more comprehensively,

$$(\mathbf{v}_G) = -\frac{\mathrm{grad}_k \Omega}{\partial\Omega/\partial\omega} \,, \tag{19}$$

where the gradient of Ω is taken with the respect to variables $k_i = 1, 2, 3$.

The group velocity describes the flux of the energy carried by the wave in contrast to the phase velocity, which responds to the velocity of the phase fronts traveling. The group and phase velocities usually differ in both the directions and the magnitude. The corresponding phase and group velocities satisfy the equation [CHU and ROKHLIN, 1994]

$$v_G = v_\varphi \cos\psi \,, \tag{20}$$

where ψ is the angle between the wave vector and the energy flux directions. This equation means that the ray surface is a tangent surface to the normal surface is a footpoint to the ray surface [BALASUBRAMANIAM and WHITNEY, 1996]. The slowness surface, which is the inverse surface to the normal surface and is polar reciprocal to the normal surface and vice versa. These geometrical relations are defined in the Section and they enable experimentally obtained ray surfaces to be converted into corresponding normal and contrariwise. However, simple relations between group velocities and directions of propagation cannot be, in general, derived.

For an elastic half-space, where the free-surface conditions must be considered, the orthogonal tripled by phase velocities, which are solutions of an equation (8) remain valid, but two other types of a wave can be observed. These are the head-wave, and the surface wave of a phase velocity very close to the slowest bulk mode. These waves are strongly attenuated with a distance from the interface, limiting the bulk solution for unbounded media.

Matrix of elastic coefficients for orthotropic material

The crystallographic axes of the orthotropic system are orthogonal to each other and elastic constants are invariant to the turning through an angle π around any crystallographic axis. The orthotropic material is described by nine independent elastic constants and the matrix of elastic coefficients has form

$$c_{ij} = \begin{pmatrix} c_{11} & c_{12} & c_{13} & 0 & 0 & 0 \\ c_{12} & c_{22} & c_{23} & 0 & 0 & 0 \\ c_{13} & c_{23} & c_{33} & 0 & 0 & 0 \\ 0 & 0 & 0 & c_{44} & 0 & 0 \\ 0 & 0 & 0 & 0 & c_{55} & 0 \\ 0 & 0 & 0 & 0 & 0 & c_{66} \end{pmatrix} \,, \tag{21}$$

with the cartesian coordinate system denoted *(x₁,x₂,x₃)*, configured identically with the natural crystallographic axes of a material, is considered.

The Christoffel equation (8) for the orthotropic material and for the wave propagating in x_1x_2 plane is

$$\begin{bmatrix} c_{11}n_1^2 + c_{66}n_2^2 - \rho\omega^2 & (c_{12} + c_{66})\, n_1 n_2 \\ (c_{12} + c_{66})\, n_1 n_2 & c_{66}n_1^2 + c_{22}n_2^2 - \rho\omega^2 \end{bmatrix} \begin{bmatrix} U_1 \\ U_2 \end{bmatrix} = 0 \,, \tag{22}$$

for the wave propagating in x_1x_3 plane it is

$$\begin{bmatrix} c_{11}n_1^2 + c_{55}n_3^2 - \rho\omega^2 & (c_{13} + c_{55})\, n_1 n_3 \\ (c_{13} + c_{55})\, n_1 n_3 & c_{55}n_1^2 + c_{33}n_3^2 - \rho\omega^2 \end{bmatrix} \begin{bmatrix} U_1 \\ U_3 \end{bmatrix} = 0 \tag{23}$$

and for the wave propagating in x_2x_3 plane it is

$$\begin{bmatrix} c_{22}n_2^2 + c_{44}n_3^2 - \rho\omega^2 & (c_{23} + c_{44})\, n_2 n_3 \\ (c_{23} + c_{44})\, n_2 n_3 & c_{44}n_2^2 + c_{33}n_3^2 - \rho\omega^2 \end{bmatrix} \begin{bmatrix} U_2 \\ U_3 \end{bmatrix} = 0 \,. \tag{24}$$

The solution of the Christoffel's coefficients for the orthotropic material is well described in literature [Auld, 1973, Geiske and Allred, 1974, Royer and Dieulesaint, 1996]. The formulae published by Rho [Rho, 1996] derived for the contact pulse transmission technique measurement of the cortical bone specimens (Figure 2) of a cubic shape are, for example, introduced subsequently. The diagonal coefficients can be determined from ultrasonic measurements in main crystallographic axes

$$\begin{aligned} c_{11} = \rho v_1^2, \quad c_{22} = \rho v_2^2, \quad c_{33} = \rho v_3^2, \\ c_{44} = \rho v_{23}^2, \quad c_{55} = \rho v_{13}^2, \quad c_{66} = \rho v_{12}^2, \end{aligned} \tag{25}$$

where v_i is velocity of quasi-longitudinal wave in direction i and v_{ij} is a velocity of a quasi-transverse wave traveling in the direction i, polarized in direction j. Elastic coefficients outside the diagonal can be measured by wave propagation in $(i+j)/\sqrt{2}$

$$\begin{aligned} c_{12} &= \sqrt{(c_{11} + c_{66} - 2\rho v_{12}^2) + (c_{22} + c_{66} - 2\rho v_{12}^2)} - c_{66} \ , \\ c_{13} &= \sqrt{(c_{11} + c_{55} - 2\rho v_{13}^2) + (c_{33} + c_{55} - 2\rho v_{13}^2)} - c_{55} \ , \\ c_{23} &= \sqrt{(c_{22} + c_{44} - 2\rho v_{23}^2) + (c_{33} + c_{44} - 2\rho v_{23}^2)} - c_{44} \ , \end{aligned} \tag{26}$$

where v_{ij} is a a velocity of a quasi-longitudinal or a quasi-transverse wave traveling in the direction $(i+j)/\sqrt{2}$ polarized in the ij plane.

The acoustic energy travels in the anisotropic materials with a group velocity v_G which differs in the direction and the magnitude from the phase velocity. However, in case of immersion measurements (Section), we directly obtain the phase velocities [Enderby *et al.*, 1998, Geiske and Allred, 1974] instead of group velocities resulting from the PS/PR measurements (Section) [Seiner, 2004, Seiner and Landa, 2003, Seiner and Landa, 2005].

Matrix of elastic coefficients for transversely isotropic material

The transversely isotropic material symmetry is a special case of the orthotropic symmetry and it is described by five independent elastic constants

$$c_{ij} = \begin{pmatrix} c_{11} & c_{12} & c_{13} & 0 & 0 & 0 \\ c_{12} & c_{11} & c_{13} & 0 & 0 & 0 \\ c_{13} & c_{13} & c_{33} & 0 & 0 & 0 \\ 0 & 0 & 0 & c_{44} & 0 & 0 \\ 0 & 0 & 0 & 0 & c_{44} & 0 \\ 0 & 0 & 0 & 0 & 0 & \frac{1}{2}(c_{11} - c_{12}) \end{pmatrix} \text{ and } c_{66} = \frac{1}{2}(c_{11} - c_{12}) \ . \tag{27}$$

An x_3 axis is directed along axis of symmetry (a fiber direction in composite materials, a direction of Haversian system in bones) and plane x_1x_2 is isotropic plane. The Christoffel equation (8) for the wave propagating in x_1x_3 plane is

$$\begin{bmatrix} c_{11}n_1^2 + c_{44}n_3^2 - \rho\omega^2 & (c_{13} + c_{44})\, n_1 n_3 \\ (c_{13} + c_{44})\, n_1 n_3 & c_{44}n_1^2 + c_{33}n_3^2 - \rho\omega^2 \end{bmatrix} \begin{bmatrix} U_1 \\ U_3 \end{bmatrix} = 0 \tag{28}$$

and for the wave propagating in x_1x_3 is

$$\begin{bmatrix} c_{11}n_1^2 + c_{66}n_2^2 - \rho\omega^2 & (c_{12} + c_{66})\, n_1 n_2 \\ (c_{12} + c_{66})\, n_1 n_2 & c_{66}n_1^2 + c_{11}n_2^2 - \rho\omega^2 \end{bmatrix} \begin{bmatrix} U_1 \\ U_2 \end{bmatrix} = 0 \ . \tag{29}$$

It is obvious from equations (28) and (29) that two modes of the wave propagation in x_1x_2 exists , i.e. the qL and qT modes. The unknown elastic constants for the transversely isotropic elastic material can be obtained by qL and qT wave propagation measurements in only two planes.

Characteristic surfaces

Three characteristic surfaces are widely described in literature [HEARMON, 1961, MUSGRAVE, 1970, ROYER and DIEULESAINT, 1996, SEINER, 2004] in order to illustrate the propagation of acoustic waves in anisotropic solids or crystals. These surfaces can be defined by means of phase $\mathbf{v}_\varphi$ and group velocities $\mathbf{v}_G$, which are dependent on the normal direction $\mathbf{n}$ running along a unit sphere and they can be treated as three closed surfaces in $\mathbf{R}^3$. The characteristic surfaces are valid for all three modes of the wave propagation (two quasi-transverse qT and one quasi-longitudinal qL).

The normal surface is formed by the radius vector $\mathbf{v}_\varphi = \mathbf{v}_\varphi(\mathbf{n})$ which is proportional to the phase velocity in the normal direction $\mathbf{n}$. The ray surface is a plot of the group velocity vector $\mathbf{v}_G = \mathbf{v}_G(\mathbf{n})$ versus corresponding normal direction $\mathbf{n}$.

The inverse surfaces can be constructed to above defined surfaces. The slowness surface is defined as $\frac{1}{\mathbf{v}_\varphi}(\mathbf{n})$ and the ray-slowness surface as $\frac{1}{\mathbf{v}_G}(\mathbf{n})$ for $\mathbf{n}$ running along the whole unit sphere in $\mathbf{R}^3$ again. The slowness surface can be also defined by means of slowness vectors $\mathbf{s}$

$$\mathbf{s} = \frac{\mathbf{n}}{v\varphi}\,. \tag{30}$$

The implementation of characteristic surfaces can be summarized as follows: The propagation of acoustic waves in anisotropic solid is possible to distinguish by twelve closed surfaces in $\mathbf{R}^3$, because each of three modes of wave propagation (2 x qT and 1 x qL) appertains to the normal surface, ray surface and two inverse surfaces running in all normal directions along the unit sphere.

Waves on a solid/fluid interface

The wave propagation in unbounded media have been studied until now. The situation is more complex if two generally anisotropic materials are in contact at their free surfaces. The model situation (solution of the Christoffel equation) is the same for both cases, but the interaction of these waves at a boundary must be dealt with. Let us define the incident wave

$$\mathbf{u}_{\mathsf{inc}} = \mathbf{U}_{\mathsf{inc}} \cdot\ e^{\mathrm{i}\omega(\mathbf{s}_{\mathsf{inc}}\cdot\mathbf{x}-t)},\ x_1 < 0\,, \tag{31}$$

where $\mathbf{s}$ denotes the slowness vector, the superscript $_{\mathsf{inc}}$ means the incident wave and the coordinate system is indicated on Figure 5. The incident wave can generate according to the Huygens principle three reflected and/or transmitted waves (1 x qL, 2x qT). These are

$$\mathbf{u}_{\mathsf{r}} = \mathbf{U}_{\mathsf{r}} \cdot e^{\mathrm{i}\omega(\mathbf{s}_{\mathsf{r}}\cdot\mathbf{x}-t)},\ x_1 < 0\,, \tag{32}$$

$$\mathbf{u}_{\mathsf{t}} = \mathbf{U}_{\mathsf{t}} \cdot e^{\mathrm{i}\omega(\mathbf{s}_{\mathsf{t}}\cdot\mathbf{x}-t)},\ x_1 > 0\,, \tag{33}$$

where the subscript $_{\mathsf{r}}$ is for the reflected waves, the subscript $_{\mathsf{t}}$ is for the transmitted waves and both subscripts run from 1 to 3 for each mode of the wave propagation. The situation, when only the reflected waves exist, is called the total reflection and it is determined by critical angle (for detailed description see [ROYER and DIEULESAINT, 1996]).

The reflection and refraction of elastic waves at a boundary between two anisotropic media is described by the Snell-Descartes law. Even in our simpler case, where one of the media is considered to be a non-viscous fluid, evaluation of paths of reflected energy fluxes is a significantly difficult issue.

An interaction between a single planar wave and an anisotropic plate-like specimen is outlined in Figure 5. The incident wave of a slowness vector $\mathbf{s}_{\mathrm{inc}}$ is refracted into more separate waves in the specimen, each travelling at its own group velocity in the direction of its energy flux. In Figure 5, only two of these waves (qL and one qT) are shown for clarity. Besides them, one more qT

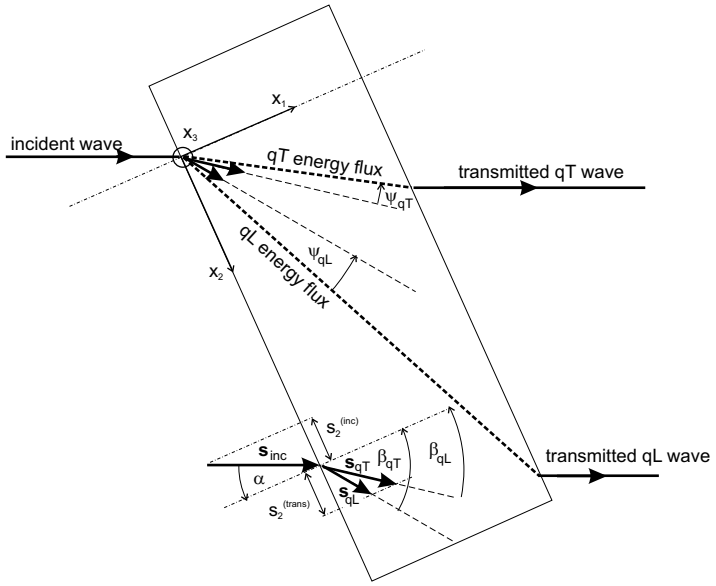

Fig. 5: An interaction of a single planar wave with an anisotropic plate-like specimen.

mode can be generated, or the surface wave can arise instead of one of the bulk modes, depending on the angle of incidence [Geiske and Allred, 1974, Royer and Dieulesaint, 1996].

According to the Snell-Descartes law, the projection of the incident wave slowness into the boundary $s_2^{(\mathrm{fluid})}$ is conserved, following conditions for refraction angles $\beta_{\mathrm{qL}}$and β_{qT}

$$\frac{v_\varphi^{\mathrm{fluid}}}{v_\varphi^{\mathrm{qL}}} = \frac{\sin\alpha}{\sin\beta_{\mathrm{qL}}} \qquad \text{and} \qquad \frac{v_\varphi^{\mathrm{fluid}}}{v_\varphi^{\mathrm{qT}}} = \frac{\sin\alpha}{\sin\beta_{\mathrm{qT}}} \ . \tag{34}$$

This relation expresses the Snell-Descartes law for elastic waves on the interface of two anisotropic media: The slowness vectors of the reflected and refracted waves are contained in the plane of incidence, defined by a vector normal to the interface and the slowness vector of the incident wave. The projections of these slowness vectors onto the interface are equal to that of the slowness vector of the incident wave.

Consequently, the angles β_{qL} and β_{qT} determine the directions of refracted wave's slowness vectors, containing angles $\Psi_{\mathrm{qL}}$and Ψ_{qT} with corresponding energy fluxes. At the second interface, the Snell-Descartes law is implemented again, resulting in a set of separate parallel planar (transmitted) waves of the same direction as the incident wave.

When the opposite surfaces of the specimen are not perfectly parallel, i.e. the specimen is slightly wedge-shaped, the transmitted waves are planar again, but their directions may vary from the direction of the incident wave. Furthermore, other deviations from a perfect rectangularity of a specimen may distort both the parallelism and the planarity of the transmitted waves.

Ultrasonic evaluation of curvilinear anisotropic samples by the simplified ray method

The simplified ray method

The well known theory of the acoustic waves propagation in solids was discussed so far. The quite original approach of the interaction between the planar acoustic wave propagating in a liquid and

a generally shaped anisotropic specimen is a subject of interest in this chapter. This interaction is modeled by virtue of simplified ray method [ČERVENÝ, 2001, PSENCIK, 2000]. The technique is based on a wavefront substitution by the closely localized energy flow (ray) in every geometrical point. The Chrristoffel's equation along rays (8) and the ray behaviour at a solid/liguid interface will be solved numerically afterwards. Rays in immersion are lines perpendicular to the wavefront - the planar wavefront is replaced by the set of respectively parallel rays.

Subsequent simplifications are used in following considerations:

1. The problem is two dimensional. Only one of the main crystallographic planes of the orthotropic material symmetry is contemplated.

2. The density is uniform in all geometrical points, only the anisotropy rotation in consequence of a general shape of the specimen is studied. This conduces to preservation of the wave vector in every ray point inside the specimen.

3. The multistage Runge-Kutta method is not used to the integration of the resultant equation of motion, the simple summation of time increments through the specimen thickness is utilized. This simplification significantly accelerates computation and will be discussed later.

The generalization of the simplified ray method into three dimensions is elementary, however, the full ray method for an inhomogeneous anisotropic medium should be used, taking the varying density into the account.

Anisotropic orientation in curvilinear specimen

Let us consider a curvilinear orthotropic homogenous specimen, whose boundaries are described by the set of points (X_i^1, Y_i^1) and (X_i^2, Y_i^2). Continuous boundaries are then replaced by bi-cubic interpolation of contemplated points. The sample is regarded as unbounded in a direction $\pm y$, the x is a direction of an incident planar wave propagation. Main directions of the orthotropic symmetry of the specimen boundary correspond with tangential (τ) and normal (ν) directions (Figure 6). The orientation within the specimen is continuously merged to normal and tangent into the boundary.

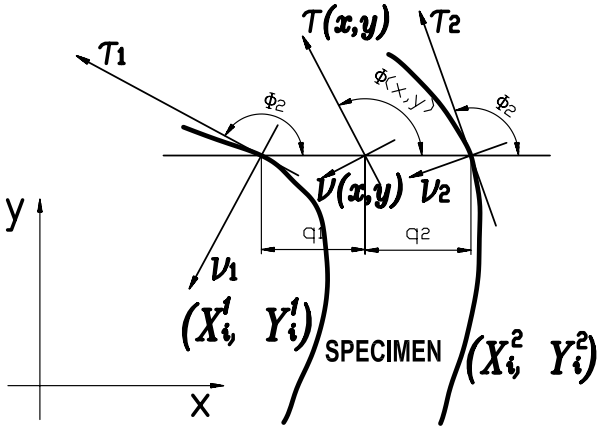

Fig. 6: The implementation of geometry and anisotropy of the specimen.

Let us introduce an angle $\phi(x, y)$ as the angle between axes x and τ in each point of the specimen. This angle describes the anisotropy orientation in every point simultaneously. The angle $\phi(x, y)$ can be expressed as

$$\phi(x,y) = \frac{\phi(X^1(y))q_2 + \phi(X^2(y))q_1}{q_1 + q_2} \,, \tag{35}$$

where q_1 and q_2 are distances of points (x, y) from the boundary along the x axis, $X^i(y)$ are corresponding boundary points and $\phi(X^i(y))$ is an anisotropy turning inside these points (Figure 6). Axes τ and ν pass continuously at boundaries into a tangential and a normal direction to the specimen upon thereby defined anisotropy.

The structure of the ray inside the specimen

Let us define the anisotropy orientation in each point of the sample by means of the angle $\phi(x, y)$. The rays in this media will be designed on the basis of Huygens axiom [Helbig, 1994, Musgrave, 1970], thus each point of the current wavefront is a new point source and those newly generated wavefronts will be superimpose into new wave fronts.

Let us consider an infinitesimal section of the wavefront in an arbitrary point (x, y), which can be approached by the plane. Let the normal to this wavefront in point (x, y) have a direction $\mathbf{n}(x, y)$. Let us design two anisotropic wavefronts $\mathbf{v}_G \mathrm{d}t$ for an infinitesimal time increment $\mathrm{d}t$ for two points of this wavefront. The orientation of these wavefronts is defined by the angle $\phi(x, y)$ (Figure 7a).

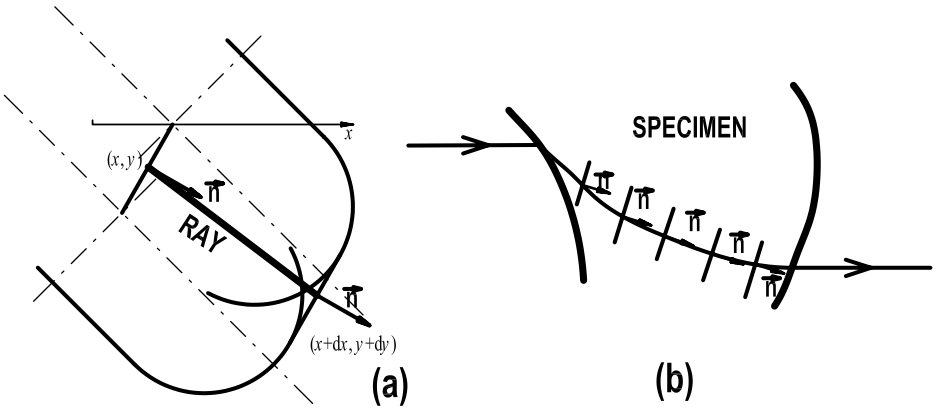

Fig. 7: (a) The ray increment according to the Huygens axiom; (b) A successive ray construction through the specimen thickness.

Tho common tangent line of these wavefronts indicates the orientation of a newly superposed wavefront. Let us label the center of this wavefront as $(x + \mathrm{d}x, y + \mathrm{d}y)$ and this will be considered as a new point. The normal of this common tangent line is identical as the normal in a point (x, y)

$$\mathbf{n}(x,y) = \mathbf{n}(x + \mathrm{d}x, y + \mathrm{d}y) \,. \tag{36}$$

The orientation of the wave vector (normal to the wavefront) doesn't change due to the arbitrarily chosen initial point.

This direction is possible to determine for every ray at an input interface (X_i^1, Y_i^1) according to the Snell-Descartes law. The output interface (X_i^2, Y_i^2) is a contrariwise determinative for the refraction back into a liquid. The successive ray design following the particular increments is demonstrated on the Figure 7b. The construction of every single ray is described by the subsequent algorithm:

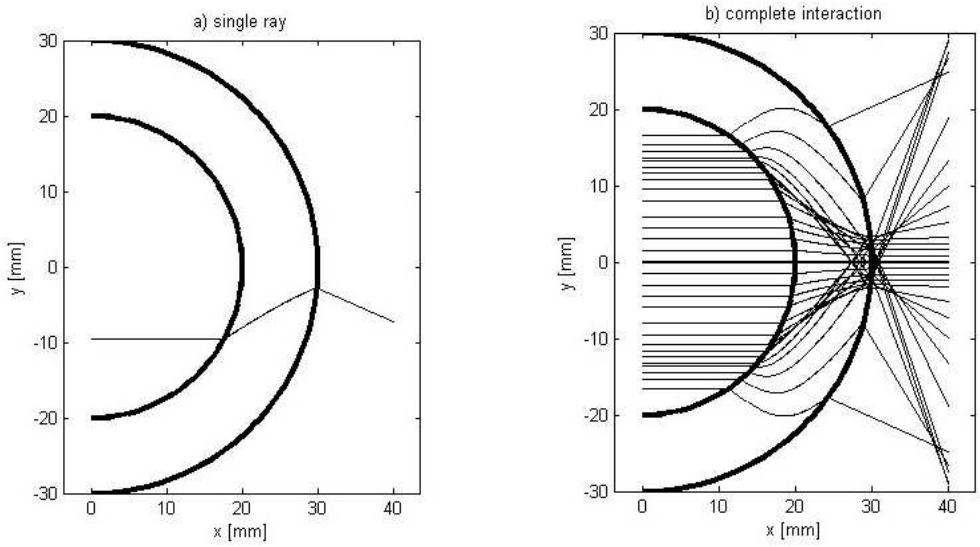

Fig. 8: The interaction of planar wave with a strongly anisotropic tube. (a) The path of one ray; (b) The complete interaction.

1. Let us select coordinate y_0 determining the location of the incident ray in a liquid. The incident ray point at the input interface of the specimen for this coordinate will be established consequently $(X_s^1, Y_s^1 = y_0)$.

2. The initial point is $(x, y) = (X_s^1, Y_s^1)$. The time of propagation is $t = 0$.

3. A new direction of the wave vector $\mathbf{n}(x, y)$ is prescribed according to the Snell-Descartes law. This direction is constant along the entire ray. The anisotropy orientation $\phi(x, y)$ at the interface point indicates a direction of the tangent line to the interface.

4. The direction corresponding to the group velocity

$$\mathbf{v}_G(\sin\phi(x, y), \cos\phi(x, y))$$

   is now calculated for the direction of the wave vector $\mathbf{n}(x, y)$ in τ a ν coordinates.

5. The projections of the wave vector into x and y axes, labeled as v_G^x a v_G^y are computed.

6. A new initial point

$$x = x + v_G^x \mathrm{d}t, \qquad y = y + v_G^y \mathrm{d}t \tag{37}$$

   is chosen, where the $\mathrm{d}t$ is a small time increment.

7. If a new point (x, y) lies inside the specimen, a time increment $t = t + \mathrm{d}t$ is added and the whole algorithms returns to item 4.

8. If the output boundary of the specimen is reached, the point of an incidence at the output interface is founded and the direction of a refraction according to the Snell-Descartes law is determined.

An example of a modelling of the complex interaction of a planar wave in an anisotropic curvilinear specimen is illustrated on Figure 8. The Carbon Fibre Reinforced Plastic (CFRP) [SEINER, 2004], the material having the transversely isotropic symmetry, is introduced as a model example.

The time increment $\mathrm{d}t = 0.05$ μs was charged during calculations, which corresponds to 100 points of every ray inside the specimen. The stability of computations was validated by a further step reducing except for 1 ns and no influence upon ray shape and the resultant ray direction was observed. The time step decreasing considerably slows down the computations and forbids the inverse problem of the elastic material properties determination.

Determination of elastic coefficients and error estimation

Determination of elastic coefficients via ultrasonic measurement

The wave propagation in anisotropic solids can be characterised by twelve close characteristic surfaces in $\mathbf{R}^3$ (section). Arbitrary three characteristic surfaces appertain to three different modes of the wave propagation (one quasi-longitudinal - qL and two quasi-transverse - qT) and remaining nine surfaces can be derived from geometrical relations. These surfaces are results of a direct problem, which consists in an evaluation of the wave fields in anisotropic media for known elastic constants. A complete knowledge of the characteristic surfaces is practically impossible, the measurement of wave velocities propagating through the examined material is often limited by the sample geometry, so only a part of characteristic surfaces can be obtained, and measured velocities are also distorted by some experimental error. If some of these surfaces can be obtained experimentally, the anisotropy of a material can be assessed, or contrariwise, if the material symmetry is known, elastic coefficient can be determined from velocity measurements for a specific direction major to the known symmetry.

Direct solution of inverse problem

The vectors of phase and group velocities are identical in the case of the elastic wave propagation through particular directions of the anisotropic solid of the higher material symmetry (e.g. cubic, orthotropic or transversely isotropic symmetry). These are axes of the crystallographic symmetry. Explicit relationships for phase velocities propagating in these directions can be easily derived. Another significant crystallographic directions are directions, which inhere in crystallographic planes, but they are not axes of the symmetry. Phase and group velocities are not identical in these directions, but the analytical relationships for the phase velocities determination can be also easily arranged especially in directions of the Cartesian coordinate system. The Christoffel matrix (14) and the solution of eigenvalue problem are significantly simplified under these circumstances.

The direct solution of the inverse problem is equivalent to the solution of the direct problem and can be resolved by the subsequent procedure:

1. The Christoffel equation (8) and the secular equation (14) assemblage for a given material symmetry.

2. A solution of the direct problem, i.e. selection of above described crystallographic directions for a given material symmetry, so that the secular equation 14 can be solved analytically and the phase velocity relationship $\mathbf{v}_\varphi = \mathbf{v}_\varphi\left(\mathbf{n}, C_{ijkl}\right)$ can be derived.

3. The experimental determination of phase velocities in selected directions and the solution of system equations for the C_{ijkl}.

The example of analytical relations for the orthotropic material are introduced in section (equations 25 and 26).

Numerical formulation of inverse problem for phase velocities

The inverse problem denotes a situation, when input data for some algorithm (function, functional, operator etc.) are to be reconstructed from that algorithm's results. In our case the inverse problem consists in determination of elastic coefficients of the examined material from a set of phase velocities in various directions [BALASUBRAMANIAM and WHITNEY, 1996], [ROKHLIN and WANG, 1992]. Then the formulation of the corresponding inverse problem is quite simple. Let us recapitulate that the phase velocities for a given wave normal $\mathbf{n}$ are evaluated from eigenvalues of the Christoffel matrix (14), which is uniquely determined by this wave normal $\mathbf{n}$ and the elastic coefficients c_{ij}.

The superscript *exp* will be used to distinguish the experimentally obtained velocities (v_φ^{exp}) from those evaluated for known elastic coefficients via the above described theory (v_φ).

Let a given wave normal $\mathbf{n}$ and a corresponding phase velocity $v_\varphi^{exp}(\mathbf{n})$ of at least one mode of the propagation is available. Then the problem consists in determination of the matrix $\Gamma(\mathbf{n})$ so that some of its eigenvalues are equal to the experimentally obtained velocity $v_\varphi^{exp}(\mathbf{n})$. For a known class of symmetry, the structure of $\Gamma(\mathbf{n})$ is known as well and the problem can be formulated by the following nonlinear equation in c_{ij} :

$$\det[\Gamma(c_{ij},\mathbf{n}) - \rho(v_\varphi^{exp}(\mathbf{n}))^2\mathbf{I}] = 0\ , \tag{38}$$

where $\mathbf{I}$ is the unit matrix.

However, the number of unknown elastic coefficients is usually too large to be uniquely determined from such single equation (38). Then the phase velocities is additional directions are taken and a system of nonlinear equations arises

$$\begin{aligned} \det\left[\Gamma\left(c_{ij},\mathbf{n}^{(1)}\right) - \rho\left(v_\varphi^{exp}\left(\mathbf{n}^{(1)}\right)\right)^2\mathbf{I}\right] &= 0 \\ \vdots \qquad\qquad & \\ \det\left[\Gamma\left(c_{ij},\mathbf{n}^{(N)}\right) - \rho\left(v_\varphi^{exp}\left(\mathbf{n}^{(N)}\right)\right)^2\mathbf{I}\right] &= 0 \end{aligned}\ . \tag{39}$$

For exactly correct values of $v_\varphi^{exp}\left(\mathbf{n}^{(1\cdots N)}\right) = v_\varphi\left(\mathbf{n}^{(1\ldots N)}\right)$ the equations (39) are not mutually independent and they can be satisfied all at once by correct values of c_{ij}. When the values $v_\varphi^{exp}\left(\mathbf{n}^{(1\cdots N)}\right)$ are experimentally distorted, the problem must be solved by an optimization procedure, which determines the coefficients c_{ij} so that the system (39) is optimally satisfied. As a suitable criterion for optimal satisfaction of (39) the least squares measure

$$\sum_{n=1}^{N}\left\{\det\left[\Gamma\left(c_{ij},\mathbf{n}^{(n)}\right) - \rho\left(v_\varphi^{exp}\left(\mathbf{n}^{(1)}\right)\right)^2\mathbf{I}\right]\right\}^2 \to \min_{c_{ij}}\ , \tag{40}$$

can be used.

When the solution of the direct problem can be obtained for every $\mathbf{n}$ and every c_{ij} in form $v_\varphi(c_{ij},\mathbf{n})$, the whole problem can be reformulated into the minimization of a quadratic sum Q

$$Q = \sum_{n=1}^{N}\left(v_\varphi\left(c_{ij},\ \mathbf{n}^{(n)}\right) - v_\varphi^{exp}\left(\mathbf{n}^{(n)}\right)\right)^2 \to \min_{c_{ij}}\ . \tag{41}$$

Let it be highlighted, that the wave normal $\mathbf{n}$ in (39), (40), (41) is known. This fact crucially simplifies both the formulation and the solution of the inverse problem for phase velocities in a comparison with a similar problem for group velocities [AUDION, 2002, CASTAGNEDE *et al.*, 1990, CASTAGNEDE *et al.*, 1991, EVERY and SACHSE, 1990, KIM and SACHSE, 1995, SACHSE *et al.*, 1998, WU and HO, 2005].

The algorithm developed to solve the optimization problem (41) is universal; it can be applied to a set of phase velocities in arbitrary general directions of every class of symmetry. Moreover, by such algorithm, the class of symmetry of the examined material can be estimated when a sufficient amount of input data is available [Sachse *et al.*, 1998].

For every wave normal $\mathbf{n}$ and for known elastic coefficients c_{ij}, all three eigenvalues of the Christoffel matrix (14) can be at least numerically evaluated. Then the resultant phase velocities $v_{\varphi}^{(1,2,3)}$, corresponding to particular modes of the propagation, can be compared with the experimental data $v_{\varphi\,1\ldots N}^{exp}$ in directions $\mathbf{n}_{1\ldots N}$. If $\tilde{c}_{ij}$ is a quess of elastic coefficients, the quadratic sum (41) takes the form

$$Q = \sum_{n=1}^{N} \left(v_{\varphi}\left(\tilde{c_{ij}}\,, \mathbf{n}_n\right) - v_{\varphi}^{exp}\left(\mathbf{n}_n\right)\right)^2 \ . \tag{42}$$

The coefficients c_{ij} that minimize the function (43) are sought.

For a numerical multidimensional minimization, a preprogrammed Matlab routine fminsearch.m [Mat, 1999] is used, which employs the simplex search method. It is a direct search method that does not use numerical or analytic gradients. A simplex in an n-dimensional space is characterized by the n+1 distinct vectors that are its vertices. In a two-dimensional space, a simplex is a triangle; in a three-dimensional space, it is a pyramid. At each step of the search, a new point in or near the current simplex is generated. The function value at the new point is compared with the function's values at the vertices of the simplex and, usually, one of the vertices is replaced by the new point, giving a new simplex. This step is repeated until the diameter of the simplex is less than the specified tolerance. Such method is especially proper when every evaluation of the minimized function is complicated and covers a considerably long time period, as it is in case of solution of the eigenvalue problem (14). The simplex method was proved suitable on many of similar optimizing procedures [Castaings *et al.*, 2000, Lematre, 2002].

The simplex method is quite immune from discontinuities of the Q (especially if these are far from the sought minimum [Mat, 1999]), but it can collapse in case of narrow extremes. When the initial guesses are close to some local extreme, the simplex method can converge to it. Therefore, the minimization is sometimes repeated by launching the simplex from the found minimum. If it was a global minimum, the simplex returns to it, if it was local, another extreme would be found.

Error estimation

To estimate the accuracy of the optimization procedure's results, no appropriate analytical approach is available. The only possible solution is, thus, the Monte Carlo simulation, based on running the whole optimization process several times with randomly distorted input data. The Gaussian statistic made over the set of results is then expected to reveal the reliability of optimized coefficients [Chu and Rokhlin, 1994, Degtyar and Rokhlin, 1997, Every and Sachse, 1992, Seiner and Landa, 2005]. In this work, we have treated the wave arrival times to be determined accurately. In other words, the inaccuracy of the wave front arrival's detection was expected to be incomparably smaller than other possible sources of the procedure's failure taken into an account. These are the variability of the specimen's thickness and, even more important, the variability of the zero angle determination. Both of these inaccuracies were involved in our Monte Carlo simulations, considering the thickness and the specimen's orientation to be normally distributed about the correct values. Moreover, for the bone specimen, some variability of the mass density was admitted. Then the procedure was repeated 30 times to generate a representative set of output data.

Although this set cannot be expected to be governed by a normal distribution, its variability can be approximatively expressed by the usual Gaussian statistic quantities, namely by the

standard deviations

$$\mathrm{SD}_{ij} = \left(\frac{1}{n-1} \sum_{k=1}^{n} \left(c_{ij}^{(k)} - \overline{c}_{ij} \right)^2 \right)^{1/2} , \tag{43}$$

where by the overlining we denote the mean value of cij , averaged for all n passes of the inverse procedure. In our case, $n = 30$.

Then we present our results in a form

$$c_{ij} = c_{ij}^{(undistorted)} \pm \mathrm{SD}_{ij} , \tag{44}$$

where the original procedure's result $c_{ij}^{(undistorted)}$ is usually not exactly equal to the mean value $\overline{c}_{ij}$.

Obviously, the presented standard deviations cannot be treated absolutely, but they bring a valuable insight in how sensitive and stable the optimization procedure is for each particular coefficient.

Experiment

The aim of the experimental part of this thesis was to develop a methodology and experimental devices for the measurement of elastic coefficients of cortical bone samples, which are considered to be an anisotropic, homogenous and linear elastic solid (according to section). The experimental technique should be suitable for a non-destructive measurement of specimens of a general shape. The methodology and the device should be proposed with a respect to a light preparation of specimens, the wave propagation in multiple variety of directions without cutting the specimen, the rapid and simple evaluation of elastic coefficients and experimental errors.

The immersion through the transmission technique was chosen as an optimal experimental technique for the elastic constants measuring according to above described requirements. The ultrasonic immersion scanner was built as an appropriate experimental device. Plate shaped composite anisotropic specimens of well known elastic properties from the previous point source - point receiver (PS/PR) measurements were used as a test material for immersion measurements at first. The isotropic PMMA tube shaped specimen was measured afterwards. The bovine femoral cortical bone, thus the specimen of a general geometry was tested lastly. Additional measurements of the bone were performed after cutting the bovine femur to cube shaped samples via the contact pulse transmission technique and the resonant ultrasound spectroscopy.

The PS/PR measurements of a composite material were not a part of this work. They were achieved previously and they are reported in the master thesis elaborated by Hanuš Seiner [SEINER, 2004]. All others ultrasonic experiments were performed in the Institute of Thermomechanics, Academy of Sciences of the Czech Republic (ASCR) under the supervision of Michal Landa and with the technical support of Hanuš Seiner and Poemysl Urbánek. The preparation of specimens was ensured in the Institute of Dental Research of the First Medical Faculty of Charles University and the General Medical Hospital in Prague in cooperations with Lucie Himmlová.

Samples

Test samples

The composite anisotropic and isotropic materials of plate and tube shapes were used in this study. These materials were utilized as etalon specimens for the experimental device and methodology testing. The plate specimens were made of an unidirectional CFRP (Carbon Fiber Reinforced Plastic, manufacturer: La-Composite Letov ATG, Ltd., prepreg: Fibredux S913C-HTA-(12k)-5-40%) with an orientation of fibres parallel to specimen's surfaces. The material

symmetry of specimens was presumed as transversally isotropic, where the rotational axis x_3 was given by the direction of the fibres. The dimensions of specimens were 120 mm x 120 mm, the approximate thicknesses were 1.95, 3.65 and 7.51 mm. All five elastic constants (c11, c12, c13, c33 and c44) were known from previous ultrasonic measurements (PS/PR technique) [26, 27, 28]. The tube specimen was made from a PMMA (inner diameter = 24 mm, the outer diameter = 30 mm). The tube was provided with the slot in the axial direction, so only one wall of the specimen was exposed to the wave propagation. The similar slot was cut into the bone sample.

Bone samples

For the ultrasonic measurements, a dry bovine cortical femur diaphysis without a marrow was used. Bovine bones were assumed to be orthotropic and the x_3 axis was parallel to the bone fibers. The x_1 axis corresponds to a radial direction and the x_2 axis corresponds to a circumferential direction. The orientation of the bone specimen in respect to the cartesian coordinate system is introduced in Table 4.

Table 4: Bone orientation in respect to the coordinate system.

x_1	Radial direction	Anterior-Posterior
x_2	Circumferential direction	Medial-Lateral
x_3	Longitudinal direction	Superior-Inferior

The epiphyses of the bovine femur were cut and a marrow was removed. Afterwards, the bone was boiled, immersed in the lye and sterilized in the autoclave. Then the axial slot was cut in order to obtain two samples (Specimen I, Specimen II - Figure 10) and then the marrow was removed.

The shape, thickness and curvature of specimens were measured by a contact probe, which was located in the CNC milling machine (Micronex FC 16 CNC - Figure 9). The scanned area is marked on Figure 11. The CAD reconstruction of shape measurements of both parts of the bone is shown on Figure 10. The knowledge of the specimen shape was important for a modelling of the wave propagation in an anisotropic media via the simplified ray method and for an evaluation of elastic constants.

The Specimen I have used for the immersion measurement of an area marked on Figure 11. All nine elastic coefficients were determined from this sample, except the constant c_{23}, which was evaluated via the contact measurement of the specimens 3 and 4. These samples were cut from the Specimen I (Figure 12). Slice shaped specimens 1,2,5 and 6 were obtained from Specimen I and they were used for the c_{33} contact measuring by the contact technique in different locations of the bone in order to detect the heterogeneity of elastic properties along the bone shape. These locations are marked by letters A, B, C, D, E and F on each slice of the specimen (Figure 12). The contact technique was also used for the measurement of elastic constants c_{11}, c_{22}, c_{33} and c_{12} of cubic samples 2, 4, 5 and 6 (Figure 13). Moreover cubic samples 2 and 6 were used for the RUS measurement. The specimen cutting was realized by the virtue of the low speed saw ISOMET.

Experimental devices and techniques

PS/PR technique

Group velocities in various directions in both specimens were experimentally obtained by a point-source/point-receiver (PS/PR) technique [Seiner and Landa, 2003, Seiner and Landa, 2005], as it is outlined in Figure 14.

Fig. 9: The bone specimen and its shape measurement.

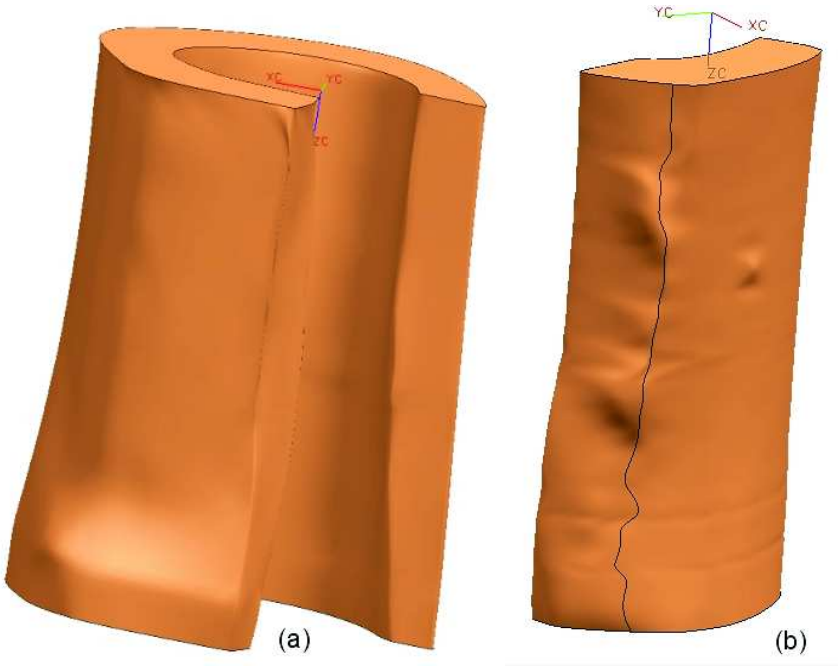

Fig. 10: CAD reconstruction of shape measurements of the bovine femur.
(a) Specimen I, (b) Specimen II.

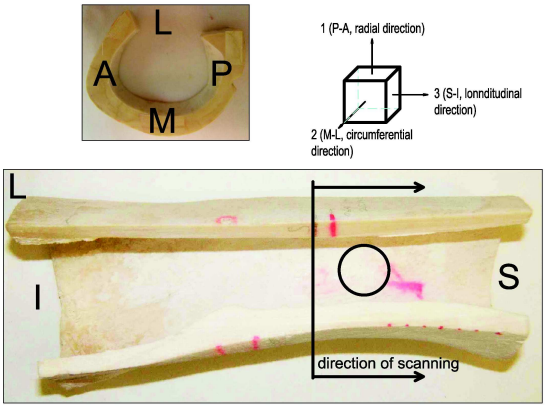

Fig. 11: The specimen I used during the immersion measurement. The circle shows area of the investigation via the immersion measurement. The arrow shows the range of shape scanning on the CNC milling machine.

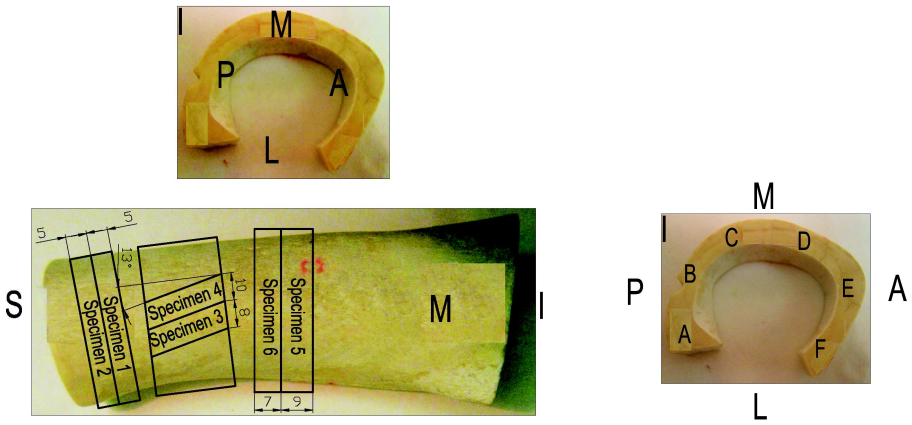

Fig. 12: Cutting the specimen I into slice shaped samples and labeling of different locations along the slice specimen for a determination of the c_{33} constant.

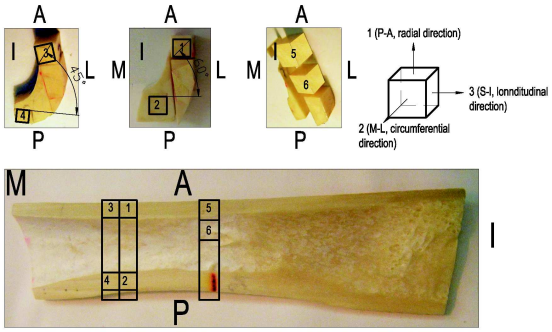

Fig. 13: Cutting the specimen II into cubic samples.

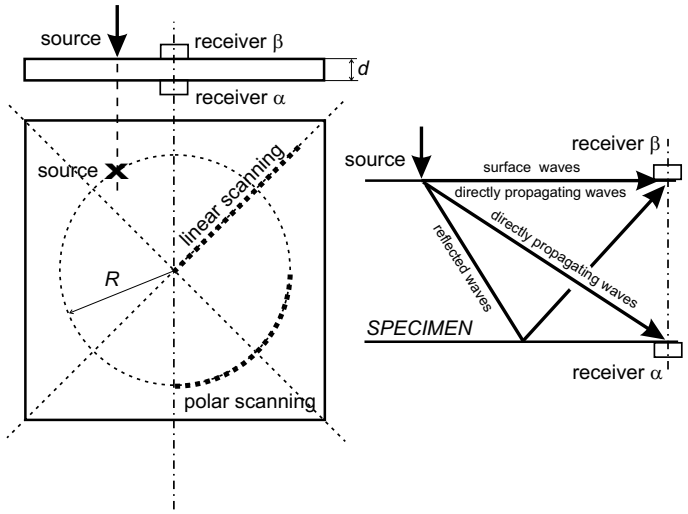

Fig. 14: Experimental set-up for PS/PR measurement.

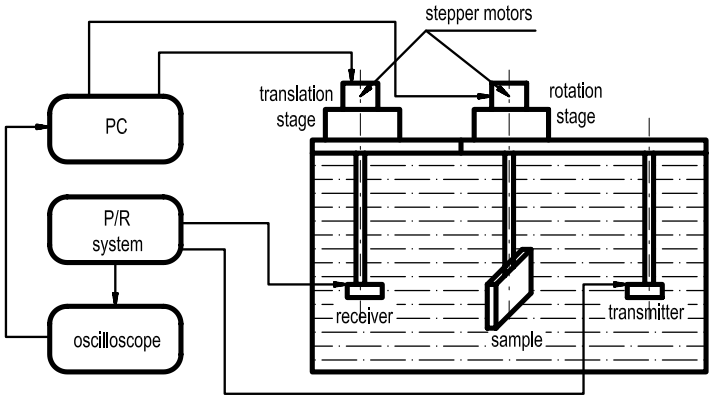

Fig. 15: Experimental set-up for immersion measurement.

The point-like source was implemented by a focused laser beam, the point-like receiver by a miniature piezoelectric transducer. Two receivers (α and β)were situated on opposite free surfaces of the specimen, facing each other. The source was equidistantly moving either along the circle (polar scanning) or along one of the symmetry directions (linear scanning). Then the signals detected on transducers corresponded to various directions of the wave propagation in the specimen.

Immersion technique

The ultrasonic immersion scanner (Figure) was designed to measure the time of flight (TOF) and the amplitude of received pulse after the transmission through a sample in the Laboratory of nondestructive testing and material evaluation in the Institute of Thermomechanics, ASCR. The specimen is rotated and immersed in a water between two ultrasonic transducers. The transmitting transducer is fixed and the receiving transducer is adjustable by the translation stage. The scanner allows to measure longitudinal and quasi-transverse waves velocities in a wide range of directions in order to recover the whole set of elastic constants without cutting the specimen. The device can be modified for a pulse-echo measurement, using a tile as an acoustic mirror instead of the receiving transducer.

The entire experimental process is controlled by a PC using two stepping motors for moving the sample and the receiver transducer. The entire measuring was controlled by the SW Testpoint. The high frequency Pulse/Receiver system (JSR Ultrasonics DPR 50+) is used for generating and receiving a pulse, which is connected with two 2.25 MHz, 0.5 in diameter ultrasonic transducers made by the Panametrics, Inc. The receiving signals from the sensors were recorded by a digital oscilloscope (DSO - LeCroy 9304AM).

Contact pulse transmission technique

The simple contact pulse transmission technique was used for a measurement of slice shaped and cubic specimen (Section) obtained by the bone cutting. The measurements were performed by using two longitudinal (Ultran - frequency 2.25 MHz, diameter 0.25") and two shear (Ultran - frequency 2 MHz, diameter 0.25") transducers. The usage of Pulse/Receiver system and the digital oscilloscope were the same as for the immersion measurement (JSR Ultrasonics DPR 50+ and DSO - LeCroy 9304AM).

Resonant ultrasound spectroscopy

Another experimental ultrasonic based technique useful for determination of matrix elastic coefficients is resonant ultrasound spectroscopy (RUS). Principles of this technique are briefly described in Section . The RUS technique is based on the measurement of amplitudes of excited harmonic vibrations and the evaluation of resonant frequencies of an examined specimen of a known shape, material symmetry and approximately known elastic coefficients. A process of the RUS measurement is schematically outlined in Figure 4 and can be described by following steps:

1. the specimen preparation. In our case were chosen the cubical specimen no. 4 and 6 (Section), because these two samples were geometrically the closest to the ideal cube.

2. the calculation of resonant frequencies - a direct problem. This approach is based on the Hamilton's variation principle (free vibrations of an elastic solid corresponds to stationary Lagrangian). The Lagrangian

$$L = \frac{1}{2}\int\int\int [\rho \dot{u}_i \dot{u}_j \delta_{ij} - \frac{1}{4}\, C_{ijkl}(\frac{\partial u_i}{\partial x_j} + \frac{\partial u_j}{\partial x_i})(\frac{\partial u_k}{\partial x_l} + \frac{\partial u_l}{\partial x_k})]\mathrm{d}V \ , \tag{45}$$

   where ρ is the density, u_i is the displacement vector, C_{ijkl} is the tensor of elastic coefficients and the integration is over the volume of the solid V; is designed for a given system, then minimized and the whole problem is conveyed to the solution of the eigenvalue problem. This procedure is described by Demarest [Demarest, 1971] in detail.

3. the measurement of a resonant spectrum. During the measurement, cubical samples were supported by their corners between two ultrasonic transducers (transmitter and receiver). This bearing provides elastically weak coupling to the transducers, hence a minimal interference with the vibration, a minimal shift in a resonant frequency and a minimal parasitic damping is expected [Wang and Lakes, 2003]. The exciting transducer was connected to the signal generator (Stanford Research Systems - Synthetyzed Function Generator - model: DS 345, 30 MHz) and the receiver was connected to the Lock-in Amplifier (Stanford Research Systems - model SR 844 RF). Both devices were linked with a PC, where the measured data were collected by means of the SW Testpoint. Both transducers, the compressional and shear ones, were used during the measurement. The shear transducer was used pursuant to a recommendation of Wang [Wang and Lakes, 2003]. The usage of a shear transducer instead of a compressional one has the advantage of the stronger signal, easier identification of vibrational modes via changing the polarization of transducers and an absence of the wave propagation in air.

4. the evaluation of the measured frequency spectrum and the determination of resonant frequencies. This task is important for the exact determination of resonant frequencies of the measured spectrum, which is afterwards used as an input argument into a minimization (next event). The simplest, but the most inaccurate method is the local maximum search in the measured spectrum. Further, more advanced approaches may be used for the evaluation of this problem such as a statistical access [**?**] or an evaluation of the transfer function from the measured data [KOZANEK, 1982]. These methods implicate the shape of a resonant peak and take the measure of a statistical fluctuation (noise).

5. the evaluation of resultant elastic coefficients - an inverse problem. The minimization of calculated and measured perturbations of resonant frequencies.

Results

Validation of immersion technique via PS/PR measurements

The results from the PS/PR (point-source/point-receiver) technique performed by Seiner and Landa [SEINER, 2004, SEINER and LANDA, 2003] on the transversely isotropic CFRP composite specimen of the thickness 7.51 mm (section) were used for a validation of the immersion technique methodology and a verification of the function of the acoustic scanner (section). Coefficients c_{11}, c_{12} and c_{44} were determined directly from velocities $v^{(L)}$ (longitudinal mode, $v^{(L)}$=3.005 mm/μs), $v^{(T1)}$ (transverse mode, polarized normal to the fibres, $v^{(T1)}$=1.447 mm/μs) and $v^{(T2)}$ (transverse mode, polarized parallel to the fibres, $v^{(T2)}$=1.819 mm/μs) lying in an isotropic plane via the pulse echo measurement. The relationships between measured phase velocities and elastic constants is given by the following formulae [EVERY and SACHSE, 2001]:

$$c_{11} = \rho(v^{(L)})^2,\ c_{12} = c_{11} - 2\rho(v^{(T1)})^2,\ \text{and}\ c_{44} = \rho(v^{(T2)})^2\ , \tag{46}$$

where ρ is a density of the examined material (ρ=1.52 g/cm^3). The remaining coefficients c_{13} and c_{33} were evaluated inversely from a set of quasi-longitudinal (qL) group velocities [SEINER, 2004] experimentally obtained from the PS/PR measurements. A slightly orthotropic behaviour of the sample was observed by a difference between the coefficient c_{11} determined from the pulse echo measurements and that from the inversion of PS/PR measurements. This error was removed by involving both, the quasi-transverse(qT) and the qL waves into the inversion procedure.

Table 5: The comparison of elastic coefficients of the 7.51 mm thick CFRP plate specimen. Elastic coefficients were experimentally obtained by the PS/PR [SEINER, 2004] and the immersion measurement (Section). Values are introduced in GPa.

Elastic constants	**PS/PR technique**	**Immersion measurement**
c_{11}	14.43	15.98
c_{12}	7.79	9.62
c_{13}	6.73	7.09
c_{33}	119.54	123.20
c_{44}	5.34	5.62

After involving the qT waves velocities, final resultant elastic coefficients are presented in Table 5. This table also contains the comparison with the immersion measurement (Section). Normal surfaces (plots of phase velocities propagating in wave normal directions) for both, the PS/PR and immersion measurements are introduced in Figure 16.

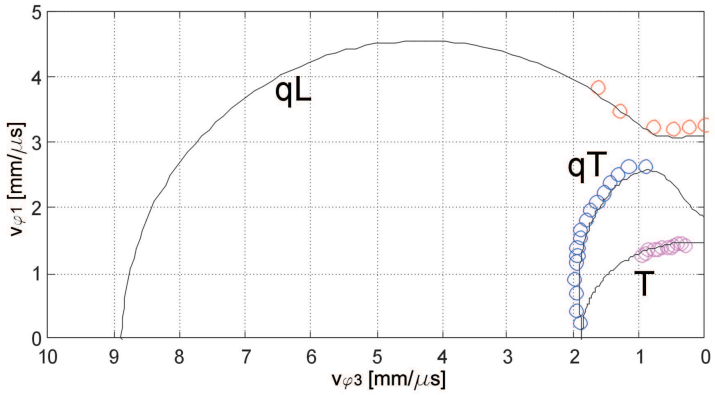

Fig. 16: Comparisons of the PS/PR measurement [Seiner, 2004] and the immersion measurement (Section) of the CFRP plate specimen (thickness 7.51 mm).
Solid lines represent normal surfaces of one qL, qT and pure transversal T waves obtained from PS/PR measurement. Circles represent adequate values of velocities obtained from the immersion measurement. The horizontal axis $v_{\varphi 3}$ corresponds to the phase velocity propagating in the x_3 direction (fiber direction). The vertical axis $v_{\varphi 1}$ corresponds to the phase velocity propagating in the x_1 direction (perpendicular to the plate).Values are introduced in [mm/μs].

Immersion measurements

The leading experimental data of this work related to the previously described ultrasonic immersion technique (Section) are introduced in this chapter. The measurement of CFRP plates of the known material symmetry (transversely isotropic) was evaluated firstly in order to provide a tuning of the experimental methodology. The ultrasonic pulsed through the transmission method with the rotating specimen immersed in a water and one stationary and one movable transducer (Figure **??**). The stationary transducer was used as a transmitter, the movable transducer served as a receiver.

The ultrasonic scanning procedure was following. The incident wave propagated through a water towards the liquid/specimen interface, where the wave was refracted into qL and qT waves (Figure 5), or pure longitudinal (L) or pure transverse waves (T) for a propagation in an isotropic plane, in an agreement with the Snell-Descartes law (34). Both refracted waves continued in the propagation inclined about the angle of refraction (34) afterwards. Refracted waves were captured by a movable receiver, which scans in a parallel way to the transmitting transducer edge. Then, the specimen was rotated about a prescribed angle and the whole process was repeated. The time of flight (TOF - the time of wave travelling on a path between two transducers) and the amplitude of a signal were monitored. The measures without a specimen had to be also performed in order to determine the wave propagation and adjust the experimental device.

The through transmission immersion measurements suggested not to be very reliable, qT and qL modes interfered with each other for some angles of the incident, the qT mode wasn't apparent for other angles (Figure 17). This situation occurred for both modes of the measurement, the propagation in isotropic and anisotropic planes of the specimen. This technique also proved to be very sensitive to the precise geometry adjustment of the experimental device.

This unsatisfactory results of the through transmission measurement were improved by a modifying of the experimental set-up into a pulse-echo configuration (Figure 18), using a tile as an acoustic mirror instead of the receiving transducer. In this set-up, only one transducer was used as a transmitter and receiver. This transducer was movable in a case of the composite plates measurement in order to examine different locations of the sample. The measuring procedure was following.

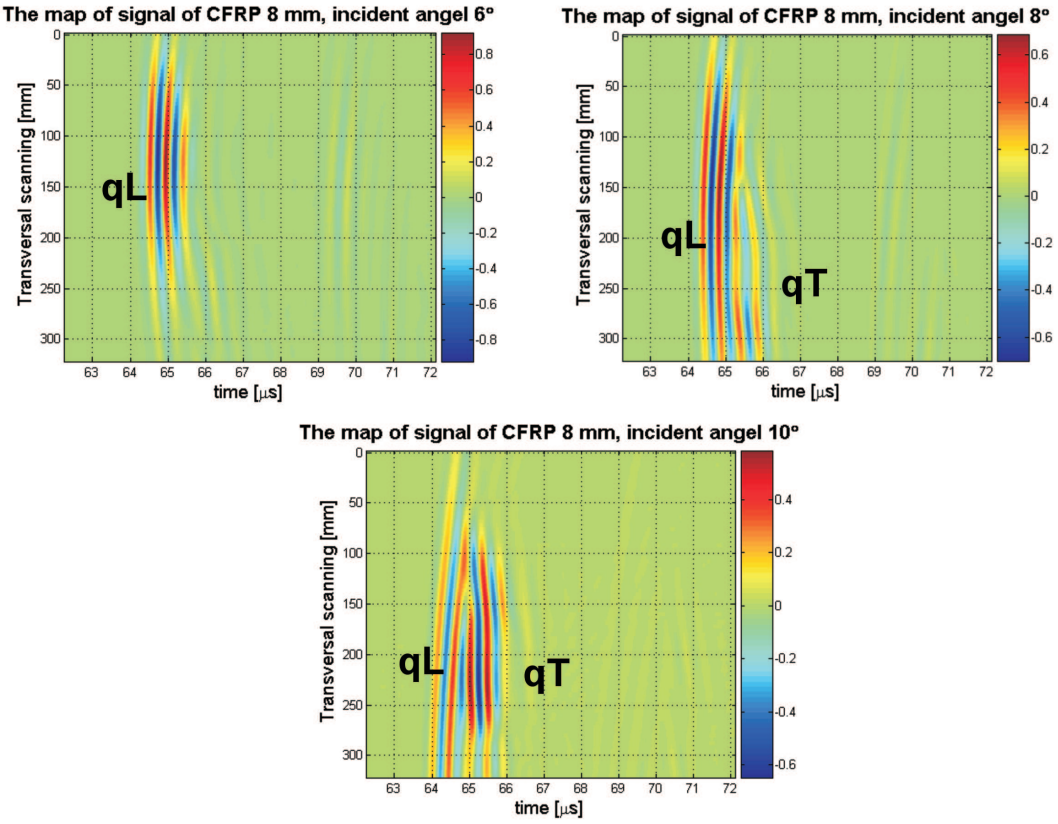

Fig. 17: The maps of signal of immersion through transmission measurement. The specimen CFRP plate, anisotropic plane, thickness 8 mm, incident angels 6°, 8° and 10 °.
qL - quasi-longitudinal wave, qT - quasi-transverse wave

The incident wave traveled towards the specimen interface where it was refracted into the qL and qT waves around the angle of refraction and hereafter both waves impacted the reflector. Reflected waves travelled back towards the transducer along the exactly same path as incident waves and both waves were received. The main advantage of the pulse-echo technique in a comparison with the through transmission technique was a clear resolution of qL and qT modes of the propagation, the explicit TOF determination and the simple and rapid adjustment of the experimental device.

The evaluation of elastic coefficients was performed by a solution of the inverse problem for phase velocities (Section). Input phase velocities and their directions of the propagation into the inverse algorithm are obtained from maps of signal (Appendix **??**). The stability of resulting data was evaluated by the statistical method based on the Monte Carlo simulation (Section) and all output data resulted from the minimization approach are presented in 44 form.

The above described procedure is sufficient for the evaluation of elastic constants of plate shaped specimens. For the specimen of a general shape and an anisotropy, the wave propagation was modelled via the simplified ray method (Section) in two dimensions. This simulation was used in the case of the wave propagation through the isotropic tube and the bone specimen and is mentioned in the following chapter.

Evaluation of elastic constants from immersion measurements

Preliminary tests on CFRP Plates The first satisfactory results of the elastic constant measurement of the CFRP (Carbon Fibre Reinforced Plastic) via the ultrasonic immersion technique

were extracted from the pulse-echo configuration of the measurement (Figure 18). This set-up consisted of one transmitting and receiving transducer and one acoustic reflector. The specimen was placed between the transducer and the reflector, and it was rotated in a wide variety of directions. The entire measuring configuration was immersed in a distilled water. The principle of this measurement was closely described in the previous section (Section).

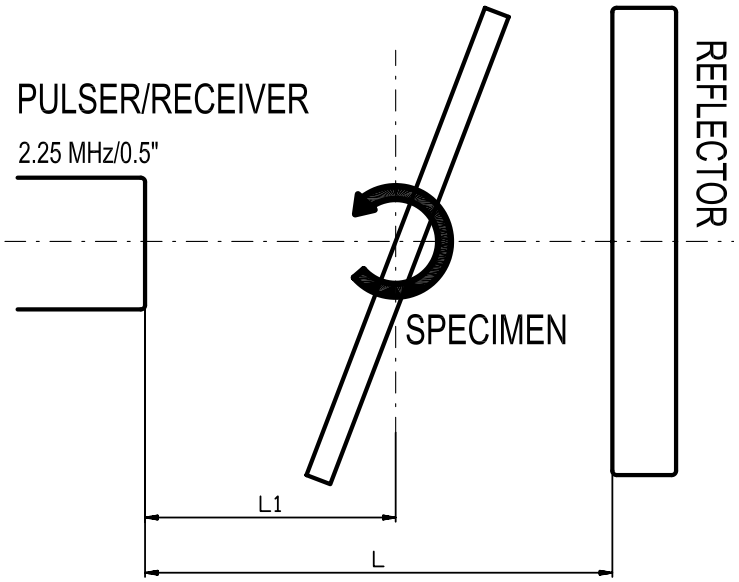

Fig. 18: The diagram of the pulse-echo measurement of CFRP plates.

The specimen was placed in the distance L1=83 mm in front of the transducer, the distance between the transducer and the reflector was L=232 mm (Figure 18). The temperature varied during measurements of all three CFRP plates from 20.7°C to 21.5°. Each specimen was examined in isotropic x_1x_2 and anisotropic x_1x_3 planes (Figure 19).

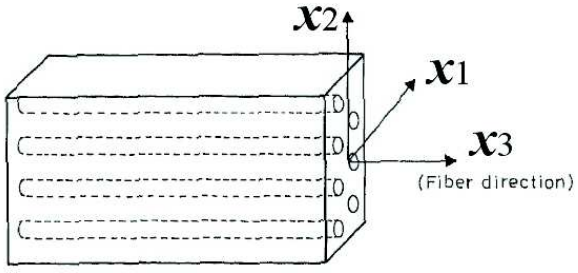

Fig. 19: Coordinates and the fiber direction of CFRP composite specimens.

During the measurement, the time arrival of the wave on its path from the transducer to the reflector and back without the immersed specimen was detected, then the specimen was rotated from the angle -40° to the angle 40° per the step of 5°, whereas the zero angle was prescribed to the parallel position of the specimen to the reflector and the face of the transducer. The raw data collected from the oscilloscope are introduced in the Appendix **??**, **??** and **??** in the form of a signal maps. This figures show the maps of signal for the measurement in isotropic and anisotropic plane for each of three CFRP plates specimens (thicknesses 1.95, 3.65 and 7.51 mm). Time arrivals (TOF) of L and T waves (pure longitudinal and transverse) in the case of isotropic plane measurements or qL and qT (quasi-longitudinal and quasi-transverse) in the case of anisotropic plane measurements were detected from the maximal amplitudes of the signal.

Thereby evaluated TOF's for different angles of the specimen rotations were used as an input data to the inverse problem (Section) in the form of phase velocities. The resultant matrix of elastic coefficients c_{ij} (27)

$$c_{ij} = \begin{pmatrix} c_{11} & c_{12} & c_{13} & 0 & 0 & 0 \\ c_{12} & c_{11} & c_{13} & 0 & 0 & 0 \\ c_{13} & c_{13} & c_{33} & 0 & 0 & 0 \\ 0 & 0 & 0 & c_{44} & 0 & 0 \\ 0 & 0 & 0 & 0 & c_{44} & 0 \\ 0 & 0 & 0 & 0 & 0 & \frac{1}{2}(c_{11} - c_{12}) \end{pmatrix} \text{ and } c_{66} = \frac{1}{2}(c_{11} - c_{12})$$

expresses in form (44) calculated from the optimization (41) is presented in the Table 6. The input inaccuracies involved into the Monte Carlo simulation (Section) are thicknesses of the specimen (d=±0.05 mm) and incident angle deviations ($\alpha = \pm 0.5°$).

Table 6: Resultant elastic coefficients c_{ij} of CFRP composite specimens in form (44). Values are expressed in GPa.

Thickness d [mm]	$\mathbf{1.95 \pm 0.05}$	$\mathbf{3.65 \pm 0.05}$	$\mathbf{7.51 \pm 0.05}$
$\mathbf{c_{11}}$ **[GPa]**	12.43 ± 0.44	13.87 ± 0.34	15.98 ± 0.22
$\mathbf{c_{12}}$ **[GPa]**	5.07 ± 0.74	7.05 ± 0.51	9.62 ± 0.22
$\mathbf{c_{13}}$ **[GPa]**	8.23 ± 0.99	7.07 ± 0.70	7.09 ± 0.39
$\mathbf{c_{33}}$ **[GPa]**	125.63 ± 8.77	123.67 ± 7.13	123.20 ± 3.35
$\mathbf{c_{44}}$ **[GPa]**	5.63 ± 0.05	5.67 ± 0.06	5.62 ± 0.06
Density ρ**[g/cm^3]**	1.6	1.6	1.52

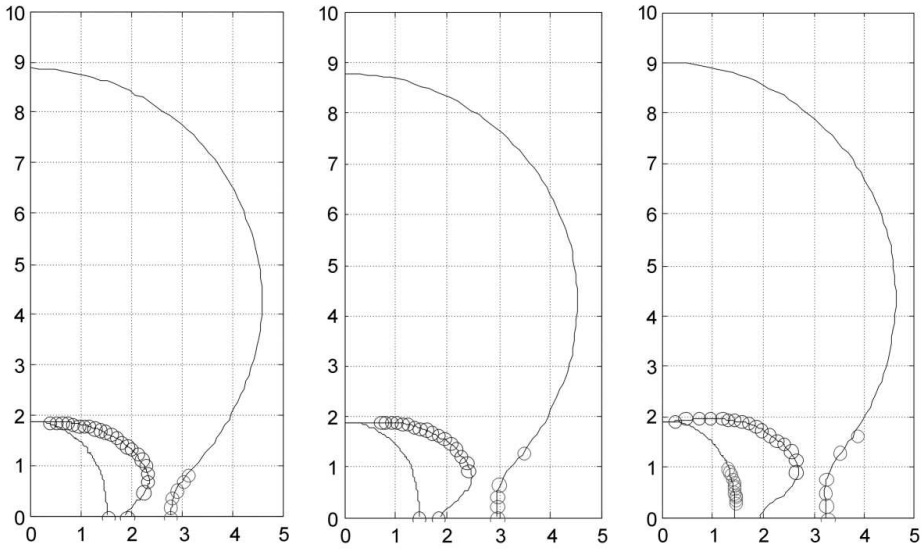

Fig. 20: Plots of the phase velocities [mm/μs] propagating in the wave normal directions through CFRP plate specimens of 1.95, 3.65 and 7.51 mm thicknesses.
Circles - experimentaly obtained data, Solid lines - phase velocities for calculated c_{ij}.
Horizontal axis - phase velocity in x_1 direction (perpendicular to the plate), Vertical axis - phase velocity in x_3 direction (fiber direction).

The normal surfaces (the plot of phase velocity $v_\varphi(\mathbf{n})$ versus the wave normal direction) of measured phase velocities of acoustic waves propagating through CFRP plate specimens of different

thicknesses in the anisotropic x_1x_3 plane are demonstrated in Figure 20. This figure represents experimentally obtained phase velocities and their fitting to the normal surfaces evaluated for c_{ij} resulting from the minimization (41). The phase velocities of the wave propagating through the 7.51 mm thick CFRP specimen obtained by the PS/PR and the immersion technique are compared in Figure 16.

Results for an isotropic PMMA tube The evaluation of an acoustic wave propagation through the bone specimen of a general shape is not, to my best knowledge, currently solved in a scientific literature. Only the work of Detti [Detti *et al.*, 2002] deals with a model of wave propagation in a cylindrical tube. This theory and the related experiment are described in the Section in detail.

This part of the experiment is focused on the wave propagation in an isotropic tube made of PMMA, which is the material of well known elastic properties. The purpose of this experiment is not only a determination of elastic constants of the specimen, but also an experimental validation of a simplified ray model described in Chapter . A successive handling of this problem is essential to the solution of a more complex problem such as the wave propagation and the elastic constant evaluation of the bone sample (more general geometry, higher class of anisotropic symmetry).

The axial slot was cut in the PMMA tube in order to simplify the propagation of wave through the specimen; the complicated solution of refracted waves inside the tube (Detti [Detti *et al.*, 2002]) falls off this way. The measuring configuration is the pulse-echo, immersed in a distilled water, similar as in the previous chapter (see Figure 18). The transmitting and receiving transducer is stationary in this case, pointed towards the center of the tube curvature. The three different modes of the measurement (mode C, D and I) are distinguished.

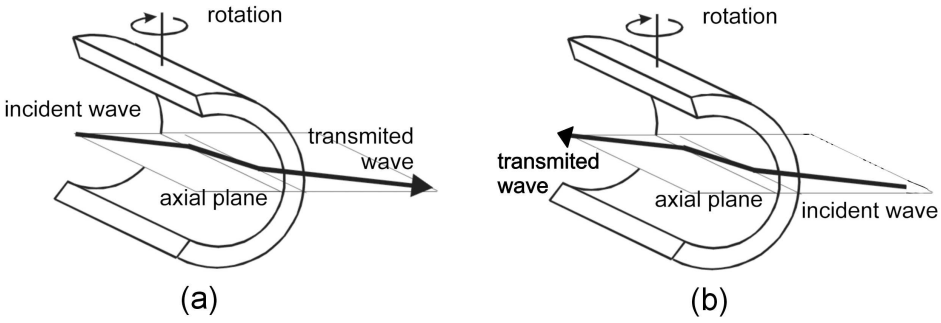

Fig. 21: Modes of the wave propagation through the PMMA tube. (a)Mode C, (b) Mode D.

Modes C and D (Figure 21) are intended for the evaluation of elastic coefficients. Both modes are configured horizontally, so the wave propagation takes place in an axial plane of the tube and is not being influenced by the curvature of the specimen at all. During the measurement, the reflector was stationary adjusted parallel to the transducer front. The specimen was rotated in the range of -50° to 50° per the step of 2° for the mode C and of -40° to 40° per the step of 2° for the mode D. The measurement without the specimen was performed at first in order to determine the velocity of wave propagation in a water.

Measured raw data from modes C and D are introduced in the form of maps signal in Appendix **??**. The shape of the signal and velocities calculated from dimensions of the experiment are identical, so the presumption, that wave is propagating in an axial plane of the tube specimen is validated. The comparison of a theoretically calculated phase velocities (calculated from dimensions of the experimental set-up and the specimen) and experimentally obtained data are shown in Figure 22. The resultant longitudinal and transverse phase velocities are consequent: $v_\phi^L = 2.764$ mm/μs and $v_\phi^T = 1.349$ mm/μs.

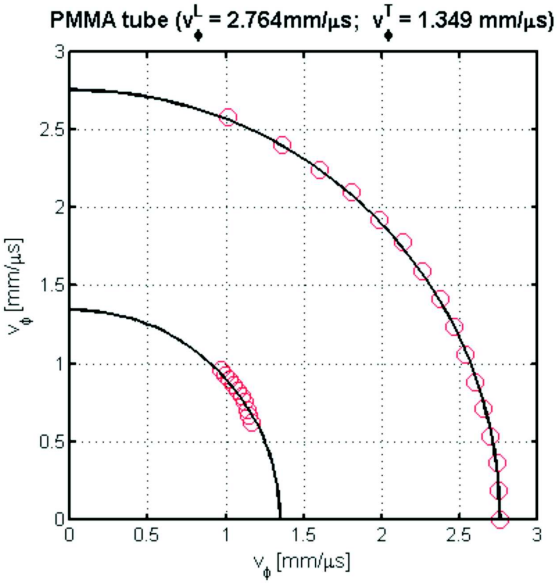

Fig. 22: Plots of phase velocities in [mm/μs] propagating through the bone specimen
Circles - experimentaly obtained data, Solid lines - theoretically calculated phase velocities.
v_ϕ^L - Longitudinal phase velocity, v_ϕ^T - Transverse phase velocity.

The isotropic material has two independent coefficients and a matrix of elastic coefficients c_{ij} can be notated in a following form:

$$c_{ij} = \begin{pmatrix} c_{11} & c_{12} & c_{12} & 0 & 0 & 0 \\ c_{12} & c_{11} & c_{12} & 0 & 0 & 0 \\ c_{12} & c_{12} & c_{11} & 0 & 0 & 0 \\ 0 & 0 & 0 & \frac{1}{2}(c_{11}-c_{12}) & 0 & 0 \\ 0 & 0 & 0 & 0 & \frac{1}{2}(c_{11}-c_{12}) & 0 \\ 0 & 0 & 0 & 0 & 0 & \frac{1}{2}(c_{11}-c_{12}) \end{pmatrix} . \tag{47}$$

Both independent constants c_{11} and c_{12} can be determined from phase velocity measurements of longitudinal v_ϕ^L and transversal v_ϕ^T waves by formulae

$$c_{11} = \rho(v_\phi^L)^2,\ c_{12} = c_{11} - 2\rho(v_\phi^T)^2\ , \tag{48}$$

which results in $c_{11} = 9.09$ GPa and $c_{12} = 4.76$ GPa, for a density of PMMA $\rho = 1.19$ g/cm^3.

Mode I (Figure 23(a)) is intended for a verification of the simplified ray method, which was introduced in the Chapter . The input arguments into a 2 dimensional simulation are the geometry of the specimen, dimensions among the transducer, specimen and reflector, the class of crystallographic symmetry (isotropic) and parameters fundamental for the satisfaction of the Snell-Descartes law (34) such as the direction of the incident wave, angles of the wave refraction and reflection on the specimen/liquid interface and the phase velocity of the wave propagating in the specimen or in a liquid. The specimen is modelled as stationary and the reflector is modelled as rotating. The results of the ray method iteration (Section) are evident from Figure 23.

The ray simulation was validated experimentally. The experimental set-up was adapted from a model. The dimensions among the transducer, the specimen and reflector as well as specimen orientation (vertical configuration - mode I Figure 23 (a)) were possibly the closest to the model. The reflector was rotated in the range of -8° to 8° per the step of 0.2°. The signal map is introduced in Appendix **??**. The calculated phase velocity of longitudinal data and its comparison with the ray model is outlined in Figure 23 (b); the very good agreement is visible.

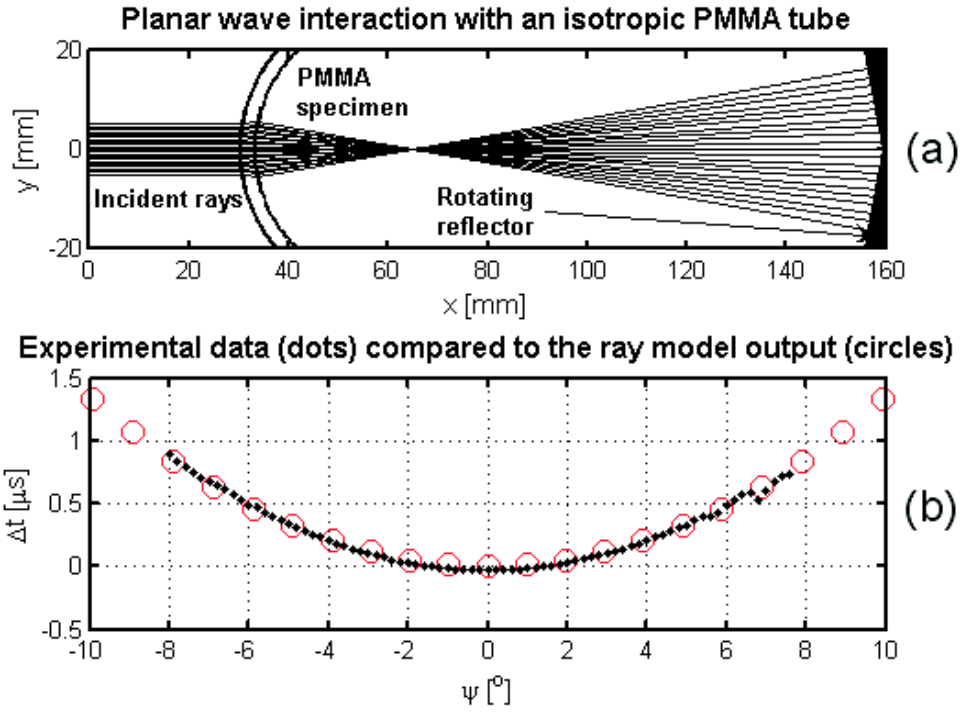

Fig. 23: The diagram of the wave propagation through the PMMA tube - mode I. (a) The ray model of wave interaction with the PMMA tube; the specimen is stationary, the reflector is rotating, (b) The comparison of the ray model and experimentally obtained data.
ψ - angle of reflector rotation; $\psi = 0$ for reflector position parallel to the transducer face.
Δt - time difference against $\psi = 0$ (Δt $= 0$, if $\psi = 0$).

Results for a bovine bone All ultrasonic pulse-echo immersion measurements were performed on one particular place of the dry bovine specimen (Section , Figure 11). The experimental configuration was similar to the measurement performed on the isotropic PMMA tube (previous chapter). The indication of modes C,D and I was also adapted from the previous experiment with respect to the similar geometry of a long bone and a cylindrical tube. The adjustment of measurements for particulars modes was following (Figure 18): Mode C - L = 219 mm (L - distance between the transducer and the reflector), T = 19.6 - 20.8°C (T - temperature of the water bath), rotation of the specimen from -40° to 40 ° per step of 0.2°; Mode D - L = 164 mm, T = 21.2°C, rotation of the specimen from -40° to 40 ° per step of 0.5°; Mode I - L = 106 mm, T= 22.2°, rotation of the reflector from -16° to 16° per step of 0.1°.

Fig. 24: The mode C of the wave propagation through the bone specimen in the x_1x_3 plane (axial plane).
Circles - experimentally obtained data, Solid lines - phase velocities for calculated c_{ij}.
qL - quasilongitudinal wave, qT - quasitransverse wave PT - pure transverse wave.

Mode D is used for the determination of elastic coefficients c_{11}, c_{33}, c_{44}, c_{55}, c_{66} and c_{13} of the orthotropic material symmetry (6 of totally 9 independent constants). These constants are calculated by a solution of the inverse optimization from the set of phase velocities qL, qT and the PT (Figure 24). The left part of the figure represents a normal surface in an approximately axial plane of the specimen, if the geometrical conformity with the tube is assumed. Two modes of the wave propagation qL and qT were observed. Their phase velocities were calculated from

maximal amplitudes of a signal arrival (Figure 24, the map of signal). The evaluation of c_{44} and c_{55} is only theoretical, because these two constants are calculated by an inverse algorithm from the PT mode of the wave propagation, which was calculated by the direct solution of the Christoffel equation (Section , Figure 24 - solid lines) and this mode is not experimentally detected. The more precise determination of c_{44} and c_{55} via another technique is necessary.

Fig. 25: The mode D of the wave propagation through the bone specimen in the x_1x_3 plane (axial plane).
Circles - experimentally obtained data, Solid lines - phase velocities for calculated c_{ij}.
qL - quasilongitudinal wave, qT - quasitransverse wave PT - pure transverse wave.

The mode D (Figure 25) serves as an independent verification of obtained results of the mode C. Only the quasi-longitudinal mode of the wave propagation was observed during this experiment.

The mode I serves for the determination of c_{22} and c_{12}, where c_{12} is calculated from the relationship $c_{12} + 2c_{66} = const$. This mode corresponds to the vertical configuration of the measurement, so the wave propagation and the elastic constant evaluation of the bone specimen with the general geometry of a bone specimen must be resolved via the ray method.

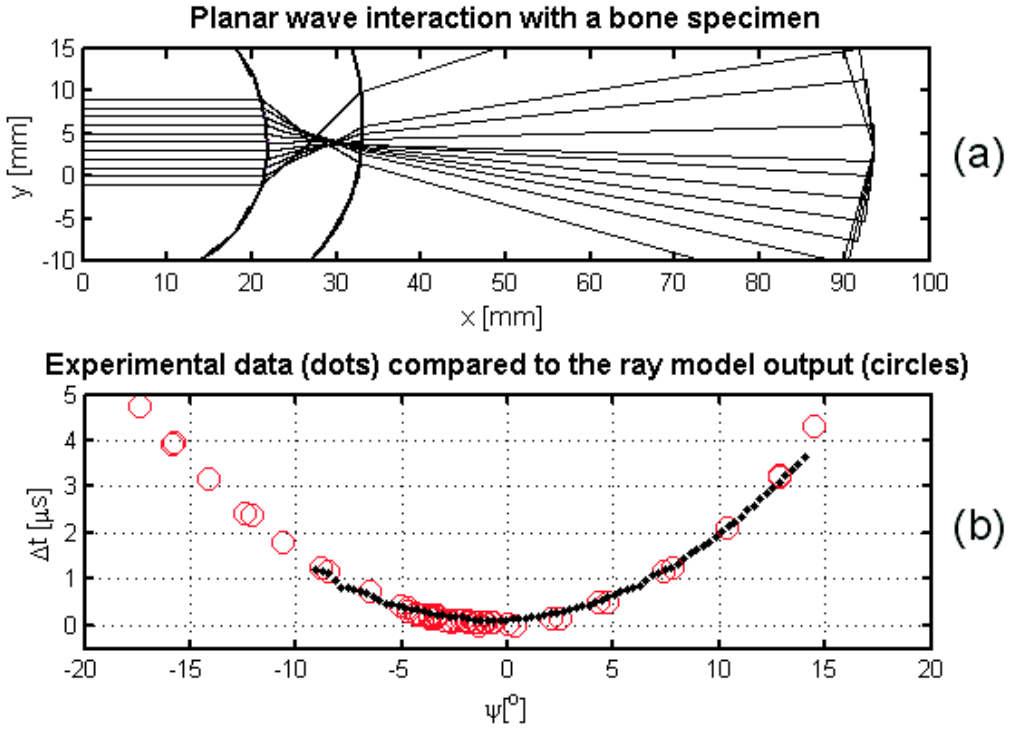

Fig. 26: The diagram of the wave propagation through the bovine bone - mode I. (a) The ray model of the wave interaction with the bovine bone sample; the specimen is stationary, the reflector is rotating, (b) The comparison of the ray model and experimentally obtained data.
ψ - the angle of the reflector rotation; $\psi = 0$ for reflector position parallel to the transducer face.
Δt - the time difference against $\psi = 0$ (Δt $= 0$, if $\psi = 0$).

The experimental procedure and the elastic constant evaluation of the mode I is subsequent. The input geometry of the bone specimen into the ray algorithm was obtained by the contact probe (Section). During the experiment, the bone sample was rotated into the vertical position, so the wave propagation in the plane perpendicular to the bone axis could be observed. The experimental set-up was the pulse-echo with the rotating reflector as described in this section

Table 7: Resultant elastic coefficients c_{ij} of the bone specimen in form (44). Values are expressed in GPa.

$\mathbf{c_{ij}}$	**Mode C, D**	**Mode I**	**Value of $\mathbf{c_{ij}}$ [GPa]**
$\mathbf{c_{11}}$	X		27.396 ± 1.557
$\mathbf{c_{33}}$	X		34.113 ± 1.737
$\mathbf{c_{13}}$	X		8.298 ± 5.335
$\mathbf{c_{44}}$	X		20.149 ± 1.295
$\mathbf{c_{55}}$	X		13.096 ± 3.732
$\mathbf{c_{66}}$	X		4.364 ± 0.073
$\mathbf{c_{22}}$		X	30.250 ± 2.811
$\mathbf{c_{12} + 2c_{66}}$		X	33.890 ± 3.583
Calculated $\mathbf{c_{12}}$		X	25.162

opening. The raw signal maps of the mode I (only qL mode was observed) as well as modes C and D are introduced in Appendix **??**. Then, the ray algorithm (Section) is solved for a different positioning of the specimen Appendix **??** until the ray model is tuned to the measured data. This situation, the final tuning in fact, and agreement of experimental data with the ray model are demonstrated in Figure 26. The Christoffel equation (8) along thereby obtained rays and behaviour of rays at the solid/specimen interface was numerically solved by means of the inverse problem (Section).

The density of the bone specimen, the necessarily known parametr for the solution of the Christoffel equation, wasn't experimentally detected by the reason of non-availability of a proper experimental device. The application of some primitive technique, such as the Archimedes principle, was not possible due to a porosity of the bone. The density of the bovine bone was finally taken over the literature [Lasayques and Pithioux, 1998, Pithioux *et al.*, 2002] where the immersion through the transmission ultrasonic technique was used for the determination of elastic constants of bovine femur. The method of a X-ray tomodensitometry was used in this work and authors used the value of density $\rho = 1.8$ g/cm^3 for a calculation of the elastic constant. This value was also applied in this case of immersion measurements (modes C,D and I) for the evaluation of all nine elastic constants. The resultant matrix of elastic coefficients c_{ij} (27)

$$c_{ij} = \begin{pmatrix} c_{11} & c_{12} & c_{13} & 0 & 0 & 0 \\ c_{12} & c_{22} & c_{23} & 0 & 0 & 0 \\ c_{13} & c_{23} & c_{33} & 0 & 0 & 0 \\ 0 & 0 & 0 & c_{44} & 0 & 0 \\ 0 & 0 & 0 & 0 & c_{55} & 0 \\ 0 & 0 & 0 & 0 & 0 & c_{66} \end{pmatrix}, \tag{49}$$

expresses in form (44) calculated from the optimization (41) is presented in the Table 7. The input inaccuracies involved into the Monte Carlo simulation (Section) are the thickness of the specimen (d = $\pm$0.5 mm), the angle of deviations of the sample (mode C,D) or the reflector (mode I) ($\alpha = \pm 0.5°$), the temperature of the water bath (T = $\pm$1°C) and the specimen density ($\rho = 1.8 \pm 0.1$ g/cm^3).

The determination of the c_{23} is not feasible by means of the immersion technique, the measurement of this constant can be performed via the contact technique for example.

Contact measurements

Determination of c_{23} and improvement of c_{44} and c_{55} from immersion

In this experiment, the contact pulse transmission technique was used in order to determinate c_{23} and improve c_{44} and c_{55} obtained from the immersion measurement. The determination of c_{23} from the immersion was not possible at all. Constants c_{44} and c_{55} were, in the immersion, obtained from the theoretically calculated pure transverse (PT) wave, so their values are not experimentally substantiated. The constant c_{44} needs to be evaluated primarily, because the knowledge of its value is necessary for the calculation of c_{23}. Coefficients c_{44} and c_{55} can be determined from contact measurements of the cubic sample number 5 and 6 and the slice sample number 5 and 6 (for sample orientation see Section) by shear transducers. Moreover, the constant c_{66} can be obtained from this experiment on the cubic sample number 5 and 6. The coefficient c_{23} is calculated from the contact measurement on slice samples number 3 and 4 in a direction diverted from the circumferential direction about an angle of 13°. The longitudinal transducers (for identification of transducers see Section) were used for this measurement.

Thicknesses of both cubic samples in all three directions (Table 4) and both slice shaped samples in the radial direction were measured by the dial indicator. In order to determine the density of cubic specimens, these specimens were weighed by a laboratory scale. The resultant density of cubic specimens no. 5 and 6 is 2.1 g/cm^3. The density of slice samples were not measured, the value of 1.8 g/cm^3 in agreement with literature [LASAYQUES and PITHIOUX, 1998, PITHIOUX *et al.*, 2002] was considered. Resultant coefficients c_{44}, c_{55} and c_{66} (Appendix 14) were calculated from the velocity measurement by formulae

$$c_{44} = \rho v_{3/2}^2,\ c_{44} = \rho v_{2/3}^2 \tag{50}$$

$$c_{55} = \rho v_{3/1}^2,\ c_{55} = \rho v_{1/3}^2 \tag{51}$$

$$c_{66} = \rho v_{2/1}^2,\ c_{66} = \rho v_{1/2}^2, \tag{52}$$

where $v_{i/j}$ are velocities measured between shear transducers, propagated in the direction i for the transducer polarized in the direction j, for $i, j = 1, 2, 3$.

Table 8: Average elastic coefficients c_{44}, c_{55} and c_{66} and their standard deviations in form (44) of cubic and slice specimens. Values are expressed in GPa.

Specificaton of c_{ij} [GPa]	**Average value of cube**	**Average value of slice**	**Average value of cube and slice**
$\mathbf{c_{44}}$	10.523 ± 0.343	8.737 ± 0.357	9.333 ± 0.942
$\mathbf{c_{55}}$	6.943 ± 0.584	7.039 ± 0.299	7.001 ± 0.391
$\mathbf{c_{66}}$	6.852 ± 0.481		

The Table 8 represents average values and their standard deviations in form (44) of cubic and slice specimens. These values are presented separately for each kind of specimen and total values are also introduced. The reason for this separation is the different location of the slice and cubes in the original sample of the bovine femur (Figures 12 and 13).

The coefficient c_{23} was calculated by the formula

$$\begin{gathered} c_{23} = \tfrac{1}{\sin(2\vartheta)}\sqrt{X^2 - 2XA + B} - c_{44},\ \text{where} \\ X = 2\rho v_L^2,\ A = c_{44} + c_{22}\cos^2\vartheta + c_{33}\sin^2\vartheta, \\ B = c_{22}c_{44}(1+\cos(2\vartheta))^2 + c_{33}c_{44}(1-\cos(2\vartheta))^2 + (c_{44}^2 + c_{22}c_{33})\sin^2(2\vartheta), \end{gathered} \tag{53}$$

where v_L is the longitudinal wave velocity propagating through slice specimens 3 and 4 in a direction diverted from the circumferential direction about an angle $\vartheta = 13°$ and ρ is the density of

the bone. This formula was derived from terms of elastic constants - the wave velocity relationship published by Every [Every and Sachse, 2001]. The velocity v_L was measured by ther contact through transmission technique, using the longitudinal transducers. The input elastic coefficients into the equation (53) are substituted from average results ofthe contact measurement of cubic samples 5 and 6 (for a further details see Section), because required constants can be measured most precisely due to a possibility of the exact density measurement and both samples are located approximately in the middle part of the femur close to the place of the immersion measurement. Values of these input quantities are following: $c_{22} = 28.63$ GPa, $c_{33} = 39.18$ GPa, $c_{44} = 10.52$ GPa, $\upsilon = 13°$ and $\rho = 2.1$ g/cm^3. Calculated resultant value of the $\mathbf{c_{23}}$ is **8.50 GPa**.

Contact measurements of cubic and slice shaped bone samples

Further contact pulse transmission experiments were performed on available cube and slice shaped samples (Section) in order to obtain the utmost possible information concerning the bone elastic properties. The main aim of this experimental part is a demonstration of the bone elastic constant heterogeneity in a geometrical sense. All measurements listed in this chapter were performed by using a longitudinal ultrasonic transducers (Section).

Table 9: Values of c_{33} for slice samples measurements.

Measurement location	c_{33} [GPa] Slice # 1	c_{33} [GPa] Slice # 2	c_{33} [GPa] Slice # 5	c_{33} [GPa] Slice # 6
A	30,84	30,11	30,85	28,94
B	30,37	29,73	30,92	28,08
C	31,82	32,70	30,48	31,83
D	32,16	32,24	33,30	32,25
E	34,41	31,92	33,75	33,85
F	32,66		33,19	34,92

Evaluation of c_{33} from slice samples Slice shaped specimens were also used, for the measurements performed by the shear transducers in order to detect c_{44} and c_{55} (previous section), for a determination of c_{33} at a different location of each slice. Totally four slices, marked as the Specimen 1,2,5,6 each at 6 different locations marked as A, B, C, D, E and F) (Figure 12), were measured. The formula

$$c_{33} = \rho v_{3/3}^2 \,, \tag{54}$$

where ρ is the density of the bovine cortical bone ($\rho = 1.8$g/cm^3 [Lasayques and Pithioux, 1998, Pithioux *et al.*, 2002]) and $v_{3/3}$ is the detected wave velocity in the direction x_3 between transducers polarized in the direction x_3, was used for c_{33} calculation. The resultant values of the c_{33} are presented in Table 9 and their graphical interpretation is represented in Figure 27.

Fig. 27: Plot of c_{33} of slice specimens 1, 2, 5 and 6 at places of measurement A, B, C, D, E, F.

Evaluation of c_{11}, c_{22} and c_{33} from cubic samples No. 5 and 6 The elastic constants c_{11}, c_{22} and c_{33} of cubic specimens no. 5 and 6 (Figure 13) were measured by the contact pulse transmission technique by means of longitudinal transducers . The elastic constants were calculated by a virtue of the following formula:

$$c_{ii} = \rho v_{i/i}^2 \,, \tag{55}$$

where ρ is a density of the cubic specimen and $v_{i/i}$ is the detected wave velocity in the direction $i = 1, 2, 3$. The density was determined from dimensions and a weight of the specimen, $\rho_{5,6} = 2.1$ g/cm^3. Calculated elastic coefficients and their average values are introduced in Table 10.

Table 10: Values of c_{11}, c_{22} and c_{33} for cubic samples No. 5 and 6 measurements.

$\mathbf{c_{ii}}$ **[GPa]**	**Cube #6**	**Cube #5**	**Average**
c_{11}	22.63	22.62	22.625
c_{22}	29.75	27.50	28.625
c_{33}	40.60	37.76	39.18

Evaluation of c_{12} from cubic samples No. 2 and 4 Cubical specimens no. 2 and 4 are appropriate for an evaluation c_{12} by the simple through transmission technique, because they are inclined about an angle $\vartheta = 30°$ and $45°$ respectively to the circumferential direction x_2 (Figure 13). Both samples are also conducive to the c_{33} measurement.

Table 11: Input parameters into (56) and the resultant value c_{12} for the contact measurement of cubical specimens No. 2 and 4.

Input/Output parameter into (56)	**Value for cube # 2**	**Value for cube # 4**	**Average**
c_{11} [GPa]	22.625	22.625	
c_{22} [GPa]	28.625	28.625	
c_{66} [GPa]	6.85	6.85	
v_L [mm/μs]	3.10	3.41	
ρ [g/cm^3]	2.4	2.1	
ϑ [°]	30	45	
$\mathbf{c_{12}}$ **[GPa]**	9.02	9.24	9.13

The coefficient c_{12} can be calculated by the following formula derived on the basis of relationships published by Every [EVERY and SACHSE, 2001]:

$$\begin{gathered} c_{12} = \tfrac{1}{\sin(2\vartheta)}\sqrt{X^2 - 2XA + B} - c_{66}, \text{ where} \\ X = 2\rho v_L^2,\ A = c_{66} + c_{11}\cos^2\vartheta + c_{22}\sin^2\vartheta, \\ B = c_{11}c_{66}(1+\cos(2\vartheta))^2 + c_{22}c_{66}(1-\cos(2\vartheta))^2 + (c_{66}^2 + c_{11}c_{22})\sin^2(2\vartheta), \end{gathered} \tag{56}$$

where v_L is the measured longitudinal velocity propagating through the specimen in the direction inclined to x_2 about the angle ϑ and ρ is a density of the specimen. Input elastic coefficients c_{11}, c_{22} and c_{66} are substituted into (56) as an average values from contact measurements on samples no. 5 and 6 (previous paragraph and Section). The density of both specimens was determined by specimens by weighting and dimensions measuring. The resultant density of the specimen no. 4 is 2.1 g/cm^3, which corresponds to a density of other cubes, but the density of the specimen no. 2 is somehow higher, $\rho_2 = 2.4$ g/cm^3.

The input parameters into the formula (56) and the resultant coefficient c_{12} for the contact measurement of samples no. 2 and 4 are presented in the Table 11.

RUS measurement

The RUS measurements were performed on specimen no. 4 and 6 which were located on the medial part of the bone sample in its superior and middle part. The procedure of the measurement and

the calculation of resonant frequencies were described in Chapter , items 1 to 3. The algorithm for

Table 12: Input parameters into the calculation of resonant frequencies of cubical specimens No. 4 and 6.

	cube #4	**cube #6**
$\mathbf{c_{11}}$ **[GPa]**	27.40	22.63
$\mathbf{c_{22}}$ **[GPa]**	30.25	27.5
$\mathbf{c_{33}}$ **[GPa]**	33.36	37.76
$\mathbf{c_{44}}$ **[GPa]**	9.33	10.25
$\mathbf{c_{55}}$ **[GPa]**	7.00	6.48
$\mathbf{c_{66}}$ **[GPa]**	6.85	7.26
$\mathbf{c_{12}}$ **[GPa]**	9.24	9.13
$\mathbf{c_{13}}$ **[GPa]**	8.30	8.30
$\mathbf{c_{23}}$ **[GPa]**	8.50	8.50
density ρ **[g/cm^3]**	2.1	2.1
dimensions [m]	5.03x5.08x5.16	6.55x6.55x6.54

the evaluation of resonant frequencies was written by Michal Landa and Hanuš Seiner from the Institute of Thermomechanics ASCR in the SW environment MATLAB. The input parameters into this computation are stated in Table 12. Input elastic coefficients are the combination of results from the immersion and the contact measurements, where elastic constants determined via contact measurements were preferred due to their higher accuracy.

The RUS scan of each cubical specimen was performed at exciting frequencies from 0.1 to 0.4 MHz. The sample no. 6 was scanned at first by compressional transducers. Then the scanning was repeated by means of shear transducers, where much stronger signal was observed (Figure **??**). The sample no. 6 was then scanned via shear transducers alone. The calculated resonant frequencies (magenta lines) as well as the comparison with the experimentally obtained resonant spectra are presented in Appendix **??**. The steps 4 and 5 of the RUS procedure (Section) weren't even evaluated due to problems with the identification of theoretically calculated and experimentally obtained resonant frequencies. Both resonant frequencies are considerably differing even from initial resonant frequencies which is evident from the visual comparison of Figures **??** and **??**. This fact excludes a reliable evaluation of bone samples elastic constants by the RUS technique.

Discussion

The main goal of this thesis is to deal with possibilities of the experimental determination of the matrix of elastic coefficients of the cortical bone by means of the dynamical, ultrasound based, mechanical tests. The cortical bone can be considered as a linear elastic material, which is approximately homogenous and anisotropic with an orthotropic material symmetry [Lasayques and Pithioux, 1998, Lee *et al.*, 2002, Pithioux *et al.*, 2002, Rho, 1996, Yoon and Katz, 1976]. The knowledge of elastic constants of the bone tissue is fundamental for modelling of a mechanical response of the bone loading. It may be useful for a mathematical modelling of the human skeleton and artificial joints via FEM analysis and results of this work should be used as an improvement of the input data into these new and existing models. The specification of elastic coefficients of bones is also very important for a micro-mechanical modelling that conduces to new findings concerning the microstructure of a bone tissue. This knowledge may, for example, help to answer a bone tissue remodelling problem. However, the benefit of this study is not to map or measure elastic constants of a number of bone samples and their statistical evaluation, but to develop an experimental methodology. This methodology

should be nondestructive, ultrasound based, appropriate for a rapid measurement, undemanding a sample preparation and automated the elastic constant result evaluation.

The ultrasonic-pulsed through-transmission method with the specimen immersed in a liquid between two opposite transducers have been chosen as a suitable technique which satisfies all declared specifications. This technique was previously used by many authors for an evaluation of elastic constants of technical composite materials [Enderby *et al.*, 1998, Geiske and Allred, 1974, Harper and Clarke, 2002, Hine *et al.*, 1997, Liaw *et al.*, 1996, Wu and Ho, 2005], but only Lasaygues and Pithioux [Lasayques and Pithioux, 1998, Pithioux *et al.*, 2002] used this method for an evaluation of bone elastic coefficients. However, in this work, the general sample geometry was not considered, the sample was presumed as a plane round examined location. The focussed transducer was used during the measurement moreover, so very precise adjustment of the experiment dimensions was necessary.

Test measurements

In this study, quite an original modification of the immersion technique was used. The unfocused transducers of larger diameters (frequency 2.25 MHz, diameter 0.5") were used in order to propagate planar acoustic waves during the measurement. The initial experimental configuration was through a transmission with a transmitting and a receiving transducer and two degrees of a freedom. The first degree of freedom was a rotation of the specimen with a view to measure velocities of waves propagation at various incident angles. The second degree of freedom was a translation of the receiver for the purpose of detection of maximal signals of refracted waves. The transmitter was stationary and the entire experimental configuration was immersed in a water. The task of this acoustic scanner was to monitor the refracted compressional (quasi-longitudinal qL waves) and shear (quasi-transversal qT waves) waves originating on the solid/fluid interface and which obey the Snell descartes laws.

Test measurements of this experimental set-up were performed on composite CFRP (Carbon Fibre Reinforced Plastic) samples of well known elastic properties [Seiner, 2004], [Seiner and Landa, 2003]. The through transmission measurements didn't acquit well, because the compression and shear modes of the wave propagation coincided with each other and it was very difficult to clearly distinguish them. Then, the pulse-echo arrangement of measurement was used with only one transducer (transmitter and receiver) and one degree of a freedom. The receiver was replaced by an acoustic reflector, so the refracted waves were reflected towards the receiver along the exactly same path as the incident waves. The one degree of a freedom consisted in a rotation of either the specimen or the reflector. The inaccurate translational scanning of maximal signals thus wasted. The resultant matrix of elastic coefficients was calculated from detected qL and qT waves by the solution of the Christoffel's equation via the formulation of an inverse problem, which led to the numerical multidimensional optimization, which was solved by the simplex search method. The stability of resulting data was evaluated by the statistical method based on the Monte-Carlo simulation. Thereby designed pulse-echo measuring configuration was validated on CFRP plates.

The algorithm based on the simplified ray method was proposed in order to deal with the wave propagation through an anisotropic specimen of a general geometry. In this algorithm, wavefronts propagating through the specimen were substituted by closely localized energy flows (rays) in every geometrical point and the Christoffel's equation along these rays was solved afterwards by the numerical minimization of an inverse problem. This theoretical model was validated on the immersion pulse-echo measurement of the PMMA tube.

Immersion measurements

Following experiments were performed on the dry bovine femur. Dry bovine bone was used instead of a wet bone [Lakes *et al.*, 1986, Lasayques and Pithioux, 1998, Lee *et al.*, 2002, Pithioux *et al.*, 2002, Rho, 1996, Yoon and Katz, 1976] for the measurement, because of the independent determination of elastic properties separately, from the natural visco-elastic behaviour of bones. The nearly elastic behaviour of the dry bovine bone against the wet one was firstly observed by Park and Lakes [Park and Lakes, 1986]. By this approach, the influences of age, weight, sample preparation and storage, which affect in particular damping and time dependent properties of bones, can be avoided. In future, the results for dried bones can be compared with these obtained on wet samples. Due to the knowledge of elastic properties of dry bones, the complex visco-elastic behaviour of bones can be decomposed into its elastic and time dependent parts. Anyway, the elastic coefficients determined for the dried bones should be close to those obtained from conventional tensile tests, where the dynamic properties of bones result complexly from their visco-elasticity, material dispersion and attenuation.

The pulse-echo arrangement of the immersion technique, which was successfully tested on the PMMA tube, was also used for the measurement of the dry bovine bone. The bone sample was slit into two parts along the bone axis in order to monitor just a simple wave propagation through one face of the bone and each part was shape-measured. During the experiment, just one particular place in a middle part of the bone localized on a medial side of the bovine femur sample was examined. The three different modes of the measurement, modes C, D and I, were performed.

Modes C and D corresponded to the horizontal positioning of the bone between the transducer and the reflector where the wave propagation in an axial plane of the bone was observed. The bone geometry was not solved in these modes, the bone geometry was considered as planar in the surrounding of a measuring position. This mode was appropriate for evaluation of 6 out of 9 elastic coefficients (c_{11}, c_{33}, c_{44}, c_{55}, c_{66} and c_{13}) of the orthotropic material symmetry. Elastic coefficients c_{11}, c_{33}, c_{66} and c_{13} were evaluated from measured qL and qT velocities via the solution of an inverse problem of the Christoffel equation. Values of c_{44} and c_{55} are only theoretical and don't correspond to real values, because they can be determined only from a pure transverse mode of the wave propagation and this mode wasn't experimentally detected. The velocities of the pure transverse wave were computed theoretically by the direct solution of the Christoffel equation.

The mode I corresponded to the vertical configuration of the measurement. In this mode, the propagation of the planar wave was observed in the plane perpendicular to the long axis of the bone, so the bone curvature needs to be considered. This is resolved by means of the simplified ray model and the solution of the Christoffel's equation along particular rays in the same way as test measurements of the PMMA tube. The mode I was used for the determination of coefficients c_{22} and c_{12}. This mode showed to be inadvisable for the evaluation of both elastic constants (c_{12} and c_{22}) from the viewpoint of a demand on the automated and rapid evaluation of elastic coefficients. The reasons for this impropriety are the time-consuming geometry measurements of every bone sample in a surrounding of the measuring location, which is the input requirement to the ray algorithm, and the complicated manual tuning of the ray model results in experimentally obtained velocities, which are very difficult to automatize.

The stability of elastic coefficients of the bovine bone sample resulting from an inverse problem optimization were evaluated by the simulation based on the Monte-Carlo statistical method. Input parameters into this simulation were variations of specimen thickness, rotations of a sample (mode C,D) or a reflector (mode I), a temperature of the water bath and a density of the specimen. The remaining coefficient c_{23} wasn't possible to determine from immersion measurements and needs to be evaluated via some other technique. The simple contact pulse through transmission technique was used in our case. The disadvantage of this method is a requirement of the specimen

sawing to exactly paralel faces. Final resultant coefficients c_{ij} can be expressed in the following form:

$$c_{ij} = \begin{pmatrix} c_{11} & c_{12} & c_{13} & 0 & 0 & 0 \\ c_{12} & c_{22} & c_{23} & 0 & 0 & 0 \\ c_{13} & c_{23} & c_{33} & 0 & 0 & 0 \\ 0 & 0 & 0 & c_{44} & 0 & 0 \\ 0 & 0 & 0 & 0 & c_{55} & 0 \\ 0 & 0 & 0 & 0 & 0 & c_{66} \end{pmatrix} =$$

$$\begin{pmatrix} 27.396 & 25.162 & 8.298 & 0 & 0 & 0 \\ 25.162 & 30.250 & ? & 0 & 0 & 0 \\ 8.298 & ? & 34.113 & 0 & 0 & 0 \\ 0 & 0 & 0 & 20.149 & 0 & 0 \\ 0 & 0 & 0 & 0 & 13.096 & \\ 0 & 0 & 0 & 0 & 0 & 4.364 \end{pmatrix} \text{GPa}$$

Contact measurements

Additional pulse through transmission contact measurements were performed on the same bone sample as in the case of immersion measurements in order to obtain the maximum possible information relevant to bone elastic properties by both kinds of transducers, the compressional and the shear ones. Two types of specimens, the cube and slice shaped specimens, were prepared by the dissection of the existing bone sample. The slice specimens were cut from a medial part and cube specimens were cut from a lateral part of the bovine femur sample. Particular contact experiments are discussed in following paragraphs.

The first contact measurement was formed with a view to acquire c_{23} which wasn't possible to evaluate from the immersion experiment. This was performed via the detection of phase velocity of the longitudinal wave propagating through the specimen, which was cut sideways in a longitudinal-circumferential plane on a medial side of the bone specimen.

The second experiment took an advantage of the contact measurements by shear transducers. It was appropriate for the improvement of c_{44} and c_{55} which were evaluated only theoretically during immersion measurements. These tests were performed on two slice shaped specimen (a middle part of the medial side of the bone sample - approximately same location as immersion measurements) and on two cube specimens (a middle part of the lateral side of the bone sample). These last cube samples were also appropriate for the determination of c_{66}. The evaluation of c_{66} via the contact technique was more precise than the evaluation via the immersion technique, because the density of the cubic sample can be easily calculated from the specimen dimensions and mass.

Another contact measurements were performed on four slice samples in order to observe the heterogeneity of bone elastic properties in different locations of the bone. The monitoring of one fairly gainable parameter was presupposed in order to suggest a rapid and simple methodology. The coefficient c_{33} expressing an elastic modulus in the direction of the bone long axis was chosen as a suitable parameter. Slice specimens were obtained by cutting the medial part of bone the sample (the Specimen I, for better orientation see Figures 10 and 12). Two slices were sawed from the superior part of the Specimen I and other two from the middle part. All four slices were cut in the perpendicular plane to the bong long axis. Each slice was examined by compressional transducers on six different positions. These positions were placed stepwise from a posterior to an anterior across the medial side of the bovine femur (Figure 12 - locations from A to F). The raw measured data of the c_{33} and their fitting by the linear least square method is introduced in Figure 28. The following conclusion can be deduced from these results: the parameter c_{33} doesn't

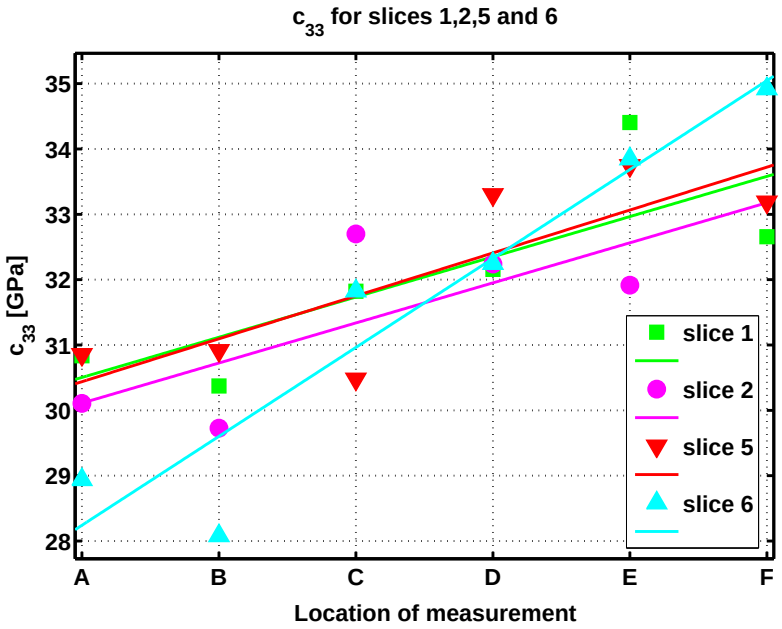

Fig. 28: The evaluation of c_{33} coefficients for the contact measurement of slice specimens 1, 2, 5 and 6.
Places of measurement A, B, C, D, E, F.
Symbols - raw data; Solid lines - data fitting by linear least square measure

notably vary along the bone long axis, but grows from the posterior to the anterior side of the bone sample.

Additional measurements were performed on available cubical specimens in order to acquire the maximum possible information concerning bone elastic coefficients. The elastic constants c_{11}, c_{22} and c_{33} in the main axis of the material symmetry were monitored during these measurements via contact measurements by longitudinal transducers. These test were performed on two cubical specimens located in a middle of the bone sample on its lateral side. Resultant values can be used as an independent verification of immersion measurements; the density of these samples was accurately measured. Another two cubical samples located on a lateral side of the bone specimen in its superior part were appropriate for the determination of c_{12} due to their suitable turning towards axes of the main material symmetry of the bone sample. The resultant value of c_{12} (resultant average value 9.13 GPa) was determined on the basis of contact measurements by longitudinal transducers and the analytical calculation. The input elastic constants c_{11}, c_{22} and c_{66} into this formula were derived from previous contact measurements.

RUS measurements

The RUS experimental technique was applied to measurements of two cubical specimens. This method was found not to be an effective tool for the determination of elastic constants of the bone due to sizable differences between theoretically calculated and experimentally obtained resonant frequencies, which is in line with the observation of Lee [Lee *et al.*, 2002]. One of the possible reasons for this conclusion may be the influence of a drying process on a bone structure; the bone structure became cracked in some locations, which may affect resonant frequencies. The influence of shear transducers usage instead of compressional ones on a strength of the resonant spectrum signal was discovered, which is consistent with the work of Wang [Wang and Lakes, 2003]. For the future work, experiments using rectangular fresh bone samples may be recommended.

Resultant matrix of elastic coefficients obtained via immersion and contact measurements

The combination of advantages of immersion and contact measurements, the final resultant matrix of elastic coefficients

$$c_{ij} = \begin{pmatrix} 27.396 & 9.130 & 8.298 & 0 & 0 & 0 \\ 9.130 & 30.250 & 8.500 & 0 & 0 & 0 \\ 8.298 & 8.500 & 34.113 & 0 & 0 & 0 \\ 0 & 0 & 0 & 9.333 & 0 & 0 \\ 0 & 0 & 0 & 0 & 7.001 & \\ 0 & 0 & 0 & 0 & 0 & 6.852 \end{pmatrix} \text{GPa} \tag{57}$$

is obtained. Elastic coefficients c_{11}, c_{22}, c_{33}, and c_{13} are results of the immersion measurement. Their values are reliably determined from the solution of the inverse problem optimization, whereas the input velocities into this problem are really experimentally obtained values of the qL (quasi-longitudinal)and the qT (quasi-transverse) waves phase velocities. These values are dependent on the specimen density, which wasn't experimentally obtained, but assumed from a literature, however the variability of the density was involved into the statistical method based on the Monte-Carlo simulation.

The coefficient c_{23} is established on the basis of the contact measurement of slice specimens via longitudinal transducers and a simple calculation, because of its determination via immersion technique was impossible without additional sample cutting. Two slice specimens designed for this experiment were located as close to the place of the immersion measurement as possible.

Table 13: Elastic coefficients and their standard deviations (where available)of various bone specimens obtained from ultrasonic measurements - literature comparison

$\mathbf{c_{ij}}$ [GPa]	This thesis	Pithioux	Yoon	Katz	Ashman	Rho
Bone specification	Dry bovine femur	Fresh, frozen bovine femur	Dry human femur	Fresh, frozen human femur	Fresh, frozen human femur	Fresh, frozen human tibia
Ultrasonic technique	Immersion & pulse transmission	Immersion transmission	Pulse transmission	Pulse transmission	Pulse transmission	Pulse transmission
$\mathbf{c_{11}}$	27.4±1.6	23.5	23.4±0.0031	21.2±0.5	18.0	19.4±1.3
$\mathbf{c_{22}}$	30.3±2.8	26.0	24.1±0.0035	21.0±1.4	20.2	20.0±1.4
$\mathbf{c_{33}}$	34.1±1.7	34.6	32.5±0.0044	29.0±1.0	27.6	30.9±1.9
$\mathbf{c_{44}}$	9.3±0.9	9.2	8.7±0.0013	6.3±0.4	6.23	5.7±0.5
$\mathbf{c_{55}}$	7.0±0.4	6.0	6.9±0.0012	6.3±0.2	5.6	5.2±0.6
$\mathbf{c_{66}}$	6.9±0.5	6.3	7.2±0.0011	5.4±0.2	4.5	4.1±0.5
$\mathbf{c_{12}}$	9.1	7.6	9.1±0.0038	11.7±0.7	10.0	11.3±0.1
$\mathbf{c_{13}}$	8.3±5.3	8.4	9.1±0.0055	11.1±0.8	10.1	12.5±0.1
$\mathbf{c_{23}}$	8.5	8.2	9.2±0.0055	12.7±0.8	10.7	12.6±0.1

$\mathbf{c_{ij}}$ [GPa]	Taylor	Van Buskirk	Maharidge	Lang	Lee
Bone specification	Fresh frozen human femur	Fresh, frozen bovine femur	Fresh, frozen bovine femur	Fresh, frozen bovine phalanx	Fresh, bovine Femur
Ultrasonic technique	Pulse transmission	Pulse transmission	Pulse transmission	Pulse transmission	RUS
$\mathbf{c_{11}}$	24.89	14.1	22.4	19.7	10.8
$\mathbf{c_{22}}$	26.16	18.4	25.0	19.7	12.4
$\mathbf{c_{33}}$	33.20	25.0	35.0	32.0	14.3
$\mathbf{c_{44}}$	7.11	7.0	8.2	5.4	5.1
$\mathbf{c_{55}}$	6.58	6.3	7.1	5.4	4.9
$\mathbf{c_{66}}$	5.71	5.28	6.1	3.8	4.2
$\mathbf{c_{12}}$	11.18	6.34	14.0	12.1	-
$\mathbf{c_{13}}$	13.59	4.84	15.8	12.6	-
$\mathbf{c_{23}}$	13.84	6.94	13.6	12.6	-

The resultant value c_{12} was substituted into the matrix c_{ij} as a result of the similar procedure as the evaluation of c_{23}, but it was performed on the cubical specimen. This value acquired from the contact measurement (c_{12}^{cont}) was at a variance with the value obtained from the immersion measurement (c_{12}^{imm}), but it is more reliably determined, because c_{12}^{imm} is a result of a complex optimization and a ray simulation, whereas c_{12}^{cont} is a result of the simple contact measurement moreover the density of the measured cube was exactly known. The value c_{12}^{cont} is also in line with the literature referred-to values (Table 13).

Resultant coefficients c_{44} and c_{55} are also evaluated from the contact measurement of two slice (each slice was scaled in different locations) and two cubic specimens by shear transducers. Their average values are represented in the matrix c_{ij}. The reason for the appliance of c_{44} and c_{55} from the contact technique instead of the immersion one is an imprecision of the immersion method evaluation in the case of both constants that are determined only from theoretical calculations.

The elastic coefficient c_{66} is used as a result of the contact measurement of two cubical specimens, because of a possibility of the exact density determination of the cubical specimen. The value of this constant resulting from the immersion technique is also reliable, but the density of the bone in the surrounding of the immersion measurement wasn't experimentally obtained.

The resultant matrix of elastic coefficients (57) of the bovine dry femur evaluated in this thesis is compared with other data in Table 13. The original presumption, that the dry bone is known to be stiffer then the wet one [Lakes *et al.*, 1986, Lee *et al.*, 2002, Park and Lakes, 1986] was satisfied. This is evident from the comparison of the elastic coefficient measured in this thesis and the work of Pithioux [Pithioux *et al.*, 2002] and from the works of Yoon and Katz [Katz *et al.*, 1984, Yoon and Katz, 1976] where both, the dry and the wet human femur, were tested by the same author team and the same methodology. The overall pattern of the highest elastic coefficient in the longitudinal direction is common to all the results presented in Table 13. The circumferential direction is the second stiffest, and the radial direction is the least stiff. Remaining coefficients are markedly lower then those in the main axes. Comparing the values of fresh bones, the elastic coefficients of the bovine and the human bone don't notably differ, except those evaluated by the RUS [Lee *et al.*, 2002].

Conclusion

In this thesis, the experimental ultrasound based methodology for the determination of elastic coefficients of composite materials CFRP (Carbon Fibre Reinforced Plastic) and the cortical bone tissue were created and evaluated. The use of the pulse ultrasonic technique applied to immersion measurements (a specimen is immersed in a liquid between ultrasonic transducers) and the inverse evaluation of all independent elastic coefficients was initially presupposed. The assumed main contribution of this work to these topical problems was to handle the evaluation of elastic constants of anisotropic specimens of a general geometry.

For understanding of the inverse process, the essential theory of the acoustic wave propagation in anisotropic solids was surveyed, including the definition of the group velocity and examples of the matrix of elastic coefficients assemblage for the orthotropic and the transversely isotropic material. Characteristic surfaces and analytic relations for the reflection and the refraction of acoustic waves at the liquid solid interface were also introduced.

The original contribution is an application of the ray method to the evaluation of elastic constants of curvilinear anisotropic samples. This method is based on the wavefront substitution by the ray (localized energy flow) and the successive determination of elastic constants by the numerical solution of the Christoffel equation along these rays at the simultaneous consideration of the ray behavior at the solid/liquid interface. The inverse problem for phase velocities was formulated and the sensitivity analysis of inverse approach based on the Monte-Carlo statistical simulation was outlined in the final theoretical part.

The description of the experimental methodology, the specimen preparation and the result evaluation were introduced in the following two chapters. The immersion ultrasonic scanner was built in the Institute of Thermomechanics, AVCR in order to realize the theoretically planned immersion ultrasonic-pulse measurements. This device was tested on CFRP plate samples (transversely isotropic material symmetry) of known elastic coefficients from previously performed PS/PR (point-source/point-receiver) measurements [Seiner, 2004, Seiner and Landa, 2003]. Originally was this experimental set-up suggested as the pulse through transmission, but this configuration

showed to be unreliable, because the detected qL (quasi-longitudinal) and qT (quasi-transverse) modes of the wave propagation interfered with one another. Then, the experimental setup was changed into the pulse-echo configuration by replacing the receiving transducer on behalf of acoustic reflector, which proved to be a very effective tool. The resultant elastic coefficients evaluated by this pulse-echo arrangement revealed a very good agreement with PS/PR experimental results, and thus the immersion scanner was validated as a reliable device for the evaluation of the matrix of elastic coefficients of anisotropic solid samples. Another experiment was performed on the PMMA tube. The PMMA is an isotropic material of very well known elastic properties so that this tube shaped sample was used as a validation of the simplified ray model for curvilinear specimens, which was created in advance.

The further immersion experiment was performed on the dry bovine femur diaphysis. The bone was dried, because our effort was to examine the elastic properties of bones separately from the natural visco-elastic behaviour. The bone was considered to be a linear elastic material of an orthotropic material symmetry. The specimen was prepared with a minimal effort, just a rough preparation was sufficient, which was one of the main reasons for the immersion measurements election. During the measurements, two experimental modes were settled; the horizontal one (wave propagation is monitored in a plane of the bone long axis - axial plane) and the vertical one (wave propagation is monitored in a plane perpendicular to the axial plane). For the horizontal bone, the geometry surrounding the place of the measurement was considered as planar, so the contemplation of the curvilinear specimen geometry wasn't required. This mode was intended for the evaluation of coefficients c_{11}, c_{33}, c_{44}, c_{55}, c_{66} and c_{13}. Coefficients c_{12} and c_{22} were determined from the vertical mode. In this mode, the general specimen geometry was reflected by using the simplified ray model of the wave propagation. The remaining coefficient c_{23} wasn't possible to measure without an additional bone sample cutting.

In the subsequent step of the experimental procedure, the bone sample was cut into cubical and slice shaped specimens in order to perform contact pulse-transmission measurements. The remaining coefficient c_{23} was determined at first. Then, coefficients c_{44}, c_{55} and c_{66} were measured on both kinds of cut specimens to improve values obtained from the immersion measurement. The cubical specimens were used for the improvement of c_{11}, c_{22} and c_{33} hereafter. One slice specimen was utilized for the improvement of c_{12}. Remaining slice specimens cut from a different location of the bone were presumed for the monitoring of the bone heterogeneity by measuring one parameter (c_{33}), where the stiffness in the direction of the bone long axis was growing from a posterior to an anterior through a medial part of the bone, in contrast to an axial direction where the value of c_{33} wasn't varied overly.

The additional experimental technique, the resonant ultrasound spectroscopy (RUS), was tested for the measurement of elastic constants of the bone tissue, but no reasonable results were evaluated.

The resultant matrix of elastic coefficients (57) is a compromise, between the immersion and the contact measurement, whereas the results from the contact technique performed on cubical samples were preferred, because of their higher accuracy due to a possibility of the precise estimation of specimens dimensions and a density.

Specific aims of this thesis, declared in the Chapter , were fulfilled and following concluding remarks and future scopes can be stated.

The application of the immersion pulse-echo technique appeared to be an effective tool for the determination of all nine elastic coefficients of the bone cortical tissue considered as the material of the orthotropic material symmetry. However, only eight elastic constants were evaluated in this work via the immersion technique. This experimental method is a very appropriate for the evaluation of five elastic constants without the additional solution of the bone geometry problem. The application of the ray model in order to deal with the complex bone geometry is necessary to the assessment of other three coefficients, which involves the elaborated shape measurement of

the bone sample and the ray model tuning. This fact partially declines the original presumption of the immersion technique usage as a method conducive to the rapid determination of all nine elastic coefficients. The determination of the remaining coefficient by the immersion technique is a matter of further specimen cutting into the slice-shaped specimens oriented perpendicularly to the long axis of the bone in order to measure the acoustic wave propagation through the bone specimen in a superior-inferior anatomical direction. The cutting of the whole bone sample into slice specimens should be performed as a prospective access to the bone tissue heterogeneity monitoring along with measuring of the entire set of elastic constants.

This work also proves suitability of the simple pulse-transmission contact technique for the measurement of all nine elastic coefficients of the cortical bone. This method is a very undemanding in the term of the performance of the respective experiment, but the specimen preparation is a quite laborious. The combination of the immersion and the contact technique, as it was accomplished in this thesis, seems to be a suitable option in the determination of elastic coefficients of the cortical bone, whereas the criterion of biological material handling and preparation should be also considered during the decision making within the type of the experimental technique preference.

Resonant ultrasonic techniques should be also tested for the evaluation of elastic coefficients of the bone tissue in the future research even through the failure of the RUS measurement realized in this work. Resonant measurements are depended on many factors such as the very precise specimen preparation regarding the exact rectangularity of the specimen, the crystallographic orientation during measurement and factors such as the experimental instrumentation. All these reasons has great influence on the determination of elastic coefficients via the minimization of measured and calculated resonant frequencies in the RUS procedure and may also influence the better identification of vibrational frequencies. Additional devices such as the laser vibrometer should be used in the conjunction with the RUS in the future in the order to obtain an information concerning vibrational modes.

The thesis has the interdisciplinary character: it associates the knowledge of medical sciences and principles of the solid phase mechanics (continuum mechanics, propagation of elastic waves in solids) and experimental techniques. The work is related to the basic research, the procedure of the elastic coefficient determination is the unique in the worldwide relevance and results are widely exercisable in many scientific fields such as the improvement of input data into FEA models of long bones implants and joint replacements. This work may contribute to the design innovation of these products and to improve theirs usage in the clinical practice.

The future research should be addicted to the mapping of such acoustical and elastic parameters that are readily detectable and appropriate for the automatized data evaluation. This direction is in line with the work of Bensamoun [Bensamoun *et al.*, 2004]. Furthermore, the viscoelastic behaviour as well as the influence of fluid components on an attenuation of the compact bone should be investigated via the measuring of the velocities and the attenuation at various frequencies. Heterogeneous characteristics such as an age, weight, a sample preparation and a storage should be taken into the account. The influence of the soft tissue should be also observed and considered in order to improve the in-vivo detection of acoustic parameters.

From the literature overview (Chapter 3) ensues, that investigation of material properties of not only the cortical, but also the cancellous bone, is the priority challenging task for the contemporary research. However, the cortical bone can't be regarded as a linear elastic continuum due to its porosity and a fluid flow. The reliable theoretical model of cancelous bone must be proposed and validated in order to obtain constitutive relations. The several attempts of such model creation were proposed, from the application of the well known Biot's theory [Hughes *et al.*, 2003], up to the more complicated cellular spring-network model [Ladd and Kinney, 1997], the model based on continuum micro-mechanics [Hellmich *et al.*, 2004] or micro-mechanical model, which also includes fluid flow [Gururaja *et al.*, 2005]. The numerical FEA models are also currently

used for the evaluation of the bone's elastic properties [TAYLOR *et al.*, 2002] or the work of Jasiuk [JASIUK and OSTOJA-STARZEWSKI, 2004], where the FEA is used for modelling at a single lamela level. The validation of such a theoretical model and the formulation of necessary parameters for the implementation of an experimental methodology is one of most important tasks in the future research of the bone tissue biomechanics.

Table 14: Resultant elastic coefficients c_{44}, c_{55} and c_{66} obtained by the contact measurement of cubic and slice samples by shear transducers.
Letters B-F: Transducer positioning on slice specimens (Figure 12); 1: Radial direction, 2: circumferential direction, 3: Longitudinal direction.

Specimen specification	**Direction of wave propagation**	**Transducers polarization**	**Velocity [mm/μs]**	**c_{ij} specification**	**Value of c_{ij} [GPa]**
Cube #5	3	1	1.913	c_{55}	7.688
	3	2	2.283	c_{44}	10.945
	2	1	1.755	c_{66}	6.468
	2	3	2.253	c_{44}	10.657
	1	2	1.750	c_{66}	6.424
	1	3	1.833	c_{55}	7.059
Cube #6	3	1	1.770	c_{55}	6.578
	3	2	2.205	c_{44}	10.208
	2	1	1.875	c_{66}	7.387
	2	3	2.213	c_{44}	10.282
	1	2	1.843	c_{66}	7.131
	1	3	1.742	c_{55}	6.374
Slice #5 - B	3	1	1.992	c_{55}	7.145
B	3	2	2.246	c_{44}	9.083
C	3	1	2.049	c_{55}	7.555
C	3	2	2.182	c_{44}	8.567
D	3	1	1.953	c_{55}	6.866
D	3	2	2.196	c_{44}	8.680
E	3	1	1.982	c_{55}	7.073
E	3	2	2.256	c_{44}	9.165
Slice #6 - C	3	1	1.909	c_{55}	6.557
C	3	2	2.108	c_{44}	7.998
D	3	1	1.986	c_{55}	7.096
D	3	2	2.210	c_{44}	8.793
E	3	1	1.945	c_{55}	6.809
E	3	2	2.214	c_{44}	8.819
F	3	1	2.001	c_{55}	7.209
F	3	2	2.210	c_{44}	8.793

Investigation of residual stresses by means of the hole drilling method regarding the infulence of eccentricity of the drilled hole

Author: Karel Doubrava

Department of Mechanics, Faculty of Mechanical Engineering, Czech Technical University in Prague, Czech Republic, Technická 4, 166 07 Prague

<Karel.Doubrava@fs.cvut.cz>

Annotation

Problem of investigation of residual stresses by means of hole drilling method with infulence of eccentricity of drilled hole is studied. State of the art is described. Aims of this work are the description of the problem of the eccentred hole, the determination of the response of the strain gauges around eccentred hole, and the conception of the method of the residual stresses calculation, which takes into account the eccentricity of the hole with respect the centre of the strain gauge rosette. This problem was simulated by means of FEM model and results of this symulation ware used to found new formula for describing state of the residual stress in a construction. Based on these results, the procedure of residual stress determination was designed. This methodology was applied to the outcome of the numerical experiment. Influence of eccentricity of the hole is described and proposed procedure of investigation can improve residual stress determination.

Seznam použitého značení

Označení	**Význam**
ε [-]	deformace
σ [MPa]	napětí
E [MPa]	modul pružnosti v tahu
μ [-]	Poissonovo číslo
A, B, C [MPa^{-1}]	analytické koeficienty odvrtávací metody
$\bar{A}, \bar{B}$ [MPa^{-1}]	kalibrační koeficienty odvrtávací metody
$\bar{a}, \bar{b}$ [-]	bezrozměrné kalibrační koeficienty odvrtávací metody
p, q, t [-]	kombinace deformací
P, Q, T [MPa]	kombinace napětí
R_0 [mm]	poloměr vrtaného otvoru
D_0 [mm]	průměr vrtaného otvoru
r_m [mm]	střední poloměr tenzometrické růžice
D [mm]	střední průměr tenzometrické růžice

Úvod

Výroba součástí sebou přináší namáhání materiálu při technologických operacích, kterým je příslušná součást podrobena. Většina těchto technologických operací má za následek vznik zbytkových napětí. Tato napětí mohou mít různý charakter ať co se týče charakteristiky orientace, hloubkového či plošného gradientu. Znalost zbytkových napětí se stává podstatnou při posuzování zatížení dané konstrukce. V současné době je po mnohých výrobcích tato znalost požadována jejich zákazníky (např. [Holý *et al.*, 2002a], [Holý *et al.*, 2002b], [Doubrava *et al.*, 2003c]).

V posledních letech lze zaznamenat znatelný nárůst možností výpočetní techniky a vzrůst významu numerických simulací při návrhu výrobků. I přes pokrok ve výkonu a ve vlastnostech numerických metod, zvláště pak metody konečných prvků, není v současné době možné u většiny součástí přesně namodelovat proces vzniku daného výrobku, čímž by bylo možné spočíst hodnoty zbytkových napětí na konci výrobního procesu. Z tohoto důvodu hrají experimentální metody stále významnou roli při určování hladiny zbytkových napětí konstrukcí.

Experimentální metody pro určování zbytkových napětí lze rozdělit podle řady kriterií, kdy můžeme zohledňovat způsob poškození konstrukce po provedení měření, fyzikální princip metody, či kterého druhu zbytková napětí daná metoda zjišťuje. Lze tedy hovořit o metodách destrukčních, semidestrukčních či nedestrukčních z hlediska míry poškození konstrukce, metodách fyzikálních, jako jsou metody rentgenové nebo neutronové difrakce [Lu, 1996], Barkhausenův šum [Gauthier *et al.*, 1998], akustoelasticita [He and Kobayashi, 2001], [Fukuoka *et al.*, 1978]

aj. a v neposlední řadě metody mechanické – metoda odvrtávací, metoda pásků, metoda Sachsova [Heténi, 1950] a další.

Jednou z nejrozšířenějších experimentálních metod pro určování zbytkových napětí je metoda odvrtávací. Tato metoda je založena na narušení silové a momentové rovnováhy uvnitř tělesa vyvrtáním kruhového otvoru, ať už slepého nebo průchozího. Velikost vyvrtaného otvoru bývá často vůči rozměrům zkoumané konstrukce zanedbatelná a proto se tato metoda řadí mezi metody semidestruktivní. Zaznamenání uvolněných deformací se nejčastěji provádí pomocí speciální tenzometrické růžice, kdy vrtání otvoru se provádí do středu této růžice. V současné době se v publikacích objevují nové metody využívající optických metod snímání uvolněných deformací. Rovněž jsou publikovány varianty této metody, kdy místo otvoru je do součásti vyfrézována mezikruhová drážka. Změřené uvolněné deformace slouží jako vstup pro metody určující zbytkové napětí u dané konstrukce. Počátky odvrtávací metody sahají do 30. let 20. století a od té doby byla publikována řada metod k vyhodnocení zbytkových deformací získaných touto metodou.

Výrobci rozličné řady produktů jsou svými zákazníky donuceni deklarovat hodnoty zbytkových napětí v jejich výrobcích, kdy požadují zjišťování zbytkových napětí dle uznávaných norem. Nejčastěji vyžadovaná norma zabývající se touto otázkou je ASTM STANDARD E837. V této normě jsou předepsány podmínky zhotovení otvoru a vyhodnocení napětí. V případě excentricity vyvrtaného otvoru vůči středu tenzometrické růžice je tato norma konzervativní a neumožňuje zohlednit vyšší hodnoty excentricity otvoru, s kterými jsme se setkali při praktické aplikaci odvrtávací metody.

V této práci je podán přehled současného stavu vyhodnocování odvrtávací metody. V další části je pomocí metody konečných prvků řešen stav v případě otvoru excentrického vůči středu tenzometrické růžice a dále navržen postup pro zohlednění excentricity otvoru. Navržený postup byl ověřen pomocí numerického experimentu a dále aplikován na reálná data.

Přehled o současném stavu vyhodnocování zbytkových napětí pomocí odvrtávací metody

Historie

Zbytková napětí I. druhu se projevují tím, že po narušení silové a momentové rovnováhy vnitřních účinků, dojde ke změně rozměrů a tvaru zkoumaného tělesa. Zbytková napětí II. druhu dosahují rovnováhy v oblasti několika zrn a v jednotlivých zrnech jsou homogenní. Zbytková napětí III. druhu se projevují v objemu několika atomových vzdáleností a jsou nehomogenní i v nejmenších oblastech materiálu. Zbytková napětí těchto tří druhů se vyskytují současně, i když pod pojmem zbytková napětí se v technické praxi zpravidla rozumí pouze zbytková napětí I. druhu. Historie přinesla mnoho metod, kdy narušení materiálu nebo jeho odebrání uvolní zbytkové deformace. Materiál je možné narušovat různými postupy od odebrání vrstev soustružením, odleptáváním, vyřezáváním drážek či vrtáním otvoru. Vrtání otvoru se nabízí jako jednoduše proveditelné pro většinu materiálů, které se v konstrukční praxi používají.

V ranné podobě tento postup publikoval Mathar [Mathar, 1934]. Pro měření uvolněných deformací používal mechanické tenzometry. Praktické použití publikoval například Soete [Soete, 1954], kdy byly řešeny problémy destrukcí lodí třídy Liberty, způsobených zbytkovým napětím. V tomto případě se závislost mezi uvolněnými deformacemi a zbytkovým napětím určovala experimentálně. Pro měření uvolněných deformací se použily jednosměrné odporové tenzometry. V rozvinutějším stádiu byla tato metoda publikována např. Rendlerem [Rendler and Vigness, 1966]. Zde se k nalezení vztahů mezi uvolněnými deformacemi a zbytkovým napětím použila experimentální kalibrace. Tato práce představuje základ dnes používaných metod a norem. Rozvoj výpočetní techniky přinesl možnost použití numerických metod, jako je třeba metoda konečných prvků nebo metoda hraničních prvků, což umožnilo přesnější určení potřebných koeficientů.

Zde je třeba zmínit práce Schajera [Schajer, 1981]. V dalších letech byly publikovány postupy pro použití odvrtávací metody v případě nekonstantního průběhu zbytkových napětí s hloubkou [Schajer, 1988a], [Schajer, 1988b] a v rovině [Kabiri, 1984], [Luh and Heang, 1999], [Nawwar and Shewchuk, 1978]. Schajer [Schajer and Yang, 1994] rovněž publikoval modifikaci odvrtávací metody pro případ ortotropických materiálů.

Teoretický základ odvrtávací metody

Základní teorie vychází z analytického řešení desky s vyvrtaným průchozím otvorem. Toto řešení bylo publikováno Prof. G. Kirchem [Timoshenko and Goodier, 1951]. Jedná se o tenkou desku zatíženou dvouosou napjatostí a s předpokládaným konstantním průběhem napětí s hloubkou.

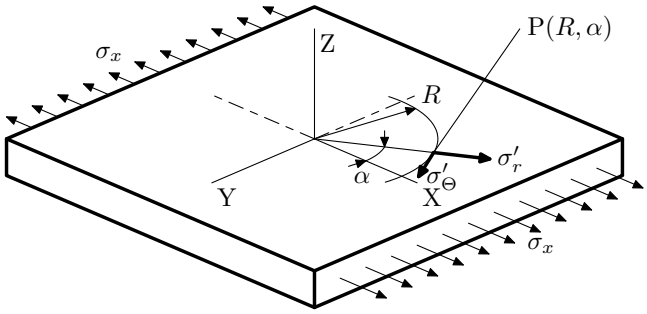

Obr. 29: Tenká deska s jednoosým namáháním

Napjatost u tenké desky (obr. 29) zatížené jednoosou napjatostí σ_x lze v jakémkoliv bodě vyjádřit pomocí polárních souřadnic vztahy:

$$\sigma'_r = \frac{\sigma_x}{2}(1 + \cos 2\alpha) \tag{58}$$

$$\sigma'_\Theta = \frac{\sigma_x}{2}(1 - \cos 2\alpha) \tag{59}$$

$$\tau'_{r\Theta} = -\frac{\sigma_x}{2} \sin 2\alpha \tag{60}$$

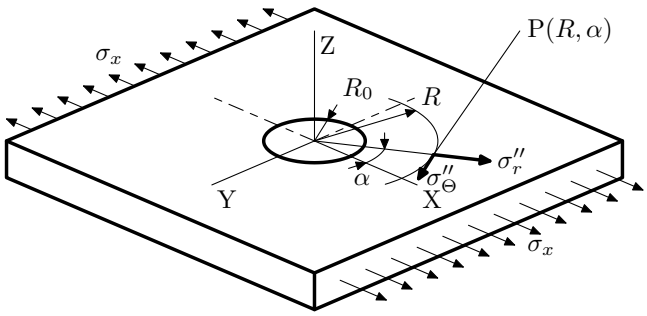

Obr. 30: Tenká deska s jednoosým namáháním s průchozím otvorem

Pro případ desky s průchozím otvorem (obr. 30) je napjatost na základě Kirschova řešení vyjádřena vztahy:

$$\sigma''_r = \frac{\sigma_x}{2}\left(1 - \frac{1}{r^2}\right) + \frac{\sigma_x}{2}\left(1 + \frac{3}{r^4} - \frac{4}{r^2}\right)\cos 2\alpha \tag{61}$$

$$\sigma''_{\Theta} = \frac{\sigma_x}{2}\left(1+\frac{1}{r^2}\right) - \frac{\sigma_x}{2}\left(1+\frac{3}{r^4}\right)\cos 2\alpha \tag{62}$$

$$\tau''_{r\Theta} = \frac{\sigma_x}{2}\left(1+\frac{3}{r^4}-\frac{4}{r^2}\right)\sin 2\alpha \tag{63}$$

kde:

$$r = \frac{R}{R_0} \quad (R \geq R_0)$$

$R_0 \ldots$ poloměr otvoru
$R \ldots$ vzdálenost od středu otvoru

Odečtením původního napětí od konečného po odvrtání otvoru získáme změnu napětí v bodě $\mathrm{P}(R,\alpha)$ po odvrtání otvoru.

$$\Delta\sigma_r = \sigma''_r - \sigma'_r \tag{64}$$

$$\Delta\sigma_{\Theta} = \sigma''_{\Theta} - \sigma'_{\Theta} \tag{65}$$

$$\Delta\tau_{r\Theta} = \tau''_{r\Theta} - \tau'_{r\Theta} \tag{66}$$

Dosazením vztahů (58) – (60) a (61) – (63) do vztahů (64) – (66) získáme úplný vztah pro vyjádření uvolněných zbytkových napětí. Pokud je zkoumaný materiál ve svých mechanických vlastnostech homogenní a izotropický a je-li možné považovat závislost napětí na deformaci za lineární, pak za použití Hookova zákona pro dvojosou napjatost lze popsat uvolněné deformace v bodě $\mathrm{P}(R,\alpha)$ vztahy:

$$\varepsilon_r = -\frac{\sigma_x(1+\mu)}{2E}\left[\frac{1}{r^2} - \frac{3}{r^4}\cos 2\alpha + \frac{4}{r^2(1+\mu)}\cos 2\alpha\right] \tag{67}$$

$$\varepsilon_{\Theta} = -\frac{\sigma_x(1+\mu)}{2E}\left[-\frac{1}{r^2} + \frac{3}{r^4}\cos 2\alpha - \frac{4\mu}{r^2(1+\mu)}\cos 2\alpha\right] \tag{68}$$

Předchozí rovnice lze upravit do následujícího tvaru

$$\varepsilon_r = \sigma_x(A + B\cos 2\alpha), \tag{69}$$

$$\varepsilon_{\Theta} = \sigma_x(-A + C\cos 2\alpha), \tag{70}$$

kde koeficienty A, B a C jsou vyjádřeny vztahy

$$A = -\frac{1+\mu}{2E}\left(\frac{1}{r^2}\right), \tag{71}$$

$$B = -\frac{1+\mu}{2E}\left[\left(\frac{4}{1+\mu}\right)\frac{1}{r^2} - \frac{3}{r^4}\right], \tag{72}$$

a

$$C = -\frac{1+\mu}{2E}\left[\left(-\frac{4\mu}{1+\mu}\right)\frac{1}{r^2} - \frac{3}{r^4}\right]. \tag{73}$$

Na obr. 31 je znázorněn průběh radiálních a tečných deformací jako funkcí poměrného poloměru r. Z obrázku je patrné, že uvolněná deformace v závislosti na vzdálenosti od otvoru se blíží k nule. Na druhou stranu v blízkosti otvoru je v případě skutečného tělesa zóna ovlivněná

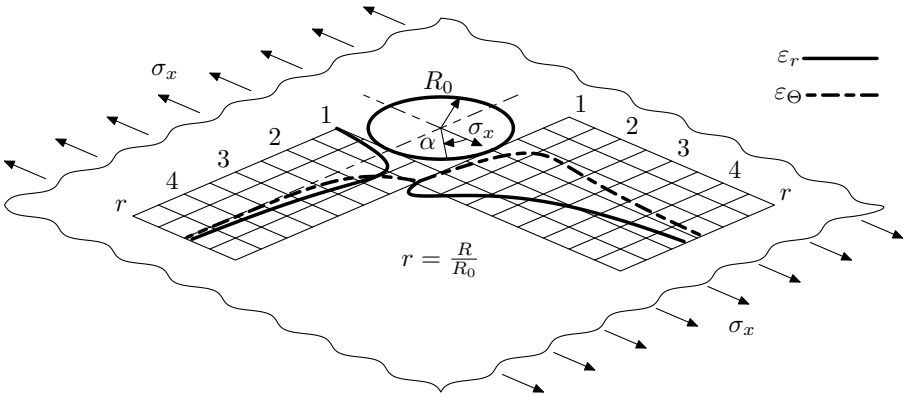

Obr. 31: Průběh radiálních a tečných deformací u desky s vyvrtaným otvorem [tn5, 1985]

vrtáním otvoru. To je důvod, proč se optimální poměrný poloměr r pro umístění tenzometru dle normy ASTM nachází v intervalu (2,5 – 3,4).

Z obrázku je zřejmé, že v případě úhlu $\alpha = 0°$ je v doporučené oblasti, odpovídající intervalu $r \in$(2,5 – 3,4), radiální deformace skoro třikrát větší než deformace tangenciální. Z tohoto důvodu je většina komerčně dodávaných tenzometrických růžic vyrobena s tenzometry orientovanými v radiálním směru. Vztahy byly odvozeny pro nejednodušší případ pro jednoosou napjatost. V reálném tělese se však předpokládá napjatost rovinná. Za předpokladu lineárně elastického materiálu lze použít princip superpozice k získání vztahů pro celkovou radiální deformaci. Působí-li napětí ve směru osy Y , lze vyjádřit radiální deformaci v bodě P(R, α) vztahem

$$\varepsilon_r^y = \sigma_y(A - B\cos 2\alpha) \tag{74}$$

a v případě jednoosé napjatosti ve směru X vztahem

$$\varepsilon_r^x = \sigma_x(A + B\cos 2\alpha). \tag{75}$$

Pokud působí obě napětí současně, princip superpozice umožňuje sečíst vztahy (74) a (75). Výsledný vztah pak popisuje radiální deformaci pro dvojosou napjatost

$$\varepsilon_r = \sigma_x(A + B\cos 2\alpha) + \sigma_y(A - B\cos 2\alpha), \tag{76}$$

respektive po malých úpravách

$$\varepsilon_r = A(\sigma_x + \sigma_y) + B(\sigma_x - \sigma_y)\cos 2\alpha. \tag{77}$$

Rovnice (76) a (77) jsou základními vztahy pro určení dvou hlavních napětí a úhlu jejich natočení. Pro určení těchto tří neznámých je potřeba získat tři rovnice. Ty můžeme získat například vyjádřením radiálních deformací ve třech různých směrech. To může být provedeno najednou pomocí tenzometrické růžice (obr. 32). Za předpokladu limitní plochy tenzometru a pro případ zobrazené 45° růžice lze pro jednotlivé tenzometry napsat odpovídající radiální deformace tenzometrů 1, 2 a 3.

$$\varepsilon_1 = A(\sigma_x + \sigma_y) + B(\sigma_x - \sigma_y)\cos 2\alpha \tag{78}$$

$$\varepsilon_2 = A(\sigma_x + \sigma_y) + B(\sigma_x - \sigma_y)\cos 2(\alpha + 45°) \tag{79}$$

$$\varepsilon_3 = A(\sigma_x + \sigma_y) + B(\sigma_x - \sigma_y)\cos 2(\alpha + 90°) \tag{80}$$

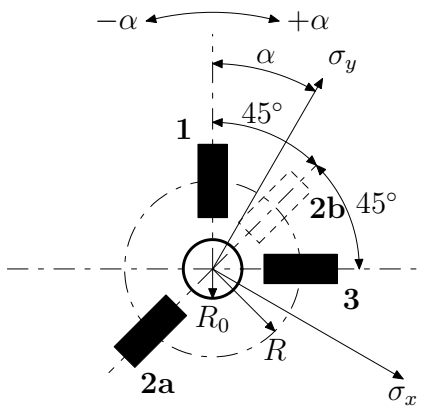

Obr. 32: Schéma tenzometrické růžice

Řešení těchto rovnic je pak možné vyjádřit vztahy (81, 82 a 83).

$$\sigma_{max} = \frac{\varepsilon_1 + \varepsilon_2}{4A} + \frac{\sqrt{2}}{4B}\sqrt{(\varepsilon_1 - \varepsilon_2)^2 + (\varepsilon_2 - \varepsilon_3)^2} \tag{81}$$

$$\sigma_{min} = \frac{\varepsilon_1 + \varepsilon_2}{4A} - \frac{\sqrt{2}}{4B}\sqrt{(\varepsilon_1 - \varepsilon_2)^2 + (\varepsilon_2 - \varepsilon_3)^2} \tag{82}$$

$$\tan 2\alpha = \frac{\varepsilon_1 - 2\varepsilon_2 + \varepsilon_3}{\varepsilon_3 - \varepsilon_1} \tag{83}$$

Takto určená napjatost odpovídá pouze ideálnímu případu, splňujícímu výše uvedené předpoklady a popisuje napjatost v bodě o souřadnicích (r, α) okolo průchozího otvoru v nekonečně rozlehlé desce a za předpokladu konstantního průběhu napětí po hloubce otvoru. Deformace změřená skutečným tenzometrem odpovídá průměrné deformaci v radiálním směru pod plochou vinutí tenzometru. Ne všechny smyčky vinutí mají směr odpovídající radiálnímu směru, takže do naměřené hodnoty radiální deformace se projeví i tangenciální složka uvolněných deformací. Koeficienty $\bar{A}$ a $\bar{B}$ pro skutečné tenzometry lze získat integrací přes skutečnou plochu vinutí tenzometru a nebo experimentální kalibrací.

Experimentální kalibrace

V následujícím odstavci je popis experimentální kalibrace publikované Rendlerem [RENDLER and VIGNESS, 1
Autoři předpokládali jednoose namáhaný vzorek, a že změnu deformace, vyvolanou vyvrtáním kroku z hloubky z do hloubky $z + \Delta z$, lze popsat vztahem

$$\Delta\varepsilon_z(\alpha) = K_z(\alpha)\sigma_z\Delta z, \tag{84}$$

kde σ_z je napětí v hloubce z, α je úhel mezi směrem radiální deformace a osou napětí, $\varepsilon_z(\alpha)$ je radiální deformace v směru daném úhlem α uvolněná vyvrtáním kroku o velikosti Δz a $K_z(\alpha)$ je parametr, který je konstantní pro dané z, Δz a α.

Pro případ vyvrtaného otvoru do koncové hloubky a stavu dvojosé napjatosti, lze radiální deformaci vyjádřit vztahem

$$\varepsilon(\alpha) = K(\alpha)\sigma_{max} + K(\alpha + 90°)\sigma_{min}, \tag{85}$$

kde úhel α je měřen od směru σ_{max}.

Rendler zavádí funkci $K(\alpha)$ ve zjednodušeném tvaru

$$K(\alpha) = \bar{A} + \bar{B}\cos(2\alpha), \tag{86}$$

kde konstanty $\bar{A}$ a $\bar{B}$ jsou závislé na materiálu a geometrii vrtaného otvoru. Hodnota $K(\alpha)$ z (86) dosazená do (85) pak představuje vztah, pomocí něhož lze ze tří signálů ze tří tenzometrů určit hlavní napětí a jejich polohu vůči geometrii růžice. Předpokladem je ale znalost konstant $\bar{A}$ a $\bar{B}$. Rendler tyto konstanty určuje pomocí experimentální kalibrace, kdy v případě jednoosé napjatosti o velikosti σ lze tyto konstanty vyjádřit jako

$$\bar{A} = \frac{\varepsilon_1 + \varepsilon_3}{2\sigma}, \tag{87}$$

$$\bar{B} = \frac{\varepsilon_1 - \varepsilon_3}{2\sigma}, \tag{88}$$

za předpokladu, že směr prvního tenzometru je totožný se směrem jednoosé napjatosti.

V případě experimentální kalibrace je třeba brát v potaz možnost přítomnosti zbytkových napětí v kalibračním vzorku. Změna deformace zaznamenaná po vyvrtání otvoru na zatíženém vzorku je poté vyvolaná, jak aplikovaným zatížením, tak i zbytkovým napětím přítomným ve vzorku. Rendler separuje zbytková napětí například způsobem znázorněným na obr. 33.

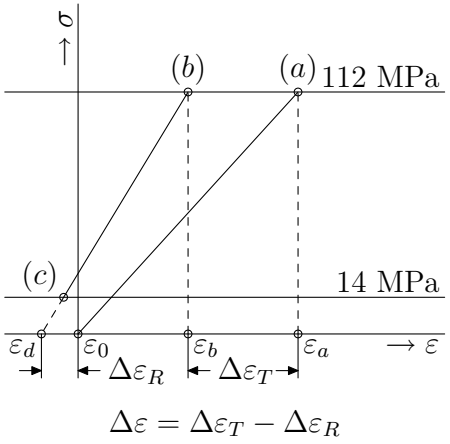

Obr. 33: Metoda separace zbytkové deformace [Rendler and Vigness, 1966]

Vzorek byl nejprve zatížen tak, aby bylo dosaženo napětí 112 MPa a byla odečtena deformace ε_a (bod a). Po odvrtání jednoho kroku hloubky byla zaznamenána uvolněná deformace $\Delta\varepsilon_T = \varepsilon_a - \varepsilon_b$. Poté bylo zatížení sníženo na hodnotu 14 MPa a byla zaznamenána hodnota deformace ε_c. Grafickou extrapolací vzniklé přímky do nulové osy byl získán bod d odpovídající deformaci ε_d, která byla způsobena zbytkovým napětím. Pokud je ε_0 deformace při nulovém zatížení vzorku před vyvrtáním přírůstku hloubky, tak deformace $\Delta\varepsilon_R = \varepsilon_0 - \varepsilon_d$ odpovídá zbytkovému napětí v materiálu v příslušné hloubce vrtu. Přírůstek deformace odpovídající čistě zatížení daného vzorku, je pak dán rozdílem $\Delta\varepsilon = \Delta\varepsilon_T - \Delta\varepsilon_R$.

Postupy používané pro vyhodnocování zbytkových napjetí

Normovaná metoda ASTM E837

Organizace ASTM vydala normu s označením E837 [E83, 2001], která prochází aktualizacemi. Tato norma předpokládá použití tříprvkové růžice, odpovídající schématu na obr. 32. Předpokládá se vyvrtání otvoru o hloubce odpovídající 0,4 násobku středního průměru růžice D ($D = 2r_m$) a odměření uvolněných deformací pomocí příslušných zařízení. Pro závislost mezi hlavními napětími a radiální uvolněnou deformací se používá vztah analogický (76):

$$\varepsilon_r = \sigma_{max}(\bar{A} + \bar{B}\cos 2\alpha) + \sigma_{min}(\bar{A} - \bar{B}\cos 2\alpha), \tag{89}$$

kde konstanty $\bar{A}$ a $\bar{B}$ lze vyjádřit následujícími vztahy

$$\bar{A} = -\bar{a}(1+\mu)/(2E), \tag{90}$$

$$\bar{B} = -\bar{b}/(2E), \tag{91}$$

kdy bezrozměrné konstanty $\bar{a}$ a $\bar{b}$ jsou materiálově téměř nezávislé [E83, 2001] a jejich hodnoty pro průchozí a slepý otvor jsou touto normou tabelovány.

Pomocí tenzometrické růžice jsou změřeny uvolněné deformace. Norma uvádí přípustné geometrie tenzometrických růžic vhodných pro určování zbytkových napětí, kde se nejčastěji používají růžice tříprvkové, ale jsou možné i jiné geometrie růžic. Například Schajer [SCHAJER and TOOTOONIAN, navrhl šestiprvkovou růžici, kdy tři tenzometry v rozložení odpovídající růžici 45° mají vinutí přesně v radiálním směru a jsou doplněny o tenzometry s vinutím v tangenciálním směru. Tyto tenzometry jsou v příslušných dvojicích zapojeny do půlmostu. Tato úprava by měla zajistit vyšší citlivost měřícího řetězce. Tenzometrické růžice odpovídající normě lze nalézt ve výrobních programech všech významných producentů tenzometrů. Pro měření uvolněných deformací norma předpokládá použití tenzometrické aparatury s rozlišením minimálně $\pm 2 \cdot 10^{-6}$ μm/m. Příprava vzorku pro instalaci tenzometrické růžice musí být provedena takovým způsobem, aby nedošlo k ovlivnění povrchových zbytkových napětí.

Vrtaný otvor nesmí svými rozměry ohrozit vinutí tenzometrů v růžici. Norma uvádí povolenu vzdálenost 0,3 mm mezi okrajem vrtaného otvoru a koncem vinutí tenzometru. Tento rozměr pak představuje maximální průměr vrtaného otvoru D_0. Minimální rozměr vrtaného otvoru je pak uveden jako 60% maximálního průměru. Norma uvádí doporučené rozměry vrtaného otvoru pro příslušné tenzometrické růžice. S rostoucím poměrem D_0/D citlivost roste přibližně dle vztahu $(D_0/D)^2$. Excentricita vrtaného otvoru a středu růžice by neměla přesahovat větší z rozměrů a to buď $\pm 0,004 \cdot D$ nebo $\pm 0,025$ mm.

Výběr vrtací techniky a nástroje by měl být proveden s ohledem na minimalizaci, případně eliminaci plastických deformací v okolí otvoru. Technologie vrtání uváděné touto normou jako vhodné jsou abrazivní odtryskávání, vrtání s vysokou řeznou rychlostí, kdy se používá vzduchová turbínka, či vrtání za nízkých řezných rychlostí. Má se za to, že pro většinu konstrukčních materiálů, s výjimkou materiálů extrémně tvrdých, je nejvhodnější technika vrtání s vysokou řeznou rychlostí.

Vzorek, jehož tloušťka je alespoň $1,2 \cdot D$, se dle normy označuje jako „tlustý“. V případě tohoto vzorku se provádí vrtání po krocích $0,05 \cdot D$ do konečné hloubky $0,4 \cdot D$. Po odvrtání každého kroku se provede odečtení uvolněných deformací. Norma umožňuje použít i jinou velikost vrtacích kroků.

Vzorek, jehož tloušťka je menší než $0,4 \cdot D$, se označuje jako „tenký“. V tomto případě se provede průchozí vrtání a poté se odečtou hodnoty uvolněných deformací.

V případě, že tloušťka vzorku je v rozmezí $(0,4 - 1,2) \cdot D$, je možné získat přibližné výsledky vyvrtáním průchozího otvoru a použitím interpolace mezi konstantami pro neprůchozí a průchozí otvor.

Pro každou sadu naměřených deformací $\varepsilon_1, \varepsilon_2$ a ε_3 je potřeba spočíst kombinace deformací:

$$p = (\varepsilon_3 + \varepsilon_1)/2 \tag{92}$$

$$q = (\varepsilon_3 - \varepsilon_1)/2 \tag{93}$$

$$t = (\varepsilon_3 + \varepsilon_1 - 2\varepsilon_2)/2 \tag{94}$$

V případě „tlustých“ vzorků je potřeba provést test pro ověření konstantnosti zbytkových napětí v závislosti na hloubce. V případě nesplnění tohoto testu není tato metoda vhodná.

Výpočet zbytkových napětí dle normy E837 předpokládá konstantní průběh zbytkových napětí.

Pro „tenké“ vzorky se měřením získají tři hodnoty uvolněných deformací ε_1, ε_2 a ε_3, což umožňuje určit hodnoty hlavních napětí a jejich směr. Norma předpokládá, že získaná napětí jsou po celé tloušťce konstantní. Největší tahové hlavní napětí σ_{max} je orientováno úhlem α od osy tenzometru 1 na obr. 32, kdy úhel α lze spočíst vztahem

$$\alpha = \frac{1}{2}\arctan\left(t/q\right) \tag{95}$$

Hlavní napětí se pak spočítají dle vztahu

$$\sigma_{max}, \sigma_{min} = -\left[p/\bar{a}(1+\mu) \pm \sqrt{(q^2+t^2)/\bar{b}}\right] E. \tag{96}$$

V případě „tlustého“ vzorku se postupuje podobně, jako u vzorku „tenkého“. Pro každou sadu naměřených deformací z každého kroku se odečtou hodnoty příslušných kalibračních konstant $\bar{a}$ a $\bar{b}$ a na jejich základě se pak spočtou tři kombinace napětí P, Q a T.

$$P = \frac{-E}{(1+\mu)} \cdot \frac{\sum \bar{a} \cdot p}{\sum \bar{a}^2} \tag{97}$$

$$Q = -E \cdot \frac{\sum \bar{b} \cdot q}{\sum \bar{b}^2} \tag{98}$$

$$T = -E \cdot \frac{\sum \bar{b} \cdot t}{\sum \bar{b}^2} \tag{99}$$

Úhel α se spočte dle obdobného vztahu jako v případě vzorku „tenkého“

$$\alpha = \frac{1}{2}\arctan\frac{-T}{-Q} \tag{100}$$

a hlavní napětí s poté určí ze vztahu

$$\sigma_{max}, \sigma_{min} = P \pm \sqrt{(Q^2+T^2)}. \tag{101}$$

V této normě je dále popsán postup experimentálního určení kalibračních konstant $\bar{a}$ a $\bar{b}$.

Určování zbytkových napětí u napětí nekonstantního s hloubkou

Metoda ASTM E837, popsaná v minulém odstavci, předpokládá průběh zbytkových napětí v závislosti na hloubce konstantní anebo jen mírně se měnící. Metody umožňující určit průběh v případě nekonstantního napětí budou předmětem tohoto pododdílu.

Přírůstková metoda Tato metoda předpokládá měření uvolněných deformací v postupných malých krocích hloubky otvoru. Velikost napětí, které bylo v odvrtaném dílku, se pak vypočítá za předpokladu, že přírůstek uvolněné deformace je celý způsoben napětím, které bylo původně v odvrtaném dílku hloubky otvoru. Pro každý dílek hloubky musí být použity vlastní hodnoty kalibračních konstant $\bar{a}$ a $\bar{b}$. Tyto kalibrační konstanty jsou pro každou hloubku díry určovány experimentálně postupným odvrtáváním vzorku se známou jednoosou napjatostí. Předpoklad, že uvolněné deformace změřené po vrtání jednoho kroku jsou způsobeny pouze zbytkovým napětím právě uvnitř dílku, však není správný. Po vyvrtání prvního kroku postupně uvolněné deformace kombinují vliv napětí uvnitř odvrtaného dílku a vliv změny geometrie otvoru. Geometrické změny způsobí další uvolnění deformací z napětí z předchozích vrtaných kroků. To má za následek, že uvolněné deformace se mohou zvětšovat, i když by nový vrtaný dílek nebyl zatížen.

Metoda průměrných napětí Tato metoda publikovaná Nickolaem [NICKOLA, 1986] měla překonat nedostatky přírůstkové metody. Metoda je založena na ekvivalentních konstantních napětích, což jsou konstantní napětí po celé hloubce otvoru, která způsobí stejné uvolněné deformace jako skutečný nekonstantní průběh zbytkových napětí. Ekvivalentní napětí jsou počítána za použití kalibračních konstant $\bar{a}$ a $\bar{b}$ pro konstantní pole napjatosti a za použití změřených uvolněných deformací. V případě metody průměrných napětí se ekvivalentní konstantní napětí počítá pomocí uvolněných deformací změřených před a po odvrtání dílku hloubky. Předpokládá se, že ekvivalentní konstantní napětí po odvrtání dílku hloubky odpovídá součtu ekvivalentního konstantního napětí před vyvrtáním dílku hloubky a napětí uvnitř odvrtaného dílku.

$$\sigma_{(z+\Delta z)}(z+\Delta z) = \sigma_{(z)} z + \sigma_{(\Delta z)} \Delta z \tag{102}$$

σ... ekvivalentní konstantní napětí uvnitř popisované oblasti
z... hloubka otvoru před odvrtáním dílku hloubky
Δz... přírůstek hloubky
$z + \Delta z$... hloubka otvoru po odvrtání přírůstku hloubky
Napětí uvnitř kroku se pak spočítá na základě řešení rovnice (102).

Integrální metoda Integrální metoda patří mezi uznávané metody pro vyhodnocování nekonstantního pole zbytkového napětí.

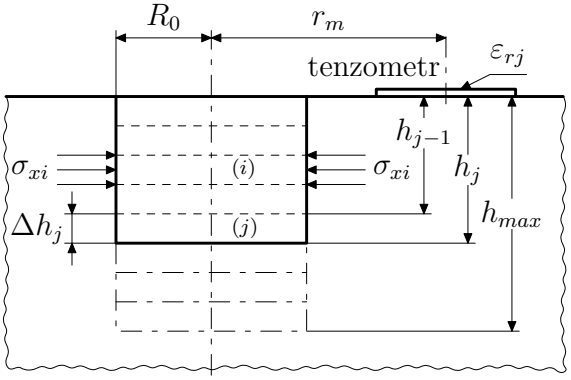

Obr. 34: Integrální metoda – schéma

Tato metoda předpokládá, že na deformaci uvolněnou po vyvrtání otvoru do hloubky h má vliv průběh zbytkového napětí po celé hloubce otvoru (obr. 34). Deformaci uvolněnou po vyvrtání otvoru do hloubky h pak lze vyjádřit vztahem

$$\varepsilon_r(h) = \frac{1}{2E} \int_0^h \left\{ (1+\mu)\hat{A}(H,h)[\sigma_x(H) + \sigma_y(H)] + \hat{B}(H,h)[\sigma_x(H) - \sigma_y(H)] \right\} dH, \tag{103}$$

kde $\sigma_x(H)$ a $\sigma_y(H)$ jsou zbytková napětí ve směrech x a y. Vztah (103) lze přepsat v diskrétním tvaru

$$\varepsilon_{rj} = \frac{1}{2E} \sum_{i=1}^{j} [\bar{a}_{ji}(1+\mu)(\sigma_{xi} + \sigma_{yi}) + \bar{b}_{ji}(\sigma_{xi} - \sigma_{yi})], \quad \text{kde} \quad 1 \le j \le n. \tag{104}$$

Při použití tříprvkové růžice vede vztah (104) při použití (92) – (94) na vztahy

$$p_j = \frac{\varepsilon_{3j} + \varepsilon_{1j}}{2}, \tag{105}$$

$$q_j = \frac{\varepsilon_{3j} - \varepsilon_{1j}}{2}, \tag{106}$$

$$t_j = \frac{\varepsilon_{3j} + \varepsilon_{1j} - 2\varepsilon_{2j}}{2}, \tag{107}$$

respektive pro napětí

$$P_j = \frac{\sigma_{3j} + \sigma_{1j}}{2}, \tag{108}$$

$$Q_j = \frac{\sigma_{3j} - \sigma_{1j}}{2}, \tag{109}$$

$$T_j = \frac{\sigma_{3j} + \sigma_{1j} - 2\sigma_{2j}}{2}. \tag{110}$$

Z rovnice (104) pak vyplývá:

$$p_j = \frac{(1+\mu)}{E} \sum_{i=1}^{j} \bar{a}_{ji} P_i \tag{111}$$

$$q_j = \frac{1}{E} \sum_{i=1}^{j} \bar{b}_{ji} Q_i \tag{112}$$

$$t_j = \frac{1}{E} \sum_{i=1}^{j} \bar{b}_{ji} T_i \tag{113}$$

Složky napětí P_j, Q_j a T_j odpovídající j-té vrstvě pak mohou být určeny na základě řešení rovnic (111) – (113).

$$P_j = \frac{1}{\bar{a}_{jj}} \left[\frac{E p_j}{(1+\mu)} - \sum_{i=1}^{j-1} \bar{a}_{ji} P_i \right] \tag{114}$$

$$Q_j = \frac{1}{\bar{b}_{jj}} \left[E q_j - \sum_{i=1}^{j-1} \bar{b}_{ji} Q_i \right] \tag{115}$$

$$T_j = \frac{1}{\bar{b}_{jj}} \left[E t_j - \sum_{i=1}^{j-1} \bar{b}_{ji} T_i \right] \tag{116}$$

Hlavní napětí $(\sigma_{max,min})_j$ v j-té vrstvě se pak spočtou dle vztahu odpovídjcímu rovnici (101)

$$(\sigma_{max,min})_j = P_j \pm \sqrt{(Q_j^2 + T_j^2)}. \tag{117}$$

Rovnice (114) – (116) lze zapsat pomocí maticového zápisu, takže například

$$\bar{\boldsymbol{A}} \boldsymbol{P} = E\boldsymbol{p}/(1+\mu), \tag{118}$$

kde pro případ čtyř kroků lze psát

$$\bar{\boldsymbol{A}} = \begin{bmatrix} \bar{a}_{11} & & & \\ \bar{a}_{21} & \bar{a}_{22} & & \\ \bar{a}_{31} & \bar{a}_{32} & \bar{a}_{33} & \\ \bar{a}_{41} & \bar{a}_{42} & \bar{a}_{43} & \bar{a}_{44} \end{bmatrix}, \ \boldsymbol{P} = \begin{bmatrix} P_1 \\ P_2 \\ P_3 \\ P_4 \end{bmatrix}, \ \boldsymbol{p} = \begin{bmatrix} p_1 \\ p_2 \\ p_3 \\ p_4 \end{bmatrix}. \tag{119}$$

Určení matice kalibračních konstant $\bar{\boldsymbol{A}}$ je pak naznačeno na obr. 35.

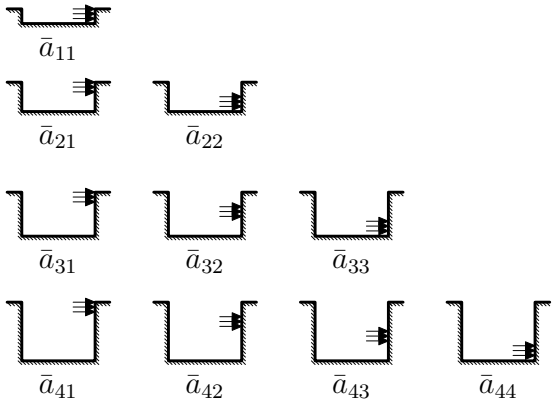

Obr. 35: Zatížení odpovídající koeficientům $\bar{a}_{ij}$ matice $\bar{\boldsymbol{A}}$ [SCHAJER, 1988a]

Určení optimálního kroku vrtání Integrální metoda je velice citlivá na chybu meření uvolněných deformací. To je způsobeno špatnou numerickou podmíněností rovnic (114) – (116). Málá chyba deformací p_j, q_j a t_j způsobí velkou chybu u napětí P_j, Q_j a T_j a následně i u odhadu zbytkových napětí. Podmíněnost pak odpovídá volbě celkového počtu kroků n. Zuccarello [ZUCCARELLO, 1999] publikoval postup pro optimalizaci volby velikosti kroku, tak aby byl zmenšen vliv chyby měření na spočtený průběch zbytkového napětí. Na obr 36 je znázorněn průběh, který byl získán za předpolkladu nahodné chyby změřené deformace v rozsahu $\pm 3\mu$m/m a při použití s počty konstantně velkých kroků $n = 4$ a $n = 9$.

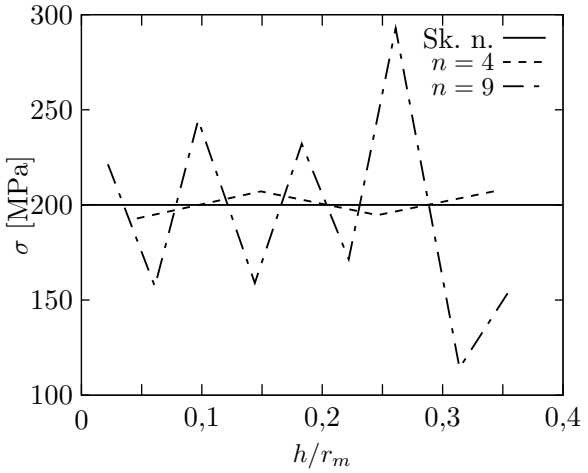

Obr. 36: Vliv počtu konstatních kroků na spočtená zbytková napětí při použití integrální metody [ZUCCARELLO, 1999] (Sk. n. ... skutečné napětí)

V současnosti je volba počtu kroků kompromisem mezi požadovanou citlovostí chyby změřených deformací a určených napětí a požadavkem na podrobný popis průběhu zbytkových napětí s hloubkou. Za předpokladu konstantní velikosti kroků a obvyklé měřící chyby při průběhu odvrtávacího experimentu, vede použití více jak tří případně čtyř kroků k velké chybě u určených zbytkových napětí.

Pro zjednodušení se přepokládalo pole zbytkového napětí, kdy $P = \sigma$ a $p = \varepsilon$ ($Q = T = 0$, $q = t = 0$). Z rovnice (118) vychází

$$\boldsymbol{\sigma} = [E/(1+\mu)]\bar{\boldsymbol{A}} \cdot \boldsymbol{\varepsilon} \tag{120}$$

a potom lze na základě (120) vyjádřit vztah mezi vektorem chyb pro napětí $\boldsymbol{D\sigma}$ a deformace $\boldsymbol{D\varepsilon}$

$$\boldsymbol{D\sigma} = [E/(1+\mu)]\bar{\boldsymbol{A}} \cdot \boldsymbol{D\varepsilon}. \tag{121}$$

Číslo podmíněnosti $K(\bar{\boldsymbol{A}})$ matice $\bar{\boldsymbol{A}}$ pak ukazuje na podmíněnost (120), malé číslo podmíněnosti odpovídá dobře podmíněné soustavě. Z rovnic (120) a (121) pak vyplývá

$$\frac{\|\boldsymbol{D\sigma}\|}{\|\boldsymbol{\sigma}\|} \leq K(\bar{\boldsymbol{A}}) \frac{\|\boldsymbol{D\varepsilon}\|}{\|\boldsymbol{\varepsilon}\|}, \tag{122}$$

kde

$$K(\bar{\boldsymbol{A}}) = \|\bar{\boldsymbol{A}}\| \cdot \|\bar{\boldsymbol{A}}^{-1}\| \tag{123}$$

a $\|\bar{\boldsymbol{A}}\|$ je normou matice $\bar{\boldsymbol{A}}$. Při použití spektrální normy lze číslo podmíněnosti vyjádřit ve tvaru

$$K(\bar{\boldsymbol{A}})_n = \frac{\sum_{i=1}^{n}\sum_{j=1}^{n}(\bar{a}_{ij})^2 + \sqrt{\left[\sum_{i=1}^{n}\sum_{j=1}^{n}(\bar{a}_{ij})^2\right]^2 - 4\prod_{i=1}^{n}(\bar{a}_{ii})^2}}{4\prod_{i=1}^{n}(\bar{a}_{ii})^2}. \tag{124}$$

Z rovnice (124) pak vyplývá, že pro nalezení nejmenšího čísla podmíněnosti $K(\bar{\boldsymbol{A}})$ musí být členy na diagonále konstantní

$$\bar{a}_{jj} = konst.. \tag{125}$$

Metoda mocninné řady Metoda mocninné řady byla publikována Schajerem [Schajer, 1981] jako přibližná, ale teoreticky akceptovatelná metoda pro výpočet nekonstantního pole zbytkové napjatosti. Při použití této metody je potřeba spočítat řadu koeficientů ${}^0\bar{a}(h)$, ${}^1\bar{a}(h)$, ${}^2\bar{a}(h)$ a ${}^0\bar{b}(h)$, ${}^1\bar{b}(h)$, ${}^2\bar{b}(h)$, které odpovídají uvolněným deformacím při vrtání otvoru do pole zbytkového napětí, které je nahrazeno mocninou řadou s proměnou odpovídající hloubce h;(${}^0\sigma(h) = 1$, ${}^1\sigma(h) = h$, ${}^2\sigma(h) = h^2$ atd.). Tento vztah je pak použit jako bázová funkce v metodě nejmenších čtverců pro analýzu naměřených dat. Při zavedení kombinace napětí ve formě $P = (\sigma_y + \sigma_x)/2$, $Q = (\sigma_y - \sigma_x)/2$ a $T = \tau_{xy}/2$ je metoda nejmenších čtverců aplikována na každou uvedenou kombinaci napětí. Transformované napětí $P(h)$ je spočítáno z transformované deformace $p(h)$ za použití vztahů

$$\begin{bmatrix} \sum^0 \bar{a}(h){}^0\bar{a}(h) & \sum^0 \bar{a}(h){}^1\bar{a}(h) \\ \sum^1 \bar{a}(h){}^0\bar{a}(h) & \sum^1 \bar{a}(h){}^1\bar{a}(h) \end{bmatrix} \begin{bmatrix} {}^0P \\ {}^1P \end{bmatrix} = \frac{E}{1+\mu} \begin{bmatrix} \sum^0 \bar{a}(h)p(h) \\ \sum^1 \bar{a}(h)p(h) \end{bmatrix}, \tag{126}$$

$$P(h) =^0 P +^1 Ph, \tag{127}$$

kde ${}^0P$ a ${}^1P$ jsou první dva členy mocninné řady, která popisuje napětí P. Tento výpočet se obdobně provede pro transformované napětí $Q(h)$ a $T(h)$ za použití deformací $q(h)$ a $t(h)$ a koeficientů $\bar{b}(h)$ místo $\bar{a}(h)$. Odvrtávací metoda nedává uspokojivé výsledky při použití více jak prvních dvou členů mocninné řady ve výrazu pro napětí. Z tohoto důvodu je omezena maximální hloubka od povrchu omezena hodnotou $0,5r_m$, kde r_m je střední poloměr tenzometrické růžice (vzdálenost středů vinutí jednotlivých tenzometrů od středu tenzometrické růžice). Použití metody nejmenších čtverců způsobuje zaokrouhlení měřících chyb, na druhou stranu v případě nehladkého průběhu zbytkových napětí tento zaokrouhlující účinek má vliv na celkovou velikost spočtených zbytkových napětí.

Porovnání vyhodnocovacích metod

Schajer [Schajer, 1988a] uvádí srovnání výše zmíněných metod, z kterého vyplývají omezení pro použití. Pro srovnání použil data získaná numerickým experimentem, kdy daná součást byla

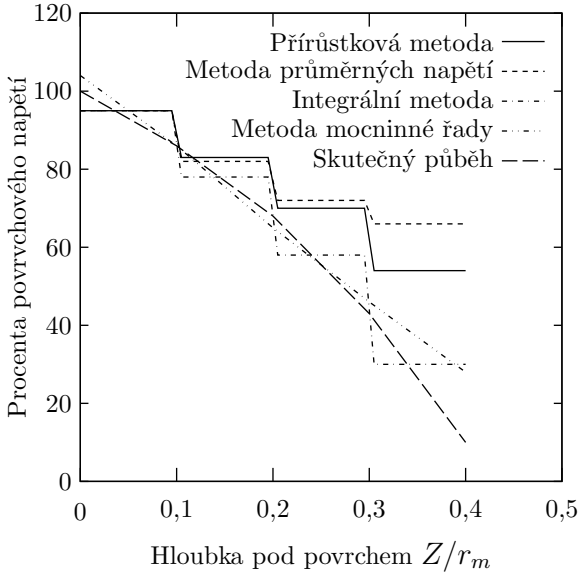

Obr. 37: Vzájemné porovnání vyhodnocovacích metod [SCHAJER, 1988a]

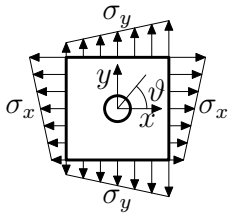

Obr. 38: Tenká deska s lineárně proměnlivým zbytkovým napětím

zatížena tak, aby průběh napětí s hloubkou měl kvadratický průběh ($\sigma = 1 - H - 2H^2$). Z obr. 37 vyplývá porovnání těchto metod.

Výsledkem integrální metody je odstupňovaný průběh napětí vcelku dobře odpovídající skutečnému průběh napětí. Průběh napětí získaný metodou mocninné řady je čára, která poměrně přesně kopíruje skutečný průběh. Metoda přírůstková a metoda průměrných napětí pak podá výsledek, který se s větší hloubkou vzdaluje skutečnému průběhu. Z uvedeného vyplývá, že v případě velice hladkého průběhu napětí je výhodnější metoda mocninné řady s použitím velkého počtu malých vrtacích kroků. Integrální metoda lépe aproximuje skutečný průběh v případě náhlých změn. Její nevýhodou je potom použití dat z malého počtu vrtacích kroků. Tento aspekt je možné eliminovat vhodnou volbou velikosti kroku, jak bylo popsáno dříve.

Modifikace odvrtávací metody v případě plošného gradientu zbytkových napětí

Určování gradientních zbytkových napětí pomocí vyvrtávací metody bylo popsáno Kabirim [KABIRI, 1984]. Pokud je průměr vrtaného otvoru poměrně malý, potom je možné nekonstantní průběh zbytkových napětí v okolí otvoru nahradit lineárním průběhem. Na obr. 38 je zobrazena tenká deska zatížená lineárně proměnnými zbytkovými napětími. Pole zbytkového napětí je možné popsat vztahy

$$\sigma_x = \sigma_a + y\sigma_c, \tag{128}$$

$$\sigma_y = \sigma_b + x\sigma_d. \tag{129}$$

V případě těchto vztahů se předpokládá konstantní průběh po celé hloubce otvoru. Průměrná

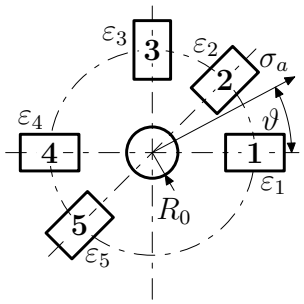

Obr. 39: Schéma pětitenzometrové růžice podle Kabiriho [Kabiri, 1984]

radiální deformace pro tento případ je vyjádřena vztahem

$$\varepsilon_r = A(\sigma_a + \sigma_b)/E + B(\sigma_a - \sigma_b)\cos 2\vartheta/E + C\sigma_c \sin\vartheta/E + \\ + C\sigma_d \cos\vartheta/E + D\sigma_c \sin 3\vartheta/E - D\sigma_d 3\vartheta/E. \tag{130}$$

Koeficienty A, B, C a D jsou funkcemi Poissonova čísla, poloměru vyvrtaného otvoru, délky a šířky tenzometru a jeho polohy vzhledem ke středu vyvrtaného otvoru. Rovnice (130) obsahuje pět neznámých: σ_a , σ_b , σ_c , σ_d a ϑ. Kabiri [Kabiri, 1984] navrhl rozložení pětitenzometrové růžice, která je zobrazena na obr. 39.

Deformace mohou být vyjádřeny pro každý tenzometr z této navržené růžice.

$$\varepsilon_1 = A(\sigma_a + \sigma_b)/E + B(\sigma_a - \sigma_b)\cos 2\vartheta/E + C\sigma_c \sin\vartheta/E + \\ + C\sigma_d \cos\vartheta/E + D\sigma_c \sin 3\vartheta/E - D\sigma_d 3\vartheta/E \tag{131}$$

$$\varepsilon_2 = A(\sigma_a + \sigma_b)/E + B(\sigma_a - \sigma_b)\cos 2(\vartheta + 45°)/E + C\sigma_c \sin(\vartheta + 45°)/E + \\ + C\sigma_d \cos(\vartheta + 45°)/E + D\sigma_c \sin 3(\vartheta + 45°)/E - D\sigma_d 3(\vartheta + 45°)/E \tag{132}$$

$$\varepsilon_3 = A(\sigma_a + \sigma_b)/E + B(\sigma_a - \sigma_b)\cos 2(\vartheta + 90°)/E + +C\sigma_c \sin(\vartheta + 90°)/E + \\ + C\sigma_d \cos(\vartheta + 90°)/E + D\sigma_c \sin 3(\vartheta + 90°)/E - D\sigma_d 3(\vartheta + 90°)/E \tag{133}$$

$$\varepsilon_4 = A(\sigma_a + \sigma_b)/E + B(\sigma_a - \sigma_b)\cos(2(\theta + 180°))/E + +C\sigma_c \sin(\vartheta + 180°)/E + \\ + C\sigma_d \cos(\vartheta + 180°)/E + D\sigma_c \sin 3(\vartheta + 180°)/E - D\sigma_d 3(\vartheta + 180°)/E \tag{134}$$

$$\varepsilon_5 = A(\sigma_a + \sigma_b)/E + B(\sigma_a - \sigma_b)\cos(2(\theta + 225°))/E + C\sigma_c \sin(\theta + 225°)/E + \\ + C\sigma_d \cos(\theta + 225°)/E + D\sigma_c \sin 3(\theta + 225°)/E - D\sigma_d 3(\theta + 225°)/E \tag{135}$$

Řešení rovnic (131) – (135) bylo Kabirim [Kabiri, 1984] provedeno. Pět neznámých σ_a , σ_b , σ_c , σ_d a ϑ může být vyjádřeno pomocí výrazů obsahující pět naměřených poměrných deformací a koeficienty. Napěťové gradienty σ_c a σ_d jsou funkcemi rozdílů v naměřených poměrných deformacích ε_1, ε_4 a ε_2, ε_5.

Modifikací výše uvedené metody je postup publikovaný Luhem a Hwangem [Luh and Heang, 1999]. Použili komerčně dostupné třítenzometrové růžice (obr. 40), kdy po vyvrtání malého otvoru do středu růžice jsou odměřeny tři radiální deformace ε_1^I – ε_3^I. Po odměření deformací je malý otvor zvětšen vyvrtáním většího otvoru a mohou být odměřeny další tři radiální deformace ε_1^{II} – ε_3^{II}. Při použití prvních pěti naměřených deformací je možné, jako v předchozím postupu, určit

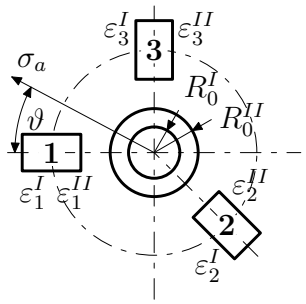

Obr. 40: Schéma růžice podle Luha [LUH and HEANG, 1999]

pět neznámých (σ_a , σ_b , σ_c , σ_d a ϑ). Zde je však na místě vyřešit otázku, zda odečtené hodnoty deformací při různých vzájemných geometriích otvoru a růžice nebudou ovlivněné různou chybou měření.

Dva výše uvedené postupy byly řešeny pro průchozí otvor s předpokládaným konstantním průběhem zbytkových napětí s hloubkou. V případě neprůchozího otvoru je situace odlišná. V tomto případě, obdobně jako pro negradientní pole, je potřeba určit koeficienty $\overline{A}, \overline{B}, \overline{C}$ a $\overline{D}$. V tomto případě by byla experimentální kalibrace obtížnější a proto se zdá výhodnější určení těchto koeficientu numerickým postupem, nejspíše pomocí metody konečných prvků.

Použití odvrtávací metody u ortotropních materiálů

V případě ortotropního materiálu by použití vztahů pro isotropní materiál vedlo k nepřesným výsledkům. Schajer [SCHAJER and YANG, 1994] publikoval postup, který vychází z analytického řešení pole posuvů v okolí otvoru v ortotropním materiálu. Uvolněnou deformaci v případě isotropního materiálu je možné vyjádřit pomocí vztahu

$$\varepsilon_r = A(\sigma_x + \sigma_y) + B(\sigma_x - \sigma_y)cos2\alpha + C\tau_{xy}\sin 2\alpha, \tag{136}$$

kde A,B a C jsou kalibrační konstanty závislé na materiálu a geometrii růžice. V případě isotropního materiálu je $C = 2B$. Při použití růžice dle ASTM (obr 32) lze rovnici (136) zapsat v maticovém tvaru

$$\begin{bmatrix} A+B & 0 & A-B \\ A & -C & A \\ A-B & 0 & A+B \end{bmatrix} \begin{bmatrix} \sigma_x \\ \tau_{xy} \\ \sigma_y \end{bmatrix} = \begin{bmatrix} \varepsilon_1 \\ \varepsilon_2 \\ \varepsilon_3 \end{bmatrix}. \tag{137}$$

V případě elastického chování ortotropního materiálu je možné rovnici (137) zobecnit do tvaru

$$\frac{1}{\sqrt{E_x E_y}} \begin{bmatrix} c_{11} & c_{12} & c_{13} \\ c_{21} & c_{22} & c_{23} \\ c_{31} & c_{32} & c_{33} \end{bmatrix} \begin{bmatrix} \sigma_x \\ \tau_{xy} \\ \sigma_y \end{bmatrix} = \begin{bmatrix} \varepsilon_1 \\ \varepsilon_2 \\ \varepsilon_3 \end{bmatrix}, \tag{138}$$

kde elastické poddajnosti c_{11}–c_{33} je třeba spočíst pro konkrétní ortotropní materiál dle vztahů uvedených v [SCHAJER and YANG, 1994].

Korekce plasticity

V případě vysokých zbytkových napětí v dané konstrukci použitím metod uvedených v předchozích oddílech získáme nepřesné výsledky. Například norma ASTM uvádí hodnotu použití do 0,5 meze kluzu daného materiálu. V tomto případě je možné použit korekční postupy úpravy koeficentů platných pro elastický materál. Yan [YAN *et al.*, 1996] uvádí následující postup: Von Misesova podmínka plasticity může být vyjdářena ve tvaru

$$\frac{1}{6}\left[(\sigma_1 - \sigma_2)^2 + (\sigma_2 - \sigma_3)^2 + (\sigma_3 - \sigma_1)^2\right] = Konst., \tag{139}$$

kde levá strana rovnice (139) zahrnuje vztah pro deformační energii. Podle rovnice (139) začne materiál klouzat, pokud deformační energie dosáhne určité hodnoty. Yan zavádí parametr S. V případě rovinné napjatosti a pokud jsou napětí σ_x a σ_y orientována v hlavních směrech, lze podmínku plasticity vyjádřit vztahem

$$\sigma_x^2 - \sigma_x\sigma_y + \sigma_y^2 = \sigma_k^2 \tag{140}$$

a dle Hookeova zákona platí

$$\varepsilon_x = \frac{1}{E}(\sigma_x - \mu\sigma_y), \tag{141}$$

$$\varepsilon_y = \frac{1}{E}(\sigma_y - \mu\sigma_x). \tag{142}$$

Levá strana rovnice (140) pak může být vyjádřena vztahem

$$\sigma_x^2 - \sigma_x\sigma_y + \sigma_y^2 = S\left(\frac{E}{1-\mu^2}\right)^2, \tag{143}$$

kde

$$S = (1+\mu^2-\mu)(\varepsilon_x^2+\varepsilon_y^2) - (1+\mu^2-4\mu)\varepsilon_x\varepsilon_y, \tag{144}$$

z čehož vyplývá, že S zastupuje velikost deformační energie odpovídající daným napětím. Yan uvádí závislost mezi S a zatížením σ, kdy je uváděna exponenciální závislost a v případě nízkých napětí je S zanedbatelné.

Norma ASTM E837 je omezena hodnotou $0,5 \cdot \sigma_k$, kdy začíná docházet k plastizaci na okraji vrtaného otvoru. Pro tento případ Yan označil hodnotu S jako S_y, z čehož vyplývá podmínka, že k plastizaci dojde v případě $S > S_y$. Hodnotu S_y je možné určit experimentálně. V tomto případě Yan navrhuje korekci kalibračních koeficientů

$$A' = -(a_A + b_A S), \tag{145}$$

$$B' = -(a_B + b_B S), \tag{146}$$

kde a_A, b_A, a_B a b_B jsou určeny na základě regrese výsledků experimentálních měření.

Excentricita otvoru

Pro případ excentricity otvoru vůči středu tenzometrické růžice byly publikovány [Lu, 1996] vztahy, kdy pro případ průchozího otvoru je možné provést korekci. Za předpokladu, že hlavní napětí σ_1 svírá s osou x' referenčního souřadného systému $x'o'y'$ úhel ϕ viz obr. 41 je možné sestavit nové vztahy pro uvolněné deformace ε_1, ε_2, ε_3 změřené tenzometrickou růžicí

$$\begin{bmatrix} A_1 & B_1 & C_1 \\ A_2 & B_2 & C_2 \\ A_3 & B_3 & C_3 \end{bmatrix} \begin{bmatrix} \sigma_1+\sigma_2 \\ (\sigma_1-\sigma_2)\cos 2\phi \\ (\sigma_1-\sigma_2)\sin 2\phi \end{bmatrix} = \begin{bmatrix} \varepsilon_1 \\ \varepsilon_2 \\ \varepsilon_3 \end{bmatrix}, \tag{147}$$

kde

$$A_i = -\frac{1}{2E}(1+\mu)r_i^2\cos 2\alpha_i,$$

$$B_i = -\frac{1}{E}\left[(1-\mu)r_i^2\cos 2\theta_i - (1-\mu)r_i^2(1-\frac{3}{2}r_i^2)\cos 2(\theta_i-\alpha_i)\right],$$

$$C_i = -\frac{1}{E}\left[(1-\mu)r_i^2\cos 2\theta_i - (1-\mu)r_i^2(1-\frac{3}{2}r_i^2)\sin 2(\theta_i-\alpha_i)\right].$$

$r_i = r/R_i$, kde r je poloměr otvoru normalizovaný s ohledem na vzdálenost mezi počátkem o' a středem i-tého tenzometru, úhly θ_i respektive α_i popisují orientaci respektive natočení i-tého tenzometru, β a e jsou pak úhel a velikost excentricity středu otvoru o' vůči středu růžice o. R je pak vzdálenost středu růžice a středu tenzometru. Úhel ζ_i pak určuje orientaci i-tého tenzometru vůči souřadnému systému xoy.

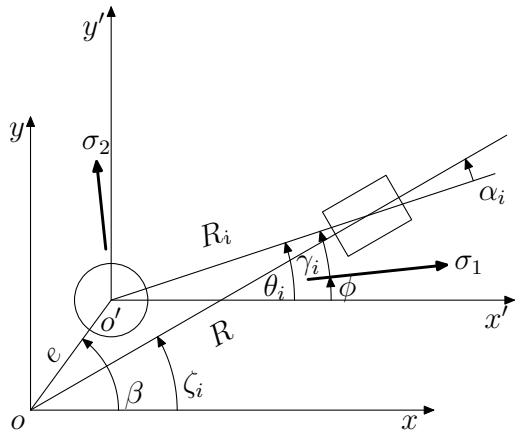

Obr. 41: Schéma růžice s excentrickým otvorem [LU, 1996]

Problematika vrtání otvoru

Sama technologie vrtání otvoru může být zdrojem vzniku zbytkových napětí. V literatuře je popsáno mnoho postupů tvorby otvoru, kdy v dnešní době k nejčastěji používaným patří vrtání se standartními řeznými rychlostmi a vrtání za vysokých řezných rychlostí (HSD). Na výsledný tvar otvoru má vliv interakce zkoumaný materiál a materiál nástroje. Při použití HSD vzniká teplo, které je přenášeno do zkoumaného materiálu a může ovlivnit signály snímané z tenzometrické růžice. Švantner [ŠVANTNER, 2004] doporučuje dostatečně dlouhé časové prodlevy mezi koncem vrtání kroku hloubky otvoru a odečtením uvolněných deformací.

Další metody využívající odvrtávacího principu

Principu uvolnění zbytkových napětí pomocí vyvrtání otvoru využívají i postupy, kdy měření deformace se neprovádí odporovým tenzometrem. Jedná se většinou o metody založené na optickém měření uvolněných deformací. Zde je možné zmínit fotoelasticimetrii, interferometrické moaré [SCHWARZ *et al.*, 2000], holografickou interferomtrii [MAKINO and NELSON, 1994], [NELSON *et al.*, 1994], optickou interferometrii [LIN, 2000] a v neposlední řadě metoda využívající optické korelace [FOCHT and SCHIFFNER, 2003], [DÍAZ *et al.*, 2000]. Jinou alternativou je vrtání mezikruhové drážky a odečítání deformací optickou cestou pomocí mikroskopu, jak uvádí Berka [BERKA *et al.*, 1998]. Další alternativní metodou je postup publikovaný Wernem [WERN *et al.*, 1997], [WERN, 1997], kdy signály z tenzometrické růžice doplňuje o změření posunutí ve směru kolmém k povrchu vyšetřované konstrukce. Zatím však nebyla publikována praktická aplikace této metody.

Cíle

Při zjišťování zbytkových napětí pomocí odvrtávací metody bylo zjištěno u některých měření excentricita otvoru větší než umožňuje norma ASTM E837. Proto byly stanoveny následující cíle:

- zjistit stav napjatosti kolem otvoru excentrického vůči středu tenzometrické růžice
- zjistit odezvu tenzometrů v okolí otvoru excentrického vůči středu tenzometrické růžice
- zpracovat metodu pro zohlednění excentricity otvoru při výpočtu zbytkových napětí
- aplikace na experimentálně zjištěná data

Postup řešení

Pro popis stavu napjatosti v okolí otvoru vzniklého aplikací odvrtávací metody byla použita metoda konečných prvků (MKP). Byl simulován experiment, tyč byla namáhána jednoosým tahem a bylo provedeno postupné vrtání otvoru.

MKP model

ABAQUS/CAE

Modelování a výpočet byl proveden pomocí programu ABAQUS verze 6.4 a 6.5. Program ABAQUS/CAE je program, který spojuje modelování, analýzu, správu úloh a vizualizaci výsledků. Jako vypočtový program je možné použít ABAQUS/Standard nebo ABAQUS/Explicit. Prostředí CAE je vytvořeno pomocí interpretačního jazyka Python, což umožňuje tvorbu maker pro zautomatizování tvorby modelu a výpočtu. Modely vytvořené v prostředí CAE je možné parametrizovat, což spolu s vytvořenými pomocnými programy umožňuje zautomatizovat výpočty modelů lišících se jen některými vlastnostmi.

Popis modelu

Cílem modelu bylo co nejpřesněji simulovat stav při exeprimentální kalibraci. Proto byla namodelována tyč zatížená jednoosým tahem a na ní se provadělo odvrtání otvoru. Model se skládá ze tří částí. Těleso tyče, které zprostředkovává přenos zatížení, detailu, v kterém se nachází místo vrtu a pro odečet radiálních deformací byl namodelován tenzometr, který svým tvarem a rozměry odpovídá vinutí tenzometru v tenzometrické růžici. Na pracovišti Ústavu mechaniky Fakulty strojní ČVUT v Praze, odboru pružnosti a pevnosti se pro aplikaci odvrtávací metody používá nejčastěji měřící souprava RESTAN dodáná firmou Hottinger Baldwin Messtechnik (HBM), a při námi prováděných experimentech se nejčastěji používá tenzometrická růžice RY61S vyráběná touto firmou.

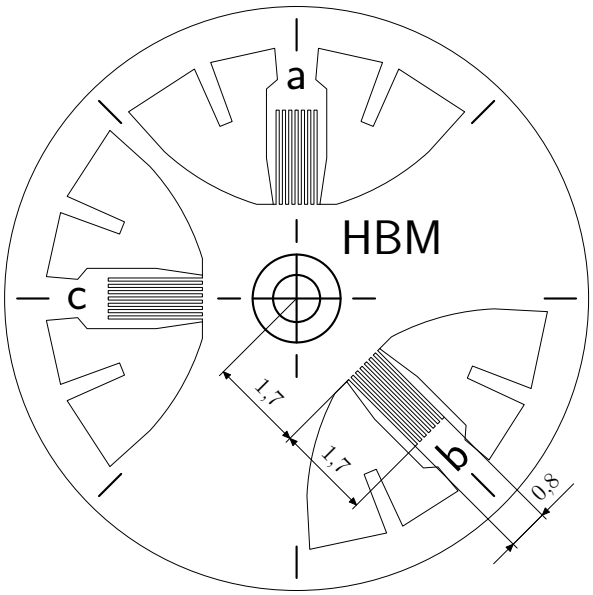

Obr. 42: Schéma tenzometrické růžice RY61S

Geometrie této růžice je znázorněná na obr. 42. Vinutí bylo namodelováno jako rovinná součást, kdy modul pružnosti v tahu materiálu vinutí byl zvolen mnohonásobně menší, než modul pružnosti materiálu tyče. Pro vytvoření sítě byly použity dvouuzlové tyčové prvky, programem

ABAQUS označené jako T3D2. Část „detail“ byla rozdělena oblastí otvoru na válcovou část a dále dělena na vrstvy odpovídající velikosti vrtacích kroků. U této části byla volena MKP síť s menší velikostí prvků.

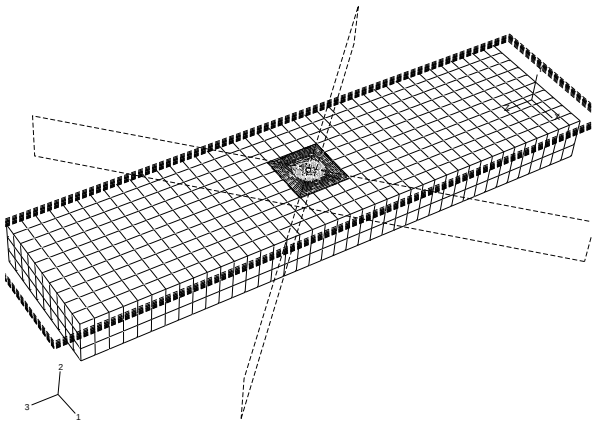

Obr. 43: MKP síť modelu tyče

Pro model tyče byly zvoleny 8 uzlové elementy, které jsou v programu ABAQUS označeny jako C3D8R.

Spojení modelu tenzometru a modelu zkušební tyče bylo provedeno pomocí vazby „tie“, tato vazba byla použita i pro spojení dílu „detail“ a „tyč“. V prostředí ABAQUS vazba „tie“ patří mezi povrchové vazby a slouží ke svázání dvou povrchů během simulace. Každý uzel „slave“ povrchu se pohybuje stejně jako nejbližší bod „master“ povrchu. V případě strukturální analýzy to znamená, že posuvné (případně rotační) stupně volnosti jsou svázány. Pro určení, který uzel „slave“ povrchu je svázán s konkrétní „master“ plochou, je rozhodující nedeformovaný tvar modelu. Standartně všechny uzly „slave“ povrchu, které leží v dané vzdálenosti od „master“ povrchu, jsou svázány. Ve výchozím nastavení programu je tato vzdálenost odvozena od velikosti prvků „master“ povrchu.

Pro zjištění stavu uvolněných deformací měřených tenzometrickou růžicí byla namodelována instalace tenzometrů okolo otvoru. Tenzometry byly instalovány paprskovitě okolo otvoru s úhlovým rozestupem 5°.

Signál z jednotlivých tenzometrů byl odečítán jako deformace jednotlivých prvků na vinutí a následnou integrací těchto deformací, kdy vzhledem ke komplikovanosti výsledného modelu byla využita objektovost prostředí CAE a pro vytvoření cesty pro odečet signálu bylo vytvořeno pomocné makro.

Odvrtání otvoru bylo namodelováno postupným odebíráním prvků z oblasti otvoru. Po odebrání vrstvy odpovídající odvrtání daného kroku byl proveden výpočet a po zkonvergování výpočtu byla odebrána další vrstva. Po ukončení výpočtu byly výsledky uloženy ve výsledkovém souboru ABAQUSu. Vzhledem ke komplexnosti výsledkového souboru bylo pro získaní signálů nutno vytvořit další skript (s. **??**).

Případ tyče s otvorem ve středu růžice

Po namodelování zkušební tyče byl proveden výpočet pro případ centrického vrtu vůči středu tenzometrické růžice. Tyč byla zatížena napětím o velikosti 1 MPa. Signály získané tímto výpočtem byly použity pro nalezení funkce popisující vztah mezi uvolněnými deformacemi a zbytkovým napětím v místě vrtu otvoru.

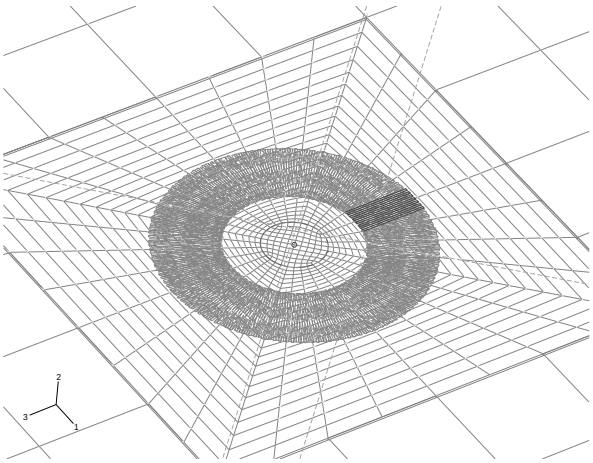

Obr. 44: Model „instalce“ MKP tenzometrů

Za předpokladu volby obecné závislosti deformace na napětí, odpovídající vztahu použitého Rendlerem (84), je možné zapsat pro deformaci ve směru udaným úhlem α

$$\varepsilon(\alpha) = K(\alpha)\sigma. \tag{148}$$

Jako bázová funkce pro $K(\alpha)$ byl zvolen rozvoj Fourierovy řady, takže pro vztah mezi napětím a deformací v případě rovinné napjatosti dané velikostí hlavních napětí σ_1 a σ_2 platí

$$\varepsilon(\alpha) = \left[\sum_j^n K_j \cos(\alpha) + L_j \sin(\alpha)\right] \cdot \sigma_1 + \left[\sum_j^n K_j \cos(\alpha + \pi/2) + L_j \sin(\alpha + \pi/2)\right] \cdot \sigma_2. \tag{149}$$

Takto získané výsledky byly použity pro analýzu dat změřených při experimentu zjišťování zbytkových napětí na trubkovém ohybu [Doubrava *et al.*, 2003c], [Doubrava *et al.*, 2004a].

Případ s otvorem excentrickým vůči středu růžice

Pro zjištění vlivu polohy excentrického otvoru vůči geometrii tenzometrické růžice byl použit konečněprvkový model popsaný v předcházejícím odstavci. Namodelování excentricity bylo provedeno posuvem tenzometrů vůči středu otvoru. Pro posuv tenzometrů bylo vytvořeno makro `posun_tenz.py`. Vstupem tohoto makra je velikost excentricity ex a úhel φ udávající směr posuvu otvoru vůči ose napětí σ_1. Po provedení výpočtu pak bylo možné s využitím dříve uvedených maker odečíst deformace po vyvrtání otvoru příslušné hloubky. Získaná data byla vyhodnocena z použití vztahu 149, kdy pro různé orientace excentricity byly získány různé keficienty a jejich aplikací pak odlišné závislosti. Z výsledků [Doubrava *et al.*, 2003a] pak vyplývá nutnost nalezení složitějšího vztahu pro uvolněnou deformaci.

Teoretický popis problému

Pro odvození vztahů pro výpočet zbytkových napětí byla použita geometrie tenzometrické růžice RY61S firmy HBM. Pro popis deformací byla zvolena funkce s násadou dvojnásobné goniometrické funkce. Zápis gonimetrické řady byl volen pomocí exponenciálního rozvoje. Potom lze obecně zapsat deformaci jako funkci napětí a bázové funkce, kdy úhel ψ udává orientaci 1. tenzometru vůči směru napětí σ_1, φ je úhel mezi směrem napětí σ_1 a polohou otvoru a ex je velikost excentricity vyvrtaného otvoru vůči středu tenzometrické růžice:

$$\varepsilon^h(\varphi,\psi) = \sum_{k,l=-K}^{K} C_{kl}^h \cdot \mathrm{e}^{\mathrm{i}k\varphi} \cdot \mathrm{e}^{\mathrm{i}l\psi}\sigma \tag{150}$$

Excentricita otvoru se přepokládá po celé hloubce otvoru konstantní. V případě deformace změřené 1. tenzometrem po vyvrtání otvoru do hloubky h a při zatížení vzorku napětím σ_1 lze vyjádřit

$$^{\sigma_1}\varepsilon_1^h(\varphi,\psi) = \sum_{k,l=-K}^{K} C_{kl}^h \cdot \mathrm{e}^{\mathrm{i}k\varphi} \cdot \mathrm{e}^{\mathrm{i}l\psi} \cdot \sigma_1. \tag{151}$$

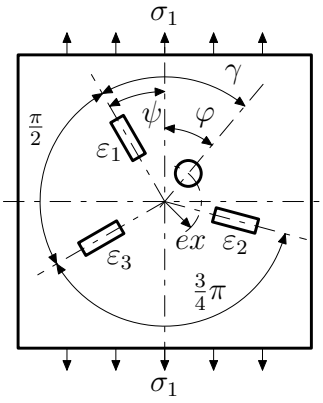

Obr. 45: Poloha prvního tenzometru při zatížení σ_1

Pokud dle obr. 45 platí

$$\varphi = \gamma - \psi, \tag{152}$$

lze vztah (151) upravit

$$^{\sigma_1}\varepsilon_1^h(\varphi,\psi) = \sum_{k,l=-K}^{K} C_{kl}^h \cdot \mathrm{e}^{\mathrm{i}k\gamma} \cdot \mathrm{e}^{\mathrm{i}(l-k)\psi} \cdot \sigma_1. \tag{153}$$

Obdobně lze psát vztah pro deformace změřené tenzometrem 2

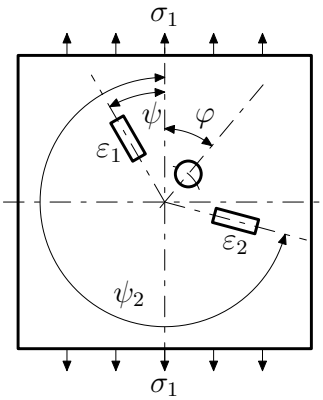

Obr. 46: Poloha druhého tenzometru při zatížení σ_1

$$^{\sigma_1}\varepsilon_2^h(\varphi,\psi_2) = \sum_{k,l=-K}^{K} C_{kl}^h \cdot \mathrm{e}^{\mathrm{i}k\varphi} \cdot \mathrm{e}^{\mathrm{i}l\psi_2} \cdot \sigma_1. \tag{154}$$

Pro zvolenou konfiguraci růžice platí

$$\psi_2 = \psi + \frac{5}{4}\pi, \tag{155}$$

proto lze (154) upravit

$${}^{\sigma_1}\varepsilon_2^h(\varphi,\psi) = \sum_{k,l=-K}^{K} C_{kl}^h \cdot \mathrm{e}^{\mathrm{i}k\varphi} \cdot \mathrm{e}^{\mathrm{i}l(\psi+\frac{5}{4}\pi)} \cdot \sigma_1. \tag{156}$$

Analogicky pro deformaci změřenou tenzometrem číslo 3 při působení napětí σ_1 a odvrtání otvoru do hloubky h lze psát:

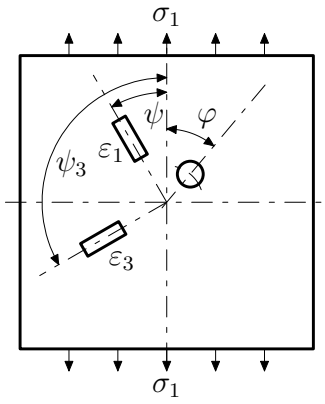

Obr. 47: Poloha třetího tenzometru při zatížení σ_1

$${}^{\sigma_1}\varepsilon_3^h(\varphi,\psi_3) = \sum_{k,l=-K}^{K} C_{kl}^h \cdot \mathrm{e}^{\mathrm{i}k\varphi} \cdot \mathrm{e}^{\mathrm{i}l\psi_3} \cdot \sigma_1 \tag{157}$$

a neboť platí

$$\psi_3 = \psi + \frac{\pi}{2}, \tag{158}$$

lze vztah (157) upravit

$${}^{\sigma_1}\varepsilon_3^h(\varphi,\psi) = \sum_{k,l=-K}^{K} C_{kl}^h \cdot \mathrm{e}^{\mathrm{i}k\varphi} \cdot \mathrm{e}^{\mathrm{i}l(\psi+\frac{\pi}{2})} \cdot \sigma_1. \tag{159}$$

Obdobně lze zapsat vztahy pro deformace změřené jednotlivými tenzometry od napětí σ_2 při vyvrtání orvoru do hloubky h. Pro 1. tenzometr

$${}^{\sigma_2}\varepsilon_1^h(\varphi_2,\eta_1) = \sum_{k,l=-K}^{K} C_{kl}^h \cdot \mathrm{e}^{\mathrm{i}k\varphi_2} \cdot \mathrm{e}^{\mathrm{i}l\eta_1} \cdot \sigma_2. \tag{160}$$

Pokud platí

$$\varphi_2 = \varphi + \frac{\pi}{2}, \qquad \eta_1 = \psi + \frac{3}{2}\pi, \tag{161}$$

lze vztah (160) upravit

$${}^{\sigma_2}\varepsilon_1^h(\varphi,\psi) = \sum_{k,l=-K}^{K} C_{kl}^h \cdot \mathrm{e}^{\mathrm{i}k(\varphi+\frac{\pi}{2})} \cdot \mathrm{e}^{\mathrm{i}l(\psi+\frac{3}{2}\pi)} \cdot \sigma_2. \tag{162}$$

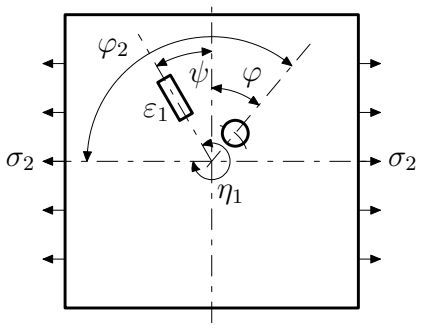

Obr. 48: Poloha prvního tenzometru při zatížení σ_2

Pro deformaci změřenou 2. tenzometrem od napětí σ_2 lze psát

$$ {}^{\sigma_2}\varepsilon_2^h(\varphi_2,\eta_2) = \sum_{k,l=-K}^{K} C_{kl}^h \cdot \mathrm{e}^{\mathrm{i}k\varphi_2} \cdot \mathrm{e}^{\mathrm{i}l\eta_2} \cdot \sigma_2. \tag{163} $$

Pokud platí

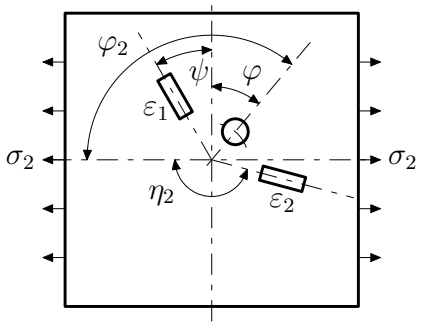

Obr. 49: Poloha druhého tenzometru při zatížení σ_2

$$ \varphi_2 = \varphi + \frac{\pi}{2}, \qquad \eta_2 = \psi + \frac{3}{4}\pi, \tag{164} $$

lze vztah (163) upravit

$$ {}^{\sigma_2}\varepsilon_2^h(\varphi,\psi) = \sum_{k,l=-K}^{K} C_{kl}^h \cdot \mathrm{e}^{\mathrm{i}k(\varphi+\frac{\pi}{2})} \cdot \mathrm{e}^{\mathrm{i}l(\psi+\frac{3}{4}\pi)} \cdot \sigma_2. \tag{165} $$

A konečně pro deformaci změřenou 3. tenzometrem od napětí σ_2 lze psát

$$ {}^{\sigma_2}\varepsilon_3^h(\varphi_2,\eta_3) = \sum_{k,l=-K}^{K} C_{kl}^h \cdot \mathrm{e}^{\mathrm{i}k\varphi_2} \cdot \mathrm{e}^{\mathrm{i}l\eta_3} \cdot \sigma_2. \tag{166} $$

Pokud platí

$$ \varphi_2 = \varphi + \frac{\pi}{2}, \qquad \eta_3 = \psi, \tag{167} $$

lze vztah (166) upravit

$$ {}^{\sigma_2}\varepsilon_3^h(\varphi,\psi) = \sum_{k,l=-K}^{K} C_{kl}^h \cdot \mathrm{e}^{\mathrm{i}k(\varphi+\frac{\pi}{2})} \cdot \mathrm{e}^{\mathrm{i}l\psi} \cdot \sigma_2. \tag{168} $$

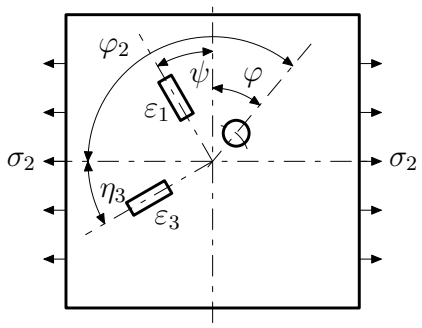

Obr. 50: Poloha třetího tenzometru při zatížení σ_2

Za předpokladu platnosti zakona superpozice je možné deformace změřené jednotlivými tenzometry od hlavních napětí sečíst. Ze vztahů (151), (160) a (152) lze vyjádřit

$$\varepsilon_1^h(\psi) = \sum_{k,l=-K}^{K} C_{kl}^h \cdot \mathrm{e}^{\mathrm{i}k(\gamma-\psi)} \cdot \mathrm{e}^{\mathrm{i}l\psi} \cdot \sigma_1 + \sum_{k,l=-K}^{K} C_{kl}^h \cdot \mathrm{e}^{\mathrm{i}k(\gamma-\psi+\frac{\pi}{2})} \cdot \mathrm{e}^{\mathrm{i}l(\psi+\frac{3}{2}\pi)} \cdot \sigma_2$$

a po úpravách

$$\varepsilon_1^h(\psi) = \sum_{k,l=-K}^{K} C_{kl}^h \cdot \mathrm{e}^{\mathrm{i}k\gamma} \cdot \mathrm{e}^{\mathrm{i}(l-k)\psi} \cdot \sigma_1 + \sum_{k,l=-K}^{K} C_{kl}^h \cdot \mathrm{e}^{\mathrm{i}k(\gamma+\frac{\pi}{2})} \cdot \mathrm{e}^{\mathrm{i}l\frac{3}{2}\pi} \cdot \mathrm{e}^{\mathrm{i}(l-k)\psi} \cdot \sigma_2. \tag{169}$$

Podobně ze vztahů (156), (165) a (152) lze vyjádřit

$$\varepsilon_2^h(\psi) = \sum_{k,l=-K}^{K} C_{kl}^h \cdot \mathrm{e}^{\mathrm{i}k(\gamma-\psi)} \cdot \mathrm{e}^{\mathrm{i}l(\psi+\frac{5}{4}\pi)} \cdot \sigma_1 + \sum_{k,l=-K}^{K} C_{kl}^h \cdot \mathrm{e}^{\mathrm{i}k(\gamma-\psi+\frac{\pi}{2})} \cdot \mathrm{e}^{\mathrm{i}l(\psi+\frac{3}{4}\pi)} \cdot \sigma_2$$

a poté

$$\varepsilon_2^h(\psi) = \sum_{k,l=-K}^{K} C_{kl}^h \cdot \mathrm{e}^{\mathrm{i}k\gamma} \cdot \mathrm{e}^{\mathrm{i}l\frac{5}{4}\pi} \cdot \mathrm{e}^{\mathrm{i}(l-k)\psi} \cdot \sigma_1 + \sum_{k,l=-K}^{K} C_{kl}^h \cdot \mathrm{e}^{\mathrm{i}k(\gamma+\frac{\pi}{2})} \cdot \mathrm{e}^{\mathrm{i}l\frac{3}{4}\pi} \cdot \mathrm{e}^{\mathrm{i}(l-k)\psi} \cdot \sigma_2, \tag{170}$$

a dále ze vztahů (159), (168) a (152) lze vyjádřit

$$\varepsilon_3^h(\psi) = \sum_{k,l=-K}^{K} C_{kl}^h \cdot \mathrm{e}^{\mathrm{i}k(\gamma-\psi)} \cdot \mathrm{e}^{\mathrm{i}l(\psi+\frac{\pi}{2})} \cdot \sigma_1 + \sum_{k,l=-K}^{K} C_{kl}^h \cdot \mathrm{e}^{\mathrm{i}k(\gamma-\psi+\frac{\pi}{2})} \cdot \mathrm{e}^{\mathrm{i}l\psi} \cdot \sigma_2,$$

$$\varepsilon_3^h(\psi) = \sum_{k,l=-K}^{K} C_{kl}^h \cdot \mathrm{e}^{\mathrm{i}k\gamma} \cdot \mathrm{e}^{\mathrm{i}l\frac{\pi}{2}} \cdot \mathrm{e}^{\mathrm{i}(l-k)\psi} \cdot \sigma_1 + \sum_{k,l=-K}^{K} C_{kl}^h \cdot \mathrm{e}^{\mathrm{i}k(\gamma+\frac{\pi}{2})} \cdot \mathrm{e}^{\mathrm{i}(l-k)\psi} \cdot \sigma_2 \tag{171}$$

Pro další úpravy lze zavést substituce a (169) upravit na rovnici

$$\varepsilon_1^h = D_{11} \cdot \sigma_1 + D_{12} \cdot \sigma_2. \tag{172}$$

Podobně lze upravit i vztahy (170) a (171).

$$\varepsilon_2^h = D_{21} \cdot \sigma_1 + D_{22} \cdot \sigma_2 \tag{173}$$

$$\varepsilon_3^h = D_{31} \cdot \sigma_1 + D_{32} \cdot \sigma_2 \tag{174}$$

Rovnici (172) lze přenásobit výrazem D_{32}, rovnici (174) výrazem D_{12} a výsledky vzájemně od sebe odečtené dají vztah pro napětí σ_1

$$\sigma_1 = \frac{\varepsilon_1^h \cdot D_{32} - \varepsilon_3^h \cdot D_{12}}{D_{11} \cdot D_{32} - D_{31} \cdot D_{12}}, \tag{175}$$

a podobně, když je rovnice (172) přenásobena výrazem D_{31}, rovnice (174) výrazem D_{11} a výsledky od sebe vzájemně odečteny, výsledkem je vztah pro napětí σ_2

$$\sigma_2 = \frac{\varepsilon_1^h \cdot D_{31} - \varepsilon_3^h \cdot D_{11}}{D_{12} \cdot D_{31} - D_{32} \cdot D_{11}}. \tag{176}$$

Z rovnic (175) a (176) lze dosadit do rovnice (173):

$$\varepsilon_2^h = \frac{D_{21}(\varepsilon_1^h \cdot D_{32} - \varepsilon_3^h \cdot D_{12})}{D_{11} \cdot D_{32} - D_{31} \cdot D_{12}} + \frac{D_{22}(\varepsilon_1^h \cdot D_{31} - \varepsilon_3^h \cdot D_{11})}{D_{12} \cdot D_{31} - D_{32} \cdot D_{11}} \tag{177}$$

Rovnici (177) lze dále upravit na tvar

$$\varepsilon_2^h(\underbrace{D_{11} \cdot D_{32} - D_{31} \cdot D_{12}}_{H_2}) + \varepsilon_3^h(\underbrace{D_{12} \cdot D_{21} - D_{22} \cdot D_{11}}_{H_3}) + \varepsilon_1^h(\underbrace{D_{22} \cdot D_{31} - D_{21} \cdot D_{32}}_{H1}) = 0 \tag{178}$$

Výrazy označené v rovnici (178) lze rozepsat , kdy indexy v druhých členech součinů byly zaměněny $k \leftrightarrow p$, $l \leftrightarrow s$

$$\begin{aligned} H_1 = &\left[\sum_{k,l=-K}^{K} C_{kl}^h \cdot \mathrm{e}^{\mathrm{i}k(\gamma+\frac{\pi}{2})} \cdot \mathrm{e}^{\mathrm{i}l\frac{3}{4}\pi} \cdot \mathrm{e}^{\mathrm{i}(l-k)\psi}\right]\left[\sum_{p,s=-K}^{K} C_{ps}^h \cdot \mathrm{e}^{\mathrm{i}p\gamma} \cdot \mathrm{e}^{\mathrm{i}s\frac{\pi}{2}} \cdot \mathrm{e}^{\mathrm{i}(s-p)\psi}\right] - \\ &- \left[\sum_{k,l=-K}^{K} C_{kl}^h \cdot \mathrm{e}^{\mathrm{i}k\gamma} \cdot \mathrm{e}^{\mathrm{i}l\frac{5}{4}\pi} \cdot \mathrm{e}^{\mathrm{i}(l-k)\psi}\right]\left[\sum_{p,s=-K}^{K} C_{ps}^h \cdot \mathrm{e}^{\mathrm{i}p(\gamma+\frac{pi}{2})} \cdot \mathrm{e}^{\mathrm{i}(s-p)\psi}\right]. \end{aligned} \tag{179}$$

Vzájemným roznásobením členů ve výrazu (179) lze získat

$$H_1 = \sum_{k,l,p,s=-K}^{K} C_{kl}^h \cdot C_{ps}^h \cdot \mathrm{e}^{\mathrm{i}k(\gamma+\frac{\pi}{2})} \cdot \mathrm{e}^{\mathrm{i}p\gamma} \cdot \mathrm{e}^{\mathrm{i}(l+s-k-p)\psi} \cdot \left(\mathrm{e}^{\mathrm{i}l\frac{3}{4}\pi} \cdot \mathrm{e}^{\mathrm{i}s\frac{\pi}{2}} - \mathrm{e}^{\mathrm{i}s\frac{5}{4}\pi}\right). \tag{180}$$

Podobně pro H_2

$$\begin{aligned} H_2 = &\left[\sum_{k,l=-K}^{K} C_{kl}^h \cdot \mathrm{e}^{\mathrm{i}k\gamma} \cdot \mathrm{e}^{\mathrm{i}(l-k)\psi}\right]\left[\sum_{p,s=-K}^{K} C_{ps}^h \cdot \mathrm{e}^{\mathrm{i}p(\gamma+\frac{\pi}{2})} \cdot \mathrm{e}^{\mathrm{i}(s-p)\psi}\right] - \\ &- \left[\sum_{k,l=-K}^{K} C_{kl}^h \cdot \mathrm{e}^{\mathrm{i}k\gamma} \cdot \mathrm{e}^{\mathrm{i}l\frac{\pi}{2}} \cdot \mathrm{e}^{\mathrm{i}(l-k)\psi}\right]\left[\sum_{p,s=-K}^{K} C_{ps}^h \cdot \mathrm{e}^{\mathrm{i}p(\gamma+\frac{\pi}{2})} \cdot \mathrm{e}^{\mathrm{i}\frac{3}{2}\pi} \cdot \mathrm{e}^{\mathrm{i}(s-p)\psi}\right] \end{aligned} \tag{181}$$

a po úpravě

$$H_2 = \sum_{k,l,p,s=-K}^{K} C_{kl}^h \cdot C_{ps}^h \cdot \mathrm{e}^{\mathrm{i}k\gamma} \cdot \mathrm{e}^{\mathrm{i}p\gamma} \cdot \mathrm{e}^{\mathrm{i}(l+s-k-p)\psi} \cdot \left(\mathrm{e}^{\mathrm{i}p\frac{\pi}{2}} - \mathrm{e}^{\mathrm{i}l\frac{\pi}{2}} \cdot \mathrm{e}^{\mathrm{i}p\frac{\pi}{2}} \cdot \mathrm{e}^{\mathrm{i}s\frac{3}{2}\pi}\right) \tag{182}$$

a konečně H_3

$$\begin{aligned} H_3 = &\left[\sum_{k,l=-K}^{K} C_{kl}^h \cdot \mathrm{e}^{\mathrm{i}k(\gamma+\frac{\pi}{2})} \cdot \mathrm{e}^{\mathrm{i}l\frac{3}{2}\pi} \cdot \mathrm{e}^{\mathrm{i}(l-k)\psi}\right]\left[\sum_{p,s=-K}^{K} C_{ps}^h \cdot \mathrm{e}^{\mathrm{i}p\gamma} \cdot \mathrm{e}^{\mathrm{i}s\frac{5}{4}\pi}\mathrm{e}^{\mathrm{i}(s-p)\psi}\right] - \\ &- \left[\sum_{k,l=-K}^{K} C_{kl}^h \cdot \mathrm{e}^{\mathrm{i}k(\gamma-\frac{\pi}{2})} \cdot \mathrm{e}^{\mathrm{i}l\frac{3}{4}\pi} \cdot \mathrm{e}^{\mathrm{i}(l-k)\psi}\right]\left[\sum_{p,s=-K}^{K} C_{ps}^h \cdot \mathrm{e}^{\mathrm{i}p\gamma} \cdot \mathrm{e}^{\mathrm{i}(s-p)\psi}\right] \end{aligned} \tag{183}$$

a po úpravách

$$H_3 = \sum_{k,l,p,s=-K}^{K} C_{kl}^h \cdot C_{ps}^h \cdot \mathrm{e}^{\mathrm{i}k\gamma} \cdot \mathrm{e}^{\mathrm{i}p\gamma} \cdot \mathrm{e}^{\mathrm{i}(l+s-k-p)\psi} \cdot \left(\mathrm{e}^{\mathrm{i}k\frac{\pi}{2}} \cdot \mathrm{e}^{\mathrm{i}l\frac{3}{2}\pi} \cdot \mathrm{e}^{\mathrm{i}s\frac{5}{4}\pi} - \mathrm{e}^{\mathrm{i}k\frac{\pi}{2}} \cdot \mathrm{e}^{\mathrm{i}l\frac{3}{4}\pi}\right). \tag{184}$$

Dosazením vztahů (180), (182) a (184) do (178) lze získat vztah, z něhož je pak možné vyjádřit úhel ψ

$$\sum_{k,l,p,s=-K}^{K} C_{kl}^h \cdot C_{ps}^h \cdot \mathrm{e}^{\mathrm{i}k\gamma} \cdot \mathrm{e}^{\mathrm{i}p\gamma} \cdot \Psi^{s+l-k-p} \left[\varepsilon_1^h \cdot \mathrm{e}^{\mathrm{i}k\frac{\pi}{2}} \cdot \mathrm{e}^{\mathrm{i}s\frac{\pi}{2}} \cdot \mathrm{e}^{\mathrm{i}l\frac{3}{4}\pi} - \varepsilon_1^h \cdot \mathrm{e}^{\mathrm{i}k\frac{\pi}{2}} \cdot \mathrm{e}^{\mathrm{i}s\frac{5}{4}\pi} + \right.$$
$$\left. + \varepsilon_2^h \cdot \mathrm{e}^{\mathrm{i}p\frac{\pi}{2}} - \varepsilon_2^h \cdot \mathrm{e}^{\mathrm{i}l\frac{pi}{2}} \cdot \mathrm{e}^{\mathrm{i}p\frac{pi}{2}} \cdot \mathrm{e}^{\mathrm{i}s\frac{3}{2}\pi} + \varepsilon_3^h \cdot \mathrm{e}^{\mathrm{i}k\frac{pi}{2}} \cdot \mathrm{e}^{\mathrm{i}l\frac{3}{2}\pi} \cdot \mathrm{e}^{\mathrm{i}s\frac{5}{4}\pi} - \varepsilon_3^h \cdot \mathrm{e}^{\mathrm{i}l\frac{3}{4}\pi} \cdot \mathrm{e}^{\mathrm{i}k\frac{pi}{2}}\right] = 0, \tag{185}$$

kde $\Psi = \mathrm{e}^{\mathrm{i}\psi}$.

Rovnici (185) je možné vyjadřit ve tvaru

$$\sum_{m=0}^{M} C_h^m \cdot \Psi^m = 0. \tag{186}$$

Řešením této rovnice je velikost úhlu ψ, který určuje orientaci hlavních napětí a po dosazení do (175) a (176) pak i jejich velikosti.

Následující úprava výše zmíněných vztahů, potřebná pro počitačové zpracování dané rovnice. Rovnici (185) lze vyjádřit symbolicky ve tvaru

$$G_{kpls} \cdot \left[\varepsilon_1^h \cdot F_{kpls}^1 + \varepsilon_2^h \cdot F_{kpls}^2 + \varepsilon_3^h \cdot F_{kpls}^3\right] \cdot \Psi^{s+l-k-p} = 0, \tag{187}$$

kdy členy F_{kpls}^1–F_{kpls}^3 popisují orientaci tenzometrů a člen G_{kpls} pak obsahuje kalibrační koeficienty určené na základě řešení numerického experimentu.

Určení kalibračních koeficientů

Dle vztahu (150) je zavedena funkce pro deformaci v případě zatížení jednotkovým napětím

$$\varepsilon^h(\varphi,\psi) = \sum_{k,l=-K}^{K} C_{kl}^h \cdot \mathrm{e}^{\mathrm{i}k\varphi} \cdot \mathrm{e}^{\mathrm{i}l\psi} = \sum C_a^h \cdot B_a(\varphi,\psi), \tag{188}$$

bázovou funkci B_a lze pak vyjádřit vztahem

$$\mathbf{B} = [\mathrm{e.\hat{}}(\mathrm{i}\cdot k\cdot\varphi) \otimes \mathrm{e.\hat{}}(\mathrm{i}\cdot k\cdot\psi)] \tag{189}$$

funkce pro deformaci pak může být vyjádřena vztahem

$$\varepsilon(\varphi,\psi) = \mathbf{B}(\varphi,\psi)\cdot\mathbf{C}. \tag{190}$$

V případě znalosti deformací pro daná φ a ψ je možné pomocí metody nejmenších čtverců (viz např. [MAREŠ, 2006d]) vyjádřit matici koeficientů při dané volbě bázové funkce

$$\varepsilon = \mathbf{B}\cdot\mathbf{C}, \tag{191}$$

kde ε je vektor odměřených deformací pro příslušná φ a ψ

$$\mathbf{C} = [\mathbf{B}^T\mathbf{B}]^{-1}\mathbf{B}^T\varepsilon. \tag{192}$$

V daném případě φ nabývalo hodnot (0,355) po 5°, ψ nabývalo hodnot (0,345) po 15° a K udávající počet členů řady bylo zvoleno 5.

Ověření metody na numerickém modelu

Pro ověření metody byly provedeny výpočty napětí na základě deformací „odměřených“ na vytvořeném konečněprvkovém modelu. Model byl zatížen jednoosou napjatostí o velikosti σ_1=1 MPa.

0.0.1 Data pro ověření

Z výsledků numerické simulace byly odečteny data, která jsou vynesena v tab. 15. Úhel φ udává orientaci mezi směrem zatížení a orientací excentrického otvoru, ψ je úhel mezi tenzometrem 1 a směrem zatížení, γ je úhel mezi směrem excentricity otvoru a směrem tenzometru 1.

Ověření	$h[mm]$	$\varphi[^\circ]$	ψ [°]	γ [°]	$\varepsilon_1[\mu i]$	$\varepsilon_2[\mu i]$	$\varepsilon_3[\mu i]$
1	0,2	15	5	20	-0,2034003046	-0,04860032732	0,03613706667
2	0,3	45	60	105	-0,0169590209	0,04707186463	-0,20248489818
3	0,4	225	10	235	-0,4246858225	-0,06139822517	0,08985523435
4	0,5	105	100	235	0,1392641593	-0,42171154746	-0,68131726039

Table 15: Data odečtená z MKP modelu pro ověření metody

0.0.2 Výsledky ověření

Výše uvedená data byla podrobena výpočtu pomocí maker uvedených v příloze. Výsledky jsou uvedeny v tab. 16.

Ověření	ψ [°]	σ_1 [MPa]	σ_2[MPa]
1	8	1,05	-0,054
2	60	1,03	0,001
3	12	1,06	-0,003
4	99	0,97	0,006

Table 16: Výsledky ověření

Z uvedených výsledků vyplývá, že odchylka od očekávaných hodnot se pohybuje v řádu procent a je tedy možné považovat na základě těchto výsledků uvedený postup jako funkční.

Experimentální data

Navržená metoda byla použita na spočtení zbytkových napětí pro data získaná v rámci experimentu prováděného na pracovišti odboru pružnosti a pevnosti ústavu mechaniky při řešení určování zbytkových napětí u trubkových ohybů [Doubrava *et al.*, 2003c]. Jednalo se o problém popisu zbytkových napětí u trubkového ohybu v případě vynechání technologické operace žíhání a následného popouštění s ohledem na možné snížení výrobních nákladů firmy Modřanská potrubní.

0.0.3 Popis zkoumaného tělesa

Zkoumaný ohyb byl vyroben z trubky o průměru 273 mm, tloušťka stěny 16 mm a délky 5,3 m. Materiál trubky 12 022.1, výrobce Vítkovice, číslo atestu 4639/92, číslo tavby 2347. Poloměr

ohybu 1250 mm, kdy poloměr ohybu trubky byl pětkrát větší než průměr trubky. Způsob ohýbání – za tepla s indukčním ohřevem na 920 – 980 °C s ochlazováním z tvářecí teploty na klidném vzduchu (bez vodní sprchy).

0.0.4 Výrobní postup

Nejprve byla zhotovena rovná část trubky (část A) se simulovaným ohřevem shodným s ohřevem při ohýbání (ale trubka nebyla ohnuta a zůstala rovná). V dalším kroku došlo ke zhotoveni ohybu 90° (část B) tvářením za tepla s indukčním ohřevem za kontrolovaných podmínek tváření. Poté byla část A odříznuta a podrobena technologické operaci normalizačního žíhání (920 °C/50 min./ochlazování na vzduchu).

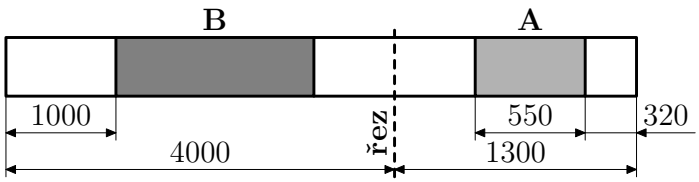

Obr. 51: Schéma trubky před tvářením

Na části B bylo vytypováno 14 míst, v kterých bylo provedeno měření. Rozmístění těchto míst je na obr. 52.

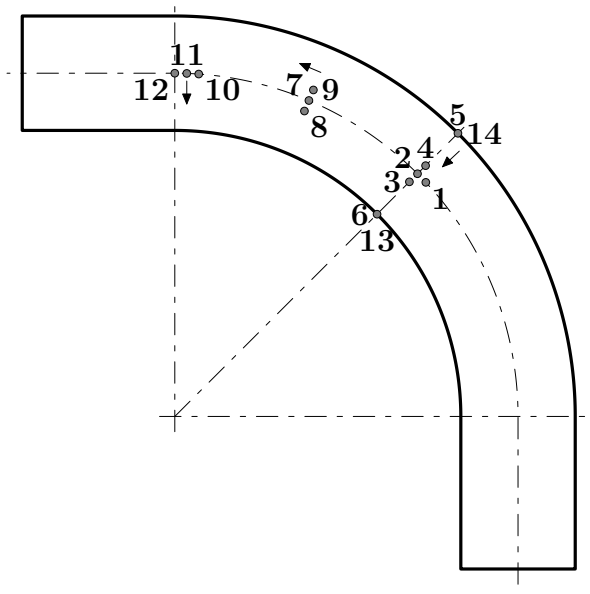

Obr. 52: Schéma měřených míst na části B

0.0.5 Souprava RESTAN

Experiment byl proveden pomocí zařízení MTS-3000 SINT-RESTAN (RESTAN). Souprava RESTAN [sin, 1999] je zařízení k experimentálnímu určování zbytkových napětí pomocí odvrtávací metody. Dodavatelem tohoto zařízení je firma Hottinger Baldwin Messtechnik a výrobcem pak italská firma SINT Technology. Souprava se skládá z vrtacího přípravku, řídící jednotky, měřící karty a tlakového ventilu. Dále byla souprava doplněna o PC, o vzduchový kompresor a dynamickou měřící ústřednu.

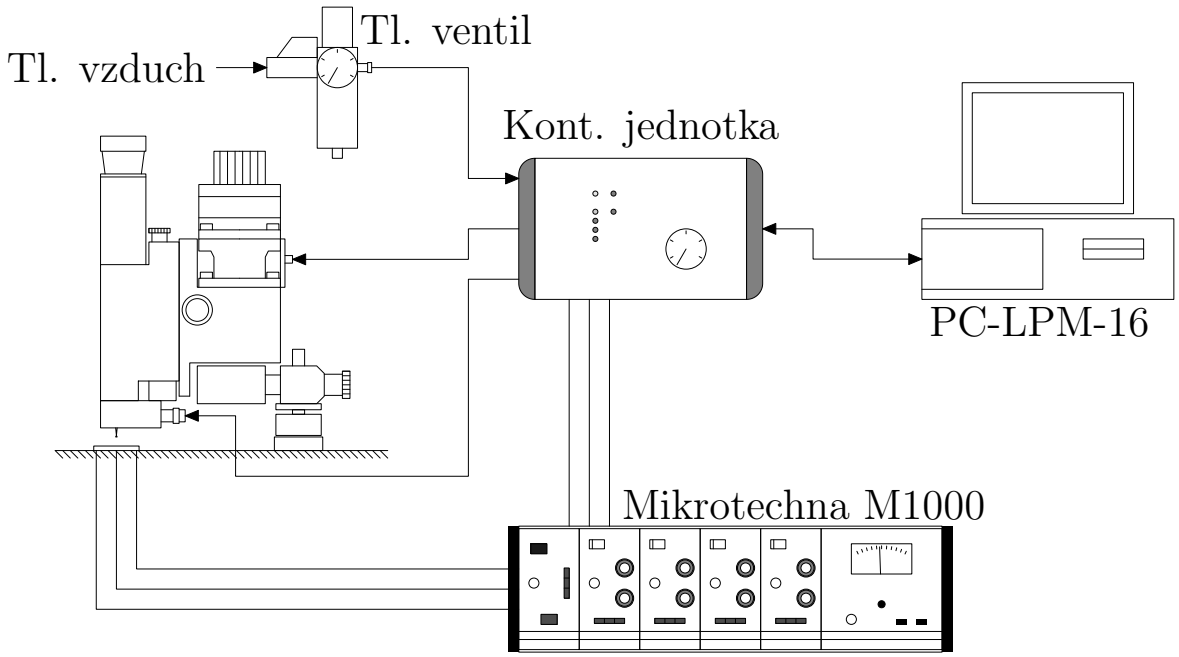

Obr. 53: Měřící řetězec při instalaci zařízení RESTAN

Vrtací přípravek

Základní konstrukce vrtacího přípravku je umístěna na třech stavitelných magnetických nohách. Ty umožňují nastavení přípravku do požadované polohy, kdy osa vrtací turbínky je kolmá k povrchu zkoumané součásti. Dále je možný horizontální posuv v směru osy x a y. Velikost posuvů je indikována měřícími hodinkami. Pomocí těchto posuvů a mikroskopu je možné na konci měření odečíst případnou excentricitu otvoru a její orientaci vůči prvnímu tenzometru. Vrtací a optický člen je spojen s tímto základem pomocí pohybového šroubu, který je ovládán krokovým motorem. Vzduchová turbínka s vrtací frézou je umístěna na výklopném rameni, kdy po odklopení turbínky je možný průzor optickým mikroskopem. Tento mikroskop spolu s posuvným zařízením umožňuje zacílení na střed tenzometrické růžice. Do kleštiny vzduchové turbínky je umístěna šestibřitá kuželová fréza. Uváděné pracovní otáčky jsou 300 000 otáček za minutu při dodržení výrobcem požadované velikosti tlaku.

Řídící elektronická jednotka

Řídící elektronická jednotka spravuje všechny vstupy a výstupy. Vstupuje do ní tlakový vzduch a řídí výstupní tlakový vzduch vstupující do vrtací turbínky. Jednotka je propojena s měřící kartou pomocí plochého kabelu. Dále jsou připojeny výstupy z analogové tenzometrické ústředny odpovídající jednotlivým tenzometrům v růžici, kontakt pro určení nulové hloubky a kabel pro řízení krokového motoru vrtacího přípravku. Na čelním panelu je tlakoměr, který měří velikost tlaku ve vnitřním okruhu tlakového vzduchu.

Regulační ventil

Tento ventil umožňuje uzavření vstupu vzduchu od kompresoru. Je vybaven tlakoměrem, jenž měří výstupní tlak. Dále obsahuje filtr, který zachytává mechanické nečistoty a kondenzovanou vlhkost, aby nevstupovala do vnitřního okruhu. Na ventilu je pak možné nastavit výstupní velikost tlaku. Pro správnou funkci se požaduje velikost 4 barů.

Měřící karta

Jedná se o 16 bitovou kartu PC–LPM–16 firmy Nationall Instruments. Karta má ISA sběrnici. Vstupní signál je možný v rozsahu ± 5 V a výstupní napětí pak v rozsahu ± 10 V.

PC

Pro instalaci měřící karty je potřeba PC vybavené ISA slotem. Minimální požadovaná konfigurace je

- AT 486–66 MHz
- MS–DOS 6.0 (nebo vyšší)
- Windows 3.1 (nebo vyšší)

Dále je pak požadováno místo na pevném disku potřebné pro instalaci měřícího a vyhodnocovacího softwaru (zhruba 20 MB).

Dynamická ústředna M1000

Pro měření uvolněných deformací byla soupravu doplněna o měřící tenzometrickou ústřednu. V popisovaném případě byla použita analogová dynamické ústředna M1000 [mik, 1982], vyrobená firmou MIKROTECHNA Praha. Tato ústředna je vybavena čtyřmi měřícími kanály–zesilovače M 1101 a indikační jednotkou M 1401. Měření na ústředně je možné v půlmostovém a nebo v celomostovém zapojení. V popisovaném případě bylo použito půlmostové zapojení, kdy pro doplnění půlmostu byly použity tenzometrické růžice nainstalované poblíž místa vrtu. Na každém zesilovači se nastavuje měřící rozsah, kdy interval hodnot je 0,1–20 mV/V. Konkrétní hodnota rozsahu musí být volena tak, aby při měření nedošlo k překročení maximálního dovoleného signálu. Napájecí napětí se nastavuje pro všechny kanály najednou a jsou možné hodnoty 1, 2, a 4 V. Tato ústředna umožňuje pouze manuální vyvážení měřícího obvodu.

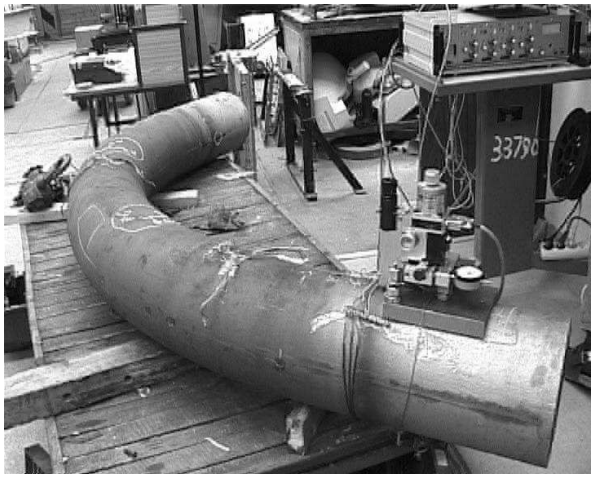

Obr. 54: Experimentální zjišťování zbytkových napětí na trubkovém ohybu

Aplikace na experimentálně změřená data

Pro případ použití navrhované metody byly vybrány dvě měřená místa: místo 8 (tab. 17 a obr. 55) a místo 10 (tab. 18 a obr. 56). V místě 8 byla změřena excentricita 0,2 mm a její orientace oproti

1. tenzometru v růžici byla $\gamma = 30°$, v místě 10 pak byla změřena excentricita o velikosti 0,17 mm a orientaci $\gamma = 85°$.

h[mm]	$\varepsilon_1[\mu$i]	$\varepsilon_2[\mu$i]	$\varepsilon_3[\mu$i]
0,02	0,23	-0,11	-0,03
0,05	2,55	-0,25	-3,49
0,11	10,32	2,21	-4,43
0,16	17,23	9,29	-1,82
0,24	27,02	19,36	0,79
0,34	39,55	32,34	4,96
0,46	54,01	46,95	8,61
0,59	68,9	63,5	15,11
0,74	80,57	74,7	18,06
0,91	95,13	87,5	21,36
1,10	103,21	92,52	23,37
1,30	109,64	97,27	21,44
1,51	113,79	98,29	20,15

Table 17: Naměřená data v místě 8

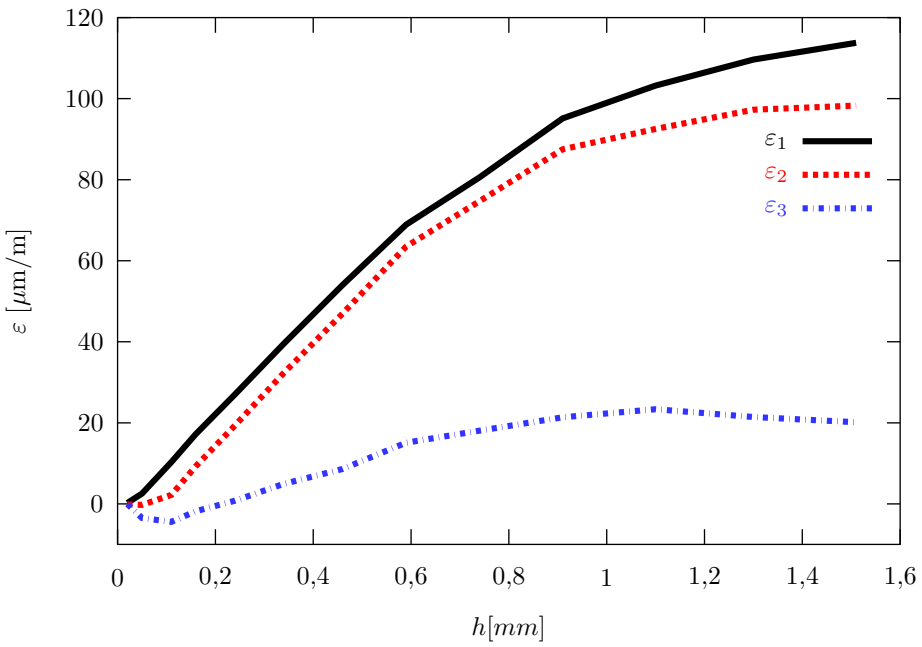

Obr. 55: Naměřená data v místě 8

Na základě deformací změřených na trubkovém ohybu byla určena zbytková napětí ve dvou vybraných místech [Karel Doubrava, 2006]. Data jsou porovnána s výsledky získanými při neuvažování excentricity otvoru [Doubrava *et al.*, 2004b].

Z uvedených grafů vyplývá rozdíl spočtených napětí při zahrnutí excentricity otvoru. Tento rozdíl je v řádu procent až desítek procent. U obou vyšetřovaných míst výsledky získané při zahrnutí excentricity dávají menší hladinu zbytkových napětí s rozdílem ca 20%.

h[mm]	$\varepsilon_1[\mu$i]	$\varepsilon_2[\mu$i]	$\varepsilon_3[\mu$i]
0,02	0,1	1,47	0,64
0,05	1,45	2,15	2,25
0,10	2,1	5,49	5,34
0,16	6,2	15,93	13,86
0,24	15,62	23,5	25,48
0,34	24,8	34,14	36,11
0,46	32,28	49,73	55,31
0,59	38,85	65,97	75,39
0,74	43,04	82,98	95,68
0,91	42,99	96,07	111,89
1,10	38,8	105,5	122,06
1,30	33,31	115,97	131,53
1,51	28,92	121,98	137,18
1,75	23,76	128,25	143,28
2,00	17,92	119,43	151,38

Table 18: Naměřená data v místě 10

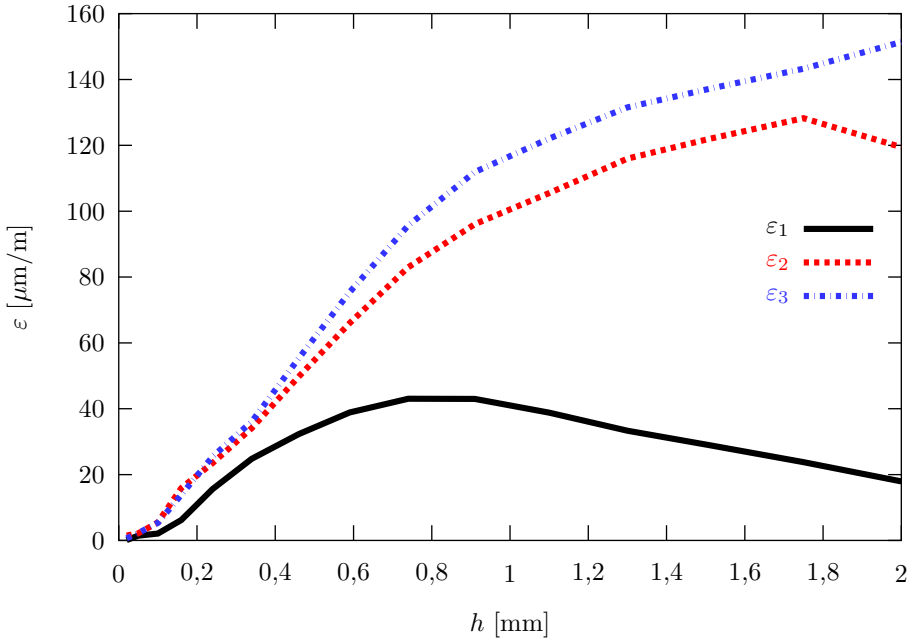

Obr. 56: Naměřená data v místě 10

h[mm]	σ_1[MPa]	σ_2[MPa]	ψ[°]
0,05	35	-94	0
0,10	-19	-109	163
0,15	-35	-109	163
0,20	-38	-107	157
0,25	-40	-95	157

Table 19: Zbytková napětí v místě 8

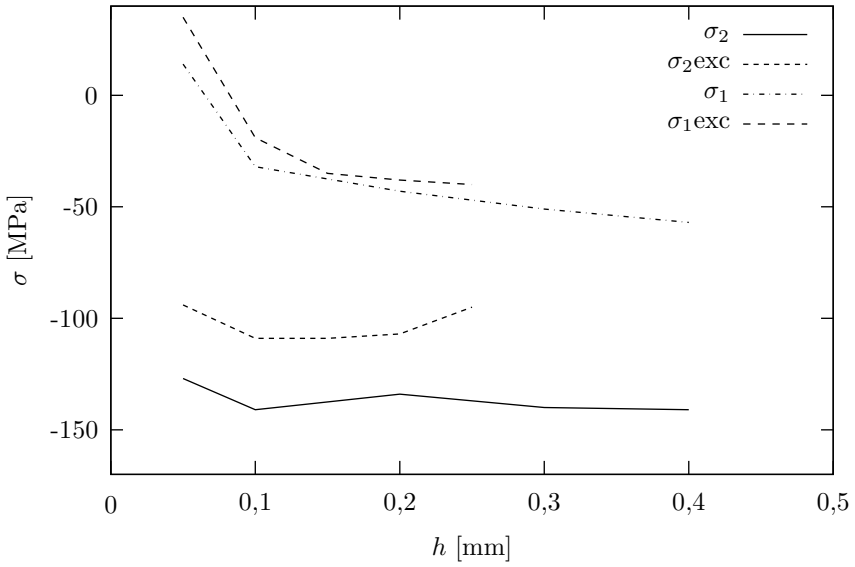

Obr. 57: Zbytková napětí v místě 8

h[mm]	σ_1[MPa]	σ_2[MPa]	ψ[°]
0,05	-38	-76	113
0,10	-76	-122	113
0,15	-87	-123	103
0,20	-94	-136	103
0,25	-75	-114	103

Table 20: Zbytková napětí v místě 10

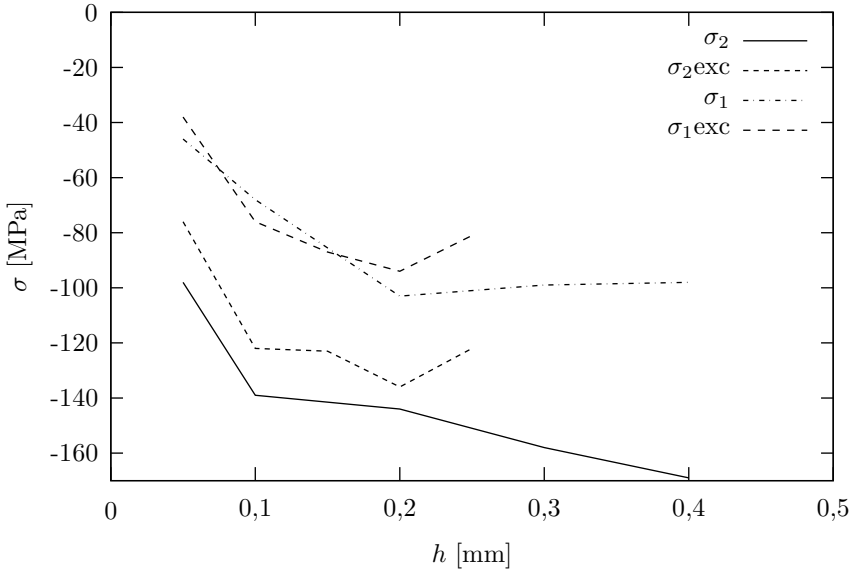

Obr. 58: Zbytková napětí v místě 10

Shrnutí a přínosy práce

Shrnutí práce

V kapitole o současném stavu byl uveden zevrubný popis metod pro vyhodnocování zbytkových napětí na základě deformací získaných odvrtávací metodou. V dnešní době je často zákazníky vyžadována znalost zbytkových napětí, kdy je nejčastěji vyžadováno určení zbytkových napětí dle normy ASTM E837. Tato norma je rovněž v přehledu zahrnuta a jsou uvedeny podmínky jejího použití. V oblasti excentricity otvoru tato norma připouští excentricitu, která nepřekročí větší z rozměrů $0{,}004 \cdot D$ nebo 0,025 mm. Vzhledem k faktu, že u některých experimentů byla zjištěna excentricita přesahující výše uvedenou mez, přistoupilo se k sestavení metody, která by umožňovala zahrnout excentricitu vrtaného otvoru vůči středu tenzometrické růřice. Byly stanoveny nasledující cíle a ty postupně řešeny:

0.0.6 Stav napjatosti kolem otvoru excentrického vůči středu tenzometrické růžice

Pro zjištění stavu napjatosti byl sestaven konečněprvkový model. Jednalo se o simulaci experimentu při určování kalibračních koeficientů dle normy ASTM E837. MKP model byl vytvořen v programu ABAQUS CAE. Prostředí CAE je vytvořeno pomocí interpretačního jazyka Python, což spolu s možností parametrizovat MKP model umožňuje určit stav napjatosti v okolí excentrického otvoru. Tímto je možné výše zmíněný cíl považovat za splněný.

0.0.7 Odezva tenzometrů v okolí otvoru excentrického vůči středu tenzometrické růžice

Vytvořený MKP model byl doplněn o tenzometry, jejichž vinutí bylo namodelováno dle rozměrů tenzmoterické růžice RY61S firmy HBM. Byla provedena instalace v okolí excentrického otvoru a pro danou excentricitu otvoru a jeho orientaci byly odečteny deformace odpovídající signálům daných tenzometrů. Pro výše uvedené bylo sestaveno makro zautomatizující načítání dat. Tímto je možné výše zmíněný cíl považovat za splněný.

0.0.8 Metoda pro zohlednění excentricity otvoru při výpočtu zbytkových napětí

Byl proveden teoretický rozbor popisující vztah mezi uvolněnými deformacemi změřenými tenzometrickou růžicí a zbytkovým napětím v případě excentrického otvoru za předpokladu konstantní velikosti excentricity a konstantního průběhu zbytkových napětí s hloubkou. Byla sestavena soustava tří rovnic, na jejichž základě je možné určit směr hlavních napětí a jejich velikost. Metoda byla ověřena na datech získaných z MKP modelu, kdy maximální odchylka byla 6%. Tímto byl daný cíl splněn.

0.0.9 Aplikace na experimentální data

Navržená metoda byla použita na data získaná v rámci řešení zakázky na zjišťování zbytkových napětí na trubkovém ohybu [Doubrava *et al.*, 2003c], [Doubrava *et al.*, 2003b]. Experiment byl proveden pomocí zařízení RESTAN. Toto zařízení umožňuje určit excentricitu vyvrtaného otovoru. Byla vybrána dvě místa a data naměřená během vrtání otvoru v těchto dvou místech byla vyhodnocena pomocí navržené metody [Karel Doubrava, 2006] a zjištěné hodnoty zbytkových napětí byly srovnány s hodnotamy získanými v případě neuvažování excentricity vyvrtaného otvoru [Doubrava *et al.*, 2004b]. Výsledky těchto dvou případů se lišili zhruba o 20%. Tímto byl splněn i poslední cíl předkládané práce.

Na základě těchto bodu je možné konstatovat, že všechny stanovené cíle byly splněny.

Přínos pro vědu

V předkládané práci byl proveden rozbor stavu napjatosti v případě otvoru excentrického ke středu tenzometrické růžice, kdy bylo použito konečněprvkového modelu simulujícího experimentální určení kalibračních konstant. Byl navržen postup pro zohlednění excentricity otvoru při určování zbytkových napětí. V literatuře, mně známé, byl publikován postup pouze pro korekci případu s průchozím otvorem. Metoda navržená v této práci vychází z předpokladu konstantního napětí po hloubce otvoru. Získané výsledky potom odpovídají ekvivalentnímu napětí, které by způsobilo danou deformaci. Předpokládá se, že toto ekvivalentní napětí je s hloubkou konstantní. Zde spatřují další možnost rozšíření, kdy kombinací navrženého postupu a například integrální metody by bylo možné vyhodnocovat i průběhy zbytkových napětí v případě skokově proměnlivého průběhu zbytkových napětí s hloubkou.

Přínos pro praxi

Odvrtávací metoda patří v praxi mezi nejčastěji používané experimentální metody určování zbytkových napětí. Při měření zbytkových napětí prováděných v laboratořích odboru pružnosti a pevnosti, ústavu mechaniky, byla u některých testů zjištěna větší excentricita otvoru oproti středu tenzometrické růžice, než umožňuje norma ASTM E837, kdy tato norma patří mezi mezinárodně uznávané postupy. Popsaná metoda umožňuje zahrnout vliv excentricity otvoru do výpočtu zbytkových napětí.

V případě uvažování excentricity, která je s hloubkou konstantní, je zřejmé, že geometrie skutečného excentrického otvoru oproti geometrii ideálního otvoru představuje zdroj chyb, kdy tato chyba bude zřejmě větší pro menší hloubky otvoru. Na druhou stranu uvolněné deformace změřené po odvtrání kroků v počátečních hloubkách jsou řádově souměřitelné s měřící chybou indikačního zařízení. Při použití popsaného postupu je možné zvýšit citlivost odvrtávací metody pro počáteční kroky vrtání otvoru i v případě excentricity vyhovující normě ASTM E837. Další možné využití by bylo možné v případě vrtání otvoru bez možnosti zaměření středu vrtacího nástroje do středu tenzometrické růžice. Zjištění excentricity by pak bylo možné například zachycením vrtaného místa pomocí digitální fotografie a jejím následným vyhodnocením.

Závěr

V této práci byly řešeny problémy spojené s problematikou excentricity otvoru vůči středu tenzometrické růžice. Byl popsán současný stav problematiky vyhodnocování zbytkových napětí pomocí odvrtávací metody.

Pro popis napjatosti v okolí excentrického otvoru byl vytvořen numerický model procesu odvrtávání. Byly rovněž namodelovány tenzometry, které odpovídaly skutečnému tvaru tenzometrické růžice, kdy signály z těchto tenzometrů byly odečítány pomocí sestavených maker.

Byl proveden rozbor problému excentrického otvoru na jehož základě byl navržen postup pro zohlednění excentricity otvoru při výpočtu zbytkových napětí. Byly sestaveny vztahy určující závislost mezi změřenými deformacemi a zbytkovým napětím. Výsledky numerických experimentů pak posloužily k určení koeficientů u navržených vztahů. Navržený postup byl ověřen dosazením hodnot deformací odečtených numerickou tenzometrickou růžicí. Bylo dosaženo dobré shody mezi vypočteným napětím a napětím, jímž byl numerický model zatížen, kdy zjištěná maximální odchylka byla 6%.

Bylo provedeno vyhodnocení dat získaných při experimentálním měření, kdy byl zaznamenán rozdíl oproti výsledkům získaným bez uvažování excentricity otvoru. Tento rozdíl se pohyboval u jednotlivých hloubek v rozmezí procent až desítek procent s průměrnou odchylkou ca 20%.

Navržený postup umožňuje zahrnout vliv excentricity při určování zbytkových napětí pomocí odvrtávací metody. Tímto postupem je možné zvýšit citlivost odvrtávací metody v případě menších hloubek otvoru a v případě excentricity menší, než povoluje norma ASTM E837.

Nanobiomechanical model of cortical bone

Author: Tomáš Mareš

Department of Mechanics, Faculty of Mechanical Engineering, Czech Technical University in Prague, Czech Republic, Technická 4, 166 07 Prague
<Tomas.Mares@fs.cvut.cz>

Geometry and internal structure of thigh bone

The femur,[1] the longest and strongest bone in the skeleton, is almost perfectly cylindrical in the greater part of its extent.

[1] [GRAY, 1918], *e.g.* at http://www.bartleby.com/107/59.html.

Geometry and nomenclature of the femur

In the following let us list some comments regarding the terms stated in Figs. 59 and 60.[2]

Proximal extremity [Upper extremity] presents for examination the head, the neck, the greater and lesser trochanter.

Caput femoris [L., head of femur] is the proximal end of the femur, articulating with the acetabulum on the *os coxae*. Called also femoral head.

Acetabulum [L., vinegar-cruet, from acetum vinegar] is the large cup-shaped cavity on the lateral surface of the *os coxae* in which the head of the femur articulates; called also acetabular bone, cotyloid cavity, and os acetabuli.

Fovea [L., a pit], *i.e.*, anatomic nomenclature for a small pit in the surface of a structure or organ.

Fovea capitis femoris, *i.e.*, fovea of head of femur: a depression in the head of the femur where the ligamentum teres is attached; called also *fossa capitis femoris* and fossa of head of femur.

Collum femoris [Femoral neck, Neck of femur] is the heavy column of bone connecting the head of the femur and the shaft. The *collum femoris* (neck) is broader laterally than medially.

Tuberculum [L., dimension of tuber], is a general term in anatomical nomenclature for a tubercle, nodule, or small eminence.

Capsula articularis [L., articular capsule] is the saclike envelope that encloses the cavity of a synovial joint by attaching to the circumference of the articular end of each involved bone; it consists of a fibrous membrane and a synovial membrane. Called also joint capsule and synovial capsule.

Linea intertrochanterica [Anterior intertrochanteric line] is a line running obliquely downward and medially from the tubercle of the femur, winding around the medial side of the body of the bone.

Musculus psoas (so'as) major [Greater psoas muscle] is a muscle with origin from the bodies of the lumbar vertebrae and the intervertebral disks from the twelfth thoracic to the fifth lumbar vertebrae and from the transverse processes of the lumbar vertebrae, with insertion into the lesser trochanter of femur, with nerve supply from the lumbar plexus, and whose action flexes the thigh or trunk.

Vastus [L., great or vast]. Description of muscles, as musculus vastus lateralis.

Musculus quadriceps femoris [Quadriceps muscle of thigh] is a name applied collectively to the rectus femoris, vastus intermedius, vastus lateralis, and vastus medialis, inserting by a common tendon that surrounds the patella and ends on the tuberosity of the tibia, and acting to extend the leg upon the thigh.

Musculus vastus lateralis has origin on capsule of hip joint, lateral aspect of femur. Insertion point: patella, common tendon of quadriceps femoris. Action: extends leg.

Musculus vastus intermedius (Crureus) is the muscle for extension of the knee joint and thus extends leg. It origins at anterior and lateral surfaces of the body of the femur in its upper two-thirds and from the lower part of the lateral intermuscular septum (Septum intermusculare femoris laterale). Its fibers end in a superficial aponeurosis, which forms the deep part of the Quadriceps femoris tendon.

Musculus vastus medialis originates on medial aspect of femur. Its insertion is on patella, common tendon of quadriceps femoris. Action: extends leg.

Septum is an anatomic nomenclature for a dividing wall or partition.

Trochanter major [Greater trochanter] is a broad, flat process at the upper end of the lateral surface of the femur, to which several muscles are attached.

Trochanter minor [Lesser trochanter] is a short conical process projecting medially from the lower part of the posterior border of the base of the neck of the femur.

[2]Cf. [Dorland and Newman, 2003] and A.D.A.M. Encyclopedia at http://www.mercksource.com.

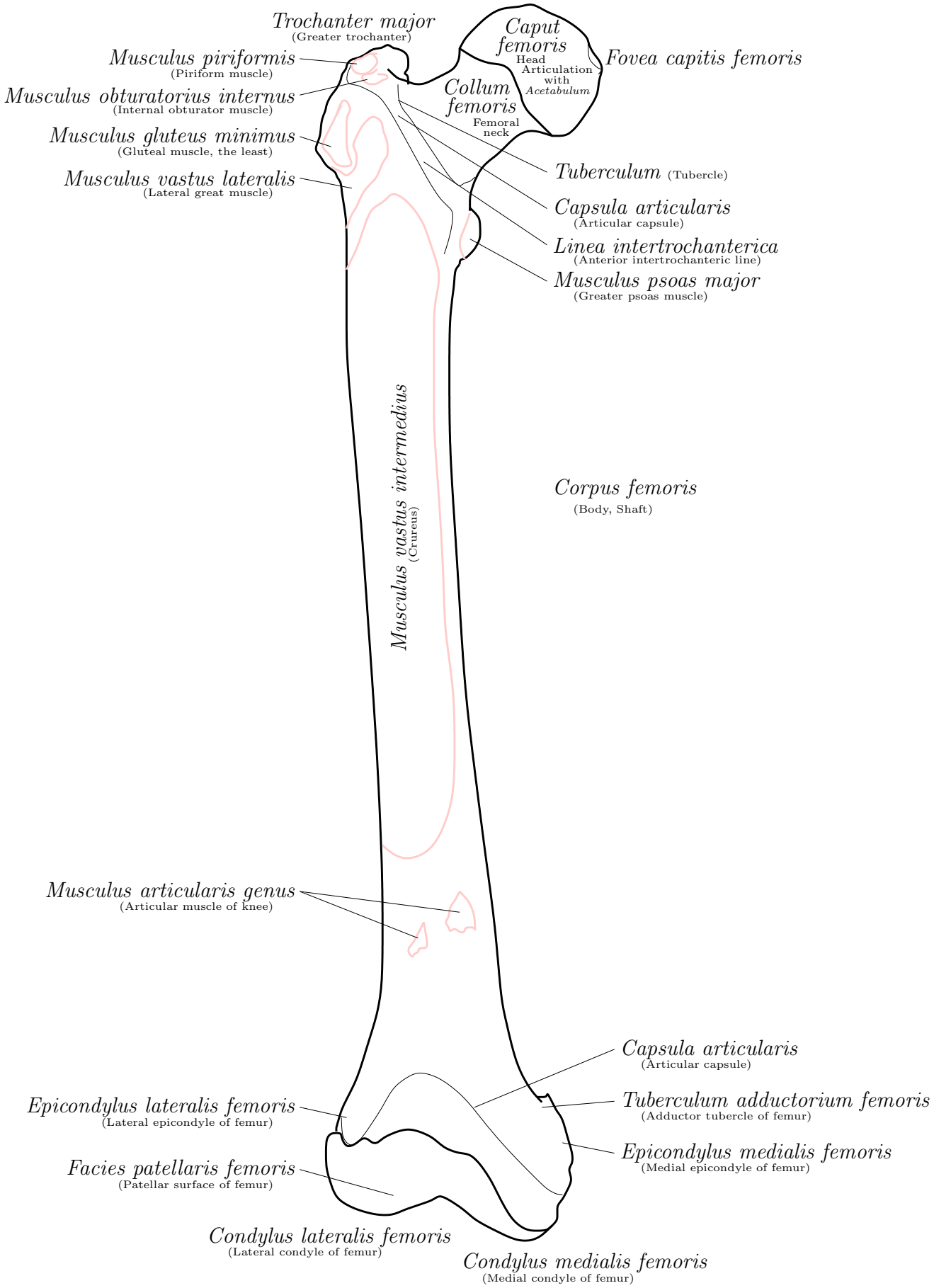

Fig. 59: Right femur—Anterior surface

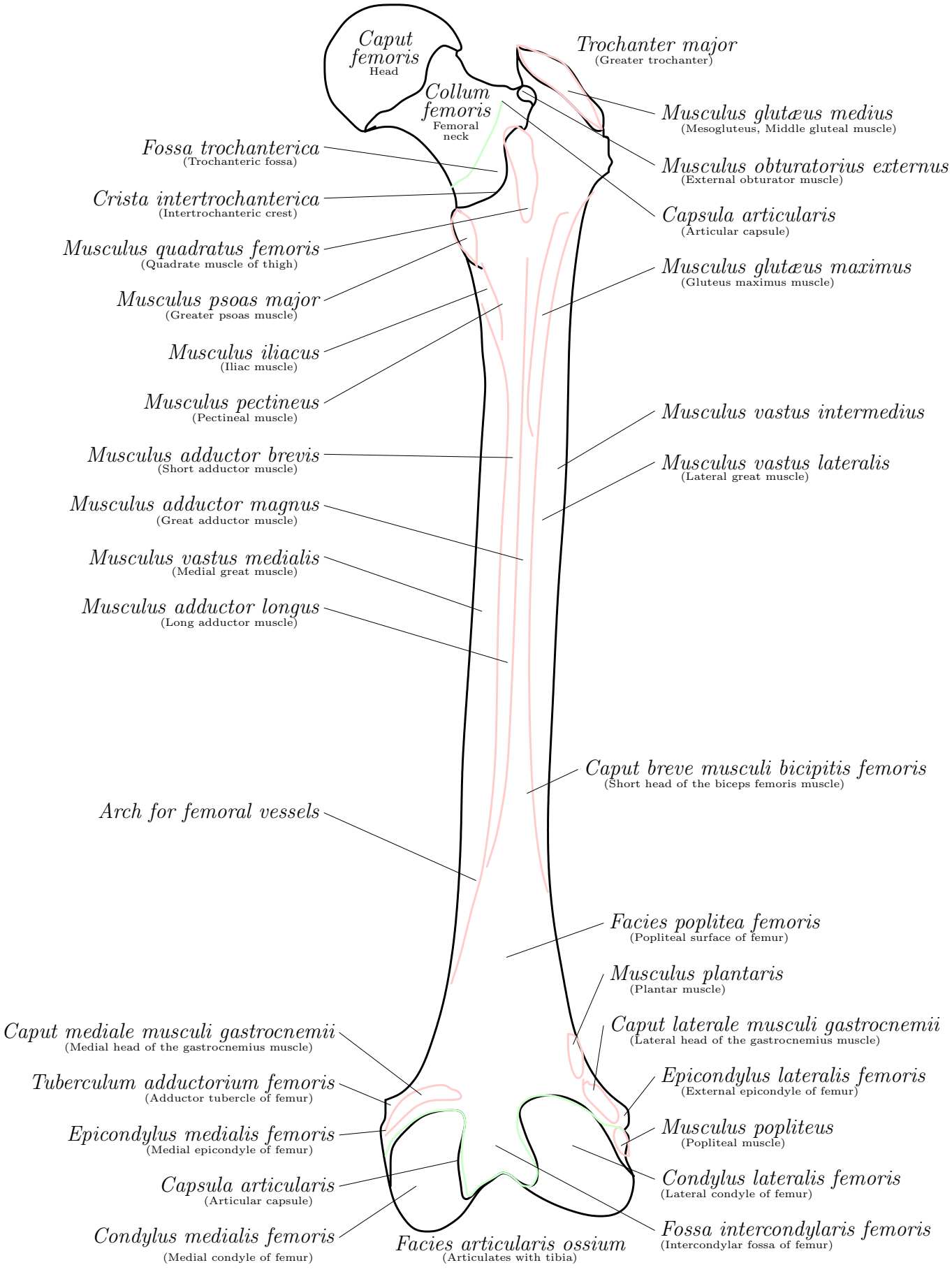

Fig. 60: Right femur—Posterior surface

Musculus piriformis [Piriform muscle] has origin on ilium, second to fourth sacral vertebrae and insertion on upper border of greater trochanter.

Musculus gemellus inferior [Inferior gemellus muscle] originates from the tuberosity of ischium and inserts on the greater trochanter of femur. It rotates thigh laterally.

Musculus gemellus superior [Superior gemellus muscle] originates from the spine of ischium and inserts on the greater trochanter of femur. Action: It rotates thigh laterally.

Obturator [L.] is any structure, natural or artificial, that closes an opening.

Musculus obturatorius internus [Internal obturator muscle] has origin on pelvic surface of hip bone, margin of obturator foramen, ramus of ischium, inferior ramus of pubis, internal surface of obturator membrane. The insertion is on greater trochanter of femur. The action is to rotate thigh laterally.

Musculus glutæus minimus [Least gluteal muscle] has origin on lateral surface of ilium between anterior and inferior gluteal lines. Insertion: greater trochanter of femur. Action: abducts, rotates thigh medially.

Musculus glutæus medius [Mesogluteus, Middle gluteal muscle] originates on lateral surface of ilium between anterior and posterior gluteal lines. Insertion is on greater trochanter of femur. Action: abducts and rotates thigh medially.

Musculus glutæus maximus [Gluteus maximus muscle] originates posteriorly from the posterior gluteal line of the ilium, aponeurosis of the erector spinae, dorsal surface of the sacrum, coccyx, and sacrotuberous ligament. It inserts at the iliotibial band and the gluteal tuberosity of the femur. The gluteus maximus is the uppermost of the three muscles. Its action is to extend and outwardly rotate hip, and extend the trunk. The direct attachment to the sacrum it may influence the stability of the joint.

Musculus articularis genus [Articular muscle of knee] originates at the distal fourth of anterior surface of shaft of femur. Insertion: synovial membrane of knee joint. Action: lifts capsule of knee joint.

Epicondylus [Epicondyle] is an eminence upon a bone, above its condyle.

Epicondylus lateralis femoris [Lateral epicondyle of femur] is a projection from the distal end of the femur, above the lateral condyle, for the attachment of collateral ligaments of the knee. Called also external epicondyle of femur.

Epicondylus medialis femoris [Medial epicondyle of femur] is a projection from the distal end of the femur, above the medial condyle, for the attachment of collateral ligaments of the knee; called also internal epicondyle of femur.

Condylus (pl. condyli) [L., from Gr. kondylos knuckle, condyle] is a rounded projection on a bone, usually for articulation with another.

Condylus lateralis femoris [Lateral condyle of femur] is the lateral of the two surfaces at the distal end of the femur that articulate with the superior surfaces of the head of the tibia. It is also called external or fibular condyle of femur.

Condylus medialis femoris [Medial condyle of femur] is the medial of the two surfaces at the distal end of the femur that articulate with the superior surfaces of the head of the tibia. Called also internal or tibial condyle of femur, and condylus tibialis femoris.

Facies patellaris femoris (Patellar surface of femur) is the smooth anterior continuation of the condyles that forms the surface of the femur articulating with the patella; called also anterior intercondylar fossa of femur and patellar fossa of femur.

Tuberculum adductorium femoris [Adductor tubercle of femur] is a small projection from the upper part of the medial epicondyle of the femur, to which the tendon of the adductor magnus muscle is attached.

Fossa (pl. fossae), [L.] is a trench, channel, or hollow place.

Fossa trochanterica [Trochanteric fossa] is a deep depression on the medial surface of the greater trochanter that receives the insertion of the tendon of the obturator externus muscle.

Musculus obturatorius externus [External obturator muscle] originates on pubis, ischium, and superficial surface of obturator membrane. Insertion is on trochanteric fossa of femur. Action: rotates thigh laterally.

Crest is a projection or projecting structure, or ridge, especially one surmounting a bone or its border; see also crista and ridge.

Crista intertrochanterica [Intertrochanteric crest] is a prominent ridge running obliquely downward and medialward from the summit of the greater trochanter on the posterior surface of the neck of the femur to the lesser trochanter; called also intertrochanteric ridge, linea intertrochanterica posterior, and posterior intertrochanteric line.

Musculus quadratus femoris [Quadrate muscle of thigh, Quadratus femoris muscle] originates on upper part of lateral border of tuberosity of ischium; inserts on quadrate tubercle of femur, intertrochanteric crest. It adducts, rotates thigh laterally.

Musculus iliacus [Iliac muscle] originates on iliac fossa and base of sacrum; inserts on greater psoas tendon and lesser trochanter of femur. Action: flexes thigh, trunk on limb.

Musculus pectineus [Pectineal muscle] originates on pectineal line of pubis; inserts on femur distal to lesser trochanter. Action: flexes, adducts thigh.

Musculus adductor brevis [Short adductor muscle, Short h. of triceps femoris muscle] originates on outer surface of inferior ramus of pubis; insertion is on upper part of linea aspera of femur. Action: adducts, rotates, flexes thigh.

Musculus adductor magnus [Great adductor muscle] (2 parts): Deep part originates on inferior ramus of pubis, ramus of ischium. Superficial part on ischial tuberosity. Deep part inserts on linea aspera of femur. Superficial part on adductor tubercle of femur. Action: Deep part adducts thigh, Superficial part extends thigh.

Musculus adductor longus [Long adductor muscle] originates on crest and symphysis of pubis. Insertion is on linea aspera of femur. Action: adducts, rotates, flexes thigh.

Caput breve musculi bicipitis femoris [Short head of the biceps femoris muscle] is arising from the linea aspera femoris.

Facies (pl. facies) is a specific surface of a body structure, part, or organ.

Facies articularis ossium is articular surface of bone: the surface by which a bone articulates with another.

Facies poplitea femoris [Popliteal surface of femur] is the triangular lower third of the posterior surface of the femur, between the medial and lateral supracondylar lines, which forms the superior part of the floor of the popliteal fossa; called also planum popliteum femoris.

Musculus plantaris [Plantar muscle] has origin on oblique popliteal ligament, lateral supracondylar line of femur; insertion on posterior part of calcaneus. Action: plantar flexes foot.

Epicondylus lateralis femoris [Lateral epicondyle of femur] is a projection from the distal end of the femur, above the lateral condyle, for the attachment of collateral ligaments of the knee. Called also external epicondyle of femur.

Musculus popliteus [Popliteal muscle] has origin on lateral condyle of femur, lateral meniscus; insertion is on posterior surface of tibia. Action: flexes leg, rotates leg medially.

Fossa intercondylaris femoris [Intercondylar fossa of femur] is the posterior depression between the condyles of the femur; called also fossa intercondyloidea femoris, intercondylar notch of femur, and popliteal notch or incisure.

Caput laterale musculi gastrocnemii [Lateral head of the gastrocnemius muscle, Lateral gastrocnemius muscle] is arising from the lateral condyle and posterior surface of the femur, and the capsule of the knee joint.

Caput mediale musculi gastrocnemii [Medial head of the gastrocnemius muscle, Medial gastrocnemius muscle] is arising from the medial condyle of the femur and the capsule of the knee joint.

Corpus femoris [Body, Shaft] is almost cylindrical in form. It is slightly arched, so as to be convex in front.

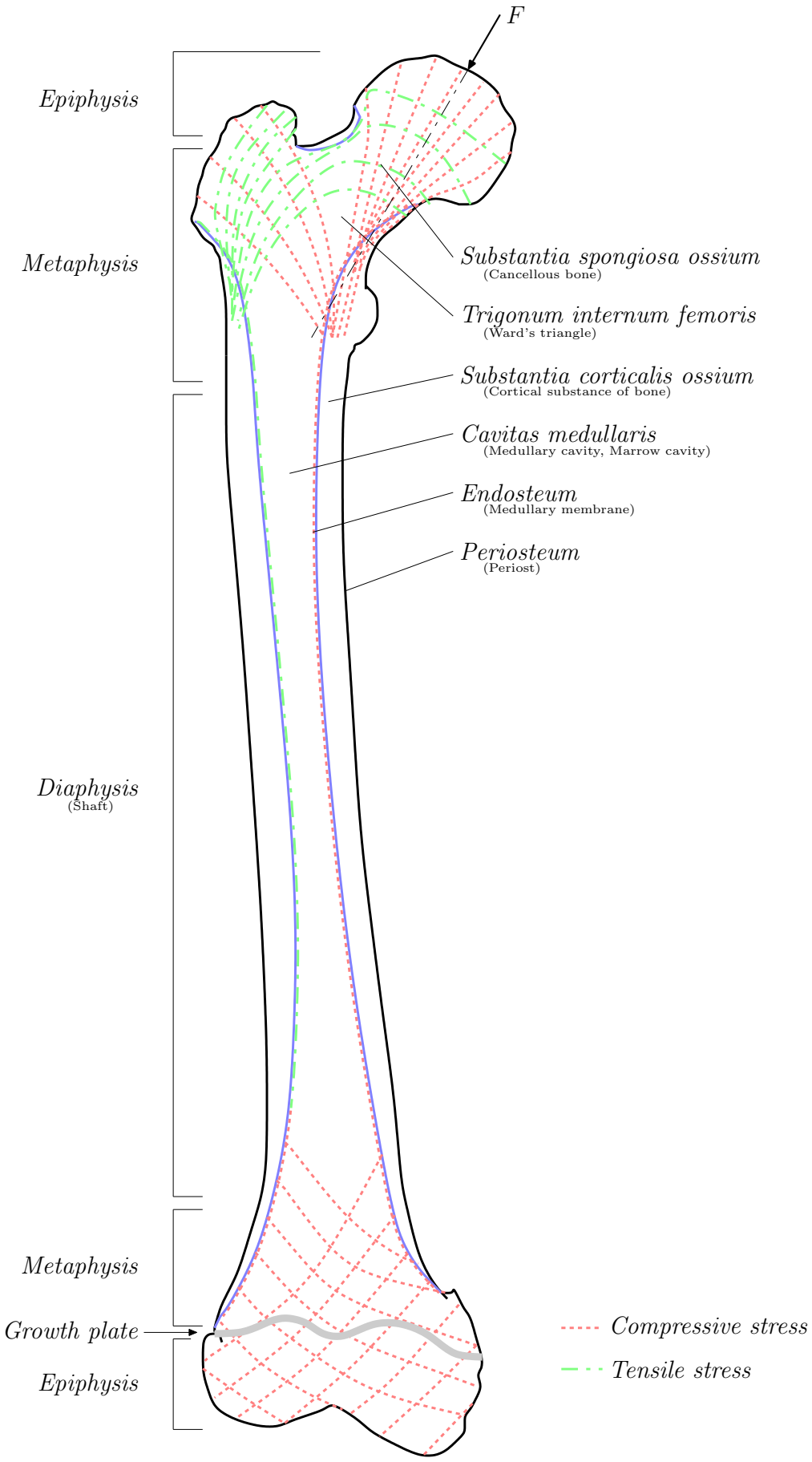

Fig. 61: Internal structure of the right femur—Anterior surface

The architecture and internal structure of the femur

John C. Koch[3] by mathematical analysis has *"shown that in every part of the femur there is a remarkable adaptation of the inner structure of the bone to the machanical requirements due to the load on the femur-head."*

It is believed that the following laws of bone structure have been demonstrated for the femur:

1. The inner structure and external form of human bone are closely adapted to the mechanical conditions existing at every point in the bone.

2. The inner architecture of a normal bone is determined by definite and exact requirements of mathematical and mechanical laws to produce a maximum of strength with a minimum of material.[4]

Trabeculae descend from the periphery of the femoral head toward the medial cortex along the direction of the resultant compressive force, exactly like the compressive trajectories obtained theoretically and by the photoelastic method. A bundle of trabeculae follows an arched course from the lateral to the medial cortex, as do the tensile trajectories derived from theory.[5]

Trigonum internum femoris [Ward's triangle] is the space formed by the angle of the trabeculae (an area of diminished density in the trabecular pattern) in the neck of the femur; a vulnerable point for fracture. It is evident by X-ray as well as by direct inspection.

Cancellus (pl. cancelli) [L., a lattice] any structure arranged like a lattice. A reticular, spongy, or lattice-like structure.

Substantia (pl. substantiae) [L., substance, called also matter] is a general anatomical nomenclature for material of which a tissue, organ, or body is composed.

Substantia spongiosa ossium [Spongy substance of bone, called also Cancellated or Cancellous bone, Spongy bone, Trabecular substance, and Substantia trabecularis ossium] is bone substance made up of thin intersecting lamellae, usually found internal to compact bone.

Corticalis [Cortical] means pertaining to or of the nature of a cortex or bark.

Substantia corticalis ossium [Cortical substance of bone] is the substance comprising the hard outer layer of a bone.

Cavitas medullaris [Medullary cavity, Marrow cavity, Medullary canal, and Medullary space] is the space in the diaphysis of a long bone containing the marrow.

Endo [L., inside, within].

Membrana (gen. and pl. membranae) [Membrane] is an anatomic nomenclature for a thin layer of tissue that covers a surface, lines a cavity, or divides a space or organ.

Endosteum [Medullary membrane] is the tissue lining the medullary cavity of a bone.

Peri (Gr., around, about).

Periosteum (Peri- + Gr. osteon, bone) [Periost] is a specialized connective tissue covering all bones of the body, and possessing bone-forming potentialities; in adults, it consists of two layers that are not sharply defined, the external layer being a network of dense connective tissue containing blood vessels, and the deep layer composed of more loosely arranged collagenous bundles with spindle-shaped connective tissue cells and a network of thin elastic fibers. Thus, the periosteum is a fibrous sheath that covers bones. It contains the blood vessels and nerves that provide nourishment and sensation to the bone.

Epiphysis (pl. epiphyses, Gr.: an ongrowth, excrescence) is the expanded articular end of a long bone, developed from a secondary ossification center, which during the period of growth is

[3][Koch, 1917]. Cf. [Gray, 1918] at `http://www.bartleby.com/107/59.html`. See also Wolff and Roux.

[4]That all is cited from [Gray, 1918]. There also is the following: Diagram of the lines of stress in the upper femur, based upon the mathematical analysis of the right femur. These result from the combination of the different kinds of stresses at each point in the femur. (After Koch.) See http://www.bartleby.com/107/illus248.html, http://www.bartleby.com/107/illus251.html, etc. Cf. second half of http://www.bartleby.com/107/59.html.

[5]See Fig. 61. Cf. [Pauwels, 1976], [Koch, 1917], [Gray, 1918] at `http://www.bartleby.com/107/59.html`.

either entirely cartilaginous or is separated from the shaft by the epiphyseal cartilage. Called also apophysis ossium.

Metaphysis (pl. metaphyses) is the wider part at the extremity of the shaft of a long bone, adjacent to the epiphyseal disk. During development it contains the growth zone and consists of spongy bone; in the adult it is continuous with the epiphysis.

Diaphysis (pl. Diaphyses, Gr.: the point of separation between stalk and branch) [Shaft] is the portion of a long bone formed from a primary center of ossification. It is the elongated cylindrical portion (the shaft) of a long bone, between the ends or extremities (the epiphyses), which are usually articular and wider than the shaft; it consists of a tube of compact bone, enclosing the medullary (marrow) cavity.

Sector of the shaft of a long bone

Osteon (Gr., bone) [Haversian system] is the basic unit of structure of compact bone, comprising a haversian canal and its concentrically arranged lamellae, of which there may be 4 to 20, each 3 to 7 micrometres thick, in a single (haversian) system. Such units are directed mainly in the long axis of the bone.[6]

Canalis nutricius [Haversian canal, Haversian space, Canalis nutriens, Nutrient canal of bone] is one of the freely anastomosing channels of the haversian system of compact bone, which contain blood vessels, lymph vessels, and nerves. Named for CLOPTON HAVERS, English physician and anatomist, 1650—1702

Volkmann's canal [ALFRED WILHELM VOLKMANN, German physiologist, 1800—1877] is a passage other than haversian canals (canales nutricii), for the passage of blood vessels through bone. It is usually transversely connecting two Haversian canals.

Haversian lamella (L., genitive and plural: lamellae) is one of the concentric bony plates surrounding a haversian canal.

Collagen fiber [collagenous fiber] is the soft, flexible, white fiber which is the most characteristic constituent of all types of connective tissue, consisting of the protein collagen, and composed of bundles of fibrils that are in turn made up of smaller units (unit fibrils or microfibrils) which show a characteristic crossbanding with a major periodicity of approximately 65 nm. In describing the hierarchy of arrangement of collagen structure, the terms fiber and fibril are sometimes loosely interchanged.

Interstitial lamella (pl. lamellae) [Ground lamella, Intermediate lamella] is one of the bony plates that fill in between the haversian systems.

Cement line is a name applied to a line, visible in microscopic examination of bone in cross section, marking the boundary of an osteon (haversian system).

Circumferential lamella (gen. and pl. lamellae) is one of the layers of bone. There are *external circumferential lamellae* and *internal circumferential lamellae*.

Trabecula (pl. trabeculae) is, in anatomical nomenclature, a supporting or anchoring strand of connective tissue, such as one extending from a capsule into the substance of the enclosed organ.

Trabeculae of bone are anastomosing bony spicules in cancellous bone which form a meshwork of intercommunicating spaces that are filled with bone marrow.

[6] Cf. [GRAY, 1918] at http://www.bartleby.com/107/18.html

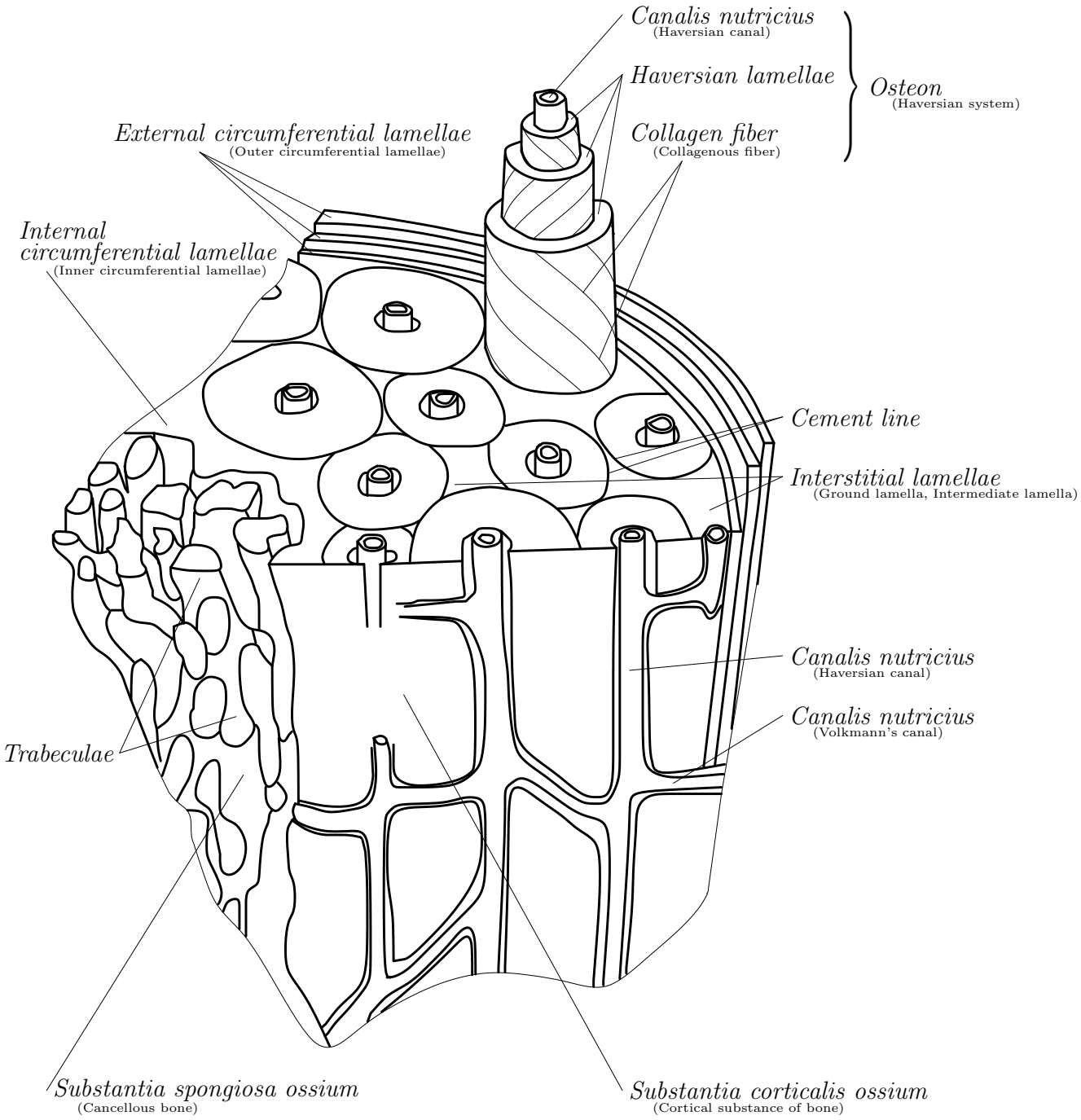

Fig. 62: Sector of the shaft of a long bone

Locally orthotropic material—the foundation of tissue mechanics

Introduction

As we are going to discuss the *locally orthotropic material—the foundation of tissue mechanics* we must spend some time in talk about the problem of biomechanical experiments. At the beginning we must stated what the biomechanics is. Surely the biomechanics is the mechanics, *i.e.*, the study of motion and its causes. (See Table of Mechanics, *Cyclopaedia*, 1728, Fig. 63.) But to what is this mechanics applied?

There is the point to be considered. It is clear, Rigid Body Mechanics is the mechanics of a

rigid body. Solid Mechanics is the mechanics of a solid (or, if you like, deformable) body. What about Biomechanics. Everyone knows the name Biomechanics has originated from biology and mechanics, and it in the sense: mechanics of biological body. And the word biology means, the science of life, from the Greek $\beta\acute{\iota}o\varsigma$, life, and logos, word or knowledge. Thus, Biomechanics is the mechanics of a living body (i.e., body that is alive).

Biomechanical experiment is said to be the experimental work in biomechanics mainly producing a better knowledge of the mechanical behaviour of some body segment and of the whole body under impact conditions. Yes, some body segment! But if it should be truly Biomechanical Experiment then the body segment must be alive. That is inside living body.

There is a wide range of truly biomechanical experiments in which the inverse mechanics and mathematical optimization methods play the great role. There are some presumptions about rational behaviour of the living body and some measured data. On this ground the extremalization of a selected objective function, such one as minimum of the consumed energy or maximum of a movement speed, is performed.

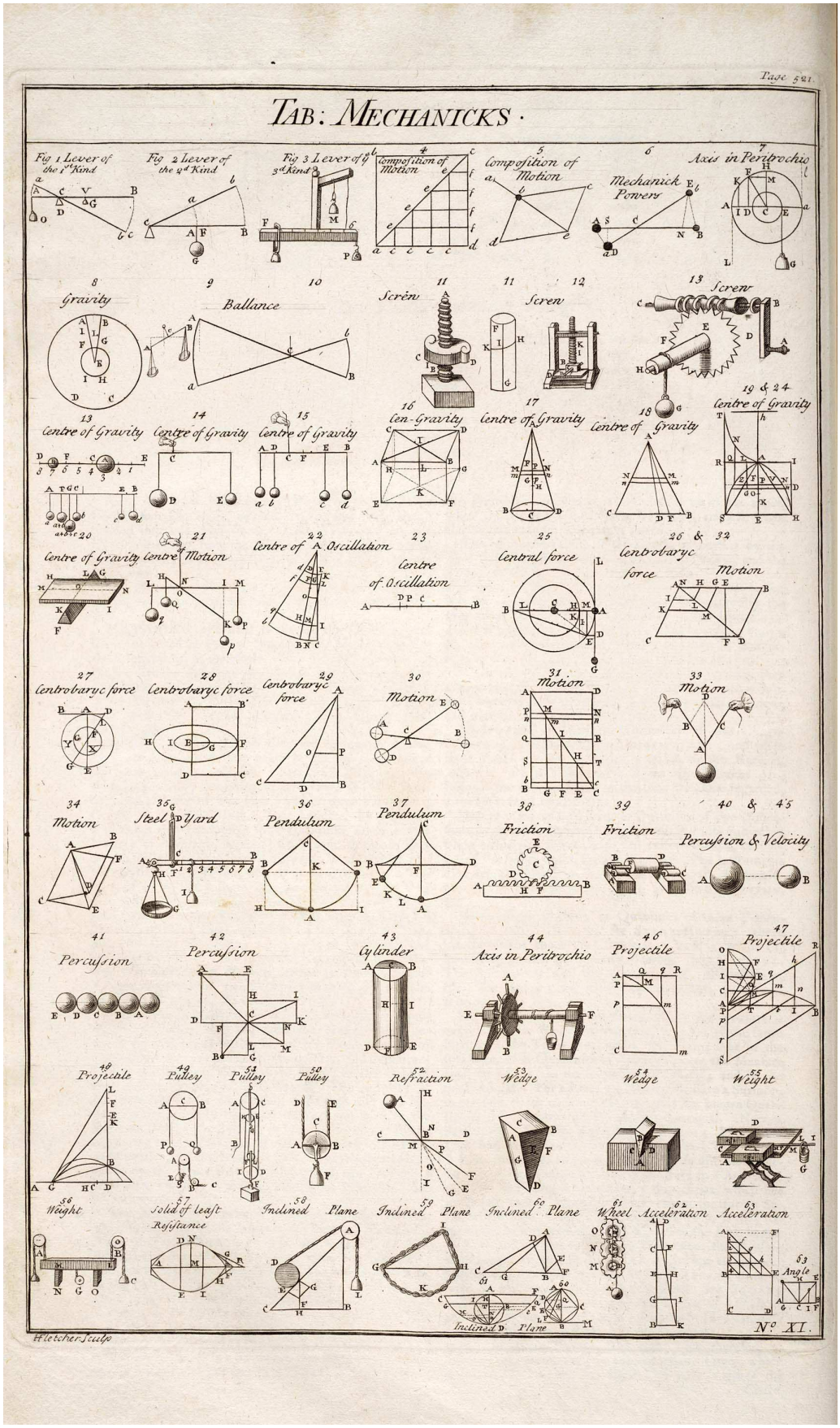

Fig. 63: Table of Mechanics, Cyclopaedia, 1728, [Chambers, 1728]

The above described approach is well known. A similar approach is possible also in the case of not entirely pure biomechanical experiments. The experiments performed in vitro are meant. At the case of experiments in vitro the great question arises: Does the biomaterial behave in vivo in the same way as in vitro? Besides this question the great spread of in vitro eperimental data is commonly observed. Also in this case the optimization methods may be of great use. For example, in the case of an anulus fibrosus of the intervertebral disc there is a possibility to utilize the method for laminate tube optimization by winding angle control[7] to predict the ratio of the first main modulus of elasticity and the second main modulus of elasticity for which the anatomical winding angle of the collagen fibres is that that maximizes stiffness. As a matter of fact in the cited example there are some stability problems of solution, but the illustrated method remains valid. The point being that geometry, internal structure, overall properties, average loading, fracture modes of body segments like bones, disks, *etc*, are known, at least to a certain degree, and thus a capability of an inverse analysis is widely opened to the material property estimation.

The other question is how to use results of biomechanical experiments, also without questioning the data validity. There is, for example, the possibility of the elastic cortical bone coefficient determination via ultrasonic measurement, cf. [ORÍAS, 2005], [GOLDMANN, 2006], where the cortical bone is regarded as an transversely isotropic material. The data obtained by this way are regarded as components of the Cartesian compliance tensor. The bone being essentially cylindrical but not thin walled there is need of a sophisticated method of transformation.

Similarly, there are some attempts, [LUKEŠ, 2005], to apportion annulus fibrosus of the intervertebral disc into fibers and test mechanical properties of these separated portions. The obtained data—data with respect to a Cartesian coordinate system—are to be transformed into the elliptical coordinates of the disc. As this case is by no means thin-walled there is once more necessity of the concept of *locally orthotropic material*.

The nomenclature *Locally orthotropic material* is meant to describe a material assembled of orthotropic material parts. The point is that every part (may be infinitesimal) can be described as an orthotropic block, that is a block with a local frame in which the elasticity tensor is of the special kind. This local frame is in a special way transformed into global reference coordinates. This local coordinate system describing a locally orthotropic body is called *Main reference frame*, *i.e.*, frame coinciding with main directions of the (infinitesimal) orthotropic block.

Another coordinate system, that may be frozen either at the material (deformed with the body) or at the space (undeformed, *i.e.*, still in the reference state), is the called *Globle material (or space) coordinate system*. This system is common for the whole ensemble of othotrpic material parts. What is essential is that in the *Cartesian frame of local orthotropy* the tensor components are physical quantities, i.e., quantities possessing the right units, however the coordinate systems are distorted in a *reference frame of computation* (Euclidian spaces with cartesian or noncartesian coordinates).

Compliance tensor and generalized Hooke's law of a (possibly infinitesimal) laminated block

Consider a laminated block, named **orthotropic (elemantary) block** and signed as νth block, as outlined in Figure 64. The coordinate system, ν_i, is the **main material reference frame**. The *main* stand for *alined with* the major/minor material axes of the orthotropic material.

Perform the following experiment: Take the block and stretch it in the direction of ν_1 axis (*i.e.*, in the direction of fibres) in such a manner that the prescribed strain ε_1^1 does not break the linear elasticity conditions. Now measure a stress σ_{11} with which you have pulled the block, and strains in transverse directions (meant the directions ν_2 and ν_3). These strains are signed ε_2^1 (*i.e.*,

[7] See [MAREŠ, 2005] and [MAREŠ and DANIEL, 2006]

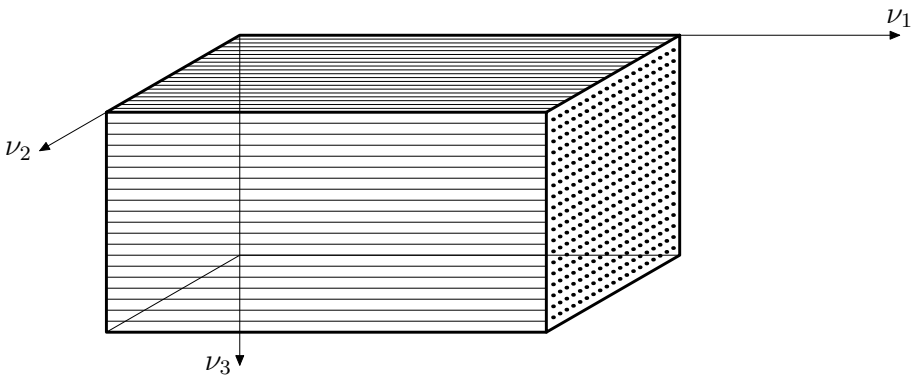

Fig. 64: The νth laminated block

a strain in the ν_2 direction, that we call the second main direction, awakened by the strain ε_1^1 in the ν_1 direction—called the first main direction) and ε_3^1, with a similar meaning of the indices.

There are successively the so-called **major Poisson ratios**

$$\nu_{12} = -\frac{\varepsilon_2^1}{\varepsilon_1^1}, \quad \nu_{13} = -\frac{\varepsilon_3^1}{\varepsilon_1^1},$$

and the **minor Poisson ratios**

$$\nu_{21} = -\frac{\varepsilon_1^2}{\varepsilon_2^2}, \quad \nu_{31} = -\frac{\varepsilon_1^3}{\varepsilon_3^3},$$

where the meaning of the indices is analogue to those first mentioned. In this way it is possible to defined also ν_{23} and ν_{32}. These ratios we will permanently need. Furthermore, from this experiment we have the ratio

$$E_{11} = \frac{\sigma_{11}}{\varepsilon_1^1}$$

called the **Hooke's law** for uniaxial stress state. Similarly we may write this law for experiments in the directions ν_2 and ν_3 as

$$E_{22} = \frac{\sigma_{22}}{\varepsilon_2^2}, \quad E_{33} = \frac{\sigma_{33}}{\varepsilon_3^3}.$$

Now we are on the way to state a **compliance tensor**. It is acceptable to think about superposition, *i.e.*, to presume the total strain is a sum of the strain in direction ν_1 uniaxially excited with stress σ_{11} (*i.e.*, ε_1^1), the strain in direction ν_1 uniaxially excited with stress σ_{22} (ε_1^2), and the strain in direction ν_1 uniaxially excited with stress σ_{33} (ε_1^3), namely

$$\varepsilon_{11} = \varepsilon_1^1 + \varepsilon_1^2 + \varepsilon_1^3,$$

or

$$\varepsilon_{11} = \varepsilon_1^1 - \nu_{21}\varepsilon_2^2 - \nu_{31}\varepsilon_3^3,$$

and at last

$$\varepsilon_{11} = \frac{\sigma_{11}}{E_{11}} - \nu_{21}\frac{\sigma_{22}}{E_{22}} - \nu_{31}\frac{\sigma_{33}}{E_{33}}.$$

As the commonly accepted relation between shear stress and strain is

$$\sigma_{12} = 2\varepsilon_{12}G_{12}, \ \sigma_{23} = 2\varepsilon_{23}G_{23}, \ \sigma_{31} = 2\varepsilon_{31}G_{31},$$

we may write the compliance relation

$$\begin{pmatrix} \varepsilon_{11} \\ \varepsilon_{22} \\ \varepsilon_{33} \\ \varepsilon_{12} \\ \varepsilon_{23} \\ \varepsilon_{31} \end{pmatrix} = \begin{pmatrix} \frac{1}{E_{11}} & -\frac{\nu_{21}}{E_{22}} & -\frac{\nu_{31}}{E_{33}} & 0 & 0 & 0 \\ -\frac{\nu_{12}}{E_{11}} & \frac{1}{E_{22}} & -\frac{\nu_{32}}{E_{33}} & 0 & 0 & 0 \\ -\frac{\nu_{13}}{E_{11}} & -\frac{\nu_{23}}{E_{22}} & \frac{1}{E_{33}} & 0 & 0 & 0 \\ 0 & 0 & 0 & \frac{1}{2G_{12}} & 0 & 0 \\ 0 & 0 & 0 & 0 & \frac{1}{2G_{23}} & 0 \\ 0 & 0 & 0 & 0 & 0 & \frac{1}{2G_{31}} \end{pmatrix} \begin{pmatrix} \sigma_{11} \\ \sigma_{22} \\ \sigma_{33} \\ \sigma_{12} \\ \sigma_{23} \\ \sigma_{31} \end{pmatrix}$$

or, as someone believes, in a more convenient form

$$\overset{\nu}{\varepsilon}{}^{ij} = \overset{\nu}{C}{}^{ij}_{kl} \overset{\nu}{\sigma}{}^{kl},$$

where the **compliance tensor**

$$\left\{ \overset{\nu}{C}{}^{ij}_{kl} \right\}_{\{ij\lceil kl\}} = \begin{pmatrix} \frac{1}{E_{11}} & 0 & 0 & 0 & -\frac{\nu_{21}}{E_{22}} & 0 & 0 & 0 & -\frac{\nu_{31}}{E_{33}} \\ 0 & \frac{1}{4G_{12}} & 0 & \frac{1}{4G_{12}} & 0 & 0 & 0 & 0 & 0 \\ 0 & 0 & \frac{1}{4G_{13}} & 0 & 0 & 0 & \frac{1}{4G_{13}} & 0 & 0 \\ 0 & \frac{1}{4G_{12}} & 0 & \frac{1}{4G_{12}} & 0 & 0 & 0 & 0 & 0 \\ -\frac{\nu_{12}}{E_{11}} & 0 & 0 & 0 & \frac{1}{E_{22}} & 0 & 0 & 0 & -\frac{\nu_{32}}{E_{33}} \\ 0 & 0 & 0 & 0 & 0 & \frac{1}{4G_{23}} & 0 & \frac{1}{4G_{23}} & 0 \\ 0 & 0 & \frac{1}{4G_{13}} & 0 & 0 & 0 & \frac{1}{4G_{13}} & 0 & 0 \\ 0 & 0 & 0 & 0 & 0 & \frac{1}{4G_{23}} & 0 & \frac{1}{4G_{23}} & 0 \\ -\frac{\nu_{13}}{E_{11}} & 0 & 0 & 0 & -\frac{\nu_{23}}{E_{22}} & 0 & 0 & 0 & \frac{1}{E_{33}} \end{pmatrix}.$$

The ν above the tensor symbol indicates that the symbol does not symbolize an abstract tensor but that it stands for the tensor components in the ν-frame of reference and $\{ij\lceil kl\}$ means to say how the entries are stored in the array, namely that the rows belong successively to the following couples of the indices $(ij = 11, 12, 13, 21, 22, 23, 31, 32, 33)$ and the columns to the couples $(kl = 11, 12, \ldots, 33)$.

A little tedious grapheme arrangement leads to **generalized Hooke's law** of the laminated block in the form

$$\overset{\nu}{\sigma}{}^{ij} = \overset{\nu}{E}{}^{ij}_{kl} \overset{\nu}{\varepsilon}{}^{kl}$$

with components of the **elasticity tensor**

$$\left\{ \overset{\nu}{E}{}^{ij}_{kl} \right\}_{\{ij\lceil kl\}} = \begin{pmatrix} \Phi_{1111} & 0 & 0 & 0 & \Phi_{1122} & 0 & 0 & 0 & \Phi_{1133} \\ 0 & G_{12} & 0 & G_{12} & 0 & 0 & 0 & 0 & 0 \\ 0 & 0 & G_{13} & 0 & 0 & 0 & G_{13} & 0 & 0 \\ 0 & G_{12} & 0 & G_{12} & 0 & 0 & 0 & 0 & 0 \\ \Phi_{2211} & 0 & 0 & 0 & \Phi_{2222} & 0 & 0 & 0 & \Phi_{2233} \\ 0 & 0 & 0 & 0 & 0 & G_{23} & 0 & G_{23} & 0 \\ 0 & 0 & G_{13} & 0 & 0 & 0 & G_{13} & 0 & 0 \\ 0 & 0 & 0 & 0 & 0 & G_{23} & 0 & G_{23} & 0 \\ \Phi_{3311} & 0 & 0 & 0 & \Phi_{3322} & 0 & 0 & 0 & \Phi_{3333} \end{pmatrix},$$

where

$$\Phi_{1111} = \frac{1 - \nu_{23}\nu_{32}}{N} E_{11}, \quad \Phi_{1122} = \frac{\nu_{21} + \nu_{23}\nu_{31}}{N} E_{11}, \quad \Phi_{1133} = \frac{\nu_{31} + \nu_{32}\nu_{21}}{N} E_{11},$$

$$\Phi_{2211} = \frac{\nu_{12} + \nu_{13}\nu_{32}}{N} E_{22}, \quad \Phi_{2222} = \frac{1 - \nu_{13}\nu_{31}}{N} E_{22}, \quad \Phi_{2233} = \frac{\nu_{32} + \nu_{31}\nu_{12}}{N} E_{22},$$

$$\Phi_{3311} = \frac{\nu_{13} + \nu_{12}\nu_{23}}{N} E_{33}, \quad \Phi_{3322} = \frac{\nu_{23} + \nu_{21}\nu_{13}}{N} E_{33}, \quad \Phi_{3333} = \frac{1 - \nu_{12}\nu_{21}}{N} E_{33},$$

and

$$N = 1 - \nu_{12}\nu_{21} - \nu_{23}\nu_{32} - \nu_{31}\nu_{13} - \nu_{12}\nu_{23}\nu_{31} - \nu_{13}\nu_{32}\nu_{21}.$$

It is well known, following energetic purposes, that in a Cartesian reference frame,[8] like the ν-frame,

$$\overset{\nu}{E}{}^{ij}{}_{kl} = \overset{\nu}{E}{}^{kl}{}_{ij} \quad \text{and} \quad \overset{\nu}{C}{}^{ij}{}_{kl} = \overset{\nu}{C}{}^{kl}{}_{ij}$$

holds which means $\Phi_{1122} = \Phi_{2211}$ and $\nu_{21}E_{11} = \nu_{12}E_{22}$, *etc.* The two last equalities imply

$$\nu_{23}\nu_{31}\nu_{12} = \nu_{13}\nu_{32}\nu_{21}.$$

Similarly, for the other two cases. We are going to use this fact at the right time.

Coordinate systems describing a locally orthotropic body

There is the above used *main reference frame* coinciding with main directions of the (infinitesimal) orthotropic block. These coordinates are denoted ν^a ($a = 1, 2, 3$) and sites of the body are described by an orthogonal grid drawn through the body in a given (reference-relaxed but not necessarily unstressed—remember residual stresses) state.

Another coordinate system in use is a global Cartesian coordinate system. This system is common for the whole ensemble of othotrpic material parts. According to the reference frame construction the transformation between the main reference frame (main coordinate system, ν^a) and a global Cartesian reference frame, z^a, should be affine, namely via the relation

$$z^a = \cos(z^a, \nu^b)\nu^b,$$

where $\cos(z^a, \nu^b)$ means the cosine of an angle contained between the direction of z^a-axis and ν^b-axis. The transformation matrix, $\cos(z^a, \nu^b)$, can be given through three consequent rotations described, according to *Euler's rotation theorem*, using three, so called *Euler*, angles in this way:

$$\cos(z^a, \nu^b) = \boldsymbol{ABC}$$

where

$$\boldsymbol{A} = \begin{pmatrix} \cos\varphi & \sin\varphi & 0 \\ -\sin\varphi & \cos\varphi & 0 \\ 0 & 0 & 1 \end{pmatrix},$$

$$\boldsymbol{B} = \begin{pmatrix} 1 & 0 & 0 \\ 0 & \cos\theta & \sin\theta \\ 0 & -\sin\theta & \cos\theta \end{pmatrix},$$

and

$$\boldsymbol{C} = \begin{pmatrix} \cos\psi & \sin\psi & 0 \\ -\sin\psi & \cos\psi & 0 \\ 0 & 0 & 1 \end{pmatrix}.$$

As the main frame of reference is orthogonal it is evident that covariant and contravariant tensor components coincide. The brief account follows:

$$\overset{\nu}{\boldsymbol{e}}_i \overset{\nu}{\boldsymbol{e}}{}^j = \delta_i^j, \ \overset{\nu}{\boldsymbol{e}}_i \overset{\nu}{\boldsymbol{e}}_j = \delta_{ij} = \delta_i^j \Rightarrow \overset{\nu}{\boldsymbol{e}}_j = \overset{\nu}{\boldsymbol{e}}{}^j$$

[8] Compare, for instance, [Salençon, 2001] p. 329.

and thus, as above uttered,

$$\overset{\nu}{E^{ij}}_{kl}=\overset{\nu}{E}_{ijkl}=\overset{\nu}{E^{ijkl}} .$$

What is essential is that these tensor components are *physical* quantities, *i.e.*, quantities possessing the right units, however the coordinate systems are distorted in a reference frame of computation.

Now we must perform a transformation from the main frozen reference frame, ν^a, into a frame of computation, say x^a. In the frame of computation the tensor entries are not necessarily physical quantities.

At this stage it is appropriate to mention the metrics. As we presumably take into account the Euclidian space, the metric is Euclidian one, h_{ab}, *i.e.*, in the orthogonal coordinates ν^a and x^a the metric has components

$$\overset{\nu}{g}_{ab}=\delta_{ab} \quad \text{and} \quad \overset{x}{g}_{ab}=\frac{\partial\nu^c}{\partial x^a}\frac{\partial\nu^d}{\partial x^b}\delta_{cd}.$$

These metrics are related to a space (frozen in the space, relaxed, undeformed) frame. There is also another frame (**material frame**), the frame that deform with the body. This frame, named also **deformed-with-body reference frame** is equipt with another metric, say $\overset{\xi}{g}_{ab}$.

Mathematical model of the cortical bone osteon

Introduction

Osteon (Gr., bone) [Haversian system] is the basic unit of structure of compact bone. The osteon consists of a number (may be 4 to 20) **Haversian lamellae**, *i.e.*, the concentric bony plates surrounding a haversian canal. Each of these lamellae is 3 to 7 microns thick.[9]

Haversian lamella is composed of **collagen fibers**. Collagen fiber is the soft, flexible, white fiber which is the most characteristic constituent of all types of connective tissue, consisting of the protein collagen, and composed of bundles of fibrils that are in turn made up of smaller units (unit fibrils or microfibrils) which show a characteristic crossbanding with a major periodicity of approximately 65 nm.

Frames of reference as a foundation of a mathematical modeling of the osteons

In the mathematical modeling it is essential to constitute a coordinate system. It is true that abstract tensor notation derives the label from *abstract* in the meaning unrelated to a specified coordinate system. Nevertheless, every mechanical modeling is connected with a body and the body has a geometry that is describable only with a coordinate system. At this stage let us look at the osteon, Fig. 65, in the b^3-direction and draw one lamella of the osteon, say $\nu = 1$, together with the global computational coordinates and one of the infinite number of local Cartesians, Fig. 66.

The relations between the coordinates of the osteon are (see carefully Fig. 66)

$$b^1 = \beta^1 \cos\beta^2,$$

$$b^2 = \beta^1 \sin\beta^2,$$

$$b^3 = \beta^3.$$

$$\beta^1 = \sqrt{(b^1)^2 + (b^2)^2},$$

[9] Cf. [GRAY, 1918] at http://www.bartleby.com/107/18.html

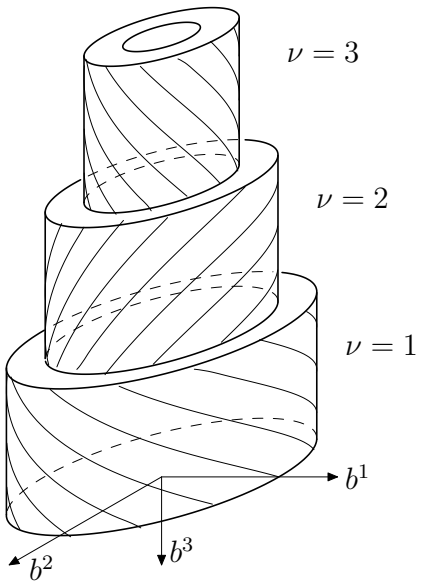

Fig. 65: Cortical bone osteon global coordinate system

$$\beta^2 = \arctan\frac{b^2}{b^1},$$
$$\beta^3 = b^3.$$
$$x^1 = \beta^1 - r_o,$$
$$x^2 = r_o\beta^2,$$
$$x^3 = \beta^3.$$
$$\beta^1 = x^1 + r_o,$$
$$\beta^2 = \frac{1}{r_o}x^2,$$
$$\beta^3 = x^3.$$

The transformation between the x-frame and the ξ-frame we postpone to another opportunity.

The matrices of tensor transformation between the above listed frames are given[10] via the following derivatives.

$$\frac{\partial b^a}{\partial \beta^b} = \begin{pmatrix} \cos\beta^2 & -\beta^1\sin\beta^2 & 0 \\ \sin\beta^2 & \beta^1\cos\beta^2 & 0 \\ 0 & 0 & 1 \end{pmatrix}$$

As

$$\frac{\partial b^a}{\partial \beta^b}\frac{\partial \beta^b}{\partial b^c} = \delta^a_c$$

we have also

$$\frac{\partial \beta^a}{\partial b^b} = \begin{pmatrix} \cos\beta^2 & \sin\beta^2 & 0 \\ \frac{-1}{\beta^1}\sin\beta^2 & \frac{1}{\beta^1}\cos\beta^2 & 0 \\ 0 & 0 & 1 \end{pmatrix}.$$

Further,

$$\frac{\partial x^a}{\partial \beta^b} = \begin{pmatrix} 1 & 0 & 0 \\ 0 & r_o & 0 \\ 0 & 0 & 1 \end{pmatrix}, \quad \frac{\partial \beta^a}{\partial x^b} = \begin{pmatrix} 1 & 0 & 0 \\ 0 & \frac{1}{r_o} & 0 \\ 0 & 0 & 1 \end{pmatrix},$$

[10][Lovelock and Rund, 1989], [Synge and Schild, 1978].

ξ^a — Local Cartesian coordinate system
b^a — Global Cartesian coordinate system of the osteon
β^a — Global computational coordinate system of the osteon
x^a — Global computational coordinate system of the unfolded osteon lamella

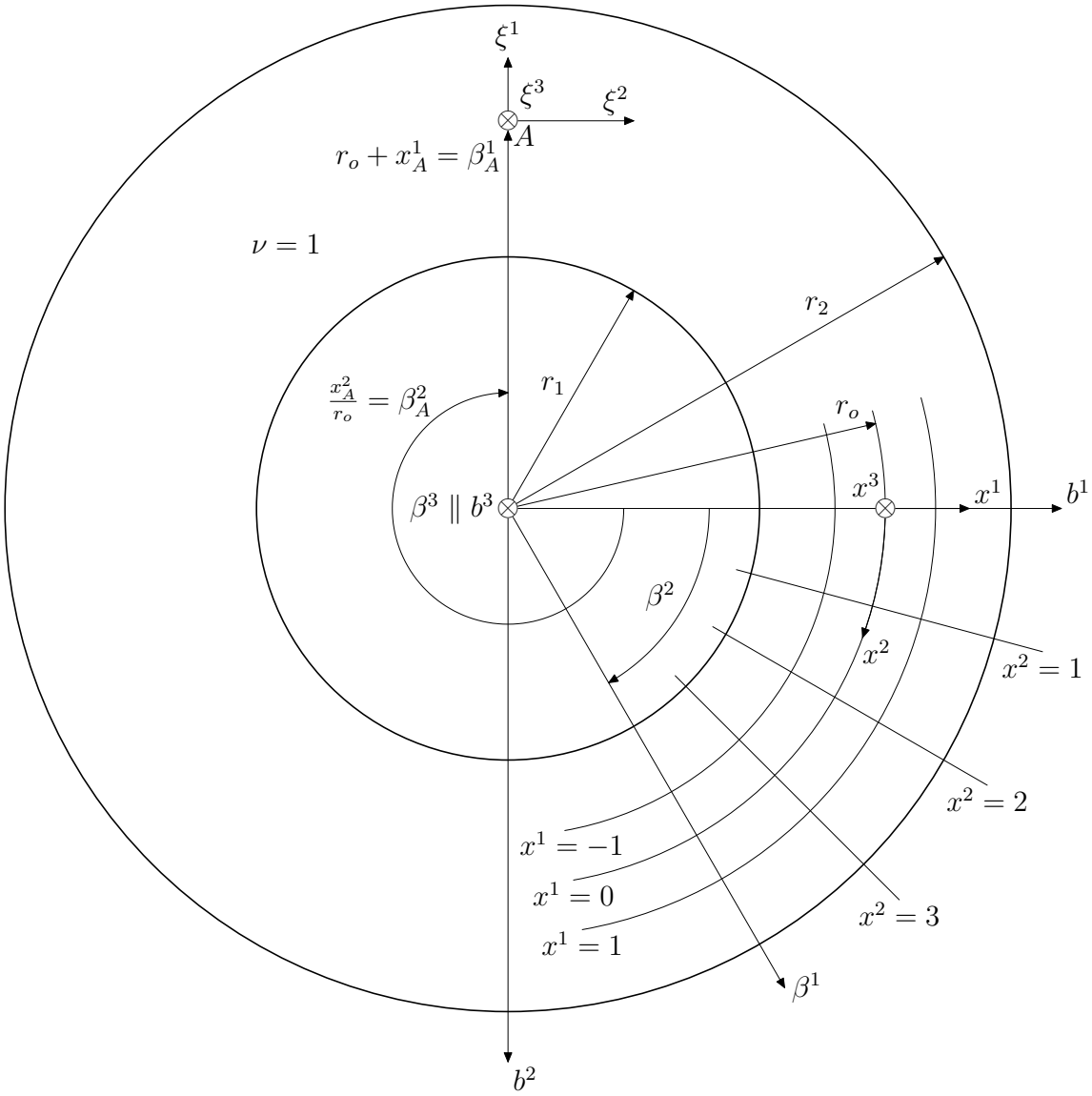

Fig. 66: Cortical bone osteon lamella coordinate system

and

$$\frac{\partial b^a}{\partial x^b} = \frac{\partial b^a}{\partial \beta^c}\frac{\partial \beta^c}{\partial x^b} = \begin{pmatrix} \cos\beta^2 & -\frac{\beta^1}{r_o}\sin\beta^2 & 0 \\ \sin\beta^2 & \frac{\beta^1}{r_o}\cos\beta^2 & 0 \\ 0 & 0 & 1 \end{pmatrix},$$

$$\frac{\partial x^a}{\partial b^b} = \frac{\partial x^a}{\partial \beta^c}\frac{\partial \beta^c}{\partial b^b} = \begin{pmatrix} \cos\beta^2 & \sin\beta^2 & 0 \\ \frac{-r_o}{\beta^1}\sin\beta^2 & \frac{r_o}{\beta^1}\cos\beta^2 & 0 \\ 0 & 0 & 1 \end{pmatrix}.$$

Now, we arrive at the constitution of the metric tensors, g_{ab}. It holds

$$\mathrm{d}s^2 = \overset{x}{g}_{ab}\,\mathrm{d}x^a\mathrm{d}x^b = \overset{\beta}{g}_{ab}\,\mathrm{d}\beta^a\mathrm{d}\beta^b = \overset{b}{g}_{ab}\,\mathrm{d}b^a\mathrm{d}b^b.$$

As the b-frame is the Cartesian one (in the Euclidian space),

$$\mathrm{d}s^2 = \mathrm{d}b^a\mathrm{d}b^a = \delta_{ab}\mathrm{d}b^a\mathrm{d}b^b$$

and thus

$$\overset{b}{g}_{ab} = \delta_{ab} = \begin{pmatrix} 1 & 0 & 0 \\ 0 & 1 & 0 \\ 0 & 0 & 1 \end{pmatrix}.$$

Transforming,

$$\overset{x}{g}_{ab} = \frac{\partial b^c}{\partial x^a}\frac{\partial b^d}{\partial x^b}\delta_{cd} = \begin{pmatrix} \cos\beta^2 & \sin\beta^2 & 0 \\ -\frac{\beta^1}{r_o}\sin\beta^2 & \frac{\beta^1}{r_o}\cos\beta^2 & 0 \\ 0 & 0 & 1 \end{pmatrix}\begin{pmatrix} \cos\beta^2 & -\frac{\beta^1}{r_o}\sin\beta^2 & 0 \\ \sin\beta^2 & \frac{\beta^1}{r_o}\cos\beta^2 & 0 \\ 0 & 0 & 1 \end{pmatrix},$$

i.e.,

$$\overset{x}{g}_{ab} = \begin{pmatrix} 1 & 0 & 0 \\ 0 & \left(\frac{\beta^1}{r_o}\right)^2 & 0 \\ 0 & 0 & 1 \end{pmatrix} = \begin{pmatrix} 1 & 0 & 0 \\ 0 & \left(\frac{x^1+r_o}{r_o}\right)^2 & 0 \\ 0 & 0 & 1 \end{pmatrix}, \tag{193}$$

the entry $\left(\frac{\beta^1}{r_o}\right)^2 = \left(\frac{x^1+r_o}{r_o}\right)^2$ being the "stretching" of the x^2-coordinate.

Similarly,

$$\overset{\beta}{g}_{ab} = \frac{\partial b^c}{\partial \beta^a}\frac{\partial b^d}{\partial \beta^b}\delta_{cd} = \begin{pmatrix} \cos\beta^2 & \sin\beta^2 & 0 \\ -\beta^1\sin\beta^2 & \beta^1\cos\beta^2 & 0 \\ 0 & 0 & 1 \end{pmatrix}\begin{pmatrix} \cos\beta^2 & -\beta^1\sin\beta^2 & 0 \\ \sin\beta^2 & \beta^1\cos\beta^2 & 0 \\ 0 & 0 & 1 \end{pmatrix},$$

and thus

$$\overset{\beta}{g}_{ab} = \begin{pmatrix} 1 & 0 & 0 \\ 0 & (\beta^1)^2 & 0 \\ 0 & 0 & 1 \end{pmatrix}.$$

Another task to look at is the *local coordinate system* of the unfolded infinitesimal ply of the lamella, ξ^a, and the connection between ξ-frame and x-frame, Fig. 67. The ξ-frame, being *Cartesian*, has the metric equal to δ_{ab} and thus the tensor transformation must be such that

$$\delta_{ab} = \overset{\xi}{g}_{ab} = \frac{\partial x^c}{\partial \xi^a}\frac{\partial x^d}{\partial \xi^b}\,\overset{x}{g}_{cd},$$

i.e., as the directions of respective axes are alined,

$$\frac{\partial x^a}{\partial \xi^b} = \begin{pmatrix} 1 & 0 & 0 \\ 0 & \frac{r_o}{\beta^1} & 0 \\ 0 & 0 & 1 \end{pmatrix} = \begin{pmatrix} 1 & 0 & 0 \\ 0 & \frac{r_o}{r_o+x^1} & 0 \\ 0 & 0 & 1 \end{pmatrix}$$

and

$$\frac{\partial \xi^a}{\partial x^b} = \begin{pmatrix} 1 & 0 & 0 \\ 0 & \frac{\beta^1}{r_o} & 0 \\ 0 & 0 & 1 \end{pmatrix} = \begin{pmatrix} 1 & 0 & 0 \\ 0 & \frac{r_o+x^1}{r_o} & 0 \\ 0 & 0 & 1 \end{pmatrix}.$$

The connection of the *main material coordinate system*, ν^a, with the *local coordinate system*, ξ^a, of an unrolled infinitesimal ply of a lamella of the osteon is apparent from the Fig. 68. It holds that

$$\frac{\partial \nu^a}{\partial \xi^b} = \begin{pmatrix} 1 & 0 & 0 \\ 0 & \cos\alpha_\nu & \sin\alpha_\nu \\ 0 & -\sin\alpha_\nu & \cos\alpha_\nu \end{pmatrix}, \quad \frac{\partial \xi^a}{\partial \nu^b} = \begin{pmatrix} 1 & 0 & 0 \\ 0 & \cos\alpha_\nu & -\sin\alpha_\nu \\ 0 & \sin\alpha_\nu & \cos\alpha_\nu \end{pmatrix}.$$

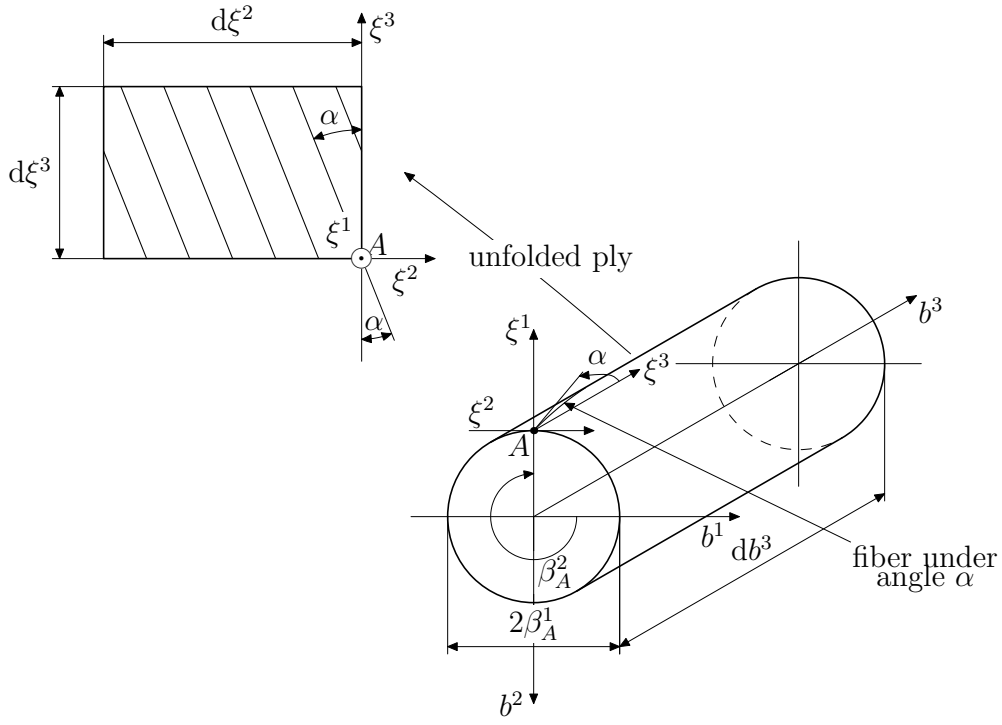

Fig. 67: Local coordinate system ξ^a of an unrolled infinitesimal ply of a lamella of the osteon

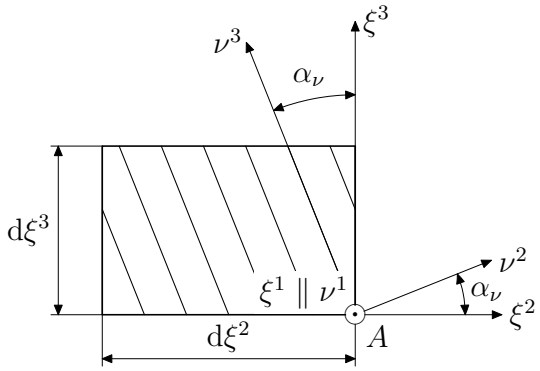

Fig. 68: Main material coordinate system ν^a of an unrolled infinitesimal part of the lamella

The stress-strain relation of a lamella of the osteon

The components of the stress tensor relevant to the ξ-frame are the physical ones, *i.e.*, the components that possess the stress units, MPa. The same holds for strains. Now, imagine that in a way the stress-strain relation of a very thin unrolled ply of an osteon lamella written in the main frame of reference was obtained.[11] Thus

$$\overset{\nu}{\sigma}{}^{ij} = \overset{\nu}{E}{}^{ij}_{kl}\,\overset{\nu}{\varepsilon}{}^{kl},$$

$$\overset{\nu}{\varepsilon}{}^{ij} = \overset{\nu}{C}{}^{ij}_{kl}\,\overset{\nu}{\sigma}{}^{kl}\,.$$

are the relations derived for an infinitesimal curved block regarded, or really adjusted, as rectangular. From the entries of the metric tensor of the x-frame, see (193), we can deduced that for

[11] The Cartesian entries of the elastic and compliance tensor see at [MAREŠ, 2006b].

$x^1 \ll r_o$ there is minimal error to put

$$\overset{x}{E}{}^{ab}{}_{cd} = \overset{\xi}{E}{}^{ab}{}_{cd} = \frac{\partial \xi^a}{\partial \nu^i}\frac{\partial \xi^b}{\partial \nu^j}\ \overset{\nu}{E}{}^{ij}{}_{kl}\ \frac{\partial \nu^k}{\partial \xi^c}\frac{\partial \nu^l}{\partial \xi^d}.$$

But if we take into account the opposite case, the case of an osteon where the thickness is not negligible compared with the radius, we must take deeper analysis:

$$\overset{x}{E}{}^{op}{}_{rs} = \frac{\partial x^o}{\partial \xi^a}\frac{\partial x^p}{\partial \xi^b}\ \overset{\xi}{E}{}^{ab}{}_{cd}\ \frac{\partial \xi^c}{\partial x^r}\frac{\partial \xi^d}{\partial x^s} = \frac{\partial x^o}{\partial \xi^a}\frac{\partial x^p}{\partial \xi^b}\frac{\partial \xi^a}{\partial \nu^i}\frac{\partial \xi^b}{\partial \nu^j}\ \overset{\nu}{E}{}^{ij}{}_{kl}\ \frac{\partial \nu^k}{\partial \xi^c}\frac{\partial \nu^l}{\partial \xi^d}\frac{\partial \xi^c}{\partial x^r}\frac{\partial \xi^d}{\partial x^s}.$$

That is

$$\frac{\partial \nu^a}{\partial x^b} = \frac{\partial \nu^a}{\partial \xi^c}\frac{\partial \xi^c}{\partial x^b} = \begin{pmatrix} 1 & 0 & 0 \\ 0 & \frac{r_o+x^1}{r_o}\cos\alpha_\nu & \sin\alpha_\nu \\ 0 & -\frac{r_o+x^1}{r_o}\sin\alpha_\nu & \cos\alpha_\nu \end{pmatrix}$$

and

$$\frac{\partial x^a}{\partial \nu^b} = \frac{\partial x^a}{\partial \xi^c}\frac{\partial \xi^c}{\partial \nu^b} = \begin{pmatrix} 1 & 0 & 0 \\ 0 & \frac{r_o}{r_o+x^1}\cos\alpha_\nu & -\frac{r_o}{r_o+x^1}\sin\alpha_\nu \\ 0 & \sin\alpha_\nu & \cos\alpha_\nu \end{pmatrix}.$$

Similarly,

$$\frac{\partial \nu^a}{\partial \beta^b} = \frac{\partial \nu^a}{\partial x^c}\frac{\partial x^c}{\partial \beta^b} = \begin{pmatrix} 1 & 0 & 0 \\ 0 & \beta^1\cos\alpha_\nu & \sin\alpha_\nu \\ 0 & -\beta^1\sin\alpha_\nu & \cos\alpha_\nu \end{pmatrix},$$

$$\frac{\partial \beta^a}{\partial \nu^b} = \frac{\partial \beta^a}{\partial x^c}\frac{\partial x^c}{\partial \nu^b} = \begin{pmatrix} 1 & 0 & 0 \\ 0 & \frac{1}{\beta^1}\cos\alpha_\nu & -\frac{1}{\beta^1}\sin\alpha_\nu \\ 0 & \sin\alpha_\nu & \cos\alpha_\nu \end{pmatrix};$$

and

$$\frac{\partial \nu^a}{\partial b^b} = \frac{\partial \nu^a}{\partial x^c}\frac{\partial x^c}{\partial b^b} = \begin{pmatrix} \cos\beta^2 & \sin\beta^2 & 0 \\ -\cos\alpha_\nu\sin\beta^2 & \cos\alpha_\nu\cos\beta^2 & \sin\alpha_\nu \\ \sin\alpha_\nu\sin\beta^2 & -\sin\alpha_\nu\cos\beta^2 & \cos\alpha_\nu \end{pmatrix},$$

$$\frac{\partial b^a}{\partial \nu^b} = \frac{\partial b^a}{\partial x^c}\frac{\partial x^c}{\partial \nu^b} = \begin{pmatrix} \cos\beta^2 & -\cos\alpha_\nu\sin\beta^2 & \sin\alpha_\nu\sin\beta^2 \\ \sin\beta^2 & \cos\alpha_\nu\cos\beta^2 & -\sin\alpha_\nu\cos\beta^2 \\ 0 & \sin\alpha_\nu & \cos\alpha_\nu \end{pmatrix}.$$

Elastic strain energy of the osteon

The *elastic strain energy* is the functional

$$a = \int_\Omega \varepsilon_{ab}\varepsilon^{cd}E^{ab}{}_{cd}\,\mathrm{d}\Omega,$$

where the differential element of a volume in a curvilinear coordinate system is related to the differentials of the coordinates by the square root of the determinate of the metric tensor g_{ab}, *e.g.*, in the β-frame,

$$\mathrm{d}\Omega = \left|\overset{\beta}{g}_{ab}\right|^{\frac{1}{2}}\mathrm{d}^3\beta = \beta^1\mathrm{d}\beta^1\mathrm{d}\beta^2\mathrm{d}\beta^3,$$

and the invariant

$$\varepsilon_{ab}\varepsilon^{cd}E^{ab}{}_{cd}$$

must be the function of the integrative coordinates. Nevertheless, components of the acting tensors may be relevant to any, but for all the same, coordinate system. If specified, in the case of the osteon,

$$a = \int_0^l \sum_{\nu=1}^{n_b} \int_{r_\nu}^{r_{\nu+1}} \beta^1 \int_0^{2\pi} \varepsilon^{\beta}_{ab} \varepsilon^{\beta}_{cd} \frac{\partial \beta^a}{\partial \nu^i} \frac{\partial \beta^b}{\partial \nu^j} E^{\nu}_{ijkl} \frac{\partial \nu^k}{\partial \beta^c} \frac{\partial \nu^l}{\partial \beta^d} \,\mathrm{d}\beta^2 \,\mathrm{d}\beta^1 \,\mathrm{d}\beta^3,$$

n_b being the number of the osteon lamellae, r_ν the inner radius of the ν-th lamella, r_{n_b+1} outer radius of the osteon, and l the regarded length of the osteon.

Method of femoral diafysis analysis

At a paper[12] the geometry and internal structure of thigh bone have been described. At another paper[13] a method of mathematical description of an osteon has been proposed. At this stage let us use the description to analyse the shaft of a thigh bone.

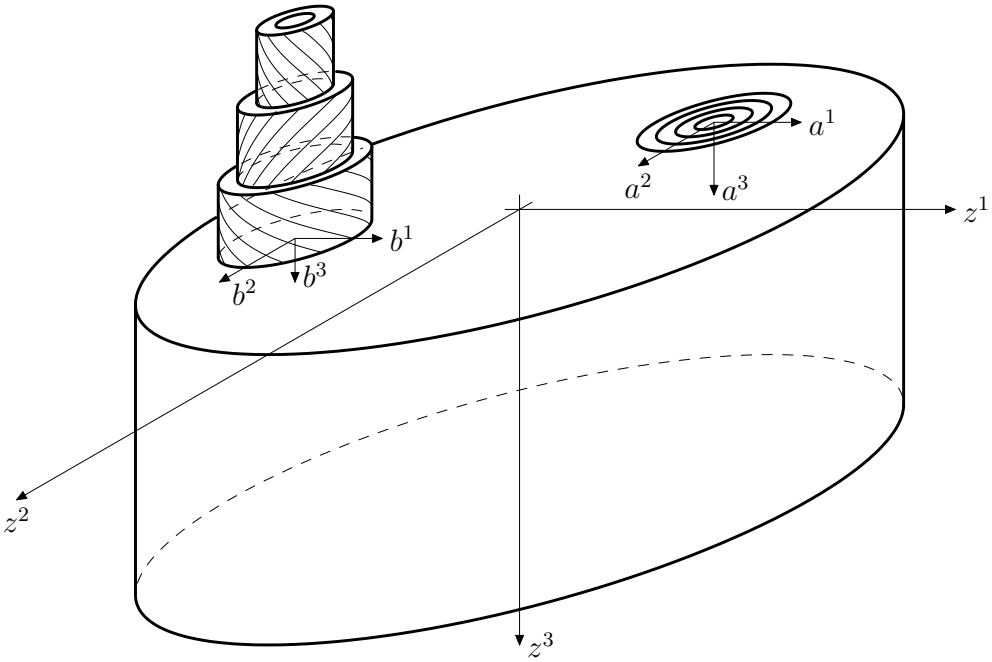

Fig. 69: Relation between the coordinate systems of long bone osteons

Osteons of a cortical bone

Let us pursue the model according to Fig. 69—something like a pair of osteons embedded in interstitial bone tissue, for our purposes considered as homogeneous isotropic material. For one osteon it holds that *elastic strain energy of the osteon* is the functional[14]

$$a_\ell = \int_{\Omega_\ell} \varepsilon_{ab} \varepsilon^{cd} E^{ab}_{\ \ cd} \,\mathrm{d}\Omega, \tag{194}$$

[12] [MAREŠ, 2006a]
[13] [MAREŠ, 2006c]
[14] [MAREŠ, 2006c]

where, in the β-frame,[15]

$$\mathrm{d}\Omega = \left|g^{\beta}_{ab}\right|^{\frac{1}{2}} \mathrm{d}^3\beta = \beta^1\mathrm{d}\beta^1\mathrm{d}\beta^2\mathrm{d}\beta^3.$$

Now, we must collect the set of osteons into one whole, *i.e.*, into the cylinder of the cortical diaphysis of a long bone. More for convenience than for absolute accuracy, let us assume the contour of the femur diaphysis as a hollow circular shaft with inner diameter, R_i, and outer diameter, R_o, respectively. The number of the osteons being n, every one of them, with its own global Cartesian coordinate system $(a, b, \ldots, n)$, consists of a number of lamellae, n_ℓ ($\ell = a, b, \ldots, n$) of known winding angles, α^ℓ_ν ($\nu = 1, 2, \ldots, n_\ell$). Besides the *global Cartesian coordinate system of the diaphysis*, z^a, consider the *global cylindrical coordinate system of the diaphysis*, θ^a.

The elastic energy stored in the hollow cylindrical shaft of the diaphysis, a, may be, as every integral, decomposed into the sum of integrals over disjunct subsets of the considered part of the diaphysis volume, Ω. Thus,

$$a = \int\limits_{\Omega} \varepsilon_{ab}\varepsilon^{cd}\mathcal{E}^{ab}{}_{cd}\,\mathrm{d}\Omega + \sum_{\ell=1}^{n}\int\limits_{\Omega_\ell} \varepsilon_{ab}\varepsilon^{cd}E^{ab}{}_{cd}\,\mathrm{d}\Omega - \sum_{\ell=1}^{n}\int\limits_{\Omega_\ell} \varepsilon_{ab}\varepsilon^{cd}\mathcal{E}^{ab}{}_{cd}\,\mathrm{d}\Omega,$$

$\mathcal{E}^{ab}{}_{cd}$ being the elasticity (stiffness) tensor of the *interstitial lamellae* modeled as a transversally isotropic material (this choice will be discussed later), $E^{ab}{}_{cd}$ elasticity (stiffness) tensor of the osteons as described at another place,[16] Ω_ℓ the volume of ℓ-th osteon. The point of expressing the elastic energy in this way is the comfortable integration over the osteons with β-frames as the chosen coordinates and over the entire cross section of diaphysis in the global cylindrical coordinate system of the diaphysis, θ^a.

At this stage we must spend some time with discussion about the modeling the *interstitial lamellae* as the transversely isotropic material with elasticity (stiffness) tensor $\mathcal{E}$. The choice of the interstitial lamellae model have been motivated by the long range of experimental works and published models of cortical bones as a homogeneous transversally isotropic material.[17] As the elasticity tensor,

$$\left\{\mathcal{E}^{\overset{z}{ij}}{}_{kl}\right\}_{\{ij\lceil kl\}} = \begin{pmatrix} e_{11} & 0 & 0 & 0 & e_{12} & 0 & 0 & 0 & e_{13} \\ 0 & G_{12} & 0 & G_{12} & 0 & 0 & 0 & 0 & 0 \\ 0 & 0 & G_{13} & 0 & 0 & 0 & G_{13} & 0 & 0 \\ 0 & G_{12} & 0 & G_{12} & 0 & 0 & 0 & 0 & 0 \\ e_{12} & 0 & 0 & 0 & e_{22} & 0 & 0 & 0 & e_{23} \\ 0 & 0 & 0 & 0 & 0 & G_{23} & 0 & G_{23} & 0 \\ 0 & 0 & G_{13} & 0 & 0 & 0 & G_{13} & 0 & 0 \\ 0 & 0 & 0 & 0 & 0 & G_{23} & 0 & G_{23} & 0 \\ e_{13} & 0 & 0 & 0 & e_{23} & 0 & 0 & 0 & e_{33} \end{pmatrix},$$

is cylindrically orthotropic (transversely isotropic, *i.e.*, the case when $e_{11} = e_{22}$, $e_{66} = 0.5(e_{11}+e_{22})$ with axis parallel to axes $z^3, a^3, b^3, \ldots$ it is not problem to performed the integration on any cylindrical coordinates. The magnitude of the constants, written in matrix form

$$\boldsymbol{E} = \begin{pmatrix} e_{11} & e_{12} & e_{13} & 0 & 0 & 0 \\ e_{12} & e_{22} & e_{23} & 0 & 0 & 0 \\ e_{13} & e_{23} & e_{33} & 0 & 0 & 0 \\ 0 & 0 & 0 & e_{44} & 0 & 0 \\ 0 & 0 & 0 & 0 & e_{55} & 0 \\ 0 & 0 & 0 & 0 & 0 & e_{66} \end{pmatrix},$$

[15] See once more [Mareš, 2006c].
[16] [Mareš, 2006b]
[17] Cf., *e.g.*, [Orías, 2005] or [Goldmann, 2006].

where $e_{44} = G_{13}, e_{55} = G_{23}, e_{66} = G_{12}$, were measured by numerous author via ultrasonic technique, for a list of them see Tab. 21.[18]

[GPa]	[1]	[2]	[3]	[4]	[5]	[6]	[7]	[8]	[9]	[0]
e_{11}	27.4±1.6	16.75±2.27	23.4±0.0031	21.2±0.5	18.0	19.4±1.3	24.89	14.1	22.4	19.7
e_{22}	30.3±2.8	19.66±2.09	24.1±0.0035	21.0±1.4	20.2	20.0±1.4	26.16	18.4	25.0	19.7
e_{33}	34.1±1.7	27.33±1.64	32.5±0.0044	29.0±1.0	27.6	30.9±1.9	33.20	25.0	35.0	32.0
e_{44}	9.3± 0.9	6.22±0.31	8.7±0.0013	6.3±0.4	6.23	5.7±0.5	7.11	7.0	8.2	5.4
e_{55}	7.0± 0.4	5.65±0.53	6.9±0.0012	6.3±0.2	5.6	5.2±0.6	6.58	6.3	7.1	5.4
e_{66}	6.9± 0.5	4.64±0.43	7.2±0.0011	5.4±0.2	4.5	4.1±0.5	5.71	5.28	6.1	3.8
e_{12}	9.1		9.1±0.0038	11.7±0.7	10.0	11.3±0.1	11.18	6.34	14.0	12.1
e_{13}	8.3±5.3		9.1±0.0055	11.1±0.8	10.1	12.5±0.1	13.59	4.84	15.8	12.6
e_{23}	8.5		9.2±0.0055	12.7±0.8	10.7	12.6±0.1	13.84	6.94	13.6	12.6

[1] (Goldmann, 2006)
[2] (Orías, 2005)
[3] (Yoon, Katz, 1976)
[4] (Katz et al., 1984)
[5] (Ashman et al., 1984)
[6] (Rho, 1996)
[7] (Taylor et al., 2002)
[8] (Buskirk et al., 1981)
[9] (Maharidge, 1984)
[0] (Lang, 1970)

Table 21: Nearly cylindrically orthotropic (transversely isotropic), in a way Catrensian, elastisity coefficients of a cortical bone

The assessment of the material characteristic of a single lamella of an osteon

If the locally orthotropic characteristics of a single lamella of an osteon were known, the model would be completed. There is a great challenge to a biomechanical experimenter: To disintegrate the osteon into lamellae and test, in a way, the mechanical behaviour. As such experiments were not accomplished, at least to the author knowledge, we must assess the characteristic in another way. Thus, let us, at this section, pursue the material characteristic of a single lamella of an osteon to meet some of the above cited transversely isotropic coefficients, *i.e.*, tune the entry of the elasticity tensor of the osteon lamella to have the overall properties such that the one measured under presumption that the cortical bone is a homogenous transversely isotropic hollow cylinder.

Now, let us accept the assumption that we know the geometry, *i.e.*, the number, location, and dimensions of the osteons, and that the interstitial tissue is transversely isotropic with the same characteristic as the material characteristics of the transversely isotropic (averaging) model.[19] Taking moreover into account the requirement that the elastic energy of both models should be the same, under the same (reasonable) strain, than we could write

$$a = \alpha,$$

where the elastic energy of our lamellar (locally orthotropic model)

$$a = \int_\Omega \varepsilon_{ab}\varepsilon^{cd}\mathcal{E}^{ab}{}_{cd}\ \mathrm{d}\Omega + \sum_{\ell=1}^{n}\int_{\Omega_\ell} \varepsilon_{ab}\varepsilon^{cd}\overset{\beta}{E}{}^{ab}{}_{cd}\ \mathrm{d}\Omega - \sum_{\ell=1}^{n}\int_{\Omega_\ell} \varepsilon_{ab}\varepsilon^{cd}\overset{\beta}{\mathcal{E}}{}^{ab}{}_{cd}\ \mathrm{d}\Omega$$

and the elastic energy of the transversely isotropic (averaging) model

$$\alpha = \int_\Omega \varepsilon_{ab}\varepsilon^{cd}\mathcal{E}^{ab}{}_{cd}\ \mathrm{d}\Omega.$$

[18] Borrowed from [GOLDMANN, 2006] and [ORÍAS, 2005].
[19] [ORÍAS, 2005], [GOLDMANN, 2006].

If, moreover, all osteons are the same the elastic energy equality holds for any osteon:

$$\int\limits_{\Omega_a} \varepsilon_{ab}\varepsilon^{cd}E^{ab}_{\ cd}\ \mathrm{d}\Omega = \int\limits_{\Omega_a} \varepsilon_{ab}\varepsilon^{cd}\mathcal{E}^{ab}_{\ cd}\ \mathrm{d}\Omega.$$

As the last equation would hold for any (reasonable) strain we may set up a number of independent equations, one of them, *e.g.* for the strain

$$\overset{z}{\varepsilon}{}^{11} = c \text{ (a constant)}, \quad \overset{z}{\varepsilon}{}^{ab} = 0 \ (ab \neq 11),$$

could look like

$$\int\limits_{\Omega_a} \overset{z}{E}_{1111}\ \mathrm{d}\Omega = \int\limits_{\Omega_a} \overset{z}{\mathcal{E}}_{1111}\ \mathrm{d}\Omega,$$

after substitution

$$\int\limits_0^l \sum_{\nu=1}^{n_a} \int\limits_{r_\nu}^{r_{\nu+1}} \beta^1 \int\limits_0^{2\pi} \frac{\partial z^1}{\partial \nu^a}\frac{\partial z^1}{\partial \nu^b}\ \overset{\nu}{E}{}^{ab}_{kl}\ \frac{\partial \nu^k}{\partial z^1}\frac{\partial \nu^l}{\partial z^1}\,\mathrm{d}\beta^2\,\mathrm{d}\beta^1\,\mathrm{d}\beta^3 =$$

$$= \int\limits_0^l \int\limits_{r_1}^{r_a} \beta^1 \int\limits_0^{2\pi} \frac{\partial z^1}{\partial \beta^a}\frac{\partial z^1}{\partial \beta^b}\ \overset{\beta}{\mathcal{E}}{}^{ab}_{cd}\ \frac{\partial \beta^c}{\partial z^1}\frac{\partial \beta^d}{\partial z^1}\mathrm{d}\beta^2\,\mathrm{d}\beta^1\,\mathrm{d}\beta^3.$$

The other equalities constructed in a similar manner will yield a system of equations. As the number of the material constants in our locally orthotropic model of osteon lamellae is nine (E_{11}, E_{22}, E_{33}, ν_{12}, ν_{23}, ν_{31}, G_{12}, G_{23}, G_{31}), the number of the equations ought to be no less than nine. To resolved this system in the case of a redundant number of equations, it is best to use the pseudoinverse method based on the singular decomposition.

Let us accomplish, as an illustration, the above mention example of the equality of the osteon elastic energy:

$$\int\limits_0^1 \sum_{\nu=1}^{n_a} \int\limits_{r_\nu}^{r_{\nu+1}} \beta^1 \int\limits_0^{2\pi} \frac{\partial z^1}{\partial \nu^a}\frac{\partial z^1}{\partial \nu^b}\ \overset{\nu}{E}{}^{ab}_{kl}\ \frac{\partial \nu^k}{\partial z^1}\frac{\partial \nu^l}{\partial z^1}\,\mathrm{d}\beta^2\,\mathrm{d}\beta^1\,\mathrm{d}\beta^3 = \pi\left(r_a^2 - r_1^2\right)\ \overset{z}{\mathcal{E}}_{1111},$$

$$\sum_{\nu=1}^{n_a} \int\limits_{r_\nu}^{r_{\nu+1}} \beta^1 \int\limits_0^{2\pi} \left(\begin{pmatrix} \cos\beta^2 \\ -\cos\alpha_\nu \sin\beta^2 \\ \sin\alpha_\nu \sin\beta^2 \end{pmatrix} \otimes \begin{pmatrix} \cos\beta^2 \\ -\cos\alpha_\nu \sin\beta^2 \\ \sin\alpha_\nu \sin\beta^2 \end{pmatrix} \otimes \begin{pmatrix} \cos\beta^2 \\ -\cos\alpha_\nu \sin\beta^2 \\ \sin\alpha_\nu \sin\beta^2 \end{pmatrix} \otimes \right.$$

$$\left. \otimes \begin{pmatrix} \cos\beta^2 \\ -\cos\alpha_\nu \sin\beta^2 \\ \sin\alpha_\nu \sin\beta^2 \end{pmatrix} \right) :: \overset{\nu}{E}_{abkl}\ \mathrm{d}\beta^2\,\mathrm{d}\beta^1\,\mathrm{d}\beta^3 = \pi\left(r_a^2 - r_1^2\right)\mathcal{E}_{1111}.$$

As

$$\int\limits_0^{2\pi} \cos^4\ \mathrm{d}\beta = \frac{3\pi}{4},$$

$$\int\limits_0^{2\pi} \cos^3\beta \sin\beta\,\mathrm{d}\beta = 0,$$

$$\int\limits_0^{2\pi} \cos^2\beta \sin^2\beta\,\mathrm{d}\beta = -\frac{1}{2},$$

$$\int_0^{2\pi} \cos\beta \sin^3\beta \,\mathrm{d}\beta = 0,$$

$$\int_0^{2\pi} \sin^4\beta \,\mathrm{d}\beta = \frac{3\pi}{4},$$

it holds

$$\sum_{\nu=1}^{n_a} \int_{r_\nu}^{r_{\nu+1}} \beta^1 \begin{pmatrix} \frac{3\pi}{4} & 0 & 0 & 0 & -\frac{\pi}{4}c_\nu^2 & \frac{\pi}{4}s_\nu c_\nu & 0 & \frac{\pi}{4}s_\nu c_\nu & -\frac{\pi}{4}s_\nu^2 \\ 0 & -\frac{\pi}{4}c_\nu^2 & \frac{\pi}{4}s_\nu c_\nu & -\frac{\pi}{4}c_\nu^2 & 0 & 0 & \frac{\pi}{4}s_\nu c_\nu & 0 & 0 \\ 0 & \frac{\pi}{4}s_\nu c_\nu & -\frac{\pi}{4}s_\nu^2 & \frac{\pi}{4}s_\nu c_\nu & 0 & 0 & -\frac{\pi}{4}s_\nu^2 & 0 & 0 \\ 0 & -\frac{\pi}{4}c_\nu^2 & \frac{\pi}{4}s_\nu c_\nu & -\frac{\pi}{4}c_\nu^2 & 0 & 0 & \frac{\pi}{4}s_\nu c_\nu & 0 & 0 \\ -\frac{\pi}{4}c_\nu^2 & 0 & 0 & 0 & \frac{3\pi}{4}c_\nu^4 & -\frac{3\pi}{4}s_\nu c_\nu^3 & 0 & -\frac{3\pi}{4}s_\nu c_\nu^3 & \frac{3\pi}{4}s_\nu^2 c_\nu^2 \\ \frac{\pi}{4}s_\nu c_\nu & 0 & 0 & 0 & -\frac{3\pi}{4}s_\nu c_\nu^3 & \frac{3\pi}{4}s_\nu^2 c_\nu^2 & 0 & \frac{3\pi}{4}s_\nu^2 c_\nu^2 & -\frac{3\pi}{4}s_\nu^3 c_\nu \\ 0 & \frac{\pi}{4}s_\nu c_\nu & -\frac{\pi}{4}s_\nu^2 & \frac{\pi}{4}s_\nu c_\nu & 0 & 0 & -\frac{\pi}{4}s_\nu^2 & 0 & 0 \\ \frac{\pi}{4}s_\nu c_\nu & 0 & 0 & 0 & -\frac{3\pi}{4}s_\nu c_\nu^3 & \frac{3\pi}{4}s_\nu^2 c_\nu^2 & 0 & \frac{3\pi}{4}s_\nu^2 c_\nu^2 & -\frac{3\pi}{4}s_\nu^3 c_\nu \\ -\frac{\pi}{4}s_\nu^2 & 0 & 0 & 0 & \frac{3\pi}{4}s_\nu^2 c_\nu^2 & -\frac{3\pi}{4}{s_\nu}^3 c_\nu & 0 & -\frac{3\pi}{4}s_\nu^3 c_\nu & \frac{3\pi}{4}s_\nu^4 \end{pmatrix} :: \overset{\nu}{E}_{abcd} \,\mathrm{d}\beta^1 = \pi\left(r_{n_a+1}^2 - r_1^2\right)\mathcal{E}_{1111}.$$

Presuming that all the lamellae are of the same behaviour we have

$$\sum_{\nu=1}^{n_a} \frac{1}{2}\left({r_{\nu+1}}^2 - {r_\nu}^2\right)\left(\Phi_{1111}\frac{3\pi}{4} + \Phi_{2222}\frac{3\pi}{4}\cos^4\alpha_\nu + \Phi_{333}\frac{3\pi}{4}\sin^4\alpha_\nu - \Phi_{1122}\frac{\pi}{2}\cos^2\alpha_\nu - \right.$$

$$\left. -\Phi_{1133}\frac{\pi}{2}\sin^2\alpha_\nu + \Phi_{2233}\frac{3\pi}{2}\cos^2\alpha_\nu\sin^2\alpha_\nu - G_{12}\pi\cos^2\alpha_\nu + G_{23}3\pi\cos^2\alpha_\nu\sin^2\alpha_\nu - G_{31}\pi\sin^2\alpha_\nu\right) =$$

$$= \pi\left(r_{n_a+1}^2 - r_1^2\right)\mathcal{E}_{1111}.$$

Prediction of the bone cross-section geometry

The problem remaining is the bad knowledge of the bone cross-section geometry in particular the knowledge of the osteon lamela winding angle.

There is the opportunity to utilize the optimization approach. According to the author[20] the best arrangement, in the case of an unknown combination of the loads, is the winding angle $\pm 45°$. This result is not in the full agreement with published findings,[21] nevertheless there are some hints in the question why the arrangement is not met.

The orther way is to tune the angle or the ratios of material tensor entries to meet the known fracture modes, under appropriate type of loading, with maximal stress.

Acknowledgement

The work described in this paper was substantially supported by the Czech Ministry of Education under Project MSM6840770012/FIS3405121.

[20] [MAREŠ, 2004] and [MAREŠ, 2005] at http://drone.fsid.cvut.cz/bulletin/20051mares.pdf.
[21] [ORÍAS, 2005]

Bibliography

[mik, 1982] (1982): *Měřící zesilovač 1101.* MIKROTECHNA, n. p., U průhonu 22 Praha 7.

[tn5, 1985] (1985): *Measurement of Residual Stresses by the Hole-Drilling Strain-Gage Method.* Measurements Group, Inc., P. O. Box 27777, Raleigh, North Carolina 27611, USA.

[Mat, 1999] (1999): *MATLAB function reference, Version 5.* The MathWorks, Inc.

[sin, 1999] (1999): *Meßsystem zur Bestimmung von Eigenspanungen mit der Borlochmethode.* SINT Technology, 243-50041 Calenzano – Italy.

[E83, 2001] (2001): *Standard Test Method for Determining Residual Stresses by the Hole-Drilling Strain-Gage Method.* ASTM International.

[Ashman *et al.*, 1989] Ashman, R. B., Rho, J. Y., and Turner, C. H. (1989): Anatomical variation of orthotropic elastic moduli of the proximal human tibia. *Journal of Biomechanics* **22**, 895–900.

[Audion, 2002] Audion, B. (2002): Non-destructive evaluation of composite materials with ultrasonic waves generated and detected by lasers. *Ultrasonics* **40**, 736–740.

[Auld, 1973] Auld, B. A. (1973): *Acoustic fields and waves in solids, Vol. 1.* John Wiley and Sons, New York.

[Balasubramaniam and Whitney, 1996] Balasubramaniam, K. and Whitney, S. C. (1996): Ultrasonic through-transmission characterization of thick fibre-reinforced composites. *NDT and E International* **29**, 225–236.

[Bayraktar *et al.*, 2004] Bayraktar, H. H., Morgan, E. F., Niebur, G. L., Morris, G. E., Wong, E. K., and Keaveny, T. M. (2004): Comparison of the elastic and yield properties of human femoral trabecular and cortical bone tissue. *Journal of Biomechanics* **37**, 27–35.

[Beaupre *et al.*, 1990] Beaupre, S. G., Orr, T. E., and Carter, D. R. (1990): An approach for time dependent bone modeling and remodeling application: a preliminary remodeling simulation. *Journal of Orthopaedic Research* **8**, 662–670.

[Bensamoun *et al.*, 2004] Bensamoun, S., Tho, M. C. H. B., Luu, S., Gherbezza, J. M., and de Belleval, J. F. (2004): Spatial distribution of acoustic and elastic properties of human femoral cortical bone. *Journal of Biomechanics* **37**, 503–510.

[Berka *et al.*, 1998] Berka, L., Sova, M., and Fisher, G. (1998): Residual Stress Evalution by Microsopic Strain Measurement. *Experimental Techniques* , 22–25.

[Biot, 1956a] Biot, M. A. (1956a): Theory of propagation of elastic waves in a fluid saturated porous solid. I. Low frequency range. *J Acoust Soc Am* **28**, 168–178.

[Biot, 1956b] Biot, M. A. (1956b): Theory of propagation of elastic waves in a fluid saturated porous solid. II. High frequency range. *J Acoust Soc Am* **28**, 179–191.

[Brown *et al.*, 1990] Brown, T. D., Pedersen, D. R., Gray, M. L., Brand, R. A., and Rubin, C. T. (1990): Toward an identiffication of mechanical parameters initiating periosteal remodeling: a combined experimental and analytic approach. *Journal of Biomechanics* **23**, 893–905.

[Buechner *et al.*, 2001] Buechner, P. M., Lakes, R. S., Swan, C., and Brand, R. A. (2001): Toward an identification of mechanical parameters initiating periosteal remodeling: a combined experimental and analytic approach. *Annals of Biomedical Engineering* **23**, 719–728.

[Burger and Klein-Nuled, 1999] Burger, E. H. and Klein-Nuled, J. (1999): Mechanotransduction in bone-role of the lacunocanalicular network. *FASEB Journal* **13**, S101–S112.

[Buskirk *et al.*, 1981] Buskirk, W. C. V., Cowin, S. C., and Ward, R. N. (1981): Ultrasonic measurement of orthotropic elstic constants of bovine femoral bone. *Journal of Biomechanical Engineering* **103**, 67–72.

[Carter, 1987] Carter, D. R. (1987): Mechanical loading history and skeletal biology. *Journal of Biomechanics* **20**, 1095–1109.

[Carter and Hayes, 1977] Carter, D. R. and Hayes, W. C. (1977): The compressive behavior of bone as a two-phase porous structure. *J Bone Jt Surg Am* , 954–962.

[Castagnede *et al.*, 1990] Castagnede, B., Jenkins, J. T., and Sachse, W. (1990): Optimal determination of the elastic constants of composite materials from ultrasonic wave-speed measurements. *J. Appl. Phys.* **69**, 2753–2761.

[Castagnede *et al.*, 1991] Castagnede, B., Kim, K. Y., Sachse, W., and Thomson, M. O. (1991): Determining of the elastic constants of anisotropic materials using laser-generated ultrasonic signals. *J. Appl. Phys.* **70**, 150–157.

[Castaings *et al.*, 2000] Castaings, A., Hosten, B., and Kundu, T. (2000): Inversion of ultrasonic, plane-wave transmission data in composite plated to infer viscoelastic material properties. *NDT and E* **33**, 377–392.

[Chambers, 1728] Chambers, E. (1728): *Cyclopaedia, or, An universal dictionary of arts and sciences: containing the definitions of the terms, and accounts of the things signify'd thereby, in the several arts, both liberal and mechanical, and the several sciences, human and divine: the figures, kinds, properties, productions, preparations, and uses, of things natural and artificial: the rise, progress, and state of things ecclesiastical, civil, military, and commercial: with the several systems, sects, opinions, &c: among philosophers, divines, mathematicians, physicians, antiquaries, criticks, &c: the whole intended as a course of antient and modern learning.* Printed for J. and J. Knapton and 18 others, London. http://images.library.wisc.edu/HistSciTech/EFacs/Cyclopaedia/, The First Volume and the Second Volume, 2 v.: ill. (some folded); 41 cm.

[Chandrasekharaiah and Debnath, 1994] Chandrasekharaiah, D. S. and Debnath, L. (1994): *Continuum Mechanics.* Academic Press, Boston.

[Chu and Rokhlin, 1994] Chu, Y. C. and Rokhlin, S. I. (1994): A method for determination of elastic constants of a unidirectional lamina from ultrasonic bulk velocity measurements on [0/90] cross-ply composites. *J. Accoust. Soc. Am* **96**, 342–352.

[Cowin, 1985] Cowin, C. (1985): The relationship between the elastic tensor and the fabric tensor. *J. Mech. Mater* **4**, 137–147.

[Cowin, 1999] Cowin, S. C. (1999): Bone poroelasticity. *Journal of Biomechanics* **217–238**.

[Cowin *et al.*, 1991] Cowin, S. C., Moss-Salentijn, L., and Moss, M. L. (1991): Candidates for the mechanosensory system in bone. *Journal of Biomechanical Engineering* **113**, 191–197.

[Cowin *et al.*, 1995] Cowin, S. C., Weinbaum, S., and Zeng, Y. (1995): A case for bone canaliculi as the anatomical site of strain generated potentials. *Journal of Biomechanics* **28**, 1281–1297.

[Cross *et al.*, 1993] Cross, S. S., Rogers, S., and Silcocs, P. B. (1993): Trabecular bone does not have a fractal structure on light microscopic examination. *Journal of Pathology* **170**, 311–313.

[Darras *et al.*, 1995] Darras, O., Duckett, R. A., Hine, P. J., and Ward, I. M. (1995): Anisotropic elasticity of oriented polyethylene materials. *Composite Science and Technology* **55**, 131–138.

[Degtyar and Rokhlin, 1997] Degtyar, A. D. and Rokhlin, S. I. (1997): Comparison of elastic constant determination in anisotropic materials from ultrasonic group and phase velocity data. *J.Acoust.Soc.Am.* **102**, 3458–3466.

[Demarest, 1971] Demarest, H. H. (1971): Cube-resonance method to determine the elastic constants of solids. *J. Acoust. Soc. Am* **49**, 768–775.

[Detti *et al.*, 2002] Detti, V., Kourtiche, D., and Nadi, M. (2002): Acoustical characterization of bone using a cylindrical model and time of flight method: edge reconstruction and ultrasound velocity determination in cortical bone and in medullar marrow. *Physiological Measurement* **23**, 313–324.

[Dong and Guo, 2004] Dong, X. N. and Guo, X. E. (2004): The dependence of transversely isotropic elasticity of human femoral cortical bone on porosity. *Journal of Biomechanics* **37**, 1281–1287.

[Dorland and Newman, 2003] Dorland, I. and Newman, W. A. (1900, 2003): *Dorland's illustrated medical dictionary*. W. B. Saunders Company, Philadelphia.

[Doubrava *et al.*, 2003a] Doubrava, K., Mareš, T., and Vítek, K. (2003a): Excentricita otvoru a její zohlednění u odvrtávací metody. In *Experimentální analýza napětí 2005*, pages 15–16. VUT, Fakulta strojní.

[Doubrava *et al.*, 2004a] Doubrava, K., Mareš, T., Španiel, M., and Vítek, K. (2004a): Problematika vyhodnocování odvrtávací metody. In *Experimentální analýza napětí 2004*, pages 47–50. Škoda Výzkum.

[Doubrava *et al.*, 2003b] Doubrava, K., Vítek, K., Kuliš, Z., and Holý, S. (2003b): Měření zbytkových napetí u trubkových ohybů. In *Summer Workshop of Applied Mechanics*, pages 102–112. ČVUT FS, Ústav mechaniky, Odbor pružnosti a pevnosti.

[Doubrava *et al.*, 2003c] Doubrava, K., Vítek, K., Kuliš, Z., and Holý, S. (2003c): *Měření zbytkových napětí na trubkovém ohybu pomocí odvrtávací metody*. Technical Report FS 2052/03/09, ČVUT v Praze FS, Ústav mechaniky, Odbor pružnosti a pevnosti.

[Doubrava *et al.*, 2004b] Doubrava, K., Vítek, K., Mareš, T., and Španiel, M. (2004b): Practical Application of Inovated Hole Drilling Method Theory for Residual Stress. In *21st Danubia-Adria Symposium on Experimental Methods in Solid Mechanics*, pages 22–23. Croatian Society of Mechanics.

[Díaz *et al.*, 2000] Díaz, G. V., Kaufmann, G. H., and Galizzi, G. E. (2000): Determination of residual stresses using hole drilling a digital speckle pattern iterferometry with automated data analysis. *Optics and Laser in Engineering* **33**, 39–48.

[Enderby *et al.*, 1998] Enderby, M. D., Clarke, A. R., Patel, M. D., Ogden, P., and Johnson, A. A. (1998): An automated ultrasonic immersion technique for the determination of three-dimensional elastic constants of polymer composites. *Ultrasonics* **36**, 245–249.

[Every and Sachse, 1990] Every, A. G. and Sachse, W. (1990): Determination of the elastic constants of anisotropic solids from acoustic-wave group-velocity measurements. *Physical Review B* **42**, 8196–8205.

[Every and Sachse, 1992] Every, A. G. and Sachse, W. (1992): Sensitivity of inversion algorithms for recovering elastic constants of anisotropic solids from longitudinal wavespeed data. *Ultrasonics* **30**, 43–48.

[Every and Sachse, 2001] Every, A. G. and Sachse, W., editors (2001): *Dynamic methods for measuring the elastic properties of solids, (Handbook of elastic properties of solids, liquids and gases, Volume I).* Academic Press, San Diego.

[Fekih and Quentin, 1983] Fekih, M. L. and Quentin, G. (1983): Scattering of short ultrasonic pulses by thin cylindrical shells: generation of guided waves inside the shell. *Phys. Lett. A* **96**, 379–384.

[Focht and Schiffner, 2003] Focht, G. and Schiffner, K. (2003): Determination of Residual Stresses by on Optical Correlative Hole-drilling Method. *Experimental Mechanics* **43**, 97–104.

[Folacci and Rossi, 1997] Folacci, A. and Rossi, J.-L. (1997): GTD analysis of scattering by two elastic spheres. *Acta Acoustica* **83**, 93–104.

[Fratzl *et al.*, 1992] Fratzl, P., Groschner, M., Vogel, G., Plenk, Jr., H., Eschberger, J., Fratzl-Zelman, N., Koller, K., and Klaushofer, K. (1992): Mineral crystals in calcified tissues: a comparative study by SAXS. *Journal of Bone and Mineral Research* **7**, 329–334.

[Frost, 1990] Frost, M. H. (1990): Skeletal structural adaptations to mechanical usage (SATMU): 2. Redefining Wolff's law: the remodeling problem. *Anatomical Record* **226**, 414–422.

[Fukuoka *et al.*, 1978] Fukuoka, H., Toda, H., and Yamane, T. (1978): Acoustoelastic Stress Analysis of Residual Stress in a Patch-welded Disk. *Experimental Mechanics* , 277–280.

[Fyhrie and Carter, 1986] Fyhrie, D. P. and Carter, D. R. (1986): A unifying principle relating stress to trabecular bone morphology. *Journal of Orthopaedic Research* **4**, 304–317.

[Gauthier *et al.*, 1998] Gauthier, J., Krause, T. W., and Atherton, D. (1998): Measurement of residual stress in steel using the magnetic Barkhausen noise technique. *NDT & E International* **31**, 23–31.

[Geiske and Allred, 1974] Geiske, J. H. and Allred, R. E. (1974): Elastic Constants of B-A1 Composites by Ultrasonic Velocity Measurements. *ExpeimentalMechanics* **14**, 158–165.

[Giesen *et al.*, 2001] Giesen, E. B. W., Ding, M., Dalstra, M., and van Eijden, T. M. G. J. (2001): Mechanical properties of cancellous bone in the human mandibular condyle are anisotropic. *Journal of Biomechanics* **34**, 799–803.

[Goldmann, 2006] Goldmann, T. (2006): *Propagation of Acoustic Waves in Composite Materials and Cortical Bone.* PhD thesis, Czech Technical University in Prague, Faculty of Mechanical Engineering, Department of Mechanics, Prague.

[Goulet *et al.*, 1994] Goulet, R. W., Goldstein, S. A., Ciarelli, M. J., Kuhn, J. L., Brown, M. B., and Feldkamp, L. A. (1994): The relationship between the structural and orthogonal compressive properties of trabecular bone. *Journal of Biomechanics* , 375–389.

[Gray, 1918] Gray, H. (1918): *Anatomy of the Human Body.* Lea & Febiger, Philadelphia.

[Gross *et al.*, 1997] Gross, T. S., Edwards, J. L., McLeod, K. J., and Rubin, C. T. (1997): Strain gradients correlate with sites of periosteal bone formation. *Journal of Bone Mineral Research* **12**, 982–988.

[Gururaja *et al.*, 2005] Gururaja, S., Kim, H. J., Swan, C. C., Brand, R. A., and Lakes, R. S. (2005): Modeling Deformation-Induced Fluid Flow in Cortical Bone's Canalicular-Lacunar System. *Annals of Biomedical Engineering* **33**, 7–25.

[Haire and Langton, 1999] Haire, T. J. and Langton, C. M. (1999): Biot Theory: A Review of Its Application to Ultrasound Propagation Through Cancellous Bone. *Bone* **24**, 291–295.

[Harper and Clarke, 2002] Harper, M. J. and Clarke, A. R. (2002): Low frequency ultrasonic propagation through fibre reinforced, polymer composites. *Ultrasonics* **40**, 555–560.

[He and Kobayashi, 2001] He, L. F. and Kobayashi, S. (2001): Acoustoelastic Determination of Residual Stress with Laser Doppler Velocimetry. *Experimental Mechanics* **41**, 190–194.

[Hearmon, 1961] Hearmon, R. F. S. (1961): *An Introduction to Applied Anisotropic Elasticity.* The Clarendon Press, Oxford.

[Helbig, 1994] Helbig, K. (1994): *Foundations of anisotropy for exploration seismics.* Pergamon Press, Oxford, 1st edition.

[Hellmich *et al.*, 2004] Hellmich, C., Ulm, F. J., and Dormieux, L. (2004): Can the diverse elastic properties of trabecular and cortical bone be attributed to only a few tissue-independent phase properties and their interactions? Arguments from a multiscale approach. *Biomechanical Modeling in Mechanobiology* **2**, 219–238.

[Hetényi, 1950] Hetényi, M., editor (1950): *Handbook of experimental stress analysis.* John Wiley & Sons, Inc.

[Hildebrand *et al.*, 1999] Hildebrand, T., Laib, A., and Muller, R. (1999): Direct three dimensional morphometric analysis of human cancellous bone: microstructural data from spine, femur, iliac crest and calcaneus. *Journal of Bone and Mineral Research* **14**, 1167–1174.

[Hine *et al.*, 1997] Hine, P. J., Wire, S., Duckett, R. A., and Ward, I. M. (1997): Hydrostatically Extruded Glass Fiber Reinforced Polyxymethylene. II: Modeling the Elastic Properties. *Polymer Composites* **18**, 634–641.

[Hollister and Kikuchi, 1992] Hollister, S. J. and Kikuchi, N. (1992): A comparison of homogenization and standard mechanics analyses for periodic porous composites. *Computational Mechanics* **10**, 73–95.

[Holý *et al.*, 2002a] Holý, S., Doubrava, K., Václavík, J., Vítek, K., and Weinberg, O. (2002a): Determination of Residual Stress in Forgings of Turbine Rotors of Different Heat Treatment. In *Abstracts of 19th Danubia-Adria Symposium*, pages 224–225. Comittee for Mechanics of the Polish Academy of Sciences.

[Holý *et al.*, 2002b] Holý, S., Doubrava, K., Václavík, J., Vítek, K., and Weinberg, O. (2002b): Určení velikosti zbytkových pnutí ve výkovcích železničních náprav s rozdílným tepelným zpracováním. In *Experimental Stress Analysis*, pages 105–108. Asociace strojních inženýrů.

[Homminga *et al.*, 2001] Homminga, J., Huiskes, R., Rietbergen, B. V., Ruegsegger, P., and Weinans, H. (2001): Introduction and evaluation of a gray-value voxel conversion technique. *Journal of Biomechanics* **34**, 513–517.

[Homminga *et al.*, 2003] Homminga, J., Mccreadie, B. R., Weinans, H., and Huiskes, R. (2003): The dependence of the elastic properties of osteoporotic cancellous bone on volume fraction and fabric. *Journal of Biomechanics* **36**, 1461–1467.

[Hosokawa and Otani, 1997] Hosokawa, A. and Otani, T. (1997): Ultrasonic wave propagation in bovine cancellous bone. *J Acoust Soc Am* **103**, 558–562.

[Hughes *et al.*, 1999] Hughes, E. R., Leighton, T. G., Petley, G. W., and White, P. R. (1999): Ultrasonic propagation in cancellous bone: A new stratified model. *Ultrasound in Med. & Biol.* **25**, 811–821.

[Hughes *et al.*, 2003] Hughes, E. R., Leighton, T. G., Petley, G. W., White, P. R., and Chivers, R. C. (2003): Estimation of critical and viscous frequencies for Biot theory in cancellous bone. *Ultrasonics* , 365–368.

[Huiskes and Hollister, 1993] Huiskes, R. and Hollister, S. J. (1993): From structure to process, from organ to cell: recent developments of FE-analysis in orthopaedic biomechanics. *Journal of Biomechanical Engineering* **115**, 520–527.

[Huiskes *et al.*, 1987] Huiskes, R., Weinans, H., Grootenboer, J. H., Dalstra, M., Fudala, B., and Sloof, T. J. (1987): Adaptive bone-remodeling theory applied to prosthetic-design analysis. *Journal of Biomechanics* **20**, 1138–1150.

[Hvid *et al.*, 1989] Hvid, I., Bentzen, S. M., Linde, F., Mosekilde, F., and Pongsoipetch, B. (1989): X-ray quantitative computed tomography: the relations to physical properties of proximal tibial trabecular bone specimens. *Journal of Biomechanics* **22**, 837–844.

[Ichitsubo *et al.*, 2002] Ichitsubo, T., Ogi, H., Hirao, M., Tanaka, K., Osawa, M., Yokokawa, T., Kobayashi, T., and Harada, H. (2002): Elastic constant measurement of Ni-base superalloy with the RUS and mode selective EMAR methods. *Ultrasonics* **40**, 211–215.

[Iyo *et al.*, 2004] Iyo, T., Maki, Y., Sasaki, N., and Nakata, M. (2004): Anisotropic viscoelastic properties of cortical bone. *Journal of Biomechanics* **37**, 1433–1437.

[Jacobs *et al.*, 1998] Jacobs, C. R., Yellowley, C. E., Davis, B. R., Zhou, Z., Cimbale, J. M., and Donahue, H. J. (1998): Differential effect of steady versus oscilating flow on bone cells. *Journal of Biomechanics* **31**, 969–976.

[Jasiuk and Ostoja-Starzewski, 2004] Jasiuk, I. and Ostoja-Starzewski, M. (2004): Modeling of bone at a single lamella level. *Biomechanical Modeling in Mechanobiology* **3**, 67–74.

[Johnson *et al.*, 1987] Johnson, D. L., Koplik, J., and Dashen, R. (1987): Theory of dynamic permeability and tortuosity in fluid-saturated porous media. *J Fluid Mech* **176**, 379–402.

[Jørgensen and Kundu, 2002] Jørgensen, C. S. and Kundu, T. (2002): Measurement of material elastic constants of trabecular bone: a micromechanical analytic study using a 1 GHz acoustic microscope. *Journal of Orthopaedic Research* **20**, 151–158.

[Junqueira *et al.*, 1995] Junqueira, L. C., Carneiro, J., and .Kelley, R. O. (1995): *Bone*. Appleton & Langer, Norwalk, CT, Basic Histology edition.

[Kabel *et al.*, 1999] Kabel, J., van Rietbergen, B., Dalstra, M., Odgaard, A., and Huiskes, R. (1999): The role of an effective isotropic tissue modulus in the elastic properties of cancellous bone. *Journal of Biomechanics* **32**, 673–680.

[Kabiri, 1984] Kabiri, M. (1984): Nonuniform Residual-stress Measurement by Hole-drilling Method. *Experimental Mechanics* , 328–336.

[Kaczmarek *et al.*, 2002] Kaczmarek, M., Kubik, J., and Pakula, M. (2002): Short ultrasonic waves in cancellous bone. *Ultrasonics* **40**, 95–100.

[Karel Doubrava, 2006] Karel Doubrava, Tomáš Mareš, K. V. a. Z. K. (2006): Excentricita u odvrtávací metody. *Bulletin of Applied Mechanics* **5**, 65–81.

[Katz *et al.*, 1984] Katz, J. L., Yoon, H. S., Lipson, S., Maharidge, R., Meunier, A., and Christel, P. (1984): The effects of remodeling on the elastic properties of bone. *Calcified Tissue International* **36**, S31–S36.

[Kim and Sachse, 1995] Kim, K. Y. and Sachse, R. S. W. (1995): Analytical and optimization procedures for determination of all elastic constants of anisotropic solids from group velocity data measured in symmetry planes. *J. Appl. Phys.* **77**, 5589–5600.

[Kinney *et al.*, 2004] Kinney, J. H., Gladden, J. R., Marshall, G. W., Marshall, S. J., So, J. H., and Maynard, J. D. (2004): Resonant ultrasound spectroscopy measurements of the elastic constants of human dentin. *Journal of Biomechanics* **37**, 437–441.

[Koch, 1917] Koch, J. C. (1917): The laws of bone architecture. *American Journal of Anatomy* **21**.

[Kozanek, 1982] Kozanek, J. (1982): Vyhodnoceni přenosové funkce z naměřených dat. *Strojnický časopis* **33**, 281–289.

[Ladd and Kinney, 1997] Ladd, A. J. C. and Kinney, J. H. (1997): Elastic constants of cellular structures. *Physica A* **240**, 349–360.

[Lakes *et al.*, 1986] Lakes, R., Yoon, H. S., and Katz, J. L. (1986): Ultrasonic wave propagation and attenuation in wet bone. *Journal of Biomechanics* **39**, 143–148.

[Lakes *et al.*, 1983] Lakes, R. S., Yoon, H. S., and Katz, J. L. (1983): Slow compressional wave propagation in wet human and bovine cortical bone. *Scince* **220**, 513–515.

[Lasayques and Pithioux, 1998] Lasayques, P. and Pithioux, M. (1998): Ultrasonic characterization of orthotropic elastic bovine bones. *Ultrasonics* **39**, 567–573.

[Lee *et al.*, 2002] Lee, T., Lakes, R. S., and LAl, A. (2002): Investigation of bovine bone by resonant ultrasound spectroscopy and transmission ultrasound. *Biomechanics and Modeling in Mechanobiology* **1**, 165–175.

[Lematre, 2002] Lematre, M. (2002): Acoustic microscopy measurements of elastic constants by using an optimization method on measured and calculated SAW velocities: effect of initial cij values on the calculation convergence and influence of the LFI transducer parameters on determination of the SAW velocity. *NDT and E* **35**, 279–286.

[Liaw *et al.*, 1996] Liaw, P. K., Hsu, D. K., Yu, N., Miriyala, N., Saini, V., and Jeog, H. (1996): Investigation of metal and ceramic-matrix composites moduli: Experiment and theory. *Acta mater.* **44**, 2101–2113.

[Liebschner, 2004] Liebschner, M. A. K. (2004): Biomechanical considerations of animal models used in tissue engineering of bone. *Biomaterials* **25**, 1697–1714.

[Lin, 2000] Lin, T. (2000): Blind-hole Residual Stress Determination Using Optical Interferometry. *Experimental Mechanics* **40**, 60–67.

[Linde *et al.*, 1989] Linde, F., Hvid, I., and Pongsoipetch, B. (1989): Energy absorptive properties of human trabecular bone specimens during axial compression. *J. Orthop. Res.* , 432–439.

[Lovelock and Rund, 1989] Lovelock, D. and Rund, H. (1989): *Tensors, Differential Forms, and Variational Principles*. Dover Publications, Inc., New York.

[Lu, 1996] Lu, J., editor (1996): *Handbook of Measuremnt of Residual Stresses*. The Fairmont Press, Inc.

[Luh and Heang, 1999] Luh, G. C. and Heang, R. M. (1999): Measuring Non-Uniform Residual Stress in Thin Plates by a Proposed Hole-Drilling Strain Gauge Method. *The International Journal of Advenced Manufacturing Technology* , 103–113.

[Lukeš, 2005] Lukeš, J. (2005): . Master's thesis, Czech Technical University in Prague, Faculty of Mechanical Engineering, Department of Mechanics, Technická 4, 166 07 Prague.

[Majumdar *et al.*, 1998] Majumdar, S., Kothari, M., and Augat, P. (1998): High resolution magnetic resonance imaging: three dimensional trabecular bone architecture and biomechanical properties. *Bone* **22**, 445–454.

[Makino and Nelson, 1994] Makino, A. and Nelson, D. (1994): Residual-stress Determination by Single-axis Holographic Interferometry and Hole Drilling–Part I: Theory. *Experimental Mechanics* **43**, 66–78.

[Mareš, 2004] Mareš, T. (2004): *Maximalizace tuhosti laminátových desek a trubek volbou orientace vrstev*. PhD thesis, Czech Technical University in Prague, Faculty of Mechanical Engineering, Department of Mechanics, Prague. http://drone.fsid.cvut.cz/staff/mares/disertace.ps.

[Mareš, 2005] Mareš, T. (2005): Laminate Tube Stiffness Maximization by Winding Angle Control. *Bulletin of Applied Mechanics* **1**, 29–54. http://drone.fsid.cvut.cz/bulletin/20051mares.pdf, ISSN 1801–1217.

[Mareš, 2006a] Mareš, T. (2006a): Geometry and internal structure of thigh bone. *Bulletin of Applied Mechanics* **7**, 141–150. http://drone.fsid.cvut.cz/archive/mares200671.pdf.

[Mareš, 2006b] Mareš, T. (2006b): Locally orthotropic material—the foundation of tissue mechanics. *Bulletin of Applied Mechanics* **7**, 151–157. http://drone.fsid.cvut.cz/archive/mares200672.pdf.

[Mareš, 2006c] Mareš, T. (2006c): Mathematical model of the cortical bone osteon. *Bulletin of Applied Mechanics* **7**, 159–165. http://drone.fsid.cvut.cz/archive/mares200673.pdf.

[Mareš, 2006d] Mareš, T. (2006d): *Základy Konstrukční Optimalizace*. Nákladem Tomáše Mareše, Praha. http://drone.fsid.cvut.cz/bulletin/zko.pdf, ISBN 80-239-6508-5.

[Mareš and Daniel, 2006] Mareš, T. and Daniel, M. (2006): *Advanced Technologies, Research–Development–Application*, chapter Application of composite lamination theory to the complex model of the intervertebral disc, pages 641—660. Pro literatur Verlag Robert Mayer-Scholz, Mammendorf, Germany.

[Martin *et al.*, 1998] Martin, R. B., B.Burr, D., and Sharkey, N. A. (1998): *Skeletal Tissue Mechanics*. Springer-Verlag, New York.

[Mathar, 1934] Mathar, J. (1934): Determination of Initial Stress by Measuring Deformation Around Drilled Hole. *Trans ASME* **56**, 249–254.

[Mueller *et al.*, 1994] Mueller, R., Hildebrand, T., and Ruegsegger, P. (1994): Non-invasive bone biopsy: A new method to analyse and display the three-dimensional structure of trabecular bone. *Physics in Medicine and Biology* **39**, 145–164.

[Musgrave, 1970] Musgrave, M. J. P. (1970): *Crystal acoustic*. Holden-Day, San Francisco, 1st edition.

[Nawwar and Shewchuk, 1978] Nawwar, A. M. and Shewchuk, J. (1978): On the Measurements of Residual-stress Gradients in Aluminium-alloy Specimens. *Experimental Mechanics* , 269–276.

[Nelson *et al.*, 1994] Nelson, D., Fuchs, E., Makino, A., and Williams, D. (1994): Residual-stress Determination by Single-axis Holographic Interferometry and Hole Drilling–Part II: Experiments. *Experimental Mechanics* **43**, 79–88.

[Nickola, 1986] Nickola, W. E. (1986): Practical Subsurface Residual Stress By The Hole–Drilling Method. In *Proceedings of the Spring Conferenc on Experimental Mechanics*, pages 47–58. Society for Experimental Mechanics.

[Odgaard and Guendersen, 1993] Odgaard, A. and Guendersen, H. J. G. (1993): Quantification of connectivity in cancellous bone, with special emphasis on 3-D reconstructions. *Bone* **14**, 173–182.

[Odgaard *et al.*, 1990] Odgaard, A., Jensen, E. B., and Guendersen, H. J. G. (1990): A direct method for fast three-dimensional serial reconstruction. *Journal of Microscopy* **159**, 335–342.

[Orías, 2005] Orías, A. A. E. (2005): *The Relationship Between the Mechanical Anisotropy of Human Cortical Bone Tissue and its Microstructure.* PhD thesis, University of Notre Dame, Indiana. http://etd.nd.edu/ETD-db/theses/available/etd-04152005-134005/unrestricted/EspinozaA042005.pdf.

[Park and Lakes, 1986] Park, H. C. and Lakes, R. S. (1986): Cosserat micromechanics of human bone: Strain redistribution by a hydration sensitive constituent. *Journal of Biomechanics* **19**, 385–397.

[Pauwels, 1973] Pauwels, F. (1973): Short survey of mechanical stress of bone and its importance for functional adaptation. *Zeitschrift fuer Orthopadie und Ihre Grenzgebiete* **111**, 681–785.

[Pauwels, 1976] Pauwels, F. (1976): *Biomechanics of the Normal and Diseased Hip.* Springer-Verlag, Berlin–Heidelberg–New York–London–Barcelona–Hong Kong–Milan–Paris–Singapore–Tokyo.

[Piekarski, 1970] Piekarski, K. (1970): Fracture of Bone. *Journal of Applied Physics* **41**, 215–223.

[Piekarski, 1973] Piekarski, K. (1973): Analysis of bone as a composite material. *International Journal of Engineering Science* **11**, 555–565.

[Pithioux *et al.*, 2002] Pithioux, M., Lasayques, P., and Chabrand, P. (2002): An alternative ultrasonic method for measuring the elastic properties of cortical bone. *Journal of Biomechanics* **35**, 961–968.

[Psencik, 2000] Psencik, I. (2000): *Basics of plane wave propagation and the seismic ray theory.* CPGG/UFBa, San Salvador.

[Rendler and Vigness, 1966] Rendler, N. J. and Vigness, I. (1966): Hole-drilling Strain-gage Method of Measuring Residual Stresses. *Experimental Mechanics* **45**, 577–586.

[Rho, 1996] Rho, J. Y. (1996): An ultrasonic method for measuring the elastic properties of human tibial cortical and cancellous bone. *Ultrasonics* **34**, 777–783.

[Rho and ad C.Turner, 1993] Rho, J. Y. and ad C.Turner, R. B. A. (1993): Young's modulus of trabecular and cortical bone material: ultrasonic and microtensile measurements. *Journal of Biomechanics* **23**, 111–119.

[Rho *et al.*, 1995] Rho, J. Y., Hobato, M. C., and Ashman, R. B. (1995): Relations of mechanical properties to density and CT numbers in human bone. *Med. Eng. Phys.* **17**, 347–355.

[Rho *et al.*, 1998] Rho, J. Y., Kuhn-Spearing, L., and Zioupos, P. (1998): Mechanical properties and the hierarchical structure of bone. *Medical Engineering & Physics* **20**, 92–102.

[Rho *et al.*, 1997] Rho, J. Y., Tsui, T. Y., and Pharr, G. M. (1997): Elastic properties of human cortical and trabecular lamellar bone measured by nanoindentation. *Biomaterials* .

[Rokhlin and Wang, 1992] Rokhlin, S. I. and Wang, W. (1992): Measurements of elastic constants of very thin anisotropic plates. *J. Acoust. Soc. Am.* **91**, 3303–3312.

[Royer and Dieulesaint, 1996] Royer, D. and Dieulesaint, E. (1996): *Elastic Waves in Solids I.* Springer-Verlag, Berlin.

[Sachse *et al.*, 1998] Sachse, W., Kim, K. Y., and Hsu, N. N. (1998): Characterizing homogenous, anisotropic elastic media. In Wirgin, A., editor, *Identification of media and structures by inversion of mechanical wave propagation, CISM Proc.*, page 26, Udine.

[Salençon, 2001] Salençon, J. (2001): *Handbook of Continuum Mechanics*. Springer-Verlag, Berlin–Heidelberg–New York–London–Barcelona–Hong Kong–Milan–Paris–Singapore–Tokyo.

[Schajer, 1981] Schajer, G. S. (1981): Application of Finite Element Calculations to Residual Stress Measurements. *Journal of Engineering Materials and Technology* **103**, 157–163.

[Schajer, 1988a] Schajer, G. S. (1988a): Measurement of Non-Uniform Residual Stresses Using the Hole-Drilling Method. Part I – Stress Calculation Procedures. *Journal of Engineering Materials and Technology* **110**, 338–343.

[Schajer, 1988b] Schajer, G. S. (1988b): Measurement of Non-Uniform Residual Stresses Using the Hole-Drilling Method. Part II – Practical Application of the Integral Method. *Journal of Engineering Materials and Technology* **110**, 344–349.

[Schajer and Tootoonian, 1991] Schajer, G. S. and Tootoonian, M. (1991): A New Rosette Design for More Reliable Hole-drilling Residual Stress Measurements. *Experimental Mechanics* **37**, 299–306.

[Schajer and Yang, 1994] Schajer, G. S. and Yang, L. (1994): Residual-stress Measurement in Orthotropic Materials Using the Hole-drilling Method. *Experimental Mechanics* , 324–333.

[Schoenberg, 1984] Schoenberg, M. (1984): Wave propagation in alternating solid and fluid layers. *Wave Motion* **6**, 303–320.

[Schwartz-Dabney and Dechow, 2002] Schwartz-Dabney, C. L. and Dechow, P. C. (2002): Accuracy of Elastic Property Measurement in Mandibular Cortical Bone is Improved by Using Cylindrical Specimens. *Journal of Biomechanical Engineering* **124**, 714–723.

[Schwartz-Dabney and Dechow, 2003] Schwartz-Dabney, C. L. and Dechow, P. C. (2003): Variations in Cortical Material Properties Throughout the Human Dentate Mandible. *American Journal of Physical Anthropology* **120**, 252–277.

[Schwarz *et al.*, 2000] Schwarz, R. C., Kutt, L. M., and Papazian, J. M. (2000): Measruing of Residual Stress Using Interferometric Moiré: A New Insight. *Experimental Mechanics* **40**, 271–281.

[Seiner, 2004] Seiner, H. (2004): *Acoustic wave propagation in anisotropic elastic media and inverse problems in quantitative nondestructive evaluation of composites*. Master's thesis, CTU in Prague.

[Seiner and Landa, 2003] Seiner, H. and Landa, M. (2003): Evaluation of all elastic muduli of anisotropic solids from ultrasonic wave inversion. *Acta Technica CSAV* **48**, 1–18.

[Seiner and Landa, 2005] Seiner, H. and Landa, M. (2005): Sensitivity analysis of an inverse procedure for determination of elastic coefficients for strong anisotropy. *Ultrasonics* **43**, 253–263.

[Silva *et al.*, 2004] Silva, M. J., Brodt, M. D., Fan, Z., and Rho, J. Y. (2004): Nanoindentation and whole-bone bending estimates of material properties in bones from the senescence accelerated mouse SAMP6. *Journal of Biomechanics* **37**, 1639–1646.

[Smalt *et al.*, 1997] Smalt, R., Mitchell, F. T., Howard, R. L., and Chambers, T. J. (1997): Induction of NO and prostaglandin E_2 in osteoblast by wall-shear stress but not mechanical strain. *American Journal of Physiology* **273**, E751–E758.

[Snyder and Hayes, 1990] Snyder, B. D. and Hayes, W. C. (1990): *Multiaxial structure-property relations in trabecular bone.* Biomechanics of Diarthrodial Joints. Springer, New York.

[Soete, 1954] Soete, W. (1954): Determination of Residual Stresses Below the Surface. In Osgood, W. R., editor, *Residual Stresses in Metals and Metal Construction*, pages 331–334. Ship Structure Committee.

[Strelitski *et al.*, 1997] Strelitski, R., Nicholson, P. H. F., and Evans, J. A. (1997): Low-frequency ultrasonic velocity measurements in human calcaneal trabecular bone. *Physiol Meas* **18**, 119–127.

[Synge and Schild, 1978] Synge, J. L. and Schild, A. (1978): *Tensor Calculus.* Dover Publications, Inc., New York.

[Tate, 2003] Tate, M. L. K. (2003): "Whither flows the fluid in bone?" An osteocyte's perspective. *Journal of Biomechanics* **36**, 1409–1424.

[Taylor *et al.*, 2002] Taylor, W. R., Roland, E., Ploeg, H., Hertig, D., Klabunde, R., Warner, M. D., Hobatho, M. C., Rakotomanana, L., and Clift, S. E. (2002): Determination of orthotropic bone elastic constants using FEA and modal analysis. *Journal of Biomechanics* **35**, 767–773.

[Timoshenko and Goodier, 1951] Timoshenko, S. and Goodier, J. M. (1951): *Theory of Elasticity.* McGraw-Hill, 2 edition.

[Turner *et al.*, 1990] Turner, C. H., Covin, S. C., and Rho, J. Y. (1990): The fabric dependence of the orthotropic elastic constants of cancellous bone. *Journal of Biomechanics* **23**, 549–561.

[Turner *et al.*, 1999] Turner, C. H., Rho, J. Y., Takano, Y., Tsui, T. Y., and Pharr, G. M. (1999): The elastic properties of trabecular and cortical bone tissues are similar: results from two microscopic measurement techniques. *Journal of Biomechanics* **32**, 437–441.

[van den Bergh *et al.*, 2000] van den Bergh, J. P., van Lenthe, G. H., Hermus, A. R. M. M., Corstens, F. H. M., Smals, A. G. H., and Huiskes, R. (2000): Speed of sound reflects Young's modulus as assessed by Microstructural Finite Element Analysis. *Bone* **26**, 519–524.

[Wang and Lakes, 2003] Wang, Y. C. and Lakes, R. S. (2003): Resonant ultrasound spectroscopy in shear mode. *Review of Scientific Instruments* **74**, 1371–1373.

[Wern, 1997] Wern, H. (1997): A new approach to triaxial residual stress evalution by the hole drilling method. *Strain* **45**, 121–125.

[Wern *et al.*, 1997] Wern, H., Cavelius, R., and Schläfer, D. (1997): A New Method to determine Triaxial Non-Uniform Residual Stresses from Measurements using the Hole Drilling Method. *Strain* **45**, 39–45.

[Whitehouse, 1974] Whitehouse, W. J. (1974): The quantitative morphology of anisotropic trabecular bone. *Journal of Microscopy* **101**, 153–168.

[Wu and Ho, 2005] Wu, T. T. and Ho, Z. H. (2005): Anisotropic wave propagation and its applications to NDE of composite materials. *Experimental Mechanics* **30**, 313–318.

[Yahia *et al.*, 1988] Yahia, L. H., Drouin, G., and Duval, P. (1988): A methodolgy for mechanical measurements of technical constants of trabecular bone. *Engineering in medicine* **17**, 169–173.

[Yan *et al.*, 1996] Yan, Z. H., Wu, S. Y., Yi, P., Pin, L., and Jun, C. Y. (1996): On the correction of plasticity effect at the hole edge when using the centre hole method for measuring high welding residual stress. *Strain* , 125–129.

[Yoon and Katz, 1976] Yoon, H. and Katz, J. (1976): Ultrasonic wave propagation in human cortical bone. II Measurements of elastic properties and microhardness. *Journal of Biomechanics* **9**, 459–464.

[Zuccarello, 1999] Zuccarello, B. (1999): Optimal Calculation Steps for th Evalution of Residual Stres by the Incremental Hole-drilling Method. *Experimental Mechanics* **39**, 117–124.

[Zysset *et al.*, 1999] Zysset, P. K., Guo, X. E., Hoffler, C. E., Moore, K. E., and Goldstein, S. A. (1999): Elastic modulus and hardness of cortical and trabecular bone lamellae measured by nanoindentation in the human femur. *Journal of Biomechanics* **32**, 1005–1012.

[Švantner, 2004] Švantner, M. (2004): *Zjišťování zbytkových napětí ve vícevrstvých strukturách.* PhD thesis, Západočeská univerzita v Plzni.

[Červený, 2001] Červený, V. (2001): *Seismic Ray Theory.* University Press, Cambridge.